TABLE OF CONTENTS

FORWARD

This Final Report of NASA Grant NAG 5-480 documents the results of research activities conducted to study the dielectric properties of vegetation material and the propagation characteristics of vegetation canopies at microwave frequencies. These results are presented in the form of reprints of papers published in the scientific literature and organized under four topics: (1) Dielectric Properties of Vegetation Material, (2) Scattering From a Vegetation Leaf, and (3) Propagation Through Vegetation Canopies, and (4) Emission From and Polarimetric Scattering by Vegetation.

MICROWAVE DIELECTRIC SPECTRUM OF VEGETATION MATERIAL

F T Ulaby & M El-Rayes

University of Michigan

ABSTRACT

A novel probe technique was developed to measure the dielectric constant of vegetation material accurately, rapidly, and non-destructively. The probe was then used to measure dielectric spectra from 0.1 GHz to 20 GHz for many types of vegetation material over a wide range of moisture content. The data were used to guide the development of a double-dispersion model that incorporates separate relaxation spectra for bound water and free water.

Keywords: Microwaves, Dielectric Constant, Vegetation.

1. INTRODUCTION

Vegetation material is a mixture of bulk vegetation, water, and various types of organic compounds. Bulk water exhibits a Debye Dispersion spectrum with a relaxation frequency $f_0 \cong 18$ GHz at 22° C [1]. Chemically bound water, as in sucrose and other sugars and proteins, is known to exhibit a dispersion spectrum also, but neither its relaxation frequency nor the shape factor of its dispersion spectrum are known. Hence, to develop a realistic model for the dielectric behavior of vegetation material, it was necessary to: (a) establish the dispersion spectrum of bound water, (b) measure the dielectric constant of vegetation material over a wide range of moisture conditions, and (c) relate the salinity of the fluid contained in the vegetation material to the moisture content. These tasks were conducted and the results are summarized in the sections that follow. A summary of previous investigations is given in [2].

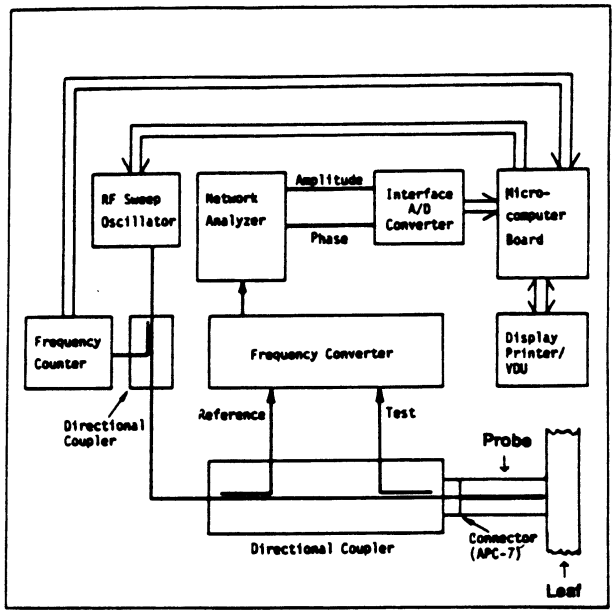

Fig. 1 Block diagram of probe dielectric system. Frequency coverage is 0.1 - 20 GHz.

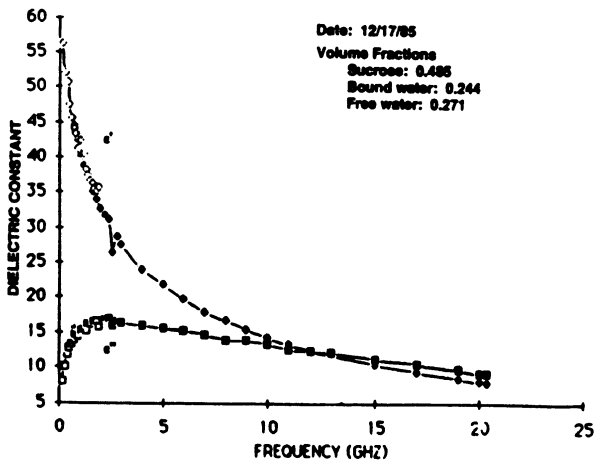

Fig. 2 Measured spectrum of sucrose-water mixture at 22°C.

Proceedings of IGARSS' 86 Symposium, Zürich, 8–11 Sept. 1986. Ref. ESA SP-254 (published by ESA Publications Division, August 1986).

2. PROBE DESIGN

Figure 1 is a block diagram of the dielectric measurement system. It consists of a network analyzer connected to coaxial probe through a directional coupler. The probe, which is an open-circuited coaxial line, may be modeled by an equivalent circuit consisting of a radiation impedance in series with a fringing capacitor. By proper choice of calibration materials, it is possible to characterize the elements of the equivalent circuit, which makes it possible to relate the magnitude and phase of the reflection coefficient measured by the network analyzer to the complex dielectric constant of the material placed in contact with the probe. The calibration procedure consists of reflection measurements made under four conditions: (a) open circuit, (b) short circuit, (c) probe immersed in pure water, and (d) probe immersed in methanol. Pure water and methanol are used for calibration because their dielectric spectra are well known. This procedure is performed at each of 50 frequencies between 0.1 GHz and 20 GHz.

3. DIELECTRIC SPECTRA

Vegetation contains proteins and sugars whose molecules can form chemical bonds with water molecules. When water is added to a sugar such as sucrose, some of the water molecules bind to the sucrose molecules and the remaining molecules remain in a free state, and the relative amounts of bound and free water can be calculated exactly. By measuring the dielectric spectra of sucrose-water mixtures of various water contents, such as the one shown in Fig. 2, it was possible to establish the dispersion spectrum of bound water. This procedure led to the Cole-Cole spectrum:

$$\varepsilon_b = \varepsilon_{b\infty} + \frac{\varepsilon_{bo} - \varepsilon_{b\infty}}{1 + (j f / f_{bo})^{1-\alpha}} \qquad (1)$$

with $\varepsilon_{b\infty} = 2.9$, $\varepsilon_{bo} = 58.9$, $f_{bo} = 0.178$ GHz, and $\alpha = 0.5$.

Next, measurements were made to determine the dielectric spectra of various types of vegetation material at several levels of moisture content. Measured spectra of the real and imaginary parts of the dielectric constant are shown in Fig. 3 for corn leaves. The moisture content M_v, which is given in volumetric units, is determined from measurements of the dry weight and wet weight values of the vegetation sample and the vegetation density. In addition, samples of the vegetation fluid were extracted and then used to determine the salinity of the solution.

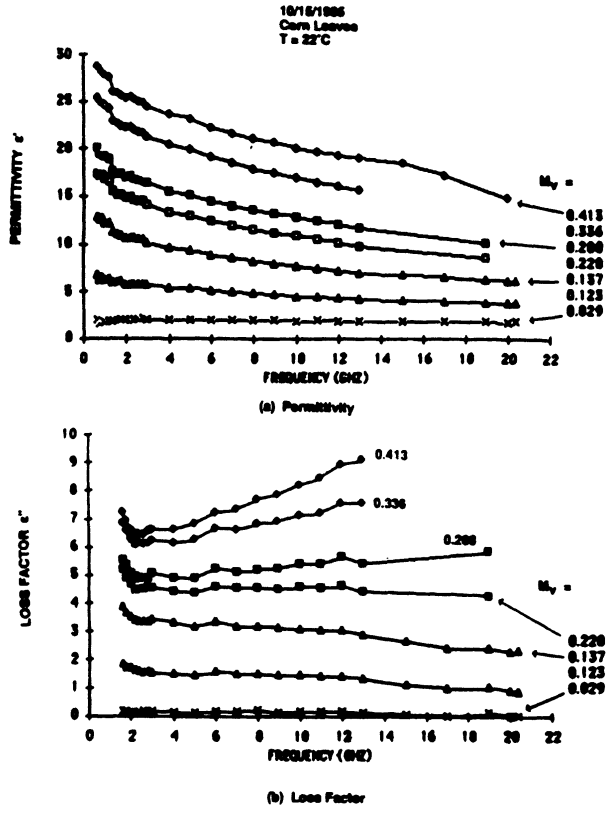

Fig. 3 Spectra of the dielectric (a) permittivity and (b) loss factor of corn leaves with volumetric moisture M_v as parameter.

4. DIELECTRIC MODEL

The vegetation dielectric constant ε is modeled as a simple mixture of three components:

$$\varepsilon = V_v \varepsilon_v + V_f \varepsilon_f + V_b \varepsilon_b , \qquad (2)$$

where V stands for volume fraction, and the subscripts v, f, and b stand for bulk vegetation material, free water, and bound water, respectively. The dielectric constant of dry corn leaves was determined to be:

$$\varepsilon_v \cong 1.5 - j\,0.01 , \qquad (3)$$

and is independent of both temperature and frequency. The magnitude of the real part is fairly accurate, but the magnitude of the imaginary part is only an estimate.

The dielectric constant of free water is given by the Debye equation

$$\varepsilon_f = \varepsilon_{f\infty} + \frac{\varepsilon_{fo} - \varepsilon_{f\infty}}{1 + j f / f_{fo}} - j \frac{\sigma}{2\pi \varepsilon_0 f} , \qquad (4)$$

where ε_0 is the permittivity of free space, $\varepsilon_{f\infty} = 4.9$, σ is the ionic conductivity of the free water and is defined by the salinity of the water, and ε_{fo} and f_{fo} are defined in terms of the water temperature and salinity [1].

The basic form of ε_b is given by (1). The values of the Cole-Cole parameters $\varepsilon_{b\infty}$, ε_{bo}, f_{bo}, and α given in conjunction with (1), however, were determined for a specific constituent of vegetation, namely sucrose. Based on a review of the literature and on a similar analysis conducted for other sugars, proteins, and starches, it is hypothesized that the general form of (1) is applicable to vegetation also.

Upon: (a) inserting (1), (3) and (4) into (2), (b) specifying the Debye parameters of free water at 22°C, and (c) introducing a free paramter ε_∞, we have

$$\varepsilon = \varepsilon_\infty + \left(\frac{75}{1 + jf/18} - j \frac{\sigma'}{f} \right) V_f + \frac{56\, V_b}{1 + (jf/0.178)^{0.5}} \quad (5)$$

where

$$\sigma' = \frac{\sigma}{2\pi\varepsilon_0} = (18.9 - 42.8\, V_f)\ \%. \quad (6)$$

The above relation was determined empirically by measuring the salinity and conductivity of the fluid contained in the vegetation material. The measurements were made for several values of the moisture content M_v, from which the free water content V_f was calculated (according to the water distribution model discussed below). It was found that for a particular vegetation type, the salinity -- and hence the conductivity also -- decreases linearly with increasing moisture content; i.e., the salt solution becomes more dilute as M_v increases.

The free parameter ε_∞ was determined through regression analysis (as discussed below) to be:

$$\varepsilon_\infty = 1.86 + 12.9\, M_v - j\, 0.01. \quad (7)$$

In order to evaluate the dielectric model, we need to use a water distribution model that defines how water is distributed between bound and free. To that end, we shall assume that when a leaf, for example, loses water to evapotranspiration, its volume shrinks accordingly, thereby maintaining the volume of air in the vegetation material constant. This assumption leads to the following relation between the volumetric moisture content M_v and gravimetric water content M_g (wet weight basis):

$$M_v = \frac{M_g}{M_g + (1 - M_g)/\rho_d}, \quad (8)$$

where ρ_d is the density of dry vegetation. For corn leaves a reasonable estimate is $\rho_d = 0.24$ g cm^{-3}. Dry vegetation consists of bulk vegetation material and air. For dry corn leaves, approximately 80% of the volume is occupied by air.

Based on the experience gained from the measurements made and models developed for sucrose and other sugars and proteins, it was hypothesized that the maximum volume fraction of the vegetation-water mixture that can be occupied by bound-water is equal to one-half of the volume fraction of the bulk vegetation material. These considerations led to the water distribution model shown in Fig. 4.

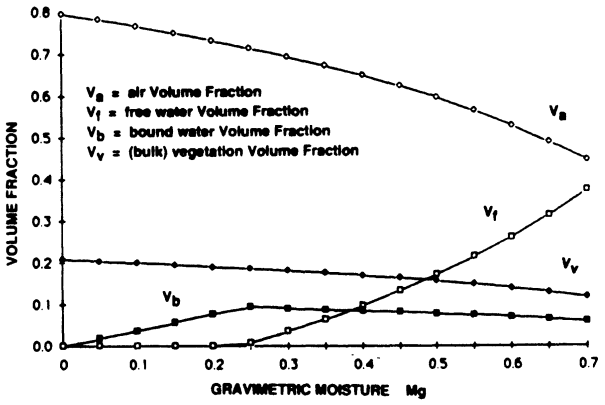

Fig. 4 Water distribution model for corn leaves.

Using a regression routine, the value of ε_∞ was determined for each value of M_v by minimizing the variance between ε calculated according to (5) and that measured directly by the dielectric probe. The results were then expressed as a linear function of M_v. This procedure led to (7). A total of 676 measurements were used in this analysis which covers the range 0.7 - 20 GHz in frequency and 0.1 to 0.7 in gravimetric moisture.

The model was evaluated by comparing calculated spectra to measured spectra at specific moisture contents, and by comparing the moisture variation predicted by the model to that measured at specific frequencies. Examples of both types are presented in Figs. 5 and 6; they include high and low moisture values, and high and low frequencies.

5. CONCLUSIONS

The model proposed in this study appears to provide a satisfactory fit to the measured dielectric spectra of vegetation-water mixtures. However, most of the data evaluated to date have been for corn leaves. The next step is to evaluate how well it can be extended to other vegetation types and to temperatures other than room temperature. These objectives will be the subject of future investigations.

6. REFERENCES

[1] Ulaby, F. T., R. K. Moore, and A. K. Fung (1986). Microwave Remote Sensing: Active and Passive. Vol. III, Appendix E., Artech House, Dedham, Ma.

[2] Ulaby, F. T., and R. P. Jedlicka (1984), Microwave Dielectric Properties of Plant Materials, IEEE Trans Geosci. Remote Sensing, GE-22, pp. 406-414

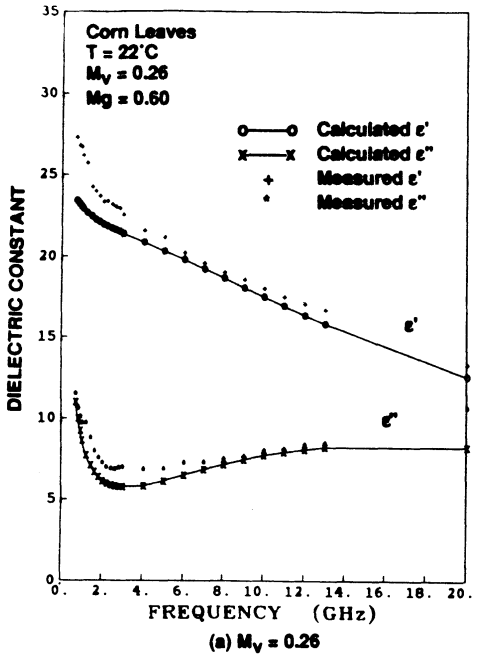

(a) M_V = 0.26

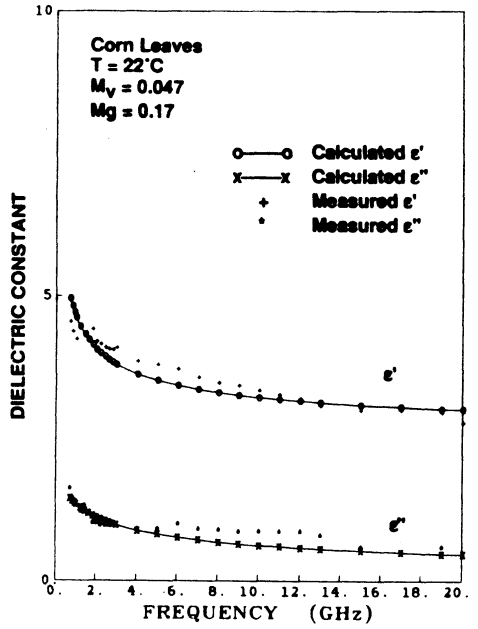

(b) M_V = 0.047

Fig. 5 Comparison of model-calculated dielectric spectra for corn leaves with (a) high volumetric moisture and (b) low volumetric moisture.

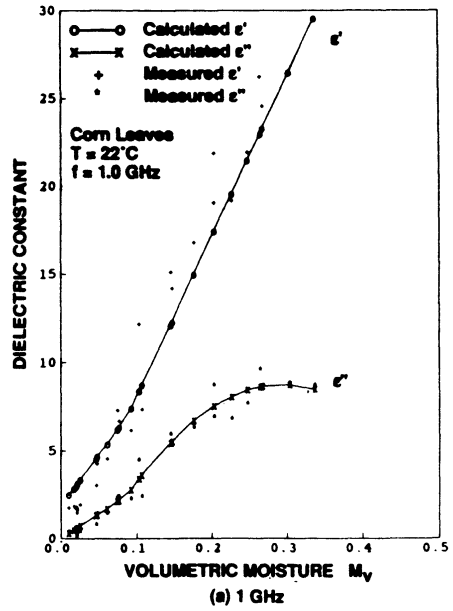

(a) 1 GHz

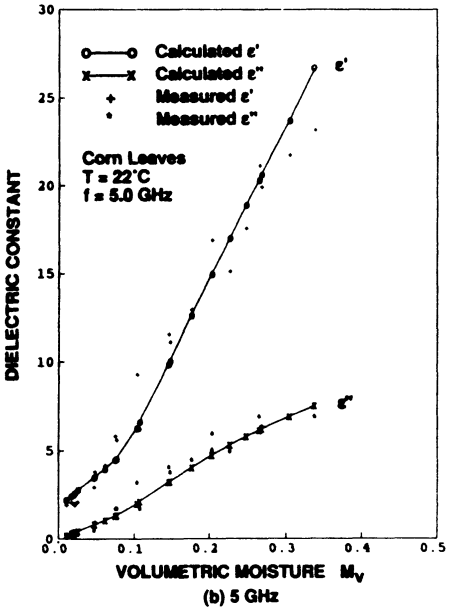

(b) 5 GHz

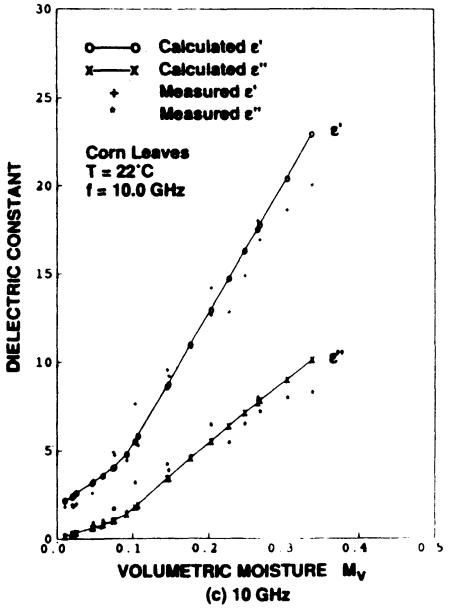

(c) 10 GHz

Fig. 6 Comparison of model-calculated moisture to measured values.

Microwave Dielectric Spectrum of Vegetation—Part I: Experimental Observations

MOHAMED A. EL-RAYES AND FAWWAZ T. ULABY, FELLOW, IEEE

Abstract—**This is the first paper in a two-part sequence that evaluates the microwave dielectric behavior of vegetation material as a function of water content, microwave frequency, and temperature. Part I presents experimental measurements of the dielectric spectrum from 0.2 to 20 GHz for various types of vegetation material including leaves, stalks, and trunks at various moisture conditions. The measurements were acquired using a coaxial probe technique suitable for measuring the dielectric constant of both thick materials, such as tree trunks, and thin materials, such as leaves.**

In Part II, the experimental data are used to guide the development of a dual-dispersion dielectric model that incorporates the dielectric properties of water in both "free" and "bound" forms.

I. Introduction

THE DIELECTRIC properties of vegetation material play a central role in the coupling between the electromagnetic properties of a vegetation canopy and its physical properties. The dielectric constant of a leaf, for example, is governed by its water content and salinity. In turn, the dielectric constants, shapes, and orientations of the vegetation elements together control the scattering and emission by the canopy. Despite its fundamental importance, however, the dielectric behavior of vegetation is not well understood, particularly in the microwave region. This is attributed to two factors: 1) very few microwave measurements of the dielectric constant ϵ of vegetation have been reported to date, as reviewed in [1], and 2) the dielectric mixture models currently in use [2] to relate the dielectric constant of vegetation to the dielectrics of its constituents—the bulk vegetation material and liquid water—are quite simplistic in form and capable of providing approximate estimates at best.

The purpose of the present study is to: 1) use a broadband measurement technique to document the dielectric behavior of vegetation material over a wide frequency range, 2) examine the temperature dependence of ϵ, and 3) develop a dielectric dispersion model based on the physical properties of the vegetation constituents. To this end, coaxial probes were developed and used in conjunction with a reflectometer system to measure the dielectric constant of both thin (such as leaves) and thick (such as trunks) vegetation samples over the range 0.2–20 GHz. The results are presented in a two-part series: Part I, this paper, describes the measurement system, proposes a technique for measuring the dielectric constant of thin slabs, and presents dielectric spectra for several vegetation types and plant parts under a variety of moisture and temperature conditions. In Part II, which follows, a new double-dispersion mixture model is proposed and its performance is evaluated in terms of some of the data presented in this paper.

Manuscript received February 24, 1987; revised June 2, 1987. This work was supported by the NASA Goddard Space Flight Center under Contract NAG 5-480.

The authors are with the Radiation Laboratory, Department of Electrical Engineering and Computer Science, The University of Michigan, Ann Arbor, MI 48109-2122.

IEEE Log Number 8716095.

II. Measurement System

The dielectric data reported in this study are based on measurements of the amplitude and phase of the reflection coefficient of a coaxial probe terminated in the material under test. The system (Fig. 1) consists of a swept RF source, a network analyzer (HP 8410C), and associated couplers and data processing instrumentation. Fig. 2(a) shows a cross section of the probe tip and the dimensions of two of the probes used in this study. The operation of open-ended coaxial lines to measure the dielectric constant of unknown materials is well-documented in the literature [3]–[5]. The input reflection coefficient at the prober tip ρ is given by

$$\rho = \frac{Z_L - Z_0}{Z_L + Z_0} = \frac{Y_0 - Y_L}{Y_0 + Y_L} \tag{1}$$

where $Y = 1/Z$, Z_0 is the line impedance, and Z_L is the load impedance, which is governed by the geometry of the probe tip and the dielectric constant of the material it is in contact with or immersed in (for liquid materials). In general, an open-ended coaxial line may be described by an equivalent circuit of the form shown in Fig. 2(b). When placed in contact with a homogeneous material whose thickness is sufficient to simulate a slab of infinite electrical thickness, an open coaxial line has an admittance $Y_L(\omega, \epsilon)$ given by

$$Y_L(\omega, \epsilon) = Y_i(\omega) + Y_e(\omega, \epsilon) \tag{2}$$

where $Y_i(\omega) = j\omega C_i$ is the "internal" admittance corresponding to the fringing capacitance C_i that accounts for the fringing field in the Teflon region between the inner and outer conductors of the line. The "external" admittance Y_e, which is a function of both ω and the complex dielectric constant ϵ of the material under test, consists of a frequency-dependent capacitor $C(\omega, \epsilon)$ in parallel with

0196/2892/87/0900-0541$01.00

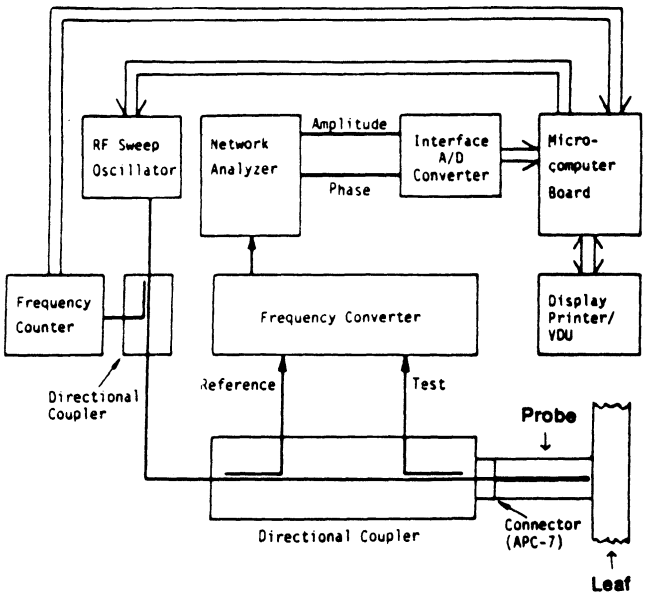

Fig. 1. Block diagram of probe dielectric system. Frequency coverage is 0.1-20 GHz.

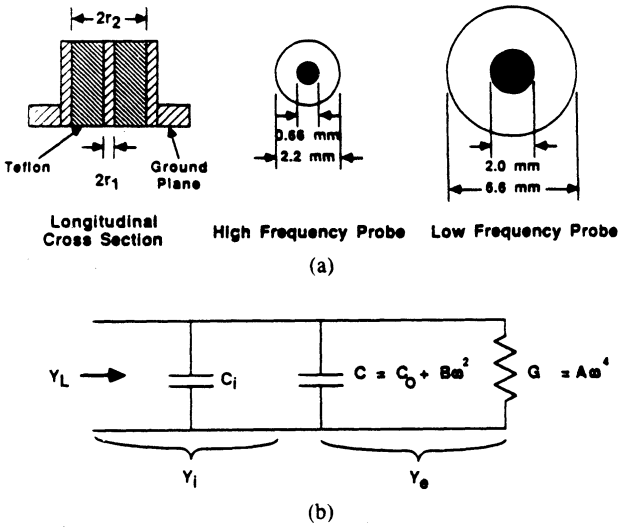

Fig. 2. (a) Coaxial probe, and (b) its equivalent circuit.

a radiation conductance $G(\omega, \epsilon)$

$$Y_e(\omega, \epsilon) = j\omega C(\omega, \epsilon) + G(\omega, \epsilon). \quad (3)$$

The capacitor $C(\omega, \epsilon)$ represents the fringing field concentration in the dielectric medium (ϵ) surrounding the probe tip, and the conductance $G(\omega, \epsilon)$ represents the radiation into the dielectric medium.

When the medium surrounding the probe tip is free space (i.e., an open-ended line), these two equivalent-circuit elements vary according to [3], [6, p. 213]

$$C(\omega, \epsilon_0) = C_0 + B\omega^2 \quad (4)$$

$$G(\omega, \epsilon_0) = A\omega^4 \quad (5)$$

where C_0, B, and A are constants for a given probe-tip geometry. If the radial dimensions of the coaxial line (namely, r_1 and r_2) are small compared to the wavelength λ, computations using the expressions given in Marcuvitz [6] yield values for A and B that are sufficiently small that the external admittance may be approximated as $Y_e(\omega, \epsilon_0) \cong j\omega C_0$. If the dielectric constant of the medium surrounding the probe tip is not the free space value ϵ_0, however, the above simplification may lead to unacceptably large errors. Hence, in the general case we have

$$Y_e(\omega, \epsilon_0) = j\omega(C_0 + B\omega^2) + A\omega^4. \quad (6)$$

According to the theorem developed by Deschamps [7], the input admittance of an antenna immersed in a medium of complex dielectric constant ϵ is related to the input admittance in free space through

$$Y_e(\omega, \epsilon) = \sqrt{\frac{\epsilon}{\epsilon_0}}\, Y_e\left(\omega\sqrt{\frac{\epsilon}{\epsilon_0}}, \epsilon_0\right). \quad (7)$$

The above expression is for materials characterized by $\mu = \mu_0$. If we regard the open-ended coaxial line as an antenna and henceforth abbreviate the relative dielectric constant ratio ϵ/ϵ_0 as simply ϵ, we can write the following expression for the total input admittance of the probe when placed in contact with a material of relative dielectric constant ϵ:

$$Y_L(\omega, \epsilon) = j\omega C_i + j\omega C_0\epsilon + jb\omega^3\epsilon^2 + A\omega^4\epsilon^{2.5}. \quad (8)$$

With the line admittance Y_0 known, measurements of the amplitude and phase of ρ by the network analyzer system (Fig. 1) lead to a measurement of Y_L. The next step is to determine ϵ from Y_L. This is accomplished by 1) calibrating the measurement probe in order to establish the values of the constants C_i, C_0, B, and A, and 2) developing an iterative program for finding a value for ϵ that minimizes the error between the measured value of Y_L and the value calculated from the expression on the right-hand side of (8).

A. Usable Frequency Range

The radii r_1 and r_2 of the coaxial line govern three important characteristics of the dielectric measurement system:

1) The ratio r_1/r_2 determines the characteristic impedance Z_0 of the line. For 50-Ω Teflon-filled lines, this ratio is approximately 0.3.

2) The difference $(r_2 - r_1)$ determines the cutoff wavelength of the TM modes [6, p. 74]; the cutoff wavelength of the TM_{01} modes is $\lambda_c \cong 2(r_2 - r_1)$. Table I provides a list of the dimensions and cutoff wavelengths of four standard coaxial lines used in this study. For a medium with a complex dielectric constant $\epsilon = \epsilon' - j\epsilon''$, the wavelength in the medium λ_ϵ is related to the wavelength in free space λ_0 by

$$\lambda_\epsilon = \lambda_0\left[\frac{\epsilon'}{2}(1 + \sec\delta)\right]^{-1/2} \quad (9)$$

where $\delta = \tan^{-1}(\epsilon''/\epsilon')$. To avoid the propagation of TM modes, the condition $\lambda_\epsilon < \lambda_c$ should be satisfied. Table II provides values of λ_ϵ for distilled water at a selected set of frequencies. If we regard distilled water as a material whose dielectric properties represent the upper end of the range of dielectric values of materials to be

TABLE I
DIMENSIONS AND CUTOFF WAVELENGTH λ_C FOR THE TM_{01} MODE FOR FOUR STANDARD-SIZE COAXIAL CABLES

Cable	Type	r_2(mm)	r_1(mm)	r_2/r_1	λ_c(mm)
0.09"	Teflon	0.84	0.26	3.28	1.18
0.14"	Teflon	1.50	0.46	3.30	2.13
0.25"	Teflon	2.66	0.82	3.22	3.76
0.35"	Teflon	3.62	1.12	3.22	5.07

TABLE II
WAVELENGTH IN DISTILLED WATER AT 22°C

f(GHz)	1.0	2.0	4.0	6.0	9.0	10.0	20.0	30.0	40.0
$(\lambda_\epsilon)_C$(mm)	33.7	16.9	11.7	5.825	4.05	3.70	2.21	1.75	1.49

tested, then both the 0.14-in probe and the 0.085-in probe are appropriate for measuring the dielectric properties of vegetation materials at frequencies below 20 GHz.

3) The probe translates variations in the dielectric constant of the test material into variations in the measured amplitude ρ_0 and phase ϕ of the reflection coefficient (i.e., $\rho = \rho_0 e^{j\phi}$). The variation in the measured phase depends on ϵ'' as well as ϵ'. However, the effects of ϵ'' on $\Delta\phi$ are of less importance compared to the effects of ϵ' [5]. The phase sensitivity to ϵ' may be defined as

$$S_{\epsilon'}^{\phi} = \frac{\epsilon'}{\phi}\frac{\partial\phi}{\partial\epsilon'} \tag{10}$$

and similar definitions may be given for the phase sensitivity to ϵ'' and the amplitude sensitivities to ϵ' and ϵ''. For a material with known ϵ' and ϵ'', it is possible to choose the probe size to optimize the measurement sensitivities, and hence the measurement accuracy [5]. In general, however, if the probe is to be used to measure ϵ for a variety of different materials, it is advantageous to use the largest possible probe because the phase and amplitude sensitivities generally increase with increasing probe dimensions.

As a compromise between the need to operate over a wide frequency range extending up to 20 GHz—which requires the use of probes with small radii—and the need to have strong sensitivities to variations in ϵ' and ϵ'', which requires the use of probes with large radii, we used the 0.141-in probe for making measurements from 0.7 to 20 GHz and the 0.25-in probe for measurements from 0.1 to 2 GHz.

B. Calibration

Calibration entails finding the values of the constants C_i, C_0, B, and A of (8) for each probe used in this study. Under ideal circumstances, one needs to determine these constants only once and at only one frequency. The equivalent-circuit model, however, is only approximate; hence, it is necessary to determine these constants at each frequency that the probe is intended to be used. For example, it was found that the *constant A* varies approximately at $1/\omega$, which means that the conductance term $G(\omega)$ varies as ω^3, not ω^4.

Each dielectric probe was calibrated by measuring the complex reflection coefficient under four termination conditions: 1) short circuit, 2) open circuit, 3) probe immersed in distilled water, and 4) probe immersed in methanol. Distilled water and methanol were used because their dispersion spectra are well known [8], [9].

Numerous tests were conducted to evaluate the measurement accuracy and precision of the dielectric system. An example is shown in Fig. 3 that compares the measured dielectric spectrum of butanol to its theoretical relaxation spectrum as reported in the literature [10]. The measured values of ϵ are in good agreement with the calculated spectrum. Based on this and other tests for both liquid and solid samples, the coaxial probes were found to have a relative accuracy of 5 percent for ϵ' and 10 percent for ϵ''.

C. Thin-Sample Measurements

In the preceding discussion, the sample under test was assumed to be electrically infinite in depth. To evaluate the effective *penetration depth* of the probe, experiments were conducted for slabs of various thicknesses. Fig. 4 is an illustrative example of the results obtained using the 0.141-in probe; three curves are shown, one depicting the permittivity of paper when measured against a metal background (but calculated as if the paper layer were infinitely thick), another measured and calculated in a similar fashion but with Plexiglas as the background, and a third (dashed curve) measured for a very thick stack of papers (representing the true value of ϵ'). We observe that the curves corresponding to the measurements for paper-over-metal and paper-over-Plexiglas approach the third curve to within $\Delta\epsilon' = 0.1$ when the thickness exceeds 3 mm. These results are based on measurements made for a low-loss material (paper) at 1 GHz. At higher frequencies and/or for lossier materials, the effective penetration depth was found to be significantly less than 3 mm. Additionally, the probe size also is a factor; as a rule of thumb, it was found that the sample thickness should be at least equal to, and preferably larger than, the radius of the probe's outer conductor.

The 3-mm thickness requirement is easy to satisfy for many materials but not for naturally thin materials such as a single leaf of vegetation. Typical leaf thickness is about 0.1 mm, thereby necessitating that a stack of 30 closely packed leaves be formed for making the dielectric measurements. It is important that the stack be under sufficient pressure to ensure that no air gaps are present between adjacent leaves.

An alternative technique was developed that allows direct measurements of thin materials. Suppose the probe is used to make a measurement of the input admittance when it is terminated with a thin dielectric slab of thickness d placed against a background consisting of an electrically thick material with dielectric constant ϵ_1. Suppose that a second measurement is made using the same thin dielectric slab, but this time placed against a different background of dielectric constant ϵ_2. Let us denote these mea-

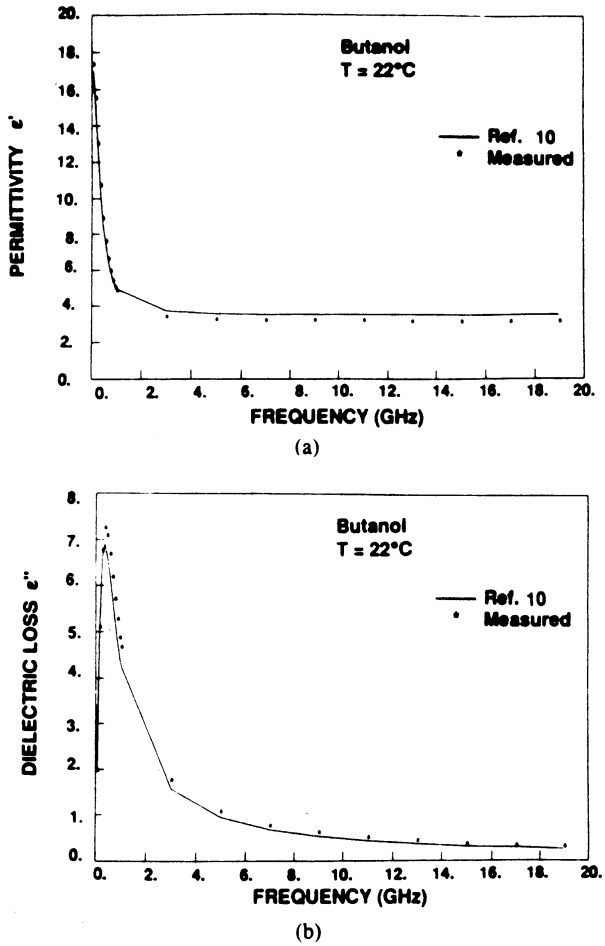

Fig. 3. Comparison of measured dielectric spectrum of Butanol to that calculated according to the dispersion equation given by Bottreau *et al.* [10].(a) ϵ'. (b) ϵ''.

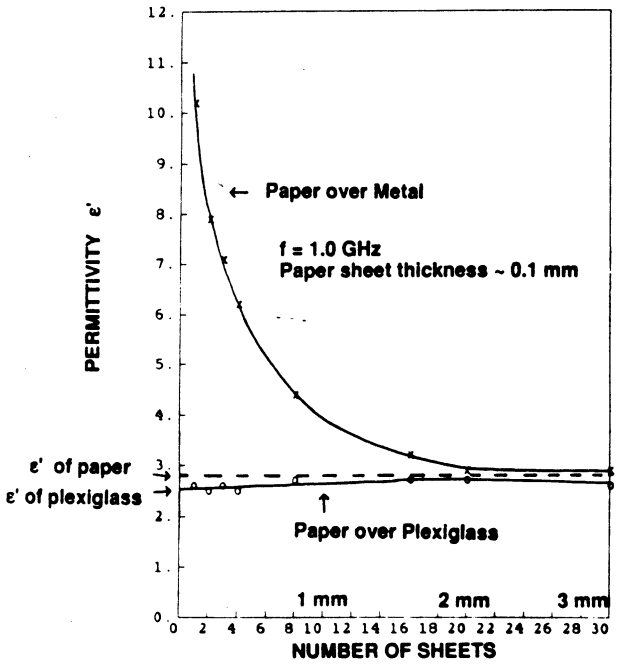

Fig. 4. Measured permittivity of paper as a function of thickness.

surements Y'_{L1} and Y'_{L2}, respectively. Fig. 5 shows the prescribed arrangement with the first background material chosen to be a metal block. If the arrangement is treated as a transmission line problem, it is easy to express Y'_{L1} in

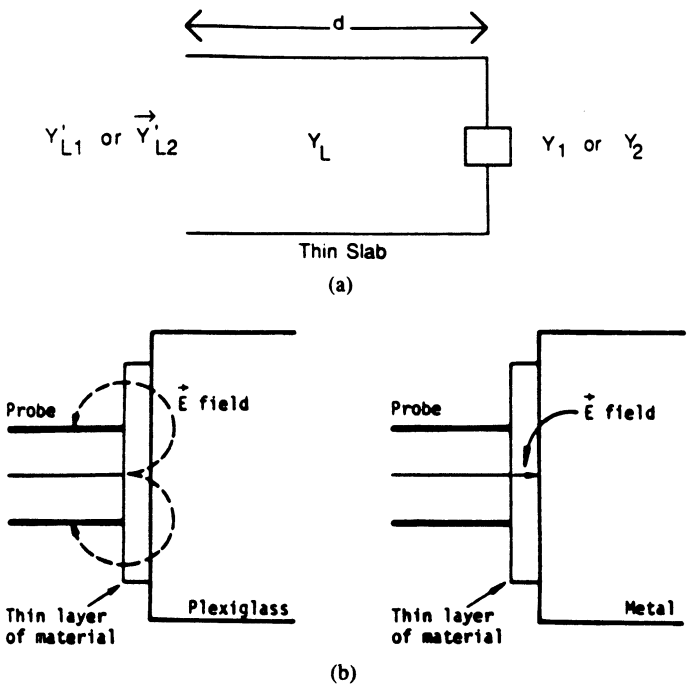

Fig. 5. Probe technique for measuring the dielectric of thin slabs; (a) transmission-line equivalent circuit of the configurations shown in (b).

terms of the unknown admittance of the thin slab Y_L, the terminating admittance Y_1 of the material with dielectric ϵ_1, and the propagation function γd of the thin slab (where γ is the propagation constant of the slab material and d is its thickness). Similarly, Y'_{L2} can be expressed in terms of Y_L, Y_2, and γd. If we eliminate γd from the two expressions and choose $Y_2 = \infty$ (metal background), we obtain the simple expression

$$Y_L = \left[Y'_{L1}Y'_{L2} + Y_1(Y'_{L1} - Y'_{L2})\right]^{1/2}. \qquad (11)$$

In the above expression Y_L represents the characteristic admittance of the thin slab, which is the load admittance that the probe would measure had the slab been infinitely thick.

The validity of this semi-empirical approach was evaluated over a wide range of frequencies for a wide range of dielectric values. In all cases the two materials used for background were metal and Plexiglas. The evaluation consisted of comparing ϵ_{thick} as measured directly for a very thick slab with ϵ_{thin} as measured for a very thin slab of the same material following the approach described above. The technique was found to yield satisfactory results as demonstrated by the comparison shown in Fig. 6 for 8 GHz. Similar results were obtained at other frequencies.

D. Sample Preparation and Handling

Solid samples are difficult to measure with the open coax method because the apparent reflection often depends on the quality of contact between the probe and the sample. Surface preparation of solid samples must be done very carefully to insure that no air gaps remain where the probe is applied. With rocks, the surface should be polished smooth prior to measurement. With semi-solid bo-

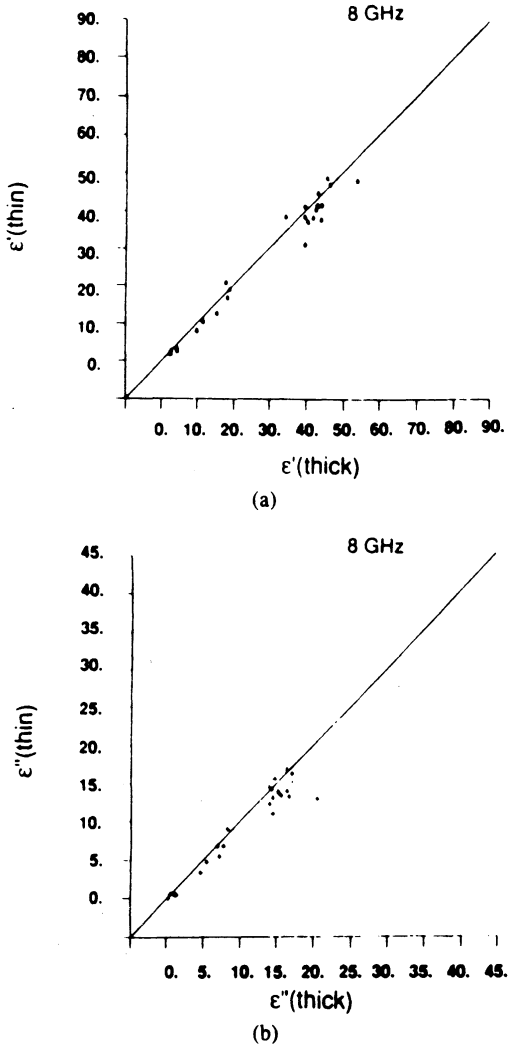

Fig. 6. Comparison of dielectric measurements made for a thick stack of corn leaves (ϵ' thick, ϵ'' thick) with measurements made for individual leaves (ϵ' thin, ϵ'' thin) using the technique described in the text. (a) Equivalent circuit. (b) Probe against thin layer with two different backgrounds.

tanical samples, excess pressure from the probe can crush the cellular structure beneath the probe, thereby changing the dielectric properties of the material being measured. In the present investigation, a pressure gauge was used to insure that the pressure was sufficient to result in good contact between the probe and the botanical sample but not too strong to crush the sample.

III. Examples of Dielectric Measurements

Over the past two years, the dielectric probe has been used to measure the dielectric spectra of many types of vegetation material under a variety of conditions. A few illustrative examples are presented in this section.

A. Balsam Fir Tree Trunk

The dielectric spectrum shown in Fig. 7(a) was measured by placing the dielectric probe against a flat cross section of a trunk section of a balsam fir tree. The volumetric moisture M_v of the wood was calculated from weight measurements (prior to and after oven drying) and density determination to be 0.17. Measurements made for other trunk samples have ranged from around 0.1 for naturally dried wood to about 0.6 for freshly cut trunks. Correspondingly, the dielectric spectra vary over a wide range of values; at 5 GHz, for example, ϵ' varies from a low value of 3.5 to a high value of 20.

B. Poplar Tree Trunk

An experiment was conducted to evaluate the radial variation of the dielectric constant of freshly cut tree trunks. An example of the results is sketched in Fig. 7(b) in the form of five concentric rings. Each ring contains the average dielectric constant (of 16 sample measurements made at different locations within that ring) and its average gravimetric moisture content. We observe that ϵ decreases from $32\text{-}j8$ at the center to $8\text{-}j1$ at the outermost ring; actually, the measurements for this outermost ring, which consisted of the tree bark, were made from the side rather than from the top. The gravimetric moisture constant, on the other hand, is essentially the same for all rings. The radial variation of ϵ is attributed to variation in volumetric moisture content M_v, which is related to the gravimetric moisture constant Mg through

$$M_v = \frac{Mg\rho}{1 - Mg(1 - \rho)} \tag{12}$$

where ρ is the dry density of the soil material. For a fixed value of Mg, M_v increases with increasing ρ. For many types of trees, including the poplar variety, the density of the trunk material is highest at the center and decreases radially outward. In all physically based dielectric mixture models [8], the concentration parameters driving the model usually are the volume fractions of the constituents, not their weights.

C. Aspen-Leaves

Three sets of spectra are presented in Fig. 8, corresponding to leaves of aspen measured at three gravimetric moisture conditions ranging from 0.20 to 0.86 by wet weight. The spectra cover only the 1–8.5 GHz range because they were made before the system's frequency range was expanded to 20 GHz.

D. Corn Leaves and Stalks

Fig. 9 presents a family of dielectric spectra for corn leaves, measured at several gravimetric moisture conditions extending from 0.83 (freshly cut) down to 0.08. The data were used in the development of the models discussed in Part II. Similar dielectric data were measured for corn stalks and found to exhibit a moisture dependence very similar to that exhibited by the dielectric constant of leaves.

E. Corn Stalk Fluid

Pressure techniques were used to extract samples of the fluids contained in some of the vegetation materials examined in this study. Fig. 10 shows the spectrum measured by the dielectric probe for a fluid sample extracted

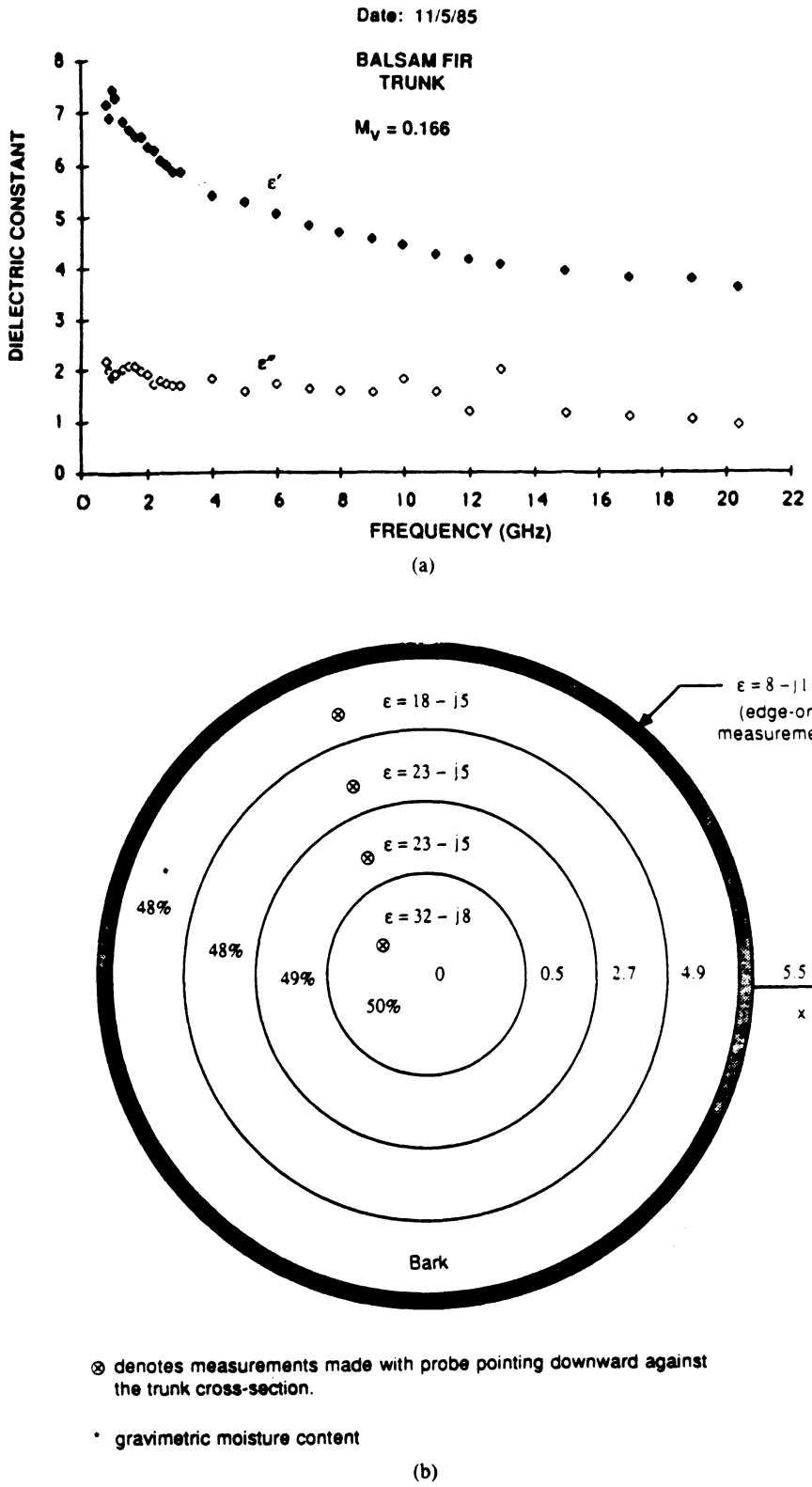

Fig. 7. Measured dielectric of the trunk of (a) a balsam fir tree and (b) a poplar tree.

from a freshly cut corn stalk. Also shown is a theoretical spectrum calculated for a slightly saline water with a salinity of 7 percent. The expressions used are due to Stogryn [11] and are available in Ulaby *et al.* [8]. Overall, the measured spectrum is in very good agreement with the calculated spectrum. The deviation between the measured and calculated curves of ϵ'' above 12 GHz is attributed to multimode propagation.

IV. Temperature Variation

To evaluate the variation of ϵ with temperature for vegetation material, use was made of a temperature chamber capable of operating over a wide range of temperatures both above and below freezing. A 2-m coaxial cable was used to connect the network analyzer system to the open-ended coaxial probe (which was placed inside the cham-

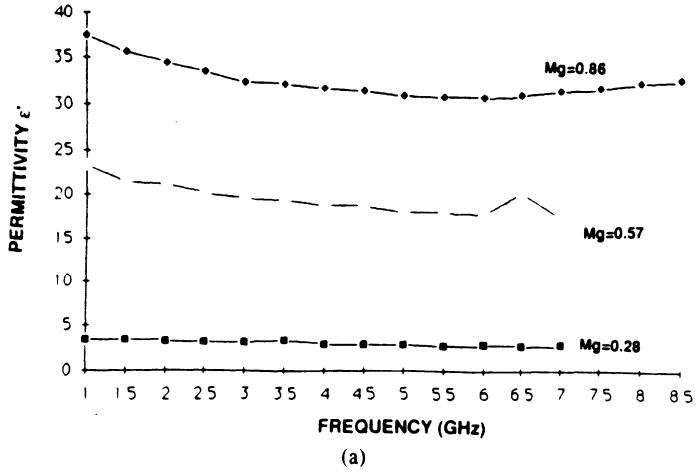

(a)

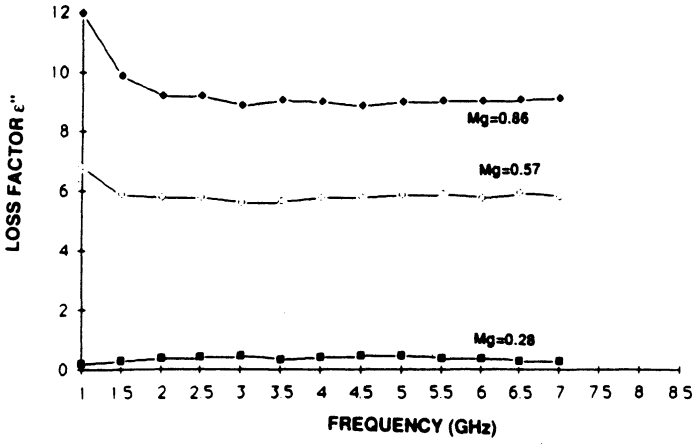

(b)

Fig. 8. Measured dielectric spectra of aspen leaves at three moisture conditions. (a) ϵ'. (b) ϵ''.

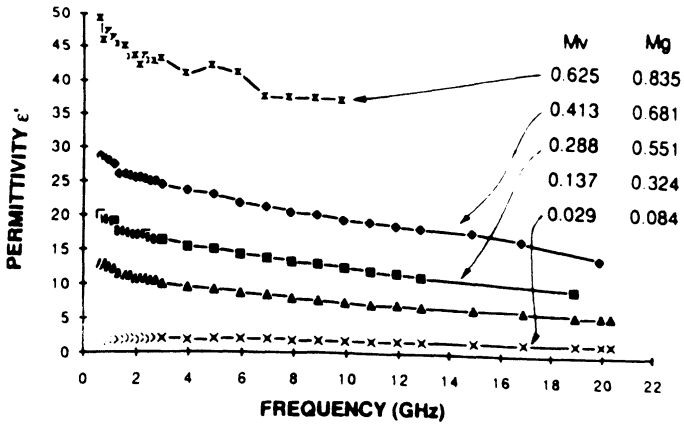

(a)

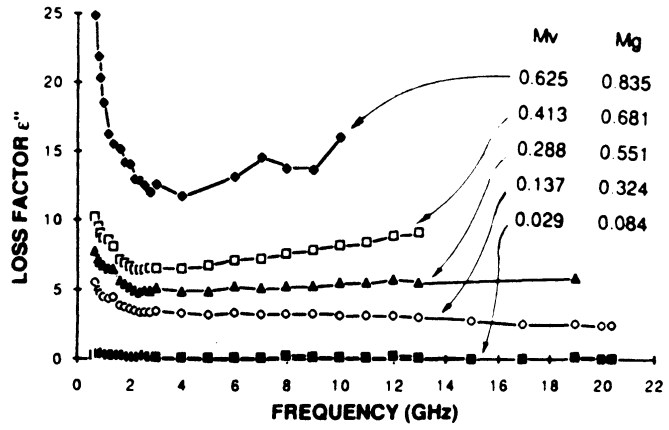

(b)

Fig. 9. Family of dielectric spectra for corn leaves at various levels of moisture content. (a) ϵ'. (b) ϵ''. T = 22°C.

ber) through a special conduit in the wall of the chamber. The curves in Fig. 11 depict the variation of the dielectric constant of a corn leaf observed as the temperature was slowly lowered from room temperature at 23°C down to −32°C. Our initial expectation was that the water in the leaves would freeze at a temperature somewhere between 0 and −1°C because its salinity is on the order of 5‰ (the freezing temperature of liquid water with such a salinity is −0.3°C). The results shown in Fig. 11 suggest that the fluid in the corn leaf goes through a supercooling state down to about −6°C and then it freezes instantaneously.

This temperature behavior was explored further by measuring ϵ as a function of temperature during three consecutive half-cycles, as shown in Fig. 12. At the start of the experiment, the sample was at 22°C; a freezing half-cycle was conducted during which the temperature dropped down to −32°C; the temperature was then raised slowly up to +3°C (this half cycle is labeled "thawing" in the figure); and finally in the last half-cycle the temperature was made to drop again to well below freezing (ending at −15°C). There are two major observations worth noting. First, at the end of the first full cycle when the temperature reached +3°C, the dielectric constant was (23-j13), compared to approximately (35-j21) at the same temperature during the first half-cycle. This difference in level is partly explainable by the loss of moisture during the thawing cycle; the moisture content was 0.83 at the start of the experiment and 0.78 at the end of the first full cycle. Second, ϵ exhibits a hysteresis-like effect as a function of the temperature T. This behavior, which was observed in this and numerous other experiments conducted for plant material at various levels of moisture content, may be related to the occurrence of some damage of the leaf cells due to water crystallization, but no adequate explanation is available at this time.

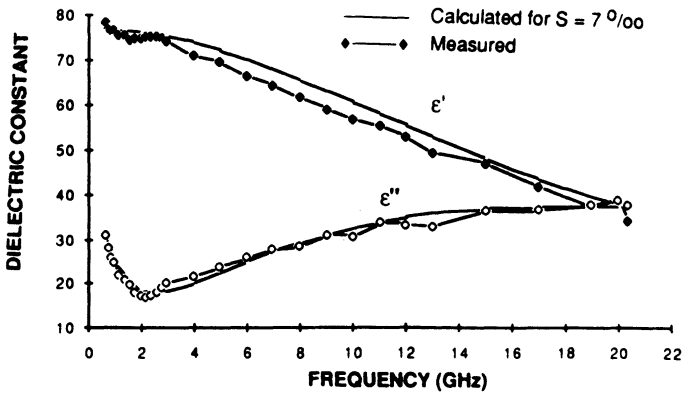

Fig. 10. Measured (◇ and ◆) dielectric spectrum of the fluid extracted from corn stalks, and calculated spectrum of saline water (——).

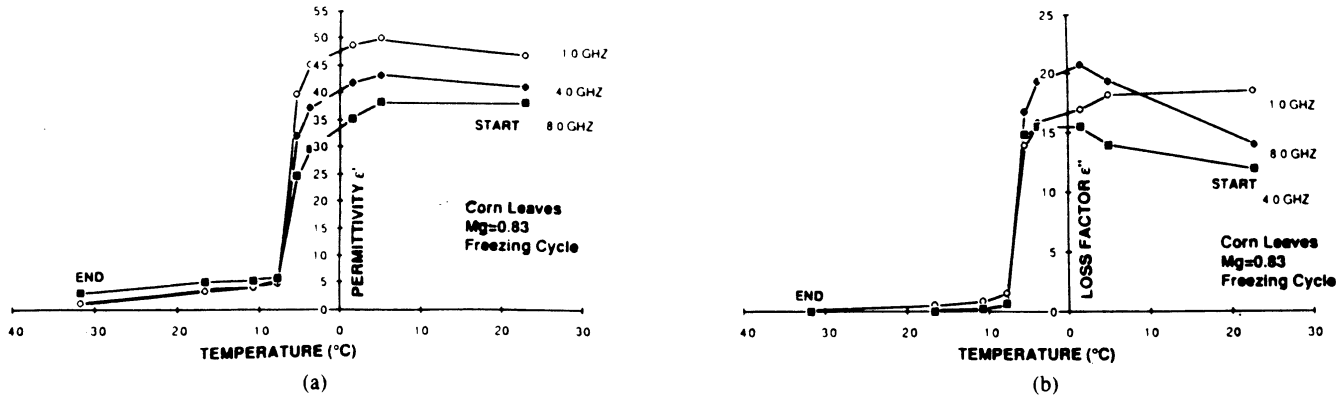

Fig. 11. Variation of ϵ of corn leaves with decreasing temperature from 22 down to $-32°C$. (a) ϵ'. (b) ϵ''.

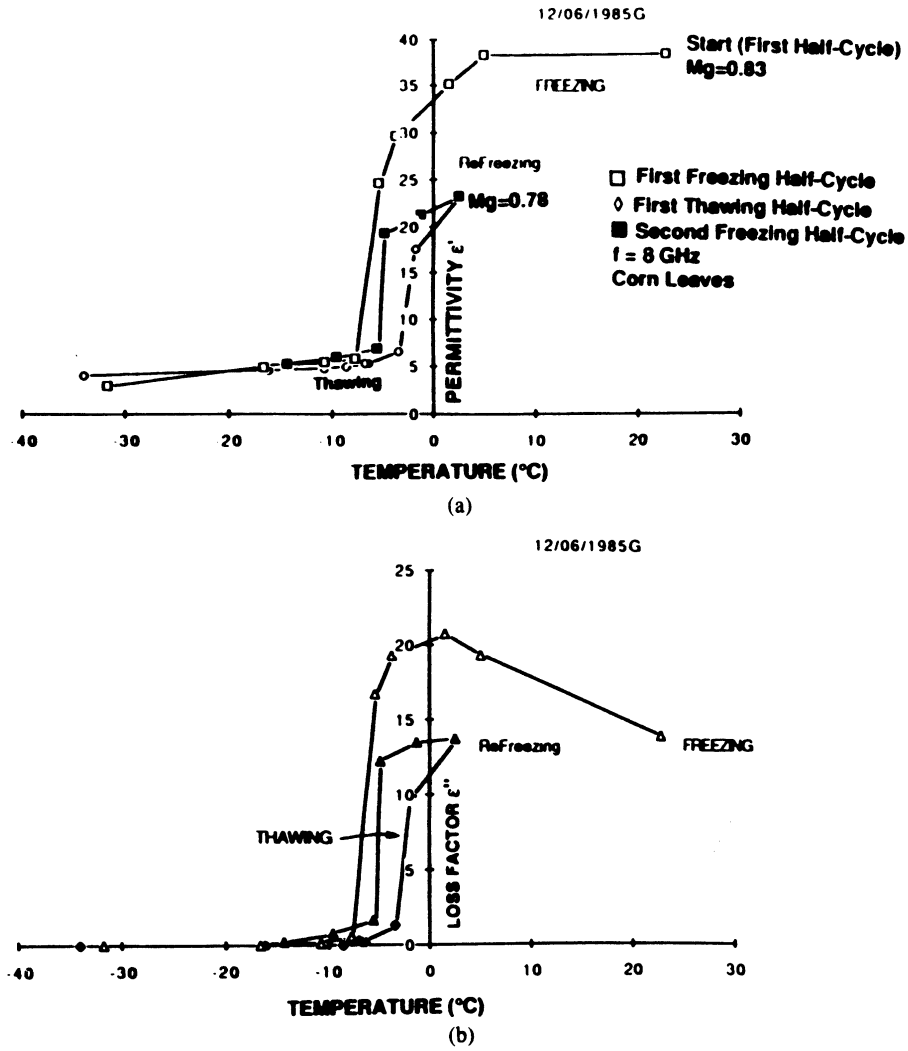

Fig. 12. Hysteresis-like behavior of the dielectric constant of vegetation as a function of temperature. (a) ϵ'. (b) ϵ''.

V. Conclusion

The coaxial probe technique proved to be an extremely useful tool for making broad frequency dielectric measurements of vegetation material. Compared to the waveguide transmission technique used previously by one of the authors [1], the coaxial probe technique is far more accurate, more convenient to use, and an experiment that used to require a full week of work to conduct with the waveguide system now can be completed in about 30 min. Already, the coaxial probe employed in this study has acquired more microwave dielectric data of vegetation material than all other previously published reports combined.

References

[1] F. T. Ulaby and R. P. Jedlicka, "Microwave dielectric properties of plant materials," *IEEE Trans. Geosci. Remote Sensing*, vol. GE-22, pp. 406–414, 1984.

[2] A. K. Fung and F. T. Ulaby, "A scatter model for leafy vegetation,"

IEEE Trans. Geosci. Electron., vol. GE-16, no. 4, pp. 281-286, Oct. 1978.

[3] M. A. Stuchly, T. W. Athey, G. M. Samaras, and G. E. Taylor, "Measurement of radio frequency permittivity of biological tissues with an open-ended coaxial line: Part II. Experimental results," *IEEE Trans. Microwave Theory Tech.*, vol. MTT-30, no. 1, pp. 87-92, Jan. 1982.

[4] E. C. Burdette, F. L. Cain, and J. Seals, "*In Vivo* probe measurement technique for determining dielectric properties at VHF through microwave frequencies," *IEEE Trans. Microwave Theory Tech.*, vol. MTT-28, no. 4, pp. 414-427, Apr. 1980.

[5] T. W. Athey, M. A. Stuchly, and S. S. Stuchly, "Measurement of radio frequency permittivity of biological tissues with an open-ended coaxial line: Part I," *IEEE Trans. Microwave Theory Tech.*, vol. MTT-30, no. 1, pp. 82-86, Jan. 1982.

[6] N. Marcuvitz, *Waveguide Handbook*. New York, Dover, 1965.

[7] G. A. Deschamps, "Impedance of antenna in a conducting medium," *IRE Trans. Antennas Propagat.*, pp. 648-650, Sept. 1962.

[8] F. T. Ulaby, R. K. Moore, and A. K. Fung, *Microwave Remote Sensing*, vol. 3. Dedham, MA: Artech, 1986, Appendix E.

[9] B. P. Jordan, R. J. Sheppard, and S. Szwarnowski, "The dielectric properties of formamide, ethanediol, and methanol," *J. Phys. D: Appl. Phys.*, vol. 11, 1978.

[10] A. M. Bottreau, Y. D. Dutuit, and J. Moreau, "On multiple reflection time domain method in dielectric spectroscopy: Application to the study of some normal primary alcohols," *J. Chem. Phys.*, vol. 66, no. 8, Apr. 15, 1977.

[11] A. Stogryn, "Equation for calculating the dielectric constant of saline water," *IEEE Trans. Microwave Theory Tech.*, vol. MIT-19, pp. 733-736, 1971.

Mohamed A. El-Rayes was born in Cairo, Egypt, on November 4, 1952. He received the B.S. degree in electrical engineering from Ain Shams University, Cairo, Egypt, in 1975, the M.S. degree in microwave engineering in 1979 from Kent University, Canterbury, England, and the Ph.D. degree from the University of Kansas in 1986. His research involves the measurement and modeling of vegetation materials at microwave frequencies.

*

Fawwaz T. Ulaby (M'68-SM'74-F'80) was born in Damascus, Syria, on February 4, 1943. He received the B.S. degree in physics from the American University of Beirut, Lebanon, in 1964 and the M.S.E.E. and Ph.D. degrees in electrical engineering from the University of Texas, Austin, in 1966 and 1968, respectively.

From 1968 to 1984, he was with the Electrical Engineering Department at the University of Kansas, where he was the J. L. Constant Distinguished Professor, and the University of Kansas Center for Research, where he was Director of the Remote Sensing Laboratory. He is currently Professor of Electrical Engineering and Computer Science, The University of Michigan, Ann Arbor. His current research interests involve microwave propagation and active and passive microwave remote sensing. Along with R. K. More and A. K. Fung, he is a coauthor of the three-volume series *Microwave Remote Sensing: Active and Passive*, (Reading, MA: Addison-Wesley). In addition, he is coeditor of the *Manual of Remote Sensing*, 2nd ed., vol. 1 (American Society of Photogrammetry).

Dr. Ulaby is a member of Eta Kappa Nu, Tau Beta Pi, and Sigma Xi. He is the Executive Editor for the IEEE TRANSACTIONS ON GEOSCIENCE AND REMOTE SENSING, 1984-1988, and was the Geoscience and Remote Sensing Society's Distinguished Lecturer for 1986-1987. He received the GRS Society's Outstanding Service Award in 1982, and its Distinguished Service Award in 1983. In 1984, he also received a Presidential Citation for Meritorious service from the American Service of Photogrammetry and the IEEE Centennial Medal. He received the University of Kansas Chancellor's Award for Excellence in Teaching in 1980, the University of Kansas Gould Award for "distinguished service to higher education" in 1973, and the Eta Kappa Nu MacDonald award as an "outstanding electrical engineering professor in the United States of America" in 1975, the University College of Engineering Research Excellence Award in 1986, and the Kuwait Prize in applied science for 1986.

Microwave Dielectric Spectrum of Vegetation—Part II: Dual-Dispersion Model

FAWWAZ T. ULABY, FELLOW, IEEE, AND MOHAMED A. EL-RAYES

Abstract—This paper is the second in a series evaluating the microwave dielectric behavior of vegetation material. It draws upon the data presented in Part I to develop a Debye-Cole dual-dispersion dielectric model consisting of a component that accounts for the volume fraction occupied by water in free form and another that accounts for the volume fraction occupied by the mixture comprised of water molecules bound to bulk-vegetation molecules. To determine the dielectric dispersion properties of the latter, measurements were made for sucrose-water solutions of known volume ratios. The proposed dielectric model is found to give excellent agreement with data over a wide range of moisture conditions and over the entire 0.2–20 GHz range examined in this study.

I. Introduction

In PART I of this two-part series, we described the experimental system used for making wide-band dielectric measurements and presented sample data to illustrate the nature of the variation of the dielectric constant of vegetation material ϵ as a function of several physical and electromagnetic parameters. The present paper draws upon the data obtained in this program to develop a dielectric mixing model for vegetation.

Available models for the dielectric constant of vegetation treat the vegetation as a simple mixture of bulk vegetation and water [1], [2], with the water sometimes subdivided into a *bound*-water component and a *free*-water component [2]. Bound water refers to water molecules that are tightly held to organic compounds by physical forces, and free water refers to water molecules that can move within the material with relative ease.

In these models the free-water component is assigned the dielectric dispersion properties of bulk water and the bound-water component is assumed to have dielectric properties similar to those of ice. As will be demonstrated in this study, bound water exhibits a dielectric behavior far different from that of ice, and this difference is responsible, in part, for the shortcomings of previously published dielectric models for vegetation [1], [2].

II. Dielectric Spectrum of Water

Direct dielectric measurements of oven-dried samples of various types of vegetation material, which henceforth shall be referred to as bulk vegetation material, give th following results:

$$1.5 \leq \epsilon_v' \leq 2.0$$

$$\epsilon_v'' \leq 0.1$$

for $0.5 \leq f \leq 20$ GHz. Although these measuremer were made at 22°C, there is no reason to expect ϵ_v to ha a temperature dependence.

In contrast to the nondispersive behavior of the bu vegetation material, bulk water is highly dispersive at m crowave frequencies because its dielectric relaxation fr quency f_0 lies in the microwave band. More specificall f_0 of pure (distilled) water is equal to 9 GHz at 0°C a increases nonlinearly with increasing temperature to GHz at 20°C, and to higher frequencies at correspon ingly higher temperatures.

The fluid contained in vegetation material may be e tracted from the material by suction. To extract a certa amount of fluid, the differential pressure that needs to l applied is far greater for a relatively dry piece of veget tion than for a fresh leaf. This is because for the relative dry leaf, the contained water is tightly bound to the bu vegetation material, whereas for the fresh leaf some of tl water is almost totally "free."

An isolated water molecule possesses a permanent ele tric dipole moment. If an electric field is applied, the mc ecule will orient itself such that its dipole moment aligned with the field. The orientation response to an i finitely fast step variation of applied electric field is cha acterized by an exponential function of the form e: $(-t/\tau)$ with time constant τ. This time constant is call the relaxation time and is governed by the interaction the H_2O molecule with its environment and by the tei perature T. If the water molecule is under the influence nonelectrical forces, such as physical forces, its respon to an applied electric field is impeded by these force which has the equivalent effect of increasing the relax tion time τ. Hence, τ of a bound-water molecule shou be much longer than that of a free-water molecule. Cc respondingly, the relaxation frequency $f_0 = (2\pi\tau)^{-1}$ o bound-water molecule should be much lower than that a free-water molecule.

To provide the background necessary for the model c veloped in Section III, we shall now give a brief revi of the dielectric properties of free water (assumed to the same as those of bulk water) and bound water. In ge

Manuscript received February 24, 1987; revised June 2, 1987. This work was supported by the NASA Goddard Space Flight Center under Contract NAG 5-480.

The authors are with the Radiation Laboratory, Department of Electrical Engineering and Computer Science, The University of Michigan, Ann Arbor, MI 48109-2122.

IEEE Log Number 8716096.

eral, free water may contain dissolved salts; hence, our review will consider the case of saline water.

As mentioned earlier, the dielectric properties of bound water are not well understood, and because bound water molecules cannot exist in bulk, it is not possible to measure their dielectric properties directly. Hence, special experiments were conducted, as discussed in Section II-B below, to measure and model the dielectric spectrum of bound water-host mixtures.

A. Free Water

The relative dielectric constant of bulk saline water is given by the Debye equation [3, pp. 2022-2025]

$$\epsilon_f' = \epsilon_{f\infty} + \frac{\epsilon_{fs} - \epsilon_{f\infty}}{1 + (f/f_{f0})^2} \tag{1a}$$

$$\epsilon_f'' = \frac{(f/f_{f0})(\epsilon_{fs} - \epsilon_{f\infty})}{1 + (f/f_{f0})^2} + \frac{\sigma}{2\pi\epsilon_0 f}. \tag{1b}$$

The subscript f denotes free water, ϵ_{fs} and $\epsilon_{f\infty}$ are the static and high-frequency limits of ϵ_f', $\epsilon_0 = 8.854 \times 10^{-12}$ F $\cdot$ m^{-1} is the permittivity of free space, f is the frequency in hertz, and σ is the ionic conductivity of the aqueous solution in siemens per meter. For computational purposes, $\epsilon_{f\infty}$ usually is taken equal to 4.9 and treated as independent of both the temperature T and salinity S of the solution. The salinity is defined as the total mass of solid salt in grams dissolved in 1 kg of solution and is expressed in parts per thousand (‰) on a weight basis. The other parameters of the dispersion equation, ϵ_{fs} and f_{f0}, are functions of both T and S and are given by empirically generated polynomial functions [4]. For pure water ($S = 0$) at $T = 0$°C, these functions yield $\epsilon_{fs} = 87.1$ and $f_{f0} = 9$ GHz.

For $S \leq 10$‰ and $T = 22$°C (room temperature), (1) may be approximated as

$$\epsilon_f = 4.9 + \frac{75}{1 + jf/18} - j\frac{18\sigma}{f} \tag{2}$$

where f is in gigahertz and σ may be related to S by

$$\sigma \cong 0.16S - 0.0013S^2 \quad S \cdot m^{-1}. \tag{3}$$

B. Bound Water

From the standpoint of dielectric theory, a water molecule is considered to be in the "bound" condition if its response to a suddenly applied electric field is inhibited as a result of some force acting upon it. Although we know that when a water molecule is in the bound condition its relaxation time τ becomes longer than when in the free state, we have no relationships by which we can quantitatively link the type of force and its magnitude to the increase in τ. In order to study the dielectric properties of bound water as they pertain to vegetation material, we have chosen to conduct dielectric measurements for sucrose-water mixtures. Sucrose was chosen because 1) it is a good example of the organic substances present in vegetation and 2) the binding arrangement of sucrose-water molecules is well known, which allows us to compute the bound water concentration in any given mixture. A sucrose molecule can bind to six water molecules, and the molecular weights of sucrose and water are 342.3 and 18.0, respectively. Hence, in a sucrose-water mixture in which the number of water molecules is equal to six times the number of sucrose molecules, the mass ratio of bound water to sucrose is given by

$$R = \frac{w_{bw}}{w_s} = 6\left(\frac{18.0}{342.3}\right) \cong \left(\frac{6}{19}\right). \tag{4}$$

The volume fractions of sucrose and bound water are

$$v_s = \rho_{bw}(\rho_{bw} + R\rho_s)^{-1} \tag{5}$$

$$= (1 + R\rho_s)^{-1} \tag{5a}$$

and

$$v_{bw} = 1 - v_s \tag{6}$$

where $\rho_s = 1.58$ g $\cdot$ cm^{-3} is the bulk density of sucrose and $\rho_{bw} = 1$ g $\cdot$ cm^{-3} was used in (5) to obtain (5a). These values lead to $v_s \cong 2v_{bw} \cong 0.667$.

Dielectric measurements were conducted from 0.1 to 20 GHz for a sucrose-water solution at room temperature (22°C). The data was fitted to a Cole–Cole dispersion equation of the form

$$\epsilon_b = \beta_{b\infty} + \frac{\epsilon_{bs} - \epsilon_{b\infty}}{1 + (jf/f_{b0})^{1-\alpha}} \tag{7}$$

where ϵ_{bs}, $\epsilon_{b\infty}$, and f_{b0} have the same definitions given earlier in connection with (2), and α is a relaxation parameter. Fig. 1 compares the measured dielectric spectrum with that calculated according to the Cole–Cole equation. The parameters of the Cole–Cole equation were selected to optimize the fit of the model to the data. Their values are $\epsilon_{b\infty} = 2.9$, $\epsilon_{bs} = 57.9$, $f_{b0} = 0.18$ GHz, and $\alpha = 0.5$, which result in

$$\epsilon_b = 2.9 + \frac{55}{1 + (jf/0.18)^{0.5}}. \tag{8}$$

The data fit the model exceptionally well; the linear correlation coefficient between ϵ_b' (measured) and ϵ_b' (calculated) is 0.99, and the same is true for ϵ_b''. Cole–Cole plots of (2) and (8) are shown in Fig. 2.

The values of $\epsilon_{b\infty}$ and ϵ_{bs} are not markedly different from the corresponding parameters for free water: at $T = 22$°C, $\epsilon_{f\infty} = 4.9$ and $\epsilon_{fs} = 80$. The relaxation frequency, on the other hand, is lower by two orders of magnitude; $f_{b0} = 0.18$ GHz compared to $f_{f0} = 18$ GHz at $T = 22$°C. Another important difference is the magnitude of α, which is equal to 0.5 for the bound-water sucrose solution, compared to zero for free water. The parameter α governs the shape of the dispersion spectrum.

III. Dielectric Model for Vegetation

In previous dielectric models for vegetation [1], [2], the vegetation-water mixture was treated as an inhomoge-

responds to a salinity $S = 8.5‰$ (from (3)). The additional result that σ was found to be approximately constant with M_g suggests that the amount of salt dissolved in the free-water solution increases with increasing M_g at exactly the same rate that v_{fw} increases with M_g.

IV. Comparison with Data

The model defined by (10) and the auxiliary relations given by (14)–(17) was evaluated by comparing it with spectral data measured for corn leaves at specific moisture contents and with data measured as a function of moisture content at specific microwave frequencies. Typical examples of these two types of comparison are given in Figs. 7 and 8. The spectral data in Fig. 7 were selected to illustrate the comparison between theory and experiment at a high moisture content of 0.68, an intermediate value of 0.26, and a low value of 0.07. The dielectric variation with M_g is illustrated in Fig. 8 at frequencies of 1.0, 4.0, and 8.0 GHz.

Statistical analysis of the 624 available measurements against the values predicted by the model gives a linear correlation coefficient of 0.99 for both ϵ_v' and ϵ_v'', and the estimated mean square error is 1.0 for ϵ_v' and 0.3 for ϵ_v''.

Overall, the model appears to provide an excellent fit to the data and is far superior in that respect to any of the traditional vegetation dielectric models used in the past. This statement is based on a detailed evaluation [5] of several empirical and theoretical models including the Polder–Van Santen mixing formulas [6], the De Loor model [7], the semi-empirical model due to Birchak *et al.* [8], and others [5]. The model also provides a physical interpretation of how water in plant material is distributed between free and bound.

A possible shortcoming of the model is the fact that it was developed using data for only one material: corn leaves. On the other hand, evaluation of the model against data measured for corn stalks, soybean leaves, aspen leaves, balsam fir trunk, potatoes, apples, and other types of vegetation material has revealed the following:

1) For ϵ_v', the value predicted by the model (as defined by (10) and the associated expressions given by (14)–(17)) agrees with the measured value within ± 20 percent of the measured value.

2) For ϵ_v'', the relative error is within ± 20 percent also, but only at frequencies above 5 GHz. This is due to salinity variations, which become unimportant when $f \geq 5$ GHz. If the salinity is known and used to compute σ according to (3) and the latter is used in (10), the ± 20-percent relative error may be extended down to 0.5 GHz.

3) If both the gravimetric moisture M_g and the density of the vegetation material are known and used to compute M_v through (19), the ± 20-percent relative error may be reduced to ± 5 percent by using expressions for ϵ_r, v_{fw}, and v_b that are based on M_v instead of M_g. These expressions are

$$\epsilon_r = 1.7 + 3.2M_v + 6.5M_v^2 \qquad (20)$$

$$v_{fw} = M_v(0.82M_v + 0.166) \qquad (21$$

$$v_b = 31.4M_v^2/(1 + 59.5M_v^2). \qquad (22$$

Moreover, the model becomes equally applicable to woody material such as tree trunks and branches.

In summary, the dielectric model given by (10) and the auxiliary equations (20)–(22) provides a good estimate of ϵ_v' for leaves, stalks, branches, and trunks. If the dry density ρ is unknown, the auxiliary equations given by (14)–(16) may be used instead, but the relative error will be as much as 20 percent for leaves and stalks and much larger for material with densities markedly different from the 0.33-g · cm^{-3} value implicit in the expressions (14)–(16). Similar statements apply to ϵ_v'' provided a reasonable estimate of the salinity S is available to use in (3) in order to compute σ.

V. Conclusions

Examination of measured dielectric spectra for vegetation material led to the development of a Deybe–Cole dual-dispersion model consisting of a Debye relaxation term representing the free water contained in the vegetation material and a Cole relaxation term with a relaxation parameter $\alpha = 0.5$ representing the bound water–bulk vegetation mixture. The model provides an excellent fit to the measured data and has led to the development of a physical model for the distribution of water in vegetation between free and bound forms.

References

[1] A. K. Fung and F. T. Ulaby, "A scatter model for leafy vegetation," *IEEE Trans. Geosci. Electron.*, vol. GE-16, no. 4, pp. 281–286, Oct. 1978.

[2] F. T. Ulaby and R. P. Jedlicka, "Microwave dielectric properties of plant materials," *IEEE Trans. Geosci. Remote Sensing*, vol. GE-22, pp. 406–414, 1984.

[3] F. T. Ulaby, R. K. Moore, and A. K. Fung, *Microwave Remote Sensing*, vol. 3. Dedham, MA: Artech, 1986, Appendix E.

[4] A. Stogryn, "Equation for calculating the dielectric constant of saline water," *IEEE Trans. Microwave Theory Tech.*, vol. MIT-19, pp. 733–736, 1971.

[5] A. M. El-Rayes and F. T. Ulaby, "Microwave dielectric behavior of vegetation material," Univ. Michigan Tech. Rep., RL-022132-3-T, 1986.

[6] D. Polder and J. H. Van Santen, "The effective permittivity of mixtures of solids," *Physica*, vol. XII, no. 5, pp. 257–271, 1946.

[7] G. P. DeLoor, "Dielectric properties of heterogeneous mixtures containing water," *J. Microwave Power*, vol. 3, pp. 67–73, 1968.

[8] J. R. Birchak, C. G. Gardner, J. E. Hipp, and J. M. Victor, "High dielectric constant microwave probes for sensing soil moisture," *Proc. IEEE*, vol. 62, no. 1, pp. 93–98, Jan. 1974.

*

Fawwaz T. Ulaby (M'68–SM'74–F'80) was born in Damascus, Syria, on February 4, 1943. He received the B.S. degree in physics from the American University of Beirut, Lebanon, in 1964 and the M.S.E.E. and Ph.D. degrees in electrical engineering from the University of Texas, Austin in 1966 and 1968, respectively.

From 1968 to 1984, he was with the Electrical Engineering Department at the University of Kansas, where he was the J. L. Constant Distinguished Professor, and the University of Kansas Center for Research, where he was Director of the Remote Sensing Labo

ratory. He is currently Professor of Electrical Engineering and Computer Science, The University of Michigan, Ann Arbor. His current research interests involve microwave propagation and active and passive microwave remote sensing. Along with R. K. More and A. K. Fung, he is a coauthor of the three-volume series *Microwave Remote Sensing: Active and Passive* (Reading, MA: Addison-Wesley). In addition, he is coeditor of the *Manual of Remote Sensing*, 2nd ed., vol. 1 (American Society of Photogrammetry).

Dr. Ulaby is a member of Eta Kappa Nu, Tau Beta Pi, and Sigma Xi. He is the Executive Editor for the IEEE TRANSACTIONS ON GEOSCIENCE AND REMOTE SENSING, 1984–1988, and was the Geoscience and Remote Sensing Society's Distinguished Lecturer for 1986–1987. He received the GRS Society's Outstanding Service Award in 1982, and its Distinguished Service Award in 1983. In 1984, he also received a Presidential Citation for Meritorious service from the American Service of Photogrammetry and the IEEE Centennial Medal. He received the University of Kansas Chancellor's Award for Excellence in Teaching in 1980, the University of Kansas Gould Award for "distinguished service to higher education" in 1973, and the Eta Kappa Nu MacDonald award as an "outstanding electrical engineering professor in the United States of America" in 1975, the University College of Engineering Research Excellence Award in 1986, and the Kuwait Prize in applied science for 1986.

*

Mohamed A. El-Rayes was born in Cairo, Egypt, on November 4, 1952. He received the B.S. degree in electrical engineering from Ain Shams University, Cairo, Egypt, in 1975, the M.S. degree in microwave engineering in 1979 from Kent University, Canterbury, England, and the Ph.D. degree from the University of Kansas in 1986. His research involves the measurement and modeling of vegetation materials at microwave frequencies.

Technique for Measuring the Dielectric Constant of Thin Materials

KAMAL SARABANDI AND FAWWAZ T. ULABY, FELLOW, IEEE

Abstract—**A practical technique for measuring the dielectric constant of vegetation leaves and similarly thin materials is presented. A rectangular section of the leaf is placed in the transverse plane in a rectangular waveguide, and the magnitude and phase of the reflection coefficient are measured over the desired frequency band using a vector network analyzer. By treating the leaf as an infinitesimally thin resistive sheet, an explicit expression for its dielectric constant is obtained in terms of the reflection coefficient. Because of the thin-sheet approximation, however, this approach is valid only at frequencies below 1.5 GHz. To extend the technique to higher frequencies, higher order approximations are derived and their accuracies are compared to the exact dielectric-slab solution. For a material whose thickness is 0.5 mm or less, the proposed technique was found to provide accurate values of its dielectric constant up to frequencies of 12 GHz or higher. The technique was used to measure the 8–12-GHz dielectric spectrum for vegetation leaves, Teflon®, and rock samples.**

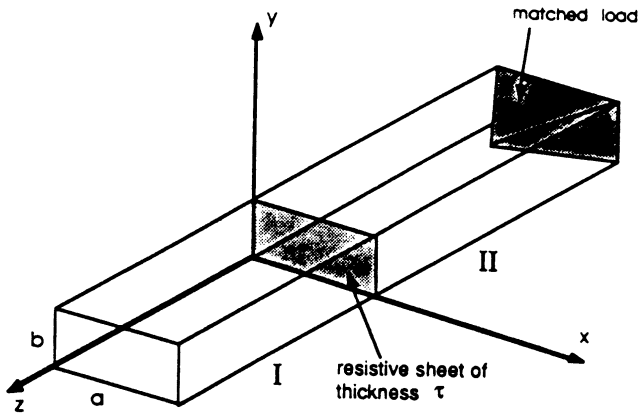

Fig. 1. Rectangular waveguide with thin resistive sheet of thickness τ a $z = 0$.

I. Introduction

PROMPTED BY THE need for a practical technique for measuring the microwave dielectric constant of vegetation leaves, solutions were sought for the voltage reflection coefficient measured at the input of a rectangular waveguide containing a thin slab placed in a plane orthogonal to the propagation direction (Fig. 1). The slab is modeled in Section II as a resistive-current-sheet [1], [2], which has proved to be an excellent approach for characterizing the radar-cross-section of a vegetation leaf over a wide range of moisture conditions (and a correspondingly wide range of the relative dielectric constant ϵ).

To evaluate the accuracy of the technique for measuring the real and imaginary parts of ϵ from measurements of the complex reflection coefficient Γ, an exact solution for Γ of the slab will be obtained in Section III and then used to simulate the measurement process for given values of ϵ. The evaluation is performed in Section IV by comparing the true value of ϵ with that predicted by the resistive-current-sheet expression. It turns out that the resistive-current-sheet solution is identical with the zeroth-order approximation of the exact solution for Γ. One of the attractive features of the zeroth-order solution is that it provides an explicit expression for ϵ in terms of Γ.

The evaluation shows that the zeroth-order solution provides an excellent estimate for the real part of the dielectric constant, ϵ', if the slab thickness τ is sufficiently small to satisfy the condition $\tau \leq 0.05\lambda_0\sqrt{|\epsilon|}$, where λ_0 is the free-space wavelength. For a typical leaf-thickness of 0.3 mm, this condition is satisfied for any moisture condition if the frequency $f \leq 15$ GHz. A much more stringent condition on τ is required in order for the zeroth-order solution to give accurate values for ϵ''; namely $\tau \leq 0.01\lambda_0\sqrt{|\epsilon|}$ and $\epsilon''/\epsilon' \geq 0.1$, or equivalently, $f \leq 1.5$ GHz for vegetation leaves. To relax this limitation, alternate solutions for Γ are obtained in Section III by invoking approximations that lead to first- and second-order solutions whose forms are invertible to explicit expressions for ϵ. Use of the second-order solution is found to extend the frequency range from 1.5–12 GHz for a leaf with a high moisture content and to higher frequencies for drier leaves.

Section V presents 8–12-GHz spectra of the dielectric constant ϵ for vegetation leaves, Teflon and rock slices, all measured using the technique developed in this paper. Where possible, the results are compared with measurements made by other techniques.

II. Model for a Thin Resistive Sheet

Consider the rectangular waveguide diagrammed in Fig. 1. The guide is terminated with a matched load, has dimensions $a \times b$, and contains a thin resistive sheet of thickness τ at $z = 0$. The waveguide dimensions are such that only the TE_{10} mode can propagate in the guide.

We seek a relationship between the input voltage reflection coefficient Γ and the relative complex dielectric

Manuscript received November 23, 1987; revised May 4, 1988 and May 28, 1988.

The authors are with the Department of Electrical Engineering and Computer Science, University of Michigan, Ann Arbor, MI 48109.

IEEE Log Number 8823465.

constant of the sheet material ϵ. To this end, we shall develop expressions for the electric and magnetic fields in Regions I and II and then apply the appropriate boundary conditions. If ψ_I and ψ_{II} are the electric potentials in Regions I and II, respectively, solutions of the scalar Helmholtz equation

$$(\nabla^2 + k^2)\Psi_{I,II} = 0 \tag{1}$$

for the TE_{10} mode leads to [4]

$$\psi_I = \cos\left(\frac{\pi x}{a}\right)\left[C_1 e^{ik_z z} + C_2 e^{-ik_z z}\right], \quad z \geq 0 \tag{2}$$

$$\psi_{II} = \cos\left(\frac{\pi x}{a}\right) \cdot C_3 e^{ik_z z}, \quad z \leq 0 \tag{3}$$

where a time factor $e^{i\omega t}$ was assumed and suppressed. The constants C_1 and C_2 represent the magnitudes of the incident and reflected waves in Region I, C_3 represents the magnitude of the wave traveling towards the matched load in Region II, and

$$k_z = \sqrt{k^2 - \left(\frac{\pi}{a}\right)^2} = \frac{\pi}{\lambda a}\sqrt{4a^2 - \lambda^2}. \tag{4}$$

The components of $\bar{E}$ and $\bar{H}$ may be obtained from (2) and (3) by applying the relations [4]

$$\bar{E} = -\nabla \times (\psi\hat{z}) \qquad \bar{H} = -i\omega\epsilon(\psi\hat{z}) + \frac{1}{i\omega\mu}\nabla\nabla \cdot (\psi\hat{z}). \tag{5}$$

The resistive sheet model [1] treats the sheet in the plane $z = 0$ as infinitesimally thin carrying an induced tangential electric current $\bar{J}$ that is related to $\bar{E}$ by

$$\hat{n} \times \hat{n} \times \bar{E} = -R\bar{J} \tag{6}$$

where $\hat{n}$ is the surface normal of the sheet ($\hat{n} = \hat{z}$ in Region I and $\hat{n} = -\hat{z}$ in Region II) and R is the sheet resistivity

$$R = \frac{-i\eta_0}{k\tau(\epsilon - 1)} \quad \text{ohms per square meter.} \tag{7}$$

In the above expression, $k = 2\pi/\lambda_0$, τ is the sheet thickness, η_0 is the free-space intrinsic impedance, and

$$\epsilon = \epsilon' - i\epsilon'' \tag{8}$$

is its relative complex dielectric constant. The condition for continuity of the tangential electric field from Region I to Region II and the boundary condition for the magnetic field requires that

$$\hat{z} \times (\bar{E}_I - \bar{E}_{II}) = 0 \qquad \hat{z} \times (\bar{H}_I - \bar{H}_{II}) = \bar{J}. \tag{9}$$

The unknown coefficients C_1, C_2, C_3 can be obtained by applying the boundary conditions given by (6) and (9). The complex voltage reflection coefficient is then found to be

$$\Gamma = \frac{C_2}{C_1} = -\frac{k^2\tau(\epsilon - 1)}{k^2\tau(\epsilon - 1) - 2ik_z} \tag{10}$$

from which an explicit expression for ϵ is obtained

$$\epsilon = 1 + \frac{2ik_z\Gamma}{k^2\tau(1 + \Gamma)} = 1 + \frac{i\left(\frac{\lambda}{2\pi a}\right)\sqrt{4a^2 - \lambda^2}}{\tau(1 + 1/\Gamma)}. \tag{11}$$

Thus by measuring the complex reflection coefficient Γ and the sheet thickness τ we can compute ϵ directly. This technique can be very useful for measuring the dielectric constant of vegetation leaves and other similarly thin slabs. Its success, however, depends on two factors: a) the ability to measure both the magnitude and phase of Γ accurately, which now is possible with the HP-8510 vector network analyzer, and b) the validity of the thin-sheet assumption underlying the derivation that led to (11). To examine the range of validity of this assumption and to quantify it in the form of specific limits, we shall first derive the expression for the reflection coefficient when a dielectric slab of arbitrary thickness is placed in the waveguide, and then compare the exact solution with the solution given by (10) and (11).

III. Model for a Slab of Arbitrary Thickness

The waveguide section shown in Fig. 2 is terminated in a matched load and contains a dielectric slab extending from $z = 0$ to $z = -\tau$. The electric potentials in Regions I, II, and III are

$$\Psi_I = \cos\left(\frac{\pi x}{a}\right)\left[C_1 e^{ik_z z} + C_2 e^{-ik_z z}\right], \quad z \geq 0 \tag{12}$$

$$\Psi_{II} = \cos\left(\frac{\pi x}{a}\right)\left[C_3 e^{ik_{z2} z} + C_4 e^{-ik_{z2} z}\right], \quad 0 \geq z \geq -\tau \tag{13}$$

$$\Psi_{III} = \cos\left(\frac{\pi x}{a}\right) \cdot C_5 e^{ik_z z}, \quad -\tau \geq z \tag{14}$$

where k_z is given by (4) and k_{z2} is given by

$$k_{z2} = \frac{\pi}{\lambda a}\sqrt{4\epsilon a^2 - \lambda^2}. \tag{15}$$

Upon using the relations given by (5) to obtain $\bar{E}$ and $\bar{H}$ in each of the three regions, and then applying the continuity conditions of the tangential $\bar{E}$ and $\bar{H}$ fields at the boundaries $z = 0$ and $z = -\tau$, we obtain the following expression for the reflection coefficient:

$$\Gamma = \frac{C_2}{C_1} = \frac{-i\left[(k_{z2}/k_z)^2 - 1\right]\sin(k_{z2}\tau)}{2\left(\frac{k_{z2}}{k_z}\right)\cos(k_{z2}\tau) + i\left[(k_{z2}/k_z)^2 + 1\right]\sin(k_{z2}\tau)}. \tag{16}$$

We shall refer to (16) as the exact solution for Γ.

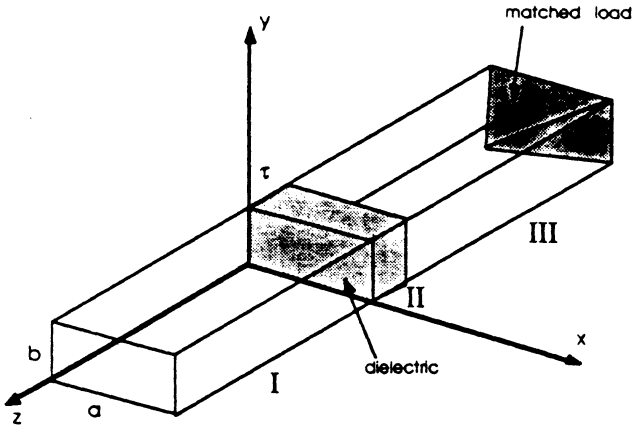

Fig. 2. Rectangular waveguide with a dielectric slab occupying region II (between $z = 0$ and $z = -\tau$).

A. Second-Order Solution

If $k_{z2}\tau$ is small and we use the approximations

$$\sin k_{z2}\tau \cong k_{z2}\tau \tag{17a}$$

$$\cos k_{z2}\tau \cong 1 - \tfrac{1}{2}(k_{z2}\tau)^2. \tag{17b}$$

The expressions given by (16) can be simplified to give the *second-order* solution

$$\Gamma \cong \frac{-(\epsilon - 1)}{\left(1 - \frac{1}{2}\left(\frac{\lambda}{a}\right)^2 - i\tau k_z\left(\frac{\lambda}{2a}\right)^2 - 2ik_z/\tau k^2\right) + (1 + i\tau k_z)\epsilon} \tag{18}$$

from which we obtain the following explicit expression for the *second-order* solution of the relative dielectric constant:

$$\epsilon \triangleq \epsilon_2 \cong \frac{1 - \left[1 - \frac{1}{2}\left(\frac{\lambda}{a}\right)^2 - i\tau k_z\left(\frac{\lambda}{2a}\right)^2 - 2ik_z/\tau k^2\right]\Gamma}{1 + (1 + i\tau k_z)\Gamma}. \tag{19}$$

B. First-Order Solution

If, instead of the approximation given by (17b), we were to set $\cos k_{2z}\tau \cong 1$ in (16) (i.e., ignoring second- and higher order powers of $(k_{z2}\tau)$), we would obtain the result

$$\Gamma \cong \frac{-1}{\left[\epsilon + \left(1 - \frac{1}{2}\left(\frac{\lambda}{a}\right)^2\right)\right]/(\epsilon - 1) - 2ik_z/(\tau k^2(\epsilon - 1))} \tag{20}$$

which can then be solved to obtain the expression

$$\epsilon \triangleq \epsilon_1 \cong \frac{1 - [1 - (\lambda^2/2a^2) - 2ik_z/\tau k^2]\Gamma}{(1 + \Gamma)} \tag{21}$$

for the first-order estimate of ϵ.

C. Zeroth-Order Solution

If $\epsilon >> 1$, we may use the approximation

$$\frac{\epsilon + \left(1 - \frac{1}{2}\left(\frac{\lambda}{a}\right)^2\right)}{\epsilon - 1} \cong 1 \tag{21}$$

because $-1 \leq 1 - \frac{1}{2}(\lambda/a)^2 < 1$. Equation (20) then leads to

$$\epsilon \triangleq \epsilon_0 \cong 1 + \frac{2ik_z\Gamma}{\tau k^2(\Gamma + 1)} = 1 + \frac{i(\lambda/2\pi a)\sqrt{4a^2 - \lambda^2}}{\tau(1 + 1/\Gamma)} \tag{22}$$

which is identical with the resistive-sheet approximation given by (11).

IV. Sensitivity Analysis

The second-order solution for Γ, given by (18), was based on assuming that $k_{z2}\tau << 1$ and on retaining terms up to and including power of 2 in the series expressions for $\sin k_{z2}\tau$ and $\cos k_{z2}\tau$, as indicated by (17). In the first-order solution, only the zeroth- and first-order terms were retained. The purpose of these derivations is to use them for computing ϵ from measured values of the complex reflection coefficient Γ. The accuracies of the approximate expressions given by (19) and (21), corresponding to the second- and first-order solutions for ϵ, respectively, depends on the magnitude of $k_{z2}\tau$. For a standard waveguide operated in the TE_{10} mode, the dimension a is on the order of $3\lambda/4$. Hence,

$$k_{z2}\tau = k\tau\sqrt{\epsilon - (\lambda/2a)^2} \cong k\tau\sqrt{\epsilon - 4/9}.$$

If we require that $k\tau\sqrt{\epsilon}$ be small, then k_{z2} will be smaller still.

The zeroth-order solution (22) is only applicable if ϵ is sufficiently large to allow the approximation given by (21) to be used in (20). Hence, for ϵ large, the first- and zeroth-order solutions should yield comparable results.

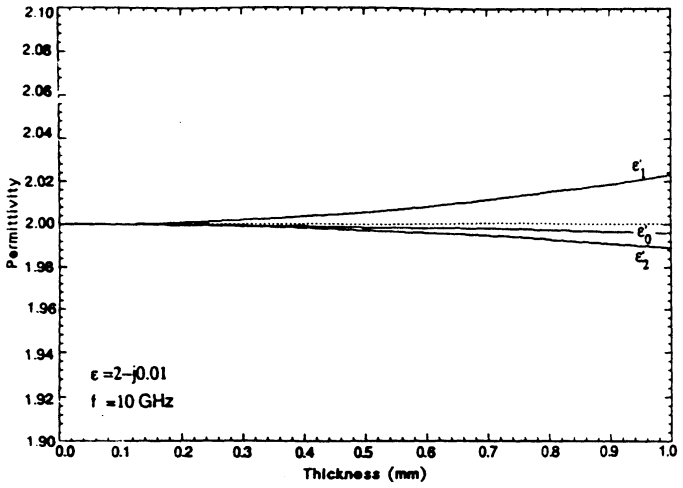

(a)

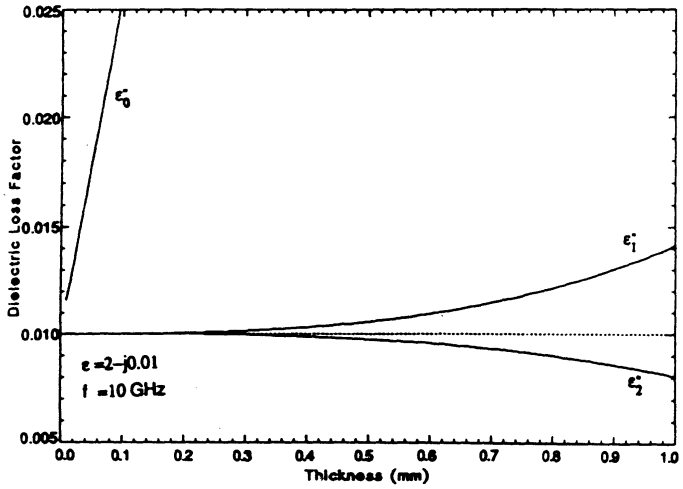

(b)

Fig. 3. Relative (a) permittivities ϵ_0', ϵ_1', and ϵ_2', and (b) dielectric loss factors.

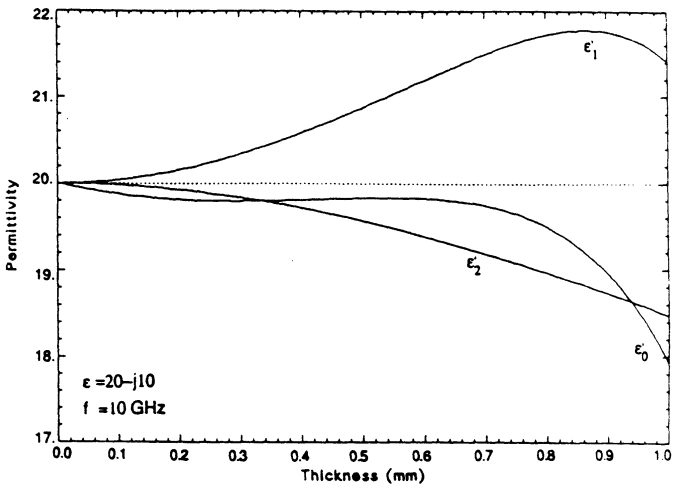

(a)

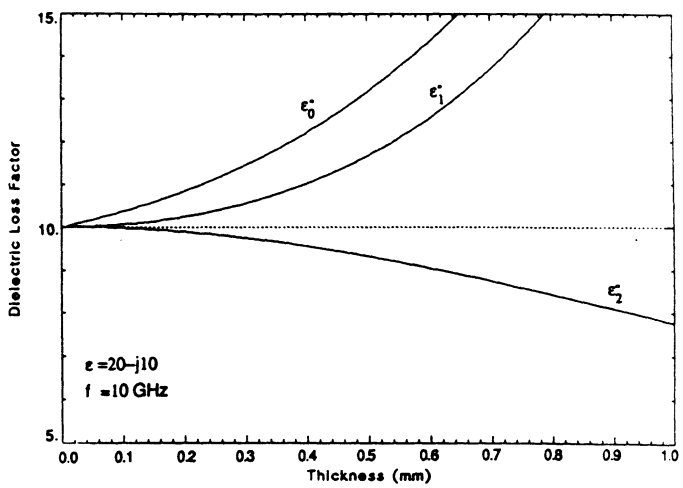

(b)

Fig. 4. Relative (a) permittivities ϵ_0', ϵ_1', and ϵ_2', and (b) dielectric loss factors.

To evaluate these approximate expressions for ϵ, we conducted the following sensitivity analysis. We selected specific values of the waveguide width a, the wavelength λ, and the relative complex dielectric constant of the slab, ϵ. We then computed Γ using the exact solution (16). The computed value of Γ was then used in (22), (21), and (19) to compute the zeroth-, first-, and second-order estimates of ϵ. We denote these ϵ_0, ϵ_1, and ϵ_2.

Our first example of this procedure is Fig. 3 where we show plots of ϵ_0, ϵ_1, and ϵ_2 at 10 GHz as a function of τ for a slab with true dielectric constant $\epsilon = 2 - i0.01$. We observe that ϵ_0', ϵ_1', and ϵ_2' in Fig. 3(a) each provide values that are within 1 percent of ϵ' for $\tau \leq 1$ mm. Among the three approximations, ϵ_0' is the most accurate, in spite of the fact that the left-hand side of (21) is equal to 2, rather than approximately equal to 1 as required by (21). This insensitivity of Γ to the first term in the denominator of (20) is because this term is much smaller than the second term in the denominator of (20), thereby exercising a minor influence on the final expression for ϵ'.

Measuring ϵ' of a material usually is not a difficult problem, but measuring ϵ'' of a low-loss material can be. The errors associated with using the approximations leading to ϵ_0'', ϵ_1'', ϵ_2'' are shown in Fig. 3(b) in the form of deviations from the true value $\epsilon'' = 0.01$. For $\tau \leq 1$ mm, the relative error is 20 percent for ϵ_2'', 50 percent for ϵ_1'', and the estimate provided by ϵ_0'' is grossly inaccurate. Hence, in spite of the result that ϵ_0' provides a good estimate of ϵ', the zeroth-order solution is inadequate for estimating ϵ''.

Fig. 4 shows results for a material with $\epsilon = 20 - i10$. Again ϵ_0' provides an adequate estimate of ϵ' over a wide range of the thickness τ. For the imaginary part, however, ϵ_2'' consistently provides more accurate estimates of ϵ'' than those provided by either ϵ_0'' or ϵ_1''.

A summary of the relative accuracies of the three approximations ϵ_0, ϵ_1, and ϵ_2, is presented in Table I for slab thicknesses τ equal to 1 and 5 percent of $\lambda_0/\sqrt{|\epsilon|}$. The entries in the table are the maximum relative errors in percent. For ϵ_0', for example, the maximum relative error is defined as

$$e_0' = \max \left| \frac{\epsilon_0' - \epsilon'}{\epsilon'} \right| \times 100$$

where ϵ_0' is the value provided by (22) and ϵ' is the true value of the slab permittivity.

TABLE I
MAXIMUM RELATIVE ERRORS ASSOCIATED WITH THE EXPRESSIONS FOR ϵ_0, ϵ_1, AND ϵ_2; THE QUANTITY e_0' IS DEFINED AS: $e_0' = \max|\epsilon' - \epsilon_0'/\epsilon| \times 100$ AND SIMILAR DEFINITIONS APPLY FOR THE REMAINING ERROR QUANTITIES

Maximum Error, %	$\tau\sqrt{\lvert\epsilon\rvert}/\lambda_0 = 0.01$			$\tau\sqrt{\lvert\epsilon\rvert}/\lambda_0 = 0.05$		
	ϵ''/ϵ'			ϵ''/ϵ'		
	10^{-2}	10^{-1}	1	10^{-2}	10^{-1}	1
e_0'	0.114	0.341	2.920	3.107	2.672	17.05
e_0''	182.8	18.35	1.445	934.0	96.70	10.11
e_1'	0.127	0.124	0.060	3.293	3.216	1.916
e_1''	0.436	0.267	0.018	33.06	8.629	2.727
e_2'	0.063	0.062	0.029	1.538	1.506	0.866
e_2''	0.215	0.132	0.091	15.11	3.926	2.238

V. DIELECTRIC MEASUREMENTS

A. Measurement System

A HP-8510A vector network analyzer was used in conjunction with a HP-8511 parameter test set and a HP-9000 computer (Fig. 5) to measure the amplitude and phase of the reflection coefficient Γ of dielectric slabs placed in a waveguide sample-holder. The arrangement shown in Fig. 5 consists of a waveguide section connected to the HP-8511 through a coax-to-waveguide adapter on one end and to a waveguide section terminated in a matched load on the other end. A thin piece of styrofoam is placed in the sample-holder section at a distance τ from the waveguide opening (junction between the two waveguide sections) where τ is equal to the thickness of the dielectric sample. Another thin piece of styrofoam is placed on the other side of the sample (in the empty waveguide section) to keep the sample in place.

After placing the sample in the waveguide, the network analyzer is used to measure the complex reflection coefficient over the frequency range of interest. In the present setup, the frequency coverage is from 8 to 12 GHz.

B. Measurement Accuracy

The accuracy of the dielectric-constant measurement is critically based upon the accuracy with which the reflection coefficient Γ can be measured. The measurement of Γ may contain some random, nonrepeatable errors caused by system noise and environmental variations as well as certain systematic errors that are repeatable and, therefore, correctable. To correct the systematic errors, the measurement system is calibrated using three independent standards whose reflection coefficients are known over the frequency range under consideration. These include a short-circuited load, a matched load, and an offset short.

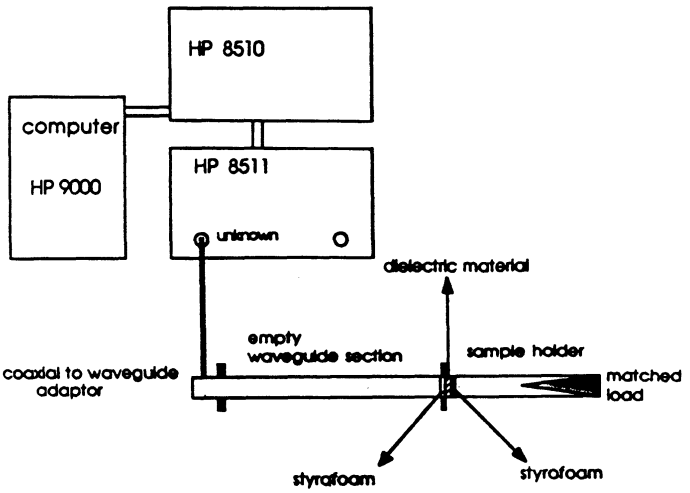

Fig. 5. Measurement system.

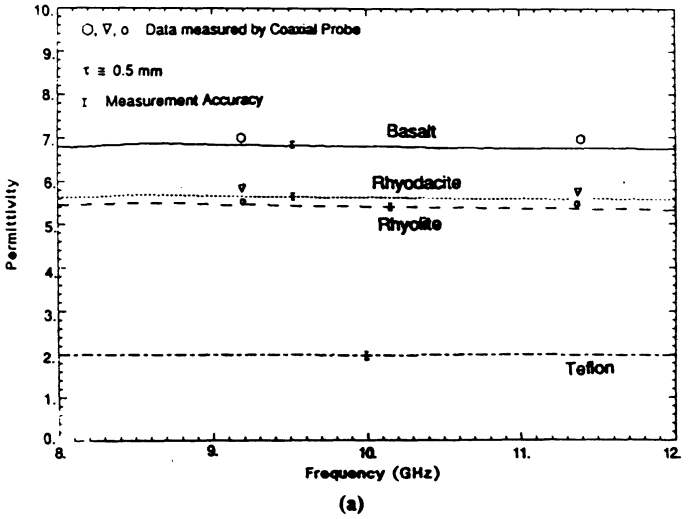

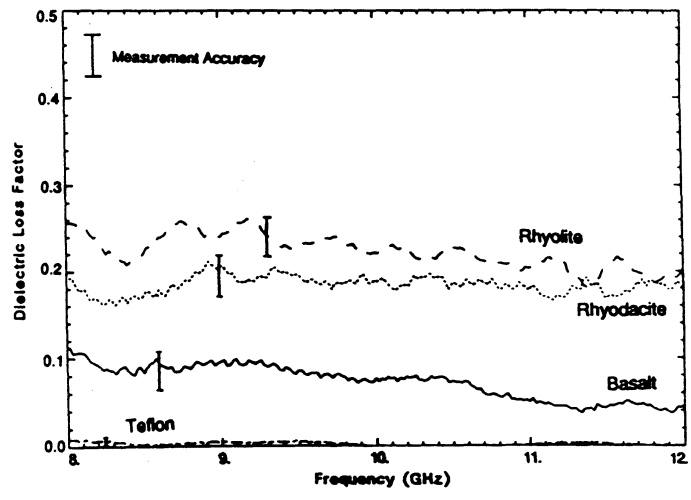

Fig. 6. Measured (a) relative permittivity and (b) dielectric loss factor of Teflon and three rock samples.

C. Sample Measurements

The technique described in the previous sections was used to measure the 8–12-GHz dielectric spectra of three types of rock materials (each cut in the shape of a thin slab with a cross-section equal to that of the waveguide's) and a thin leaf of vegetation material with a gravimetric

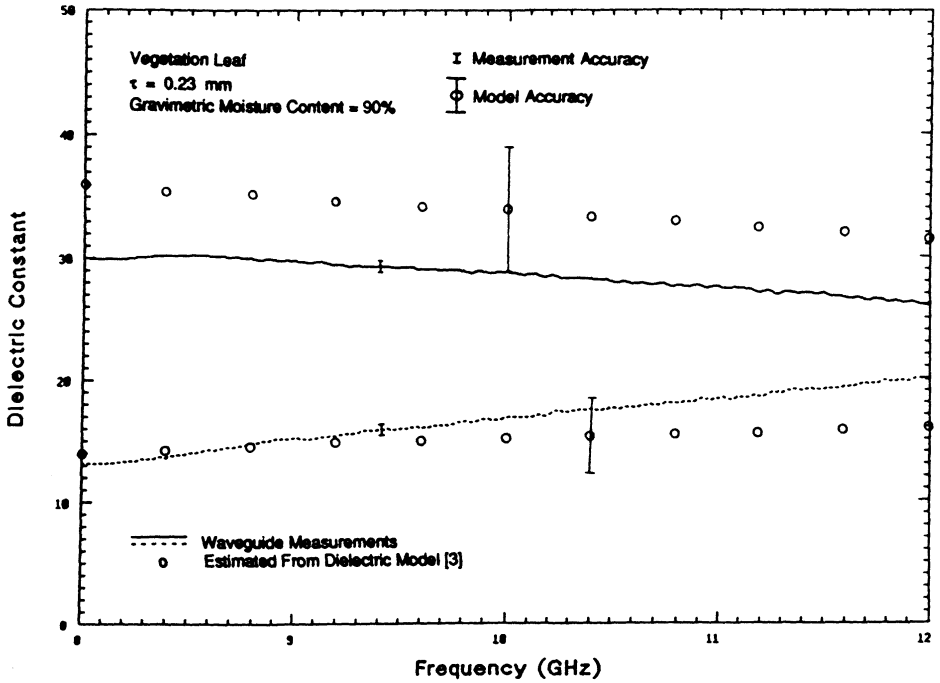

Fig. 7. Measured relative dielectric constant of a vegetation leaf.

moisture content of 90 percent. In addition, a thin slab of Teflon with $\epsilon = 2.0 - j0.005$ was measured also. The results are given in Figs. 6 and 7. The results for Teflon were found to be in excellent agreement with those measured for a thick sample for both ϵ' and ϵ''. The measured permittivities of the rock samples are essentially constant over the 8–12-GHz band (Fig. 6(a)), and for two of the samples (rhyolite and rhyodlacite) the measured permittivity compares very well with values measured by a coaxial probe using an approximate reflection technique [5].

The plots of Fig. 6(b) display ϵ'', the relative dielectric loss factor for Teflon, and the three rock samples. We have no reason to expect ϵ of rocks to exhibit a dispersive behavior in the 8–12-GHz frequency region, and therefore, we suspect that the observed variability, particularly in the 8–9-GHz range, is an artifact of the measurement system.

The example shown in Fig. 7 is for a leaf vegetation. Its gravimetric moisture was 0.9 and its thickness 0.23 mm. The continuous curves represent the values of ϵ' and ϵ'' measured with the waveguide technique and the circles represent values calculated using a model [3] with an accuracy of ± 20 percent. Within this range of accuracy, both the data and model are in good agreement.

VI. Conclusions

The technique presented in this paper for measuring the dielectric constant of thin slabs is based on measuring the complex reflection coefficient of the input of a waveguide section with the slab placed in the transverse plane of the waveguide. The dielectric constant of the leaf is then calculated from the measured reflection coefficient.

An explicit expression for the dielectric constant is obtained in terms of the reflection coefficient by simplifying the exact solution for reflection from a dielectric slab using a thin-sheet approximation. The technique is found to provide accurate measurements of the complex dielectric constant for natural materials, including vegetation leaves and rocks, up to 12 GHz if the thickness is 0.55 mm or less.

It is worth mentioning that the technique can be extended to measure the relative permeability by modifying (12)–(14). Because such a modification results in having four unknowns, it will be necessary to measure the reflection coefficient corresponding to two different sample thicknesses in order to determine both ϵ and μ. Alternatively, one can measure the reflection and transmission coefficients of one sample to realize the same objective.

References

[1] R. F. Harrington and J. R. Mautz, "An impedance sheet approximation for thin dielectric shells," *IEEE Trans. Antennas Propagat.*, vol. AP-23, pp. 532–534, 1975.

[2] T. B. A. Senior, K. Sarabandi, and F. T. Ulaby, "Measuring and modeling the backscattering cross section of a leaf," *Radio Sci.*, vol. 22, no. 6, pp. 1109–1116, Nov. 1987.

[3] F. T. Ulaby and M. A. El-Rayes, "Microwave dielectric spectrum of vegetation—Part II: Dual-dispersion model," *IEEE Trans. Geosci. Remote Sensing.*, vol. GE-25, pp. 550–557, 1987.

[4] R. F. Harrington, *Time-Harmonic Electromagnetic Fields*. New York: McGraw-Hill, 1961, p. 130.

[5] M. A. El-Rayes and F. T. Ulaby, "Microwave dielectric spectrum of vegetation—Part I: Experimental observations," *IEEE Trans. Geosci. Remote Sensing.*, vol. GE-25, pp. 541–549, 1987.

Measuring and modeling the backscattering cross section of a leaf

T. B. A. Senior, K. Sarabandi, and F. T. Ulaby

Radiation Laboratory, Electrical Engineering and Computer Science Department, University of Michigan, Ann Arbor

(Received February 25, 1987; revised June 15, 1987; accepted June 17, 1987.)

Leaves are a significant feature of any vegetation canopy, and for remote sensing purposes it is important to develop an effective model for predicting the scattering from a leaf. From measurements of the X band backscattering cross section of a coleus leaf in varying stages of dryness, it is shown that a uniform resistive sheet constitutes such a model for a planar leaf. The scattering is determined by the (complex) resistivity which is, in turn, entirely specified by the gravimetric moisture content of the leaf. Using an available asymptotic expression for the scattering from a rectangular resistive plate which includes, as a special case, a metallic plate whose resistivity is zero, the computed backscattering cross sections for both principal polarizations are found to be in excellent agreement with data measured for rectangular sections of leaves with different moisture contents. If the resistivity is sufficiently large, the asymptotic expressions do not differ significantly from the physical optics ones, and for naturally shaped leaves as well as rectangular sections, the physical optics approximation in conjunction with the resistive sheet model faithfully reproduces the dominant features of the scattering patterns under all moisture conditions.

1. INTRODUCTION

At centimeter wavelengths, a vegetation canopy consists of scatterers with sizes that span a wide range of values extending from a fraction of a wavelength to several wavelengths. The scattering and extinction properties of an individual scatterer are governed by its shape, size, orientation, and dielectric properties. For purposes of modeling the backscattering from a forest canopy, the canopy is often treated as an inhomogeneous layer containing sparsely distributed, randomly positioned discrete scatterers [*Lang*, 1981; *Levine et al.*, 1983, 1985; *Tsang et al.*, 1984]. The sizes, shapes and orientation of the scatterers are specified by probability density functions.

Leaves are a major constituent of many types of plants, and a knowledge of their scattering and extinction properties is very important in microwave remote sensing. Although most leaves are irregular in shape and are not flat, they are often modeled as flat circular discs with known radius, thickness, and dielectric constant [*Levine et al.*, 1983, 1985]. This brings up the following set of fundamental questions:

1. What formulation might one use to characterize the backscattering and extinction cross se tions of a regularly shaped (elliptical or rectangula flat leaf?
2. How does one relate the radar cross section to the leaf moisture content Mg?
3. Is it possible to approximate the scattering ar extinction cross sections of a flat irregularly shape leaf using the formulations for a rectangular leaf equal physical area?
4. What is the effect of leaf curvature on its sca tering behavior?

In this paper we shall address the first tw questions by proposing a resistive sheet model an verifying the model with experimental measuremen conducted for sections of leaves (all cut in the shap of a rectangle) at various levels of moisture conten and partially examine the third question by com paring the scattering pattern calculated for a re tangular plate with measurements obtained for a irregularly shaped leaf. Exploration of the effects leaf curvature will be the subject of future work.

2. EXPERIMENTAL PROCEDURE

The radar cross section (RCS) measurements re ported in this paper were made at 10 GHz using small rectangular horn antenna connected to a H 8510A network analyzer, as illustrated by the sketc in Figure 1. The horn antenna, whose aperture mea

Paper number 7S0540.
0048-6604/87/007S-0540$08.00

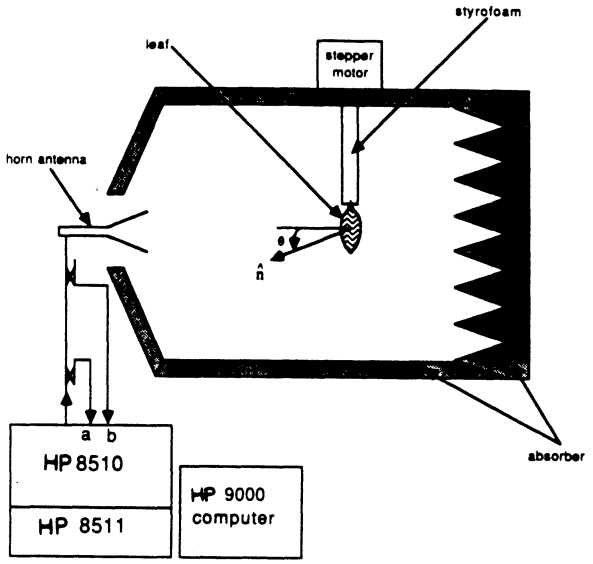

Fig. 1. Schematic of the RCS measurement system.

sured 6 cm × 6 cm, was located at the throat of a small anechoic chamber, and the leaf was suspended from the top by a thin styrofoam cylinder. The center of the top edge of the leaf was glued to the styrofoam cylinder which could be rotated to any angle θ between the backscattered direction and the normal to the plane of the leaf.

2.1. *System sensitivity and calibration*

The HP 8510A is a vector network analyzer capable of measuring both the amplitude and phase of the reflected signal (channel b in Figure 1) relative to a sample of the transmitted signal (channel a in Figure 1). To enhance the measurement sensitivity of the system, two measurements are made: one for the background alone, which includes the styrofoam cylinder, and another with the target present. By subtracting the complex signal recorded for the background alone from that measured in the presence of the target, significant improvement is obtained in the target-to-background ratio.

Absolute calibration of the system was achieved by measuring the cross section σ of a metal sphere. According to these measurements, the noise-equivalent σ of the system is about -80 dBsm. Consequently, in most cases only data above -60 dBsm was recorded, which corresponds to a target-to-background ratio of 20 dB or greater.

To test the linearity of the system and establish the extent of its dynamic range, RCS measurements were performed for seven metal spheres with diameters from 0.79 cm to 3.81 cm. The largest sphere was used to calibrate the system and the other six were used to evaluate the system accuracy by comparing the measured RCS with theoretical values computed from the Mie series. The continuous curve in Figure 2 is a plot of σ/λ^2 as a function of D/λ for a perfectly conducting sphere of diameter D, and the "stars" represent the measured data. The rms error, computed for the six test spheres, is 0.33 dB.

2.2. *Leaf moisture and dielectric constant*

The leaf moisture content was determined by measuring its weight immediately after measuring its RCS, and once again at the conclusion of the experiment. The latter measurement was made after drying the leaf in an oven at 70°C until equilibrium was reached. The difference in weight represents the weight of liquid water that was present in the leaf when its RCS was measured. The gravimetric moisture content Mg is the weight fraction of water in the leaf to the total weight.

Using the data measured and the models developed by *Ulaby and El-Rayes* [1986] for the dielectric constant of vegetation, the following simple expressions were generated to characterize the relative dielectric constant ε at 10 GHz and room temperature ($T = 22$°C):

$$\begin{aligned} \varepsilon' &= 3.95 \exp(2.79\ \mathrm{Mg}) - 2.25 \\ \varepsilon'' &= 2.69 \exp(2.15\ \mathrm{Mg}) - 2.68 \end{aligned} \tag{1}$$

2.3. *Types of RCS measurements*

Two sets of RCS measurements were conducted. The first data set involved a leaf that had been cut in

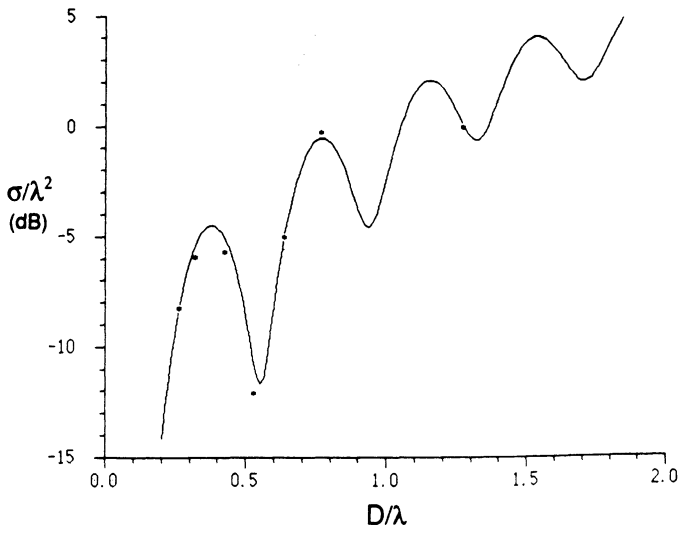

Fig. 2. The calibration accuracy and dynamic range of the measurement system were evaluated by comparing the measured RCS of metal spheres (asterisks) with theory.

the form of a rectangular plate 4 cm × 6 cm in area. With the long dimension oriented vertically, the cross section of the leaf was measured as a function of the angle of rotation θ about a vertical axis, with $\theta = 0$ corresponding to normal incidence. Each measurement scan consisted of σ versus θ in 5° steps from −90° to +90°. Usually, two scans were made, one with the antenna polarized with the electric vector vertical (E polarization) and the other with the magnetic vector vertical (H polarization). The first data set consisted of four pairs of scans corresponding to the rectangular leaf at Mg = 85% (freshly cut), 77% (a few hours later), 62% (a day later), and 0% (dry). The data comprising the second set are similar to those in the first except that the leaf was measured in its natural state without altering its shape. A profile is shown in the inset of Figure 7.

Maintaining the leaf flat to within a fraction of a wavelength was a consistent problem in this phase of the investigation, particularly for the "naturally" shaped leaf after it had been allowed to dry for a few days. Leaf thickness, which was measured using a micrometer, was found to decrease slowly with time after cutting as a result of shrinking due to loss of water. The variation of leaf thickness τ (mm) with Mg is given by the empirical expression

$$\tau = 0.032\ \mathrm{Mg}^2 + 0.091\ \mathrm{Mg} + 0.075 \tag{2}$$

In addition, it was observed that the drying took place from the outer edges of the leaf inwards, so that the moisture content was no longer uniform across the leaf.

3. THEORETICAL MODEL

3.1. *A resistive sheet*

A leaf can be viewed as a thin layer (of thickness τ) of a nonmagnetic dielectric material whose complex relative permittivity is ε, and a widely used model for such a layer is an infinitesimally thin resistive sheet whose resistivity is

$$R = \frac{iZ}{k\tau(\varepsilon - 1)} \tag{3}$$

ohms per square. In (3) k and $Z(=1/Y)$ are the propagation constant and intrinsic impedance, respectively, of the surrounding free space medium, and a time factor $e^{-i\omega t}$ has been assumed. When $R = 0$ the sheet appears perfectly conducting and when $R = \infty$ it ceases to exist.

The sheet is simply an electric current sheet whose strength is proportional to the local tangential electric field [*Harrington and Mautz*, 1975] via the single measurable quantity R. If n is the unit vector normal drawn outwards to the upper (positive) side of the sheet and $[\ ]_-^+$ denotes the discontinuity across the sheet, the boundary conditions are

$$[\hat{n} \times \bar{E}]_-^+ = 0 \tag{4}$$

implying continuity of the tangential electric field (a consequence of the absence of any magnetic current) and

$$\hat{n} \times (\hat{n} \times \bar{E}) = -RJ \tag{5}$$

where

$$\bar{J} = [\hat{n} \times \bar{H}]_-^+ \tag{6}$$

is the total electric current supported. In recent years resistive sheets have been sucessfully employed in simulating a variety of dielectric structures. Diffraction effects have been studied analytically (see, for example, *Senior* [1979]) and, in addition, computer programs have been written to determine the field scattered by resistive strips and plates of arbitrary shape.

3.2. *Scattering by an infinite planar sheet*

The scattering properties of a resistive sheet are most easily understood by considering the simple problem of a plane wave incident on an infinite sheet lying in the plane $y = 0$ of a Cartesian coordinate system (x, y, z).

For the case of E polarization in which the incident electric vector is perpendicular to the xy plane of incidence, we assume

$$\bar{E}^i = \hat{z}e^{ik(x \sin\theta_0 - y\cos\theta_0)} \qquad (|\theta_0| \le \pi/2) \tag{7}$$

implying

$$\bar{H}^i = -Y(\hat{x}\cos\theta_0 + \hat{y}\sin\theta_0)e^{ik(x\sin\theta_0 - y\cos\theta_0)}$$

The reflected and transmitted electric vectors can be written as

$$\bar{E}^r = -\hat{z}\Gamma_E e^{ik(x\sin\theta_0 + y\cos\theta_0)}$$

and

$$\bar{E}^t = \hat{z}T_E e^{ik(x\sin\theta_0 - y\cos\theta_0)}$$

respectively, where Γ_E and T_E are constants still to be determined, and by applying the boundary con-

ditions (4)–(6), we obtain

$$\Gamma_E = \left(1 + \frac{2R}{Z}\cos\theta_0\right)^{-1} \tag{8}$$

$$T_E = \frac{2R}{Z}\cos\theta_0\,\Gamma_E \tag{9}$$

The current density $\bar{J}$ supported by the sheet is $\bar{J} = \hat{z}J_z$ with

$$J_z = 2Y\cos\theta_0\,\Gamma_E e^{ikx\sin\theta_0} \tag{10}$$

and recognizing that for a perfectly conducting sheet $\Gamma_E = 1$, it follows that

$$J_z = \Gamma_E J_z^{pc} \tag{11}$$

where the superscript pc refers to the perfectly conducting case.

The analysis for H polarization in which the incident magnetic vector is perpendicular to the plane of incidence is very similar. The reflection and transmission coefficients are

$$\Gamma_H = \left(1 + \frac{2R}{Z}\sec\theta_0\right)^{-1} \tag{12}$$

and

$$T_H = \frac{2R}{Z}\sec\theta_0\,\Gamma_H \tag{13}$$

respectively, and the current density $\bar{J}$ supported by the sheet is $\bar{J} = \hat{x}J_x$ with

$$J_x = 2\Gamma_H e^{ikx\sin\theta_0} \tag{14}$$

Thus

$$J_x = \Gamma_H J_x^{pc} \tag{15}$$

If $R \neq 0$, Γ_H decreases with increasing θ_0 and vanishes at grazing incidence ($\theta_0 = \pm\pi/2$).

3.3. *Scattering by a rectangular resistive plate*

As a simple model of a leaf we consider a rectangular resistive plate occupying the region $|x| \leq a/2$, $|z| \leq b/2$ of the plane $y = 0$, and seek the physical optics approximation to the bistatic scattered field. From the expressions (11) and (15) for the currents on an infinite sheet it is evident that the analysis is very similar to that for a perfectly conducting plate, and it is sufficient to summarize the derivation.

For E polarization in which the incident electric vector is (7), the physical optics approximation to the current induced in the plate is given in (10). Since only an electric current is supported, the scattered field can be attributed to the electric Hertz vector

$$\bar{\pi}(\bar{r}) = \hat{z}\frac{iZ}{4\pi k}\int_{-a/2}^{a/2}\int_{-b/2}^{b/2} J_z(x', z')\frac{e^{ik|\bar{r}-\bar{r}'|}}{|\bar{r}-\bar{r}'|}\,dx'\,dz'$$

where

$$\bar{r} = r(-\hat{x}\sin\theta + \hat{y}\cos\theta) \qquad \bar{r}' = \hat{x}x' + \hat{z}z'$$

and in the far field

$$\bar{\pi}(\bar{r}) = \hat{z}\frac{e^{ikr}}{kr}\frac{i}{2\pi}\Gamma_E\cos\theta_0\int_{-b/2}^{b/2}dz'\int_{-a/2}^{a/2}e^{ikx'(\sin\theta+\sin\theta_0)}\,dx'$$

$$= \hat{z}\frac{e^{ikr}}{kr}\frac{i}{2\pi}ab\cos\theta_0\,\Gamma_E\frac{\sin X}{X}$$

with

$$X = \frac{ka}{2}(\sin\theta + \sin\theta_0)$$

The scattered electric field is then

$$\bar{E}^s = \hat{z}\frac{e^{ikr}}{kr}S_E(\theta, \theta_0)$$

where the far-field amplitude is

$$S_E(\theta, \theta_0) = \frac{i}{2\pi}k^2ab\cos\theta_0\,\Gamma_E\frac{\sin X}{X} \tag{16}$$

In terms of the far-field amplitude the bistatic scattering cross section is

$$\sigma = \frac{\lambda^2}{\pi}|S|^2 \tag{17}$$

implying

$$\sigma_E(\theta, \theta_0) = 4\pi\left|\frac{ab}{\lambda}\cos\theta_0\,\Gamma_E\frac{\sin X}{X}\right|^2 \tag{18}$$

For H polarization in which the incident magnetic vector is in the z direction, the analysis is similar. The physical optics approximation to the current is (14), and in the far field the resulting electric Hertz vector is

$$\bar{\pi}(\bar{r}) = \hat{x}\frac{e^{ikr}}{kr}\frac{iZ}{2\pi}ab\,\Gamma_H\frac{\sin X}{X}$$

The scattered magnetic field is then

$$\bar{H}^s = \hat{z}\frac{e^{ikr}}{kr}S_H(\theta, \theta_0)$$

with

$$S_H(\theta, \theta_0) = -\frac{i}{2\pi} k^2 ab \cos\theta \, \Gamma_H \frac{\sin X}{X} \tag{19}$$

and the bistatic scattering cross section is

$$\sigma_H(\theta, \theta_0) = 4\pi \left| \frac{ab}{\lambda} \cos\theta \, \Gamma_H \frac{\sin X}{X} \right|^2 \tag{20}$$

In the backscattering direction ($\theta_0 = \theta$) the only polarization dependence is provided by the parameter Γ and

$$\sigma_{E,H}(\theta, \theta) = |\Gamma_{E,H}|^2 \sigma_{pc} \tag{21}$$

where σ_{pc} is the backscattering cross section of the perfectly conducting plate:

$$\sigma_{pc} = 4\pi \left\{ \frac{A}{\lambda} \cos\theta \frac{\sin(ka \sin\theta)}{ka \sin\theta} \right\}^2 \tag{22}$$

in which $A = ab$ is the plate area. In terms of the far-field amplitude $S(\theta, \theta_0)$ the extinction cross section is

$$\sigma^{ext} = \frac{\lambda^2}{\pi} \operatorname{Im} S(\theta, \theta + \pi) \tag{23}$$

and thus

$$\sigma^{ext}_{E,H} = 2A \cos\theta \operatorname{Re} \Gamma_{E,H} \tag{24}$$

We recognize $2A \cos\theta$ as the extinction cross section of a perfectly conducting plate of area A, and at normal incidence

$$\sigma^{ext}_E = \sigma^{ext}_H$$

4. COMPARISON WITH MEASURED DATA

In addition to the RCS of an actual leaf and a rectangular cutout, measurements were also made using a rectangular plate to gain confidence in the accuracy of the experimental procedures and the theoretical approximations. It is convenient to discuss them in the reverse order.

4.1. *Rectangular metal plate*

When a rectangular plate is illuminated with the direction of incidence in a principal plane, an approximate expression for the backscattered field can be obtained by treating the plate as a length b of an infinite strip or ribbon of width a. For a perfectly conducting strip, a uniform second order GTD expression for the bistatic scattered field has been developed by *Senior* [1979]. If the incident field is H polarized, the formula is equivalent to an asymptotic expansion of the uniform results of *Khaskind and Vainshteyn* [1964], and when specialized to the case of backscattering, the far-field amplitude of the plate is

$$S_H(\theta, \theta) = -\frac{kb}{4\pi \sin\theta} \left\{ (1 + \sin\theta) \left[1 - \frac{2}{\sqrt{\pi}} e^{-i\pi/4} \cdot \cos\left(\frac{\pi}{4} - \frac{\theta}{2}\right) F\left(\sqrt{2ka} \sin\left(\frac{\pi}{4} - \frac{\theta}{2}\right)\right) \right]^2 e^{ika \sin\theta} - (1 - \sin\theta) \left[1 - \frac{2}{\sqrt{\pi}} e^{-i\pi/4} \sin\left(\frac{\pi}{4} - \frac{\theta}{2}\right) \cdot F\left(\sqrt{2ka} \cos\left(\frac{\pi}{4} - \frac{\theta}{2}\right)\right) \right]^2 e^{-ika \sin\theta} \right\} \tag{25}$$

for $|\theta| \leq \pi/2$, where the phase origin has been chosen at the center of the plate and $F(x)$ is the Fresnel integral

$$F(x) = \int_x^\infty e^{i\mu^2} \, d\mu \tag{26}$$

We remark that S_H is finite and continuous for all θ including $\theta = 0$ corresponding to normal incidence, and in terms of S_H the backscattering cross section is given in (17).

In the case of E polarization, a similar approach applied to the uniform results of *Fialkovskiy* [1966] gives

$$S_E(\theta, \theta) = \frac{kb}{4\pi \sin\theta} \left\{ (1 - \sin\theta) \left[1 - \frac{2}{\sqrt{\pi}} e^{-i\pi/4} \cdot \cos^3\left(\frac{\pi}{4} - \frac{\theta}{2}\right) G\left(\sqrt{2\,ka} \sin\left(\frac{\pi}{4} - \frac{\theta}{2}\right)\right) \right]^2 e^{ika \sin\theta} - (1 + \sin\theta) \left[1 - \frac{2}{\sqrt{\pi}} e^{-i\pi/4} \sin^3\left(\frac{\pi}{4} - \frac{\theta}{2}\right) \cdot G\left(\sqrt{2\,ka} \cos\left(\frac{\pi}{4} - \frac{\theta}{2}\right)\right) \right]^2 e^{-ika \sin\theta} \right\} \tag{27}$$

[*Senior*, 1979], where

$$G(x) = F(x) - \frac{i}{2x} e^{ix^2} \tag{28}$$

In Figure 3 the theoretical expressions are compared with measured data for a plate having $b = 2\lambda$ and $a = 1.33\lambda$. Overall the agreement is excellent

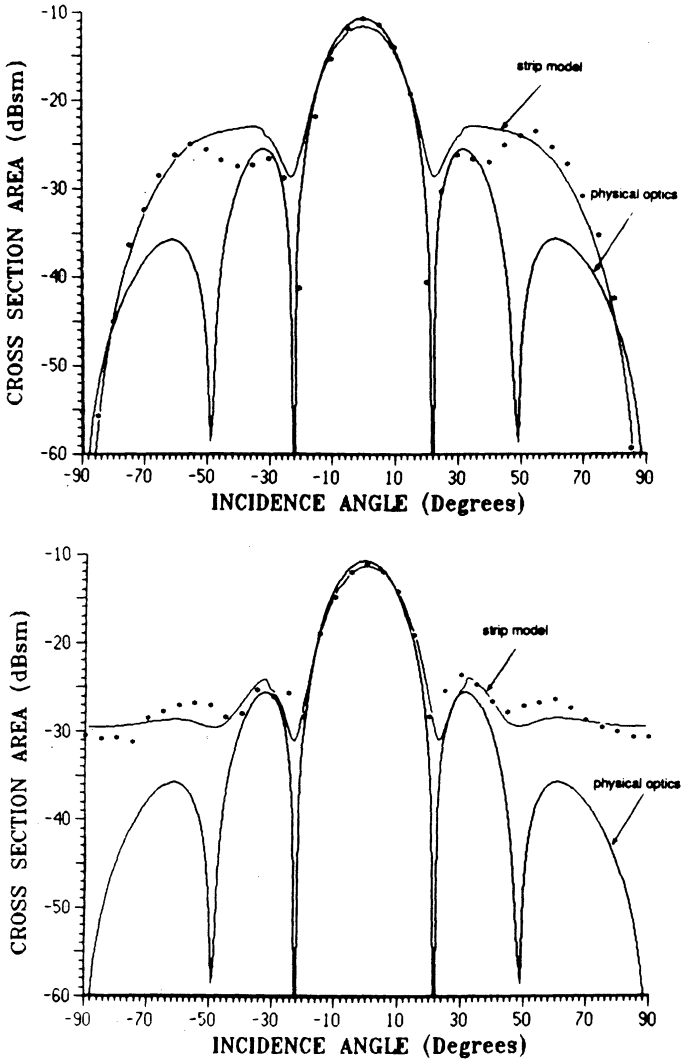

Fig. 3. The measured RCS (asterisks) of a thin metal plate (a = 4 cm, b = 6 cm) for (*a*) H polarization and (*b*) E polarization. The theoretical expressions (25) and (27) are much more accurate than the physical optics approximation (22).

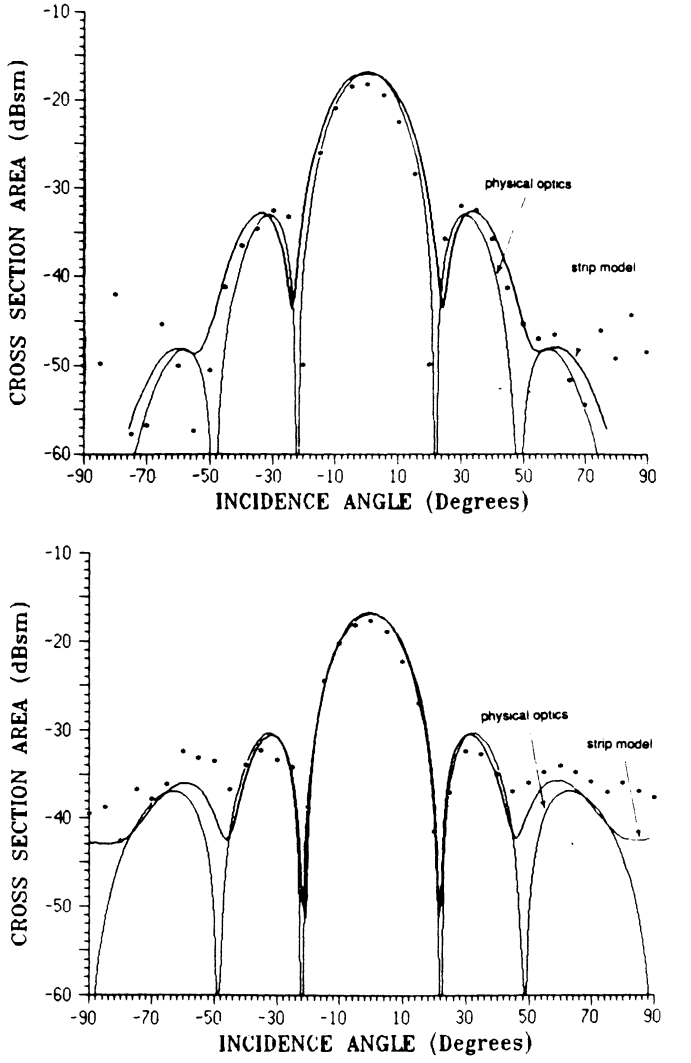

Fig. 4. The measured RCS (asterisks) of a rectangular section (a = 4 cm, b = 6 cm) of a freshly cut coleus leaf (Mg = 0.85) for (*a*) H polarization and (*b*) E polarization. The strip model provides very little improvement over the physical optics approximation (21).

With (25) used to compute σ_H, the strip model accurately reproduces the main features of the scattering pattern of a plate for H polarization, including the traveling wave lobes whose maxima occur at $\theta = \pm 54°$ and which override the outer side lobes of the specular flash. A similar agreement is found for E polarization, and the failure of (27) to reproduce the observed oscillation at angles close to grazing can be attributed to the effect of the currents borne by the side edges of the plate that are not accounted for by the strip model. The physical optics approximation (22) is included in Figure 3, and the improved accuracy provided by (25) and (27) is most evident at angles within (about) 45° from grazing.

4.2. *Rectangular resistive plate*

For a rectangular plate of uniform resistivity R, formulas analogous to (25) and (27) can be derived from the GTD expression for the bistatic scattered field of a resistive strip [*Senior*, 1979; *Herman and Volakis*, 1987], but as the resistivity increases, the improvement over the physical optics formula for a resistive plate diminishes. Even a resistivity as low as 20 ohms per square effectively eliminates the traveling wave lobe for H polarization [*Senior*, 1985] and exposes the underlying side lobes of the specular flash. Similarly, for E polarization, the resistivity reduces the strong edge effects, including the influence of the side edges of the plate.

The net result is to improve the accuracy of the physical optics approximation (21), and this is illustrated in Figure 4, where the measured data for a rectangular leaf are compared with the strip model [*Herman and Volakis*, 1987] and physical optics. The rectangle was cut from a fresh coleus leaf having Mg = 0.85, and the (complex) resistivity was com-

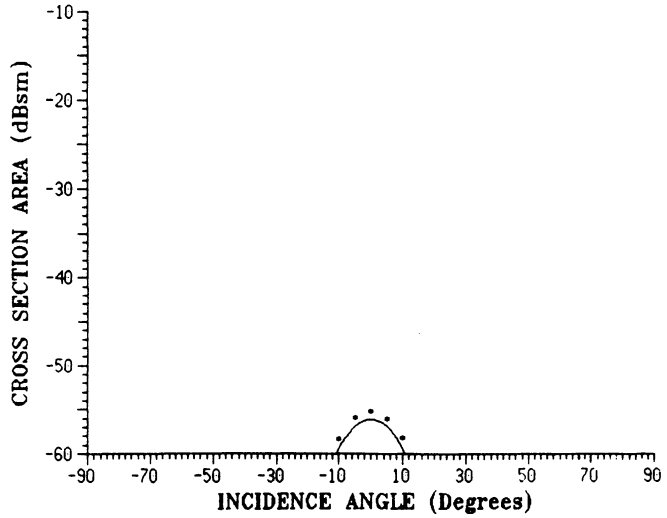

Fig. 5. The measured RCS (asterisks) of the dried leaf section (Mg = 0) compared with the physical optics approximation (21) for E polarization. The results for H polarization are the same.

puted from (3) using (1) and (2). The only significant differences between the strip and physical optics formulas occur for incidence angles within a few degrees of grazing, and the physical optics approximation is in good agreement with the measured data over most of the angular range. Similar agreement was found for other moisture contents, and Figure 5 shows the results for a dried leaf having Mg = 0. Even at this low level of reflectivity the physical optics approximation (21) retains its accuracy, and the dynamic range is illustrated in Figure 6.

4.3. *Natural leaf*

In the light of the above results it was anticipated that the physical optics approximation applied to the

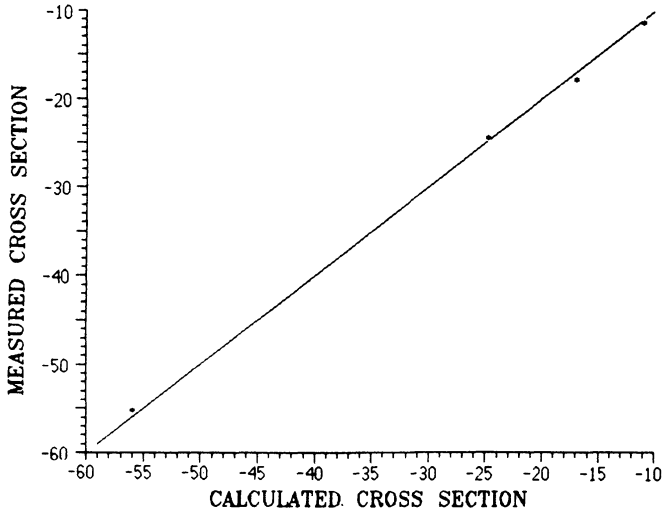

Fig. 6. The measured RCS (asterisks) of the leaf section for various moisture contents at normal incidence are in excellent agreement with the physical optics values. The 1 : 1 line is shown.

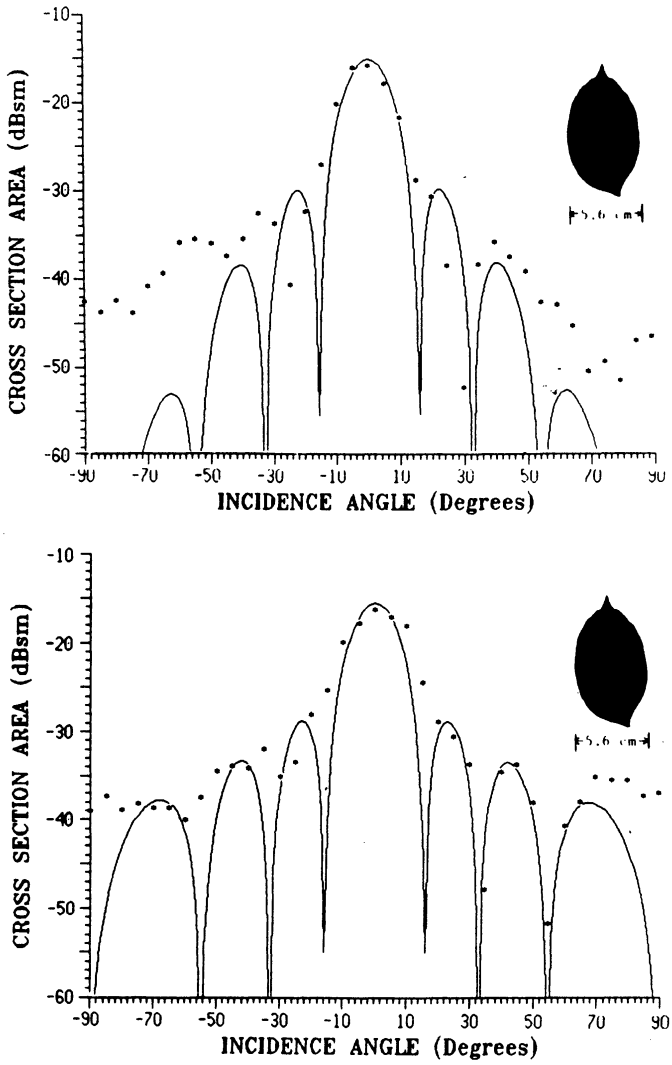

Fig. 7. The measured RCS (asterisks) of a natural coleus leaf having $A = 39.5$ cm^2 and Mg = 0.77 for (*a*) H polarization and (*b*) E polarization, compared with the physical optics approximation (21) assuming $a = 5.6$ cm.

resistive sheet model would provide a good approximation to the RCS of an actual leaf at most angles of incidence. To test this, measurements were made using a coleus leaf whose area was $A = 39.5$ cm^2. The width of the equivalent rectangle was chosen as 5.6 cm, implying $b = 7.1$ cm, and the measured RCS of the freshly cut leaf (Mg = 0.77) is compared with the physical optics approximation (21) in Figure 7. In view of the obvious uncertainty in the specification of a (or b), the agreement is good down to at least 20 dB below the broadside peak. Similar agreement was found for the same leaf with Mg = 0.85, 0.62, and 0.04.

The theoretical extinction and backscattering cross sections (24) and (21) respectively, normalized to their perfectly conducting values, are plotted as functions of the moisture content Mg for normal incidence ($\theta = 0$) in Figure 8. The measured values of σ/σ_{pc} for

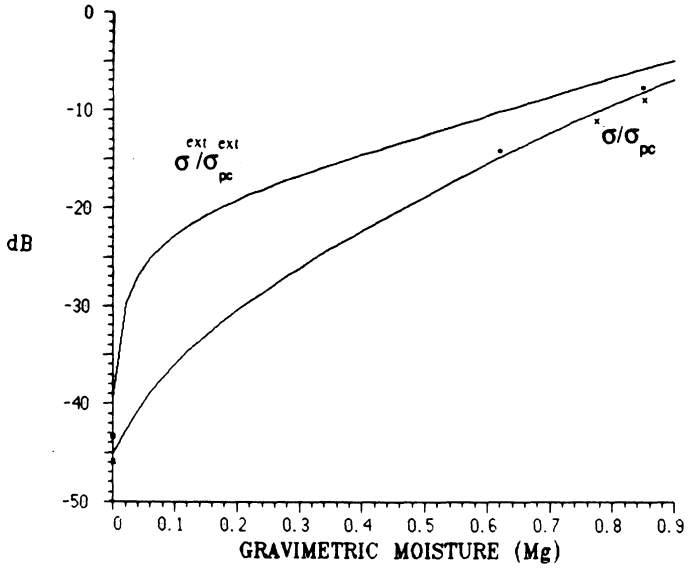

Fig. 8. The measured values of the normalized RCS of rectangular (asterisks) and natural (pluses) leaves as functions of Mg at normal incidence are accurately approximated by the physical optics expression (21). The normalized extinction cross section (24) is also shown.

the rectangular and natural leaves are included, and the agreement is excellent.

5. CONCLUSIONS

Using measurements of the backscattered field of coleus leaves in varying stages of dryness, it has been shown that a resistive sheet constitutes an effective model of a leaf. The resistivity is entirely specified by the moisture content, and for a rectangular section of a leaf, the predicted backscattering cross sections are in excellent agreement with the measured data for both principal polarizations, including the special case of a rectangular metal plate whose resistivity is zero. As the resistivity increases, the effect of the currents borne by the edges of the plate diminishes, and the accuracy of the physical optics approximation improves. Indeed, for a natural leaf, the physical optics approximation in conjunction with the resistive sheet model faithfully reproduces the dominant features of the scattering patterns for all of the moisture conditions investigated, representing a dynamic range of more than 50 dB. The simplicity of the formulation is such that the bistatic and extinction cross sections can also be computed, and the aspect angle averaging that may be necessary in a practical situation is easily performed.

Acknowledgment. This work was supported by NASA grant NAG5-480, NASA/GSFC, Beltsville, Maryland.

REFERENCES

Fialkovskiy, A. T., Diffraction of planar electromagnetic waves by a slot and a strip, *Radio Eng. Electron., 11*, 150–157, 1966.

Harrington, R. F., and J. R. Mautz, An impedance sheet approximation for thin dielectric shells, *IEEE Trans. Antennas Propag., 23*, 531–534, 1975.

Herman, M. I., and J. L. Volakis, High-frequency scattering by a resistive strip and extensions to conductive and impedance strips, *Radio Sci., 22*, 335–349, 1987.

Khaskind, M. D., and L. A. Vainshteyn, Diffraction of plane waves by a slit and a tape, *Radio Eng. Electron., 9*, 1492–1502, 1964.

Lang, R. H., Electromagnetic backscattering from a sparse distribution of lossy dielectric scatterers, *Radio Sci., 16*, 15–30, 1981.

LeVine, D. M., R. Meneghini, R. H. Lang, and S. S. Seker, Scattering from arbitrarily oriented dielectric disks in the optics region, *J. Opt. Soc. Am., 73*, 1255–1262, 1983.

LeVine, D. M., A. Snyder, R. H. Lang, and H. G. Carter, Scattering from thin dielectric disks, *IEEE Trans. Antennas Propag., 33*, 1410–1413, 1985.

Senior, T. B. A., Scattering by resistive strips, *Radio Sci., 14*, 911–924, 1979.

Senior, T. B. A., Scattering by resistive strips and plates, *Rep. 388919-1-F*, Univ. of Mich. Radiat. Lab., Ann Arbor, Mich., 1985.

Tsang, L., J. A. Kong, and R. T. Shin, Radiative transfer theory for active remote sensing of a layer of nonspherical particles, *Radio Sci., 19*, 629–642, 1984.

Ulaby, F. T., and M. El-Rayes, Microwave dielectric spectrum of vegetation material, paper presented at Geoscience Remote Sensing Symposium, IEEE, Zurich, Switzerland, Sept. 8–11, 1986.

K. Sarabandi, T. B. A. Senior, and F. T. Ulaby, Radiation Laboratory, Electrical Engineering and Computer Science Department, University of Michigan, Ann Arbor, MI 48109.

Journal of Electromagnetic Waves and Applications, Vol. 2, No. 7, 653-670, 1988

Effect of Curvature on the Backscattering from a Leaf

K. Sarabandi, T. B. A. Senior and F. T. Ulaby

Radiation Laboratory
The University of Michigan
Department of Electrical Engineering and Computer Science
Ann Arbor, MI 48109-2122, USA

Abstract– Using a model previously developed for the backscattering cross section of a planar leaf at X-band frequencies and above, the effect of leaf curvature is examined. For normal incidence on a rectangular section of a leaf curved in one and two dimensions, an integral expression for the backscattered field is evaluated numerically and by a stationary phase approximation, leading to a simple analytical expression for the cross section reduction produced by the curvature. Numerical results based on the two methods are virtually identical, and in excellent agreement with measured data for rectangular sections of coleus leaves applied to the surfaces of styrofoam cylinders and spheres of different radii.

1. INTRODUCTION

Leaves are an obvious part of any vegetation canopy. They can vary in size, shape, orientation, moisture content, etc., and if we are to model the backscattering from a canopy, it is necessary to compute the backscattering from a single leaf [1,2]. In a recent study [3] it was shown that for a typical planar leaf at X-band frequencies and above, a resistive sheet model in conjunction with the physical optics approximation accurately predicts the backscattering cross section at almost all angles of incidence. The (complex) resistivity of the sheet is a function of the gravimetric moisture content Mg of the leaf, and for all moisture contents, the accuracy of the resulting prediction is adequate for most practical purposes.

In their natural state leaves are not generally planar, and any curvature may reduce their backscattering cross sections. To explore this effect, measurements have been carried out using a rectangular portion of a coleus leaf attached to the surfaces of styrofoam cylinders and spheres of different radii. For a wide range of curvatures, the reduction in the backscattering cross section at X-band is accurately predicted by the physical optics approximation, and the results of a numerical evaluation of the physical optics integral are almost identical to a Fresnel integral expression derived from a stationary phase evaluation.

2. LEAF MODEL

A leaf can be regarded as a thin, non-magnetic lossy dielectric layer, and an effective model for such a layer is an infinitesimally thin resistive sheet. The sheet is simply an electric current sheet characterized by a (complex) resistivity

R where

$$R = \frac{iZ}{k\tau(\varepsilon - 1)} \tag{1}$$

Here, k and Z are the propagation constant and intrinsic impedance respectively of free space, τ is the layer thickness, ε is the complex dielectric constant of the material, and a time factor $e^{-i\omega t}$ has been assumed and suppressed.

The dielectric constant $\varepsilon = \varepsilon' + i\varepsilon''$ of a leaf is primarily determined by its gravimetric moisture content Mg, and can be found using a Debye-Cole dual-dispersion dielectric model [4]. The model predicts ε' and ε'' in terms of the frequency, temperature and Mg, and approximate empirical expressions valid at X-band and room temperatures are available [3]. The accuracy is within $\pm 20\%$. The thickness τ of a leaf also depends on its moisture content and decreases with decreasing Mg. In reality, however, the thickness generally decreases from base to tip and may vary by as much as 50 percent over the surface. For a class of coleus leaves, an approximate expression for the average thickness in terms of Mg was given in [3], but for the coleus leaves used in the present study the thickness was measured at several points using calipers, and the averages determined. It is worth noting that the resulting resistivity of the leaf was in good agreement with the value of R measured using a leaf section placed in a waveguide.

At X-band frequencies and up to where the leaf thickness is comparable to $\lambda/20$ the physical optics approximation applied to the resistive sheet model provides an accurate estimate of the backscattering cross section of a planar leaf for all moisture contents and most angles of incidence [3]. For a sheet lying in the plane $\xi = 0$ of a Cartesian coordinate system (ξ, η, ζ) and illuminated by a plane electromagnetic wave having

$$\overline{E}^i = (\hat{\xi}\sin\alpha\sin\phi + \hat{\eta}\sin\alpha\cos\phi + \hat{\zeta}\cos\alpha)e^{-ik(\xi\cos\phi - \eta\sin\phi)} \tag{2}$$

(see Fig. 1), the induced electric current is

$$\overline{J} = 2Y\left\{\hat{\eta}\sin\alpha\,\Gamma_H(\phi) + \hat{\zeta}\cos\alpha\cos\phi\,\Gamma_E(\phi)\right\}e^{ik\eta\sin\phi} \tag{3}$$

where Y is intrinsic admittance of free space and [3]

$$\Gamma_H(\phi) = \left(1 + \frac{2R}{Z}\sec\phi\right)^{-1}$$

$$\Gamma_E(\phi) = \left(1 + \frac{2R}{Z}\cos\phi\right)^{-1}$$

Γ_H and $-\Gamma_E$ respectively are the plane wave reflection coefficients for H-polarization ($\alpha = \pi/2$) when the magnetic vector is perpendicular to the plane of incidence and for E-polarization ($\alpha = 0$) when the electric vector is similarly inclined. Since $R = 0$ corresponds to perfect conductivity, Γ_H and Γ_E show how the current differs from the current $\overline{J}_{pc}$ supported by a perfectly conducting surface. Indeed,

$$\overline{J} = \overline{J}_{pc}\cdot\hat{\eta}\Gamma_H(\phi) + \overline{J}_{pc}\cdot\hat{\zeta}\Gamma_E(\phi) \tag{4}$$

where $\hat{\eta}$ and $\hat{\zeta}$ are unit tangent vectors in and perpendicular to the plane of incidence respectively.

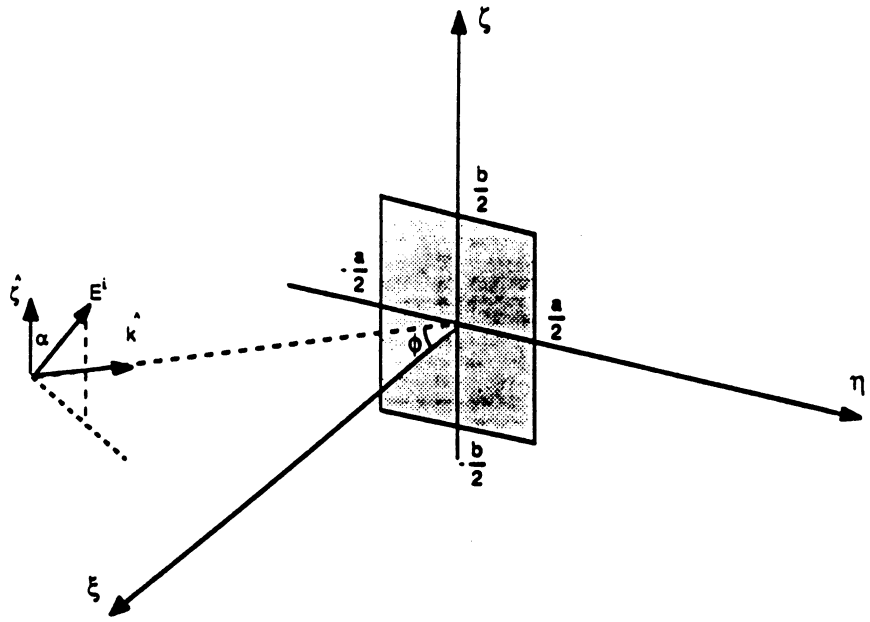

Figure 1. Geometry for the scattering of a plane wave from a resistive sheet lying in the plane $\xi = 0$.

3. ONE DIMENSIONAL CURVATURE

In the Appendix, expressions are derived for the backscattering cross section of a rectangular resistive plate of dimensions a, b as a function of the angle of incidence, and we now examine the effect of giving the plate a constant radius of curvature ρ in a principal plane. As a result of the bending, the plate conforms to a portion of the surface of a right circular cylinder of radius ρ as shown in Fig. 2.

If the flat plate has length a in the z-direction and width b in the y-direction, then $b = 2\rho\phi_o$. The illuminating field is a plane wave propagating in the negative x-direction with

$$\overline{E}^i = (\hat{y}\sin\alpha + \hat{z}\cos\alpha)e^{-ik(x-\rho)} \tag{5}$$

and in the backscattering direction the far field expression for the Hertz vector $\overline{\pi}$ is

$$\overline{\pi}(\overline{x}) = \frac{e^{ikx}}{kx}\frac{iZ}{4\pi}a\rho\int_{\theta-\phi_o}^{\theta+\phi_o}\overline{J}(\phi')e^{ik\rho(1-\cos\phi')}d\phi'$$

where the phase origin has been chosen at the front of the cylinder. To ensure that no portion of the outer surface of the plate is shadowed, it is necessary that $|\theta| \leq \frac{\pi}{2} - \phi_o$. The resistive sheet current $\overline{J}$ is given by (3) with the identification

$$\phi = \phi', \quad \hat{\eta} = -\hat{x}\sin\phi' + \hat{y}\cos\phi', \quad \hat{\zeta} = \hat{z}$$

Recognizing that the exponent in (5) is simply the incident field phase at the

surface,

$$\overline{J}(\phi') = 2Y\Big\{(-\hat{x}\sin\phi' + \hat{y}\cos\phi')\sin\alpha\,\Gamma_H(\phi') + \hat{z}\cos\alpha\cos\phi'\,\Gamma_E(\phi')\Big\}e^{ik\rho(1-\cos\phi')}$$

and hence

$$\overline{\pi}(\overline{x}) = \frac{e^{ikx}}{kx}\frac{ia\rho}{2\pi}\int_{\theta-\phi_o}^{\theta+\phi_o}\Big\{(-\hat{x}\sin\phi' + \hat{y}\cos\phi')\sin\alpha\,\Gamma_H(\phi') + \hat{z}\cos\alpha\cos\phi'\,\Gamma_E(\phi')\Big\}e^{2ik\rho(1-\cos\phi')}\,d\phi'$$

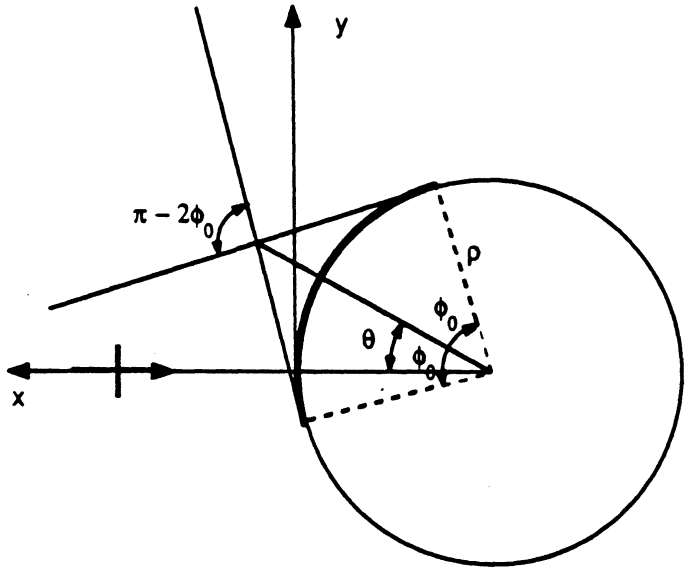

Figure 2. Geometry for the scattering of a plane wave from a resistive sheet which conforms to a portion of the surface of right circular cylinder of radius ρ.

The scattered electric field in terms of the Hertz vector $\overline{\pi}$ is given by

$$\overline{E}^s = \nabla\times\nabla\times\overline{\pi}$$

and the far field approximation in the backscattering direction is

$$\overline{E}^s(\overline{x}) = ik\hat{x}\times ik\hat{x}\times\overline{\pi}(\overline{x}) = \frac{e^{ikx}}{kx}\overline{S}$$

where $\overline{S}$ is the far field amplitude. The resulting expression for $\overline{S}$ is

$$\overline{S} = \frac{ik^2a\rho}{2\pi}\int_{\theta-\phi_o}^{\theta+\phi_o}\{\hat{y}\sin\alpha\,\Gamma_H(\phi') + \hat{z}\cos\alpha\,\Gamma_E(\phi')\}\cos\phi'\,e^{2ik\rho(1-\cos\phi')}d\phi' \quad (6)$$

in terms of which the like- and cross-polarized backscattering cross sections are

$$\sigma = \frac{\lambda^2}{\pi}\left|(\hat{y}\sin\alpha + \hat{z}\cos\alpha)\cdot\overline{S}\right|^2 \quad (7)$$

$$\sigma_{\text{cross}} = \frac{\lambda^2}{\pi}\left|(\hat{y}\cos\alpha - \hat{z}\sin\alpha)\cdot\overline{S}\right|^2 \quad (8)$$

Two methods were employed to evaluate the integral expression (6) for $\overline{S}$. In the first, the arc $\theta - \phi_o < \phi' < \theta + \phi_o$ was subdivided into $2M$ segments and each replaced by a planar strip of width $\Delta = \rho\phi_o/M$ centered at $\phi' = \phi'_m$, $m = 1, 2, \ldots, M$, and tangential to the cylinder. From the formula $(A.3)$ for the backscattered far field amplitude of an inclined plate, we then have

$$\overline{S} = \frac{ik^2 a\Delta}{2\pi} \sum_{m=1}^{2M} \left\{ \hat{y} \sin\alpha\, \Gamma_H(\phi'_m) + \hat{z} \cos\alpha\, \Gamma_E(\phi'_m) \right\} \cos\phi'_m e^{2ik\rho(1-\cos\phi'_m)} \frac{\sin U'}{U'} \tag{9}$$

with $U' = k\Delta \sin\phi'_m$. The summation was carried out numerically, and a comparison with data obtained from a moment method solution of the integral equation for a curved resistive strip is given in Section 5.

The second method is entirely analytical and is based on the stationary phase (SP) approximation. The SP point of the integral in (6) is $\phi' = 0$ and on the assumption that $k\rho \gg 1$, with $\theta < \phi_o$ so that the SP point lies within the range of integration,

$$\overline{S} = \frac{ika}{2\pi} \sqrt{k\rho} \left\{ \hat{y} \sin\alpha \Gamma_H(0) + \hat{z} \cos\alpha \Gamma_E(0) \right\} \cdot \left\{ \mathcal{F}\left[\sqrt{k\rho}(\phi_o + \theta)\right] + \mathcal{F}\left[\sqrt{k\rho}(\phi_o - \theta)\right] \right\}$$

where

$$\mathcal{F}(\tau) = \int_0^\tau e^{iu^2} du \tag{10}$$

is the finite range Fresnel integral. We remark that for $|\tau| \ll 1$

$$\mathcal{F}(\tau) = \tau + O(\tau^3) \tag{11}$$

whereas for $|\tau| \gg 1$

$$\mathcal{F}(\tau) \sim \frac{1}{2}\sqrt{\pi} e^{i\pi/4} \tag{12}$$

Since $\Gamma_E(0) = \Gamma_H(0)$ it now follows that

$$\overline{S} = \frac{ika}{2\pi} \sqrt{k\rho} (\hat{y} \sin\alpha + \hat{z} \cos\alpha) \Gamma_H(0) \left\{ \mathcal{F}\left[\sqrt{k\rho}(\phi_o + \theta)\right] + \mathcal{F}\left[\sqrt{k\rho}(\phi_o - \theta)\right] \right\} \tag{13}$$

showing that to this approximation there is no depolarization in the backscattering direction.

It is instructive to examine separately the special case of symmetric (normal) incidence when $\theta = 0$. The argument of the Fresnel integrals in (13) is then $b/2\sqrt{k/\rho}$, and if $\rho \gg kb^2/4$, the approximation (11) implies

$$\overline{S} = \frac{ik^2 ab}{2\pi} (\hat{y} \sin\alpha + \hat{z} \cos\alpha) \Gamma_H(0) \tag{14}$$

in agreement with the known expression for the backscattered far field amplitude of a planar resistive plate at normal incidence. On the other hand, if $\rho \ll kb^2/4$, (12) gives

$$\overline{S} = -\frac{ka}{2} \sqrt{\frac{k\rho}{\pi}} (\hat{y} \sin\alpha + \hat{z} \cos\alpha) \Gamma_H(0) e^{-i\frac{\pi}{4}}$$

which is the result for a resistive circular cylinder of radius ρ and length a. For intermediate values of ρ the Fresnel integral must be retained, and when the far field amplitude is normalized to the flat plate expression (14), denoted by the affix fp,

$$\frac{S}{Sfp} = \frac{1}{\gamma}\mathcal{F}(\gamma) \tag{15}$$

independent of the resistivity, where

$$\gamma = \frac{b}{2}\sqrt{\frac{k}{\rho}} \tag{16}$$

The above results are also valid for concave curvature if $\mathcal{F}(\gamma)$ is replaced by its complex conjugate. Calculations based on the formulas (9), (13) and (15) are compared with numerical results obtained using the moment method and with measured data in Section 5.

4. TWO DIMENSIONAL CURVATURE

We now consider the effect of giving the plate the same curvature in both principal planes, so that the plate conforms to a portion of a spherical surface of radius r. For simplicity the analysis is carried out for a plane wave incident symmetrically, and the geometry is then as shown in Fig. 3.

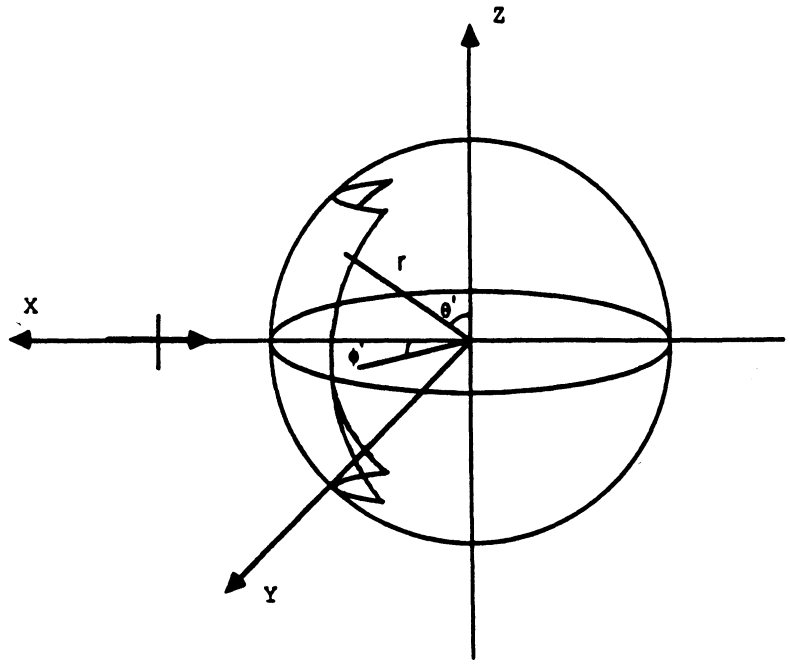

Figure 3. Geometry for the scattering of a plane wave from a resistive sheet which occupies a portion of the surface of a sphere of radius r at normal incidence.

In terms of the spherical polar coordinates r, θ', ϕ' such that $x = r\sin\theta'\cos\phi'$, $y = r\sin\theta'\sin\phi'$ and $z = r\cos\theta'$, the plate occupies the surface region $\frac{\pi}{2} - \theta_o < \theta' < \frac{\pi}{2} + \theta_o, -f(\theta') < \phi' < f(\theta')$ where $\theta_o = b/(2r)$ and $f(\theta') = a/(2r\sin\theta')$.

The incident electric field is the same as that in Section 3, and for a perfectly conducting plate the physical optics expression for the induced electric current at a point θ', ϕ' on the surface is

$$\overline{J}_{\rm pc} = 2Y\Big\{\sin\alpha\sin\theta'(-\hat{x}\sin\phi' + \hat{y}\cos\phi') + \cos\alpha(-\hat{x}\cos\theta' + \hat{z}\sin\theta'\cos\phi')\Big\} e^{ikr(1-\sin\theta'\cos\phi')}$$

Unit vectors tangential to the surface and parallel and perpendicular respectively to the plane of incidence are

$$\hat{\eta}_1 = Q\Big\{-\hat{x}(1-\sin^2\theta'\cos^2\phi') + (\hat{y}\sin\theta'\sin\phi' + \hat{z}\cos\theta')\sin\theta'\cos\phi'\Big\}$$

$$\hat{\zeta}_1 = Q(-\hat{y}\cos\theta' + \hat{z}\sin\theta'\sin\phi')$$

where

$$Q = (1-\sin^2\theta'\cos^2\phi')^{-\frac{1}{2}}$$

and in terms of $\hat{\eta}_1$ and $\hat{\zeta}_1$ the perfectly conducting plate current is

$$\overline{J}_{\rm pc} = 2Y\Big\{(\sin\alpha\sin\theta'\sin\phi' + \cos\alpha\cos\theta')\hat{\eta}_1 - \sin\theta'\cos\phi' \cdot(\sin\alpha\cos\theta' - \cos\alpha\sin\theta'\sin\phi')\hat{\zeta}_1\Big\} Qe^{ikr(1-\sin\theta'\cos\phi')}$$

From (4) it now follows that for a resistive plate the current is

$$\overline{J} = 2Y\Big\{(\sin\alpha\sin\theta'\sin\phi' + \cos\alpha\cos\theta')\Gamma_H(\phi)\hat{\eta}_1 - \sin\theta'\cos\phi' \cdot(\sin\alpha\cos\theta' - \cos\alpha\sin\theta'\sin\phi')\Gamma_E(\phi)\hat{\zeta}_1\Big\} Qe^{ikr(1-\sin\theta'\cos\phi')} \quad (17)$$

where the angle ϕ is such that

$$\cos\phi = \sin\theta'\cos\phi'$$

In the backscattering direction the far field expression for the Hertz vector $\overline{\pi}$ is

$$\overline{\pi}(x) = \frac{e^{ikx}}{kx}\frac{iZr^2}{4\pi}\int_{\frac{\pi}{2}-\theta_o}^{\frac{\pi}{2}+\theta_o}\int_{-f(\theta')}^{f(\theta')}\overline{J}(\theta',\phi')e^{ikr(1-\sin\theta'\cos\phi')}\sin\theta'\,d\theta'\,d\phi'$$

and when the formula (17) for $\overline{J}$ is inserted, the backscattering far field amplitude for the curved resistive plate is found to be

$$\begin{aligned}\overline{S} = \frac{ik^2r^2}{2\pi}\int_{\frac{\pi}{2}-\theta_o}^{\frac{\pi}{2}+\theta_o}\int_{-f(\theta')}^{f(\theta')}\Big[&\sin\alpha\hat{y}\Big\{\sin^2\theta'\sin^2\phi'\Gamma_H(\phi) + \cos^2\theta'\Gamma_E(\phi)\Big\} \\ &+ \cos\alpha\hat{z}\Big\{\sin^2\theta'\sin^2\phi'\Gamma_E(\phi) + \cos^2\theta'\Gamma_H(\phi)\Big\} \\ &+ (\cos\alpha\hat{y} - \sin\alpha\hat{z})\sin\theta'\cos\theta'\sin\phi'\Big\{\Gamma_E(\phi) - \Gamma_H(\phi)\Big\}\Big] \\ &\cdot Q^2\sin^2\theta'\cos\phi' e^{2ikr(1-\sin\theta'\cos\phi')}\,d\theta'\,d\phi' \end{aligned} \quad (18)$$

The like- and cross-polarized backscattering cross sections can be computed by substituting (18) in (7) and (8), and depolarization occurs to the extent that Γ_H and Γ_E differ over those portions of the plate that contribute to the integral.

The expression for $\overline{S}$ was evaluated using methods similar to those employed in Section 3. The first method is numerical. By subdividing the θ' and ϕ' ranges into $2L$ and $2M$ increments respectively and treating each elementary patch as a rectangular flat plate centered at $\theta' = \theta'_\ell$, $\phi' = \phi'_m$ ($\ell = 1,2,\ldots,L$; $m = 1,2,\ldots,M$) with dimensions $\Delta_1 = r\Delta\theta'$, $\Delta_2 = r\sin\theta'_2\Delta\phi'$ where $\Delta\theta' = \theta_o/L$ and $\Delta\phi' = f(\theta')/M$, the result is

$$\overline{S} = \frac{ik^2}{2\pi}\sum_{\ell=1}^{2L}\sum_{m=1}^{2M}\Big[\ \Big]\Delta_1\Delta_2 Q^2\sin\theta'_\ell\cos\phi'_m e^{2ikr(1-\cos\theta'_\ell\cos\phi'_m)}\frac{\sin U_1}{U_1}\frac{\sin V_1}{V_1} \tag{19}$$

Here

$$U_1 = k\Delta_1\cos\theta'_\ell\cos\phi'_m$$
$$V_1 = k\Delta_2\sin\phi'_m$$

and [ ] denotes the terms in square brackets in (18).

The second method is based on the stationary phase approximation. The (double) SP point of the integrand in (18) is $\theta' = \pi/2, \phi' = 0$, and when all the non-exponential terms are removed from the integrand at this point, we have

$$\overline{S} = \frac{ik^2r^2}{2\pi}(\hat{y}\sin\alpha + \hat{z}\cos\alpha)\Gamma_H(0)\int_{\frac{\pi}{2}-\theta_o}^{\frac{\pi}{2}+\theta_o}\int_{-f(\theta')}^{f(\theta')} e^{2ikr(1-\sin\theta'\cos\phi')}d\theta'\,d\phi'$$

where we have used the fact that $\Gamma_E(0) = \Gamma_H(0)$. By expanding the exponent about the SP point and retaining only the quadratic terms, we then obtain

$$\overline{S} = \frac{2ikr}{\pi}(\hat{y}\sin\alpha + \hat{z}\cos\alpha)\Gamma_H(0)\mathcal{F}\Big(\frac{a}{2}\sqrt{\frac{k}{r}}\Big)\mathcal{F}\Big(\frac{b}{2}\sqrt{\frac{k}{r}}\Big) \tag{20}$$

showing that to this approximation there is no depolarization. The amplitude normalized to its flat plate value (14) is

$$\frac{S}{S^{fp}} = \frac{1}{\gamma_1}\mathcal{F}(\gamma_1)\cdot\frac{1}{\gamma_2}\mathcal{F}(\gamma_2) \tag{21}$$

independent of the resistivity where

$$\gamma_1 = \frac{a}{2}\sqrt{\frac{k}{r}}, \qquad \gamma_2 = \frac{b}{2}\sqrt{\frac{k}{r}} \tag{22}$$

and the reduction in S_{fp} is simply the product of the factors appropriate to a one-dimensional curvature in each of the principal planes of the plate.

The extension to the case of a plane wave which is not incident symmetrically is trivial. If the plate is rotated through an angle θ about the y-axis (see Fig. 3) with $|\theta| \le \frac{\pi}{2} - \theta_o$ so that no part of the plate is shadowed, the far field amplitude corresponding to (20) is

$$\overline{S} = \frac{ikr}{\pi}(\hat{y}\sin\alpha + \hat{z}\cos\alpha)\Gamma_H(0)\mathcal{F}\Big(\frac{a}{2}\sqrt{\frac{k}{r}}\Big)$$
$$\cdot\left\{\mathcal{F}\left[\frac{b}{2}\sqrt{\frac{k}{r}}\left(1+\frac{\theta}{\theta_o}\right)\right] + \mathcal{F}\left[\frac{b}{2}\sqrt{\frac{k}{r}}\left(1-\frac{\theta}{\theta_o}\right)\right]\right\} \tag{23}$$

Here also the expression is a natural extension of the formula for a one-dimensional curvature.

5. COMPARISON WITH EXPERIMENTAL DATA

To test the validity of the resistive sheet model and to explore the effect of leaf curvature, a series of measurements was carried out using rectangular leaf sections. Coleus leaves were chosen because they retain their moisture after being cut: at room temperature (23°C) the change in moisture content after 20 minutes was less than one percent. The scattering measurements were made at X-band in a small tapered anechoic chamber using an HP 8510A network analyzer. A schematic of the equipment is shown in Fig. 4, and the general procedures employed are described in [3]. The only significant improvements made to the original system were the introduction of an automatic target positioner to permit measurements at specified increments in angle, and the use of strings stretched between synchronously rotating stepper motors at the top and bottom of the chamber to facilitate the target support. Since a single linearly-polarized horn antenna was used to radiate and receive the signals, only the like-polarized backscattering cross section could be measured. A small metal sphere was employed for calibration.

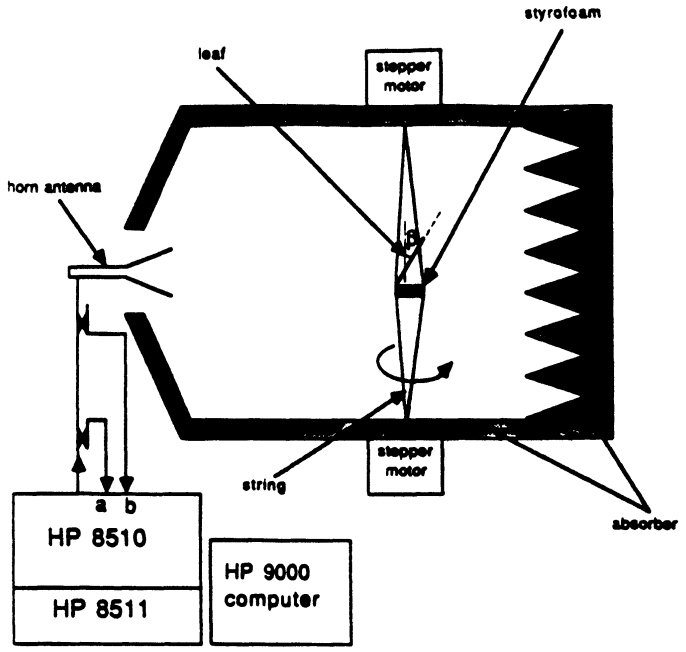

Figure 4. Schematic of the RCS measurement system.

Some results for a plane rectangular section of a leaf having $a = 1.33\lambda$ and $b = 2\lambda$ with $Mg = 0.7$ and $\tau = 0.5$ mm are shown in Figs. 5 and 6. E polarization ($\alpha = 0$) was used in both cases. In Fig. 5 the leaf was initially vertical ($\beta = 0$) and the data as a function of the rotation angle ϕ are in good agreement with the curve computed from $(A.4)$. In Fig. 6 the leaf was tilted back ($\beta = 8$ deg.) and a similar comparison with $(A.8)$ is shown. For completeness, the cross polarized cross section computed using $(A.9)$ is included in Fig. 6.

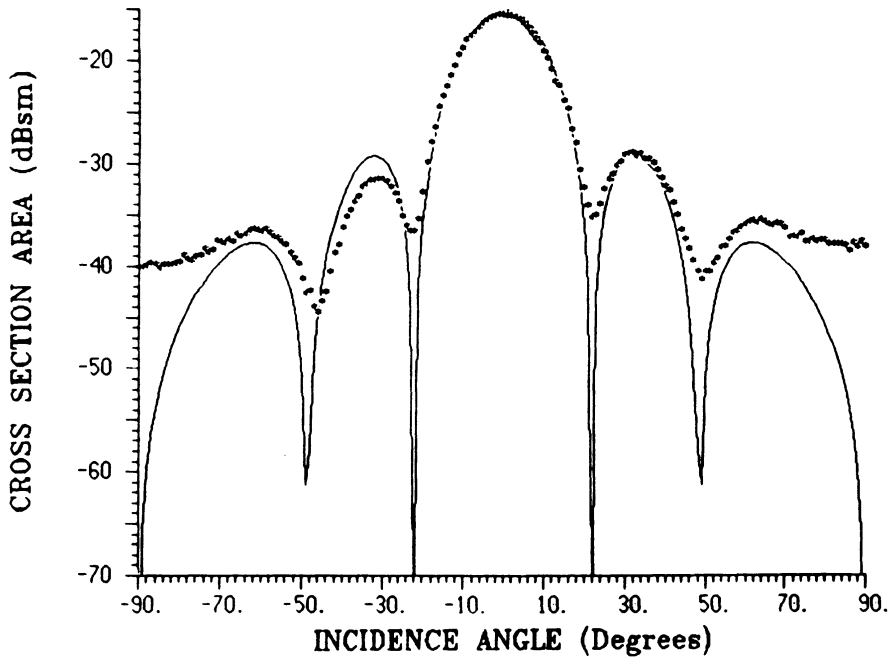

Figure 5. Comparison of the measured RCS (* * *) with the theoretical expression (*A*.4) (—) for a rectangular section ($a = 4$ cm, $b = 6$ cm) of a cut coleus leaf with $Mg = 0.7$ and $\tau = 0.5$ mm for E-polarization ($\alpha = 0$), $\beta = 0$ and $\lambda = 3$ cm.

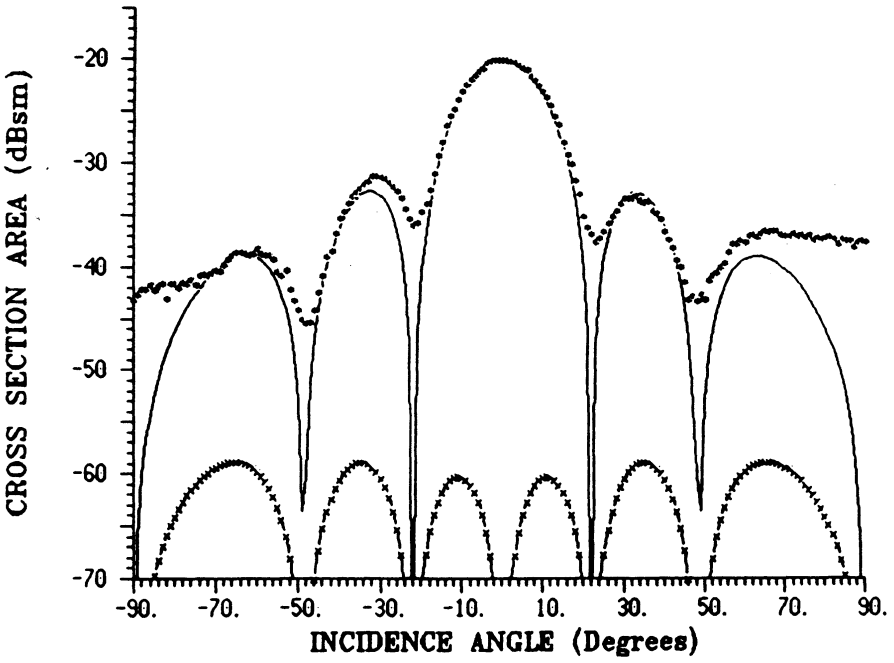

Figure 6. Comparison of the measured RCS (* * *) with the theoretical expression (*A*.8) (—) for the rectangular section of the coleus leaf with $Mg = 0.7$ and $\tau = 0.5$ mm for E-polarization ($\alpha = 0$), $\beta = 8$ deg and $\lambda = 3$ cm. The theoretical cross polarized RCS (*A*.9) (xxx) is also shown.

With the confidence that physical optics in conjunction with the resistive sheet model is adequate for planar leaves, we now compare the predictions for curved leaves with moment method data and with experimental results. To check the accuracy of (9), the scattering was computed using a two-dimensional moment method code [5] for resistive strips extended to the three-dimensional case by assuming that the current is independent of z, and in Fig. 7 the backscattering cross section computed using (9) is compared with moment method data for a curved leaf having radius of curvature $\rho = 2\lambda$ and for a flat leaf ($\rho = \infty$). The overall agreement is good out to 50 and 70 degrees respectively, where the lower limit for the curved leaf corresponds to the onset of shadowing. In Fig. 8 the Fresnel integral approximation (13) is compared with (9) for curved leaves having $\rho = 2\lambda$ and 3λ. The agreement is excellent as long as the stationary phase point is on the leaf, i.e., for $|\theta| < 28$ and 19 degrees respectively, but remains good for incidence angles out to about 45 degrees.

Experimental measurements were also performed. In the first experiment a rectangular leaf section of the same size as before was attached to the surface of a right circular cylinder of styrofoam and the normal incidence backscattering cross section was measured. Cylinders of six different radii were used and the cross sections were normalized to that of the planar leaf. The measured cross section reductions for E polarization are plotted as a function of ρ in Fig. 9 and compared with the curves computed using the numerical summation (9) and the stationary phase approximation (15). The agreement is excellent. As ρ decreases from 33 to 3, γ increases from 0.76 to 3.14. Over the entire range, (9) and (15) yield virtually identical results, and (15) provides a simple and accurate expression for the cross section reduction.

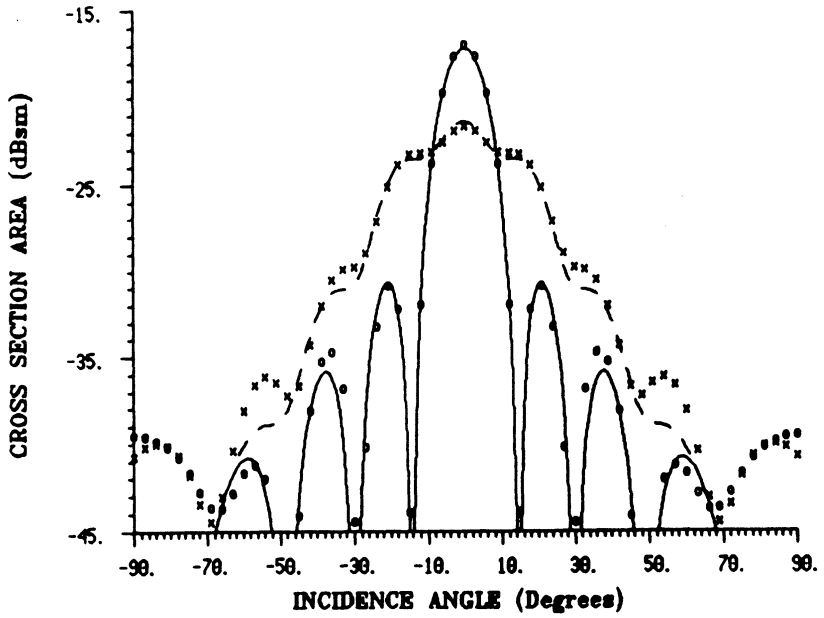

Figure 7. RCS of a rectangular resistive sheet computed using the moment method (lines) and the numerical summation (9) (points) for $\rho = 2\lambda$ (---, xxx) and $\rho = \infty$ (—, 000). The size and resistivity of the sheet are the same as in Fig. 5 with $\tau = 0.32$ mm and $\lambda = 3$ cm.

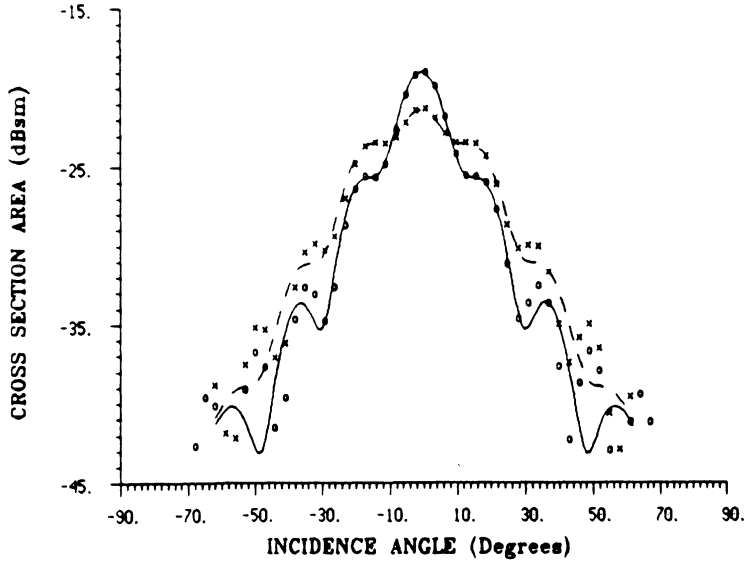

Figure 8. RCS of a rectangular resistive sheet computed using the numerical summation (9) (lines) and the Fresnel integral approximation (13) (points) for $\rho = 2\lambda$ (---, xxx) and $\rho = 3\lambda$ (—, 000). The size and resistivity of the sheet are the same as in Fig. 5 with $\tau = 0.32$ mm and $\lambda = 3$ cm.

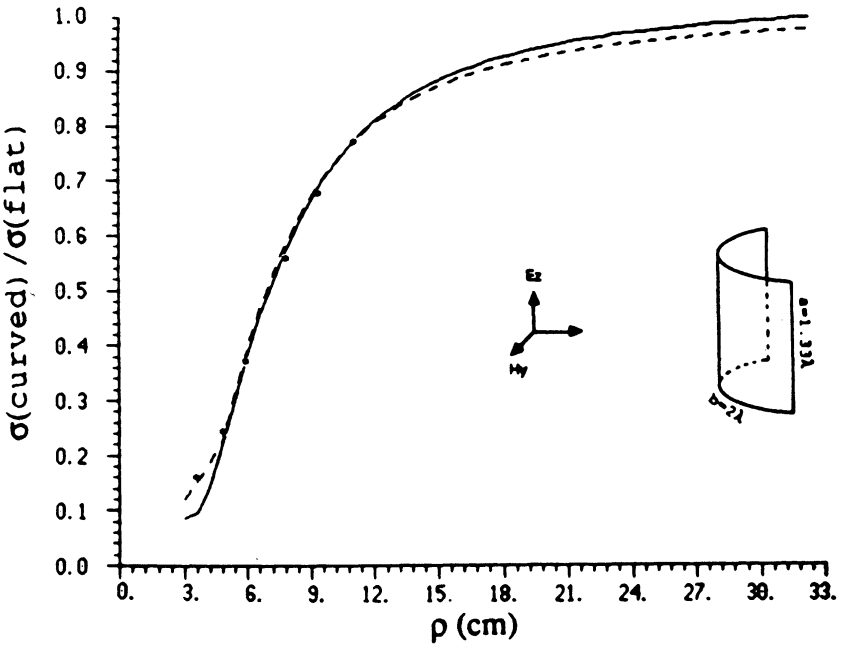

Figure 9. Comparison of the measured RCS (* * *) reduction at normal incidence with the numerical summation (19) (—) and the Fresnel integral approximation (15) (---) for a one dimensionally curved rectangular section of a coleus leaf versus radius of curvature ($\tau = 0.32$ mm, $\lambda = 3$ cm).

For the case of a two dimensional curvature a similar experiment was performed in which a leaf section was mounted on the surface of a styrofoam sphere. Spheres

of six different radii were used. To facilitate the mounting a naturally-curved leaf was chosen and cut to conform to the spherical region $\frac{\pi}{2}-\theta_o < \theta' < \frac{\pi}{2}+\theta_o$, $-\phi_o < \phi' < \phi_o$ where $\theta_o = b/(2r), \phi_o = a(2r\sin\theta_o)$, with $a = 1.33\lambda$ and $b = 2\lambda$. The region is slightly different from that specified in Section 5, and the leaf sections are no longer rectangular when flattened out, but calculations based on the summation (19) showed that the cross section reduction is the same for both. The measured data are compared with the numerical and analytical results (19) and (21) in Fig. 10. The agreement is again excellent and confirms the validity of the simple formula (21) for curvature in two dimensions.

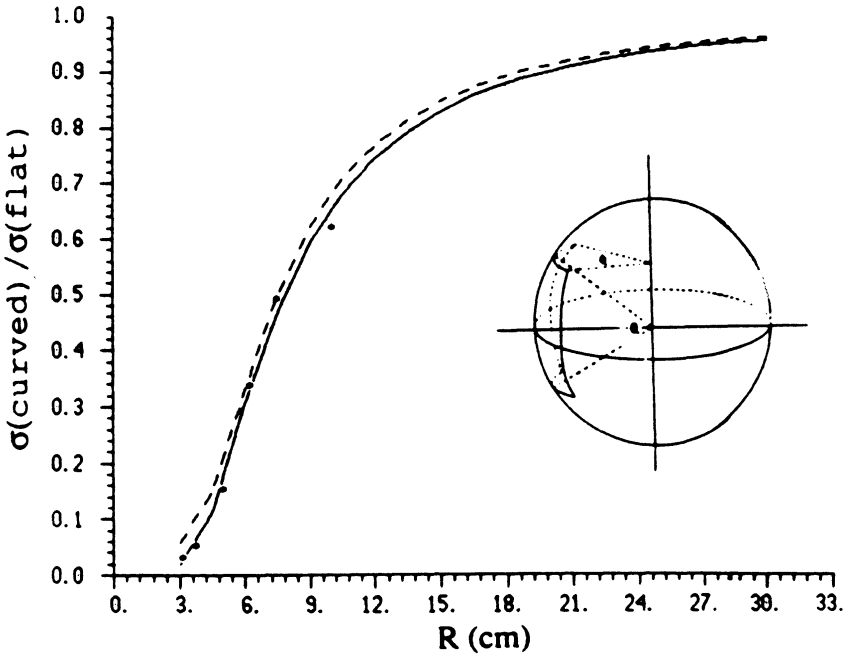

Figure 10. Comparison of the measured RCS (* * *) reduction at normal incidence with the numerical summation (19) (—) and the Fresnel integral approximation (21) (---) for a spherically curved section of a coleus leaf versus radius of curvature (τ = 0.32 mm, $\lambda = 3$ cm).

As evident from the preceding figures, curvature can have a significant effect on the backscattering cross section, and in a practical situation, it is important to know the frequency range where any curvature of a leaf must be taken into account. To this end, Fig. 11 shows the normal incidence cross section reductions versus frequency for three leaf sections 6 cm on a side, curved in one dimension with radii 3, 6 and 12 cm. In all three cases $Mg = 0.7$, $\tau = 0.5$ mm and the frequency dependence implied by (1) and the Debye-Cole dielectric model was included. Once again (9) and (15) yield virtually identical results and if, for example, $\rho = 12$ cm, the curvature produces a significant effect only at C-band frequencies and above.

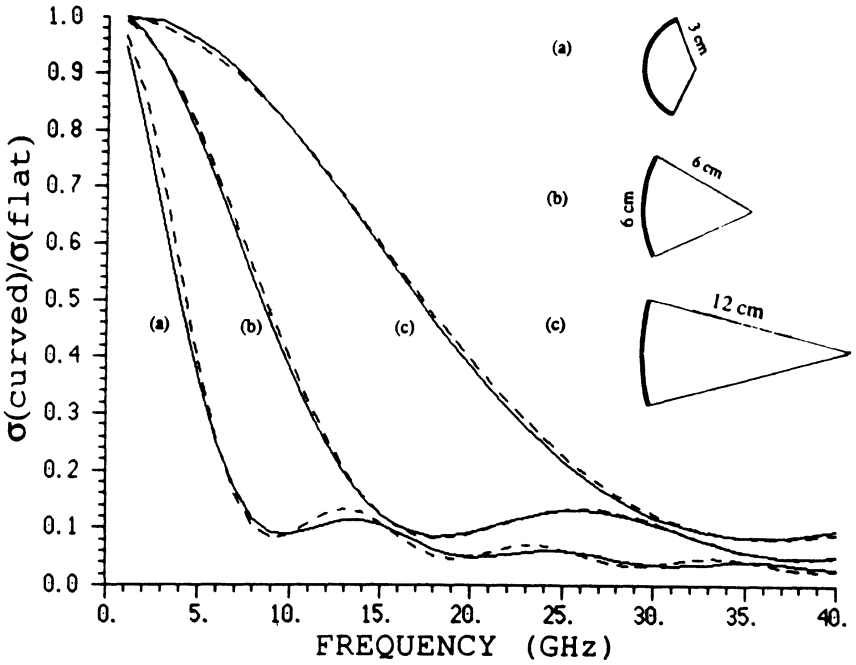

Figure 11. Normal incidence RCS reduction versus frequency due to the one dimensional curvature of a rectangular section of a leaf with $Mg = 0.7$ and $\tau = 0.5$ mm for three different radii of curvature using the numerical (9) (—) and analytical (15) (---) expressions.

6. CONCLUSIONS

The resistive sheet model in conjunction with the physical optics approximation which was previously shown [3] to accurately predict the backscattering cross section of a planar leaf has now been extended to the case of a curved leaf. For a rectangular section of a leaf curved in one and two dimensions, the physical optics expression for the backscattered field as a function of the angle of incidence was evaluated numerically and by a stationary phase approximation. The latter leads to simple analytical expressions for the cross section reduction produced by the curvature. Numerical results based on the two methods are virtually identical over a wide range of incidence angles and in excellent agreement with measured X-band data for rectangular sections of coleus leaves applied to surfaces of styrofoam cylinders and spheres of different radii. As a result of these comparisons, it is concluded that the curvature effect is accurately simulated by a multiplicative factor involving a Fresnel integral whose argument is a function of the relevant leaf dimension, the radius of curvature, the frequency, and the angle of incidence, but independent of the material properties of the leaf.

APPENDIX: FLAT PLATE ANALYSIS

To illustrate the application of the formulas in Section 2, consider a rectangular resistive plate occupying the region $-a/2 < \eta < a/2$, $-b/2 < \zeta < b/2$ of the plane $\zeta = 0$ and illuminated by the plane wave (2) as shown in Fig. 1. Since

there is only an electric current induced in the plate, the scattered field can be attributed to an electric Hertz vector $\overline{\pi}$. In the backscattering direction the far field expression for $\overline{\pi}$ is

$$\overline{\pi}(\overline{r}) = \frac{e^{ikr}}{kr}\frac{iZ}{4\pi}\iint \overline{J}(\eta,\zeta)e^{ik\eta\sin\phi}\,d\eta d\zeta$$

where the integration is over the illuminated surface of the plate, and if the physical optics approximation is employed, it is a trivial matter to determine $\overline{\pi}$. From (3)

$$\begin{aligned}\overline{\pi}(\overline{r}) &= \frac{e^{ikr}}{kr}\frac{i}{2\pi}\int_{-a/2}^{a/2}\int_{-b/2}^{b/2}\left\{\hat{\eta}\sin\alpha\,\Gamma_H(\phi)+\hat{\zeta}\cos\alpha\cos\phi\,\Gamma_E(\phi)\right\}e^{2ik\eta\sin\phi}\,d\eta d\zeta \\ &= \frac{e^{ikr}}{kr}\frac{iab}{2\pi}\left\{\hat{\eta}\sin\alpha\,\Gamma_H(\phi)+\hat{\zeta}\cos\alpha\cos\phi\,\Gamma_E(\phi)\right\}\frac{\sin U}{U} \qquad (A.1)\end{aligned}$$

where

$$U = ka\sin\phi \qquad (A.2)$$

and the backscattered far field amplitude is

$$\overline{S} = \frac{ik^2ab}{2\pi}\left\{(\hat{\xi}\sin\phi+\hat{\eta}\cos\phi)\sin\alpha\,\Gamma_H(\phi)+\hat{\zeta}\cos\alpha\,\Gamma_E(\phi)\right\}\cos\phi\frac{\sin U}{U} \qquad (A.3)$$

In terms of $\overline{S}$ the like-polarized backscattering cross section is

$$\sigma = \frac{\lambda^2}{\pi}\left|(\hat{\xi}\sin\alpha\sin\phi+\hat{\eta}\sin\alpha\cos\phi+\hat{\zeta}\cos\alpha)\cdot\overline{S}\right|^2$$

and the cross-polarized cross section is

$$\sigma_{\text{cross}} = \frac{\lambda^2}{\pi}\left|(\hat{\xi}\cos\alpha\sin\phi+\hat{\eta}\cos\alpha\cos\phi-\hat{\zeta}\sin\alpha)\cdot\overline{S}\right|^2$$

Thus

$$\sigma = 4\pi\left|\frac{ab}{\lambda}\left\{\sin^2\alpha\,\Gamma_H(\phi)+\cos^2\alpha\,\Gamma_E(\phi)\right\}\cos\phi\frac{\sin U}{U}\right|^2 \qquad (A.4)$$

and

$$\sigma_{\text{cross}} = 4\pi\left|\frac{ab}{\lambda}\sin\alpha\cos\alpha\left\{\Gamma_H(\phi)-\Gamma_E(\phi)\right\}\cos\phi\frac{\sin U}{U}\right|^2 \qquad (A.5)$$

and we observe that the cross-polarized return vanishes if at least one of $\sin\alpha$, $\cos\alpha$, or $\cos\phi$ is zero or $\Gamma_E(\phi)=\Gamma_H(\phi)$. This last condition is satisfied for a perfectly conducting plate.

The above example corresponds to the rotation of the direction of incidence in the $\xi\eta$-plane and is equivalent to the rotation of the plate through an angle ϕ about the ζ-axis with the illumination fixed in space. A more general situation is that in which the plate is first tilted back through an angle β (see Fig. $A.1$) prior to rotation. In terms of a rotated coordinate system ξ',η',ζ' where $\hat{\xi}' = \hat{\xi}\cos\beta+\hat{\zeta}\sin\beta$, $\hat{\eta}'=\hat{\eta}$, $\hat{\zeta}' = -\hat{\xi}\sin\beta+\hat{\zeta}\cos\beta$, the plate now occupies $-a/2 < \eta' < a/2$, $-b/2<\zeta'<b/2$, and the incident electric field is

$$\overline{E}^i = (\hat{\xi}\sin\alpha\sin\phi+\hat{\eta}\sin\alpha\cos\phi+\hat{\zeta}\cos\alpha)e^{-ik(\xi'\cos\beta\cos\phi-\eta'\sin\phi-\zeta'\sin\beta\cos\phi)}$$

Since the unit vector normal to the plate is $\hat{\xi}'$, the physical optics expression for the current that would be induced if the plate were perfectly conducting is

$$\overline{J}_{pc} = 2Y \left\{ -\hat{\xi} \cos\alpha \sin\beta \cos\phi + \hat{\eta}(\sin\alpha \cos\beta + \cos\alpha \sin\beta \sin\phi) + \hat{\zeta} \cos\alpha \cos\beta \cos\phi \right\} e^{ik(\eta' \sin\phi + \zeta' \sin\beta \cos\phi)}$$

which can be written as

$$\overline{J}_{pc} = 2Y \left\{ (\sin\alpha \cos\beta \sin\phi + \cos\alpha \sin\beta)\hat{\eta}_1 - (\sin\alpha \sin\beta - \cos\alpha \cos\beta \sin\phi) \cdot \cos\beta \cos\phi \, \hat{\zeta}_1 \right\} P e^{ik(\eta' \sin\phi + \zeta' \sin\beta \cos\phi)}$$

where

$$P = (1 - \cos^2\beta \cos^2\phi)^{-\frac{1}{2}}$$

and

$$\hat{\eta}_1 = P(-\hat{\xi} \sin^2\beta \cos\phi + \hat{\eta} \sin\phi + \hat{\zeta} \sin\beta \cos\beta \cos\phi)$$
$$\hat{\zeta}_1 = P(-\hat{\xi} \sin\beta \sin\phi - \hat{\eta} \sin\beta \cos\phi + \hat{\zeta} \cos\beta \sin\phi)$$

are, respectively, unit vectors in and perpendicular to the plane of incidence, lying in the plane of the plate. The current induced in the resistive plate is therefore

$$\overline{J} = 2Y \left\{ (\sin\alpha \cos\beta \sin\phi + \cos\alpha \sin\beta)\Gamma_H(\phi_1)\hat{\eta}_1 - (\sin\alpha \sin\beta - \cos\alpha \cos\beta \sin\phi) \cdot \cos\beta \cos\phi \, \Gamma_E(\phi_1)\hat{\zeta}_1 \right\} P e^{ik(\eta' \sin\phi + \zeta' \sin\beta \cos\phi)} \qquad (A.6)$$

where ϕ_1 is the angle between the negative of the incident field direction and the normal to the plate, i.e., $\cos^{-1}(\cos\beta \cos\phi)$.

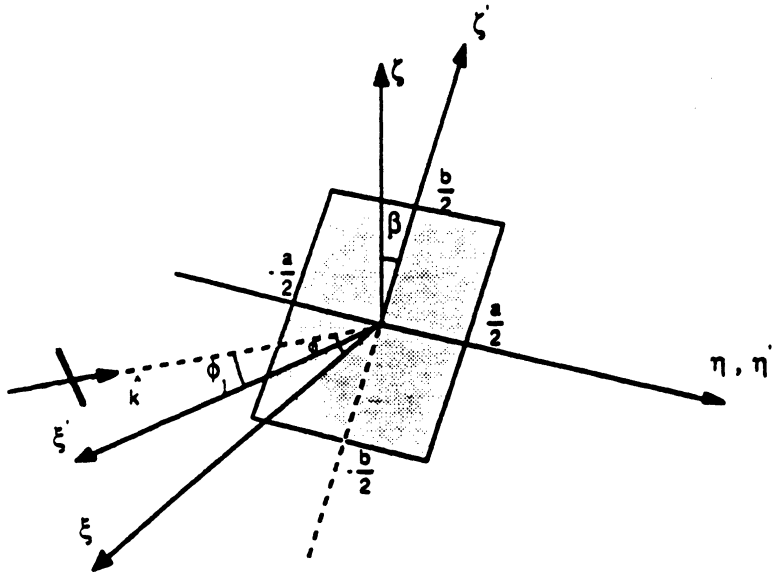

Figure *A*.1. Geometry for the scattering of a plane wave by a tilted resistive sheet.

The Hertz vector defining the backscattered field is

$$\overline{\pi}(\overline{r}) = \frac{e^{ikr}}{kr}\frac{iZ}{4\pi}\int_{-a/2}^{a/2}\int_{-b/2}^{b/2}\overline{J}(\eta',\zeta')e^{ik(\eta'\sin\phi+\zeta'\sin\beta\cos\phi)}\,d\eta'd\zeta'$$

and when the integration is performed we obtain

$$\overline{\pi}(\overline{r}) = \frac{e^{ikr}}{kr}\frac{iab}{2\pi}\Big[(\sin\alpha\cos\beta\sin\phi+\cos\alpha\sin\beta)\Gamma_H(\phi_1)\hat{\eta}_1-(\sin\alpha\sin\beta - \cos\alpha\cos\beta\sin\phi)\cos\beta\cos\phi\,\Gamma_E(\phi_1)\hat{\zeta}_1\Big]\,P\frac{\sin U}{U}\frac{\sin V}{V}$$

where U is given in $(A.2)$ and

$$V = kb\sin\beta\cos\phi$$

The resulting expression for the backscattered far field amplitude is

$$\begin{aligned}\overline{S} = \frac{ik^2ab}{2\pi}\Big[&(\hat{\xi}\sin\phi+\hat{\eta}\cos\phi)\Big\{\sin\alpha\Big[\cos^2\beta\sin^2\phi\,\Gamma_H(\phi_1)+\sin^2\beta\,\Gamma_E(\phi_1)\Big]\\&+\cos\alpha\sin\beta\cos\beta\sin\phi\,[\Gamma_H(\phi_1)-\Gamma_E(\phi_1)]\Big\}\\&+\hat{\zeta}\Big\{\cos\alpha\Big[\sin^2\beta\,\Gamma_H(\phi_1)+\cos^2\beta\sin^2\phi\,\Gamma_E(\phi_1)\Big]\\&+\sin\alpha\sin\beta\cos\beta\sin\phi\,[\Gamma_H(\phi_1)-\Gamma_E(\phi_1)]\Big\}\Big]P^2\cos\beta\cos\phi\frac{\sin U}{U}\frac{\sin V}{V}\end{aligned} \tag{A.7}$$

and we note that this reduces to $(A.3)$ when $\beta = 0$. The backscattering cross sections are

$$\sigma = 4\pi\left|\frac{ab}{\lambda}\Big\{(\sin\alpha\cos\beta\sin\phi+\cos\alpha\sin\beta)^2\Gamma_H(\phi_1)+(\sin\alpha\sin\beta - \cos\alpha\cos\beta\sin\phi)^2\Gamma_E(\phi_1)\Big\}P^2\cos\beta\cos\phi\frac{\sin U}{U}\frac{\sin V}{V}\right|^2 \tag{A.8}$$

and

$$\sigma_{\text{cross}} = 4\pi\left|\frac{ab}{\lambda}(\sin\alpha\cos\beta\sin\phi+\cos\alpha\sin\beta)(\sin\alpha\sin\beta-\cos\alpha\cos\beta\sin\phi)\cdot\Big\{\Gamma_H(\phi_1)-\Gamma_E(\phi_1)\Big\}P^2\cos\beta\cos\phi\frac{\sin U}{U}\frac{\sin V}{V}\right|^2 \tag{A.9}$$

As required, these reduce to $(A.4)$ and $(A.5)$ when $\beta = 0$, and for all β the cross-polarized return vanishes for a perfectly conducting plate. A comparison with measured data for a leaf is given in Section 5.

ACKNOWLEDGMENTS

This work was supported by NASA Grant NAG5-480, NASA/GSFC, Beltsville, MD.

The Editor thanks C. Matzler, R. E. McIntosh, and Ari Sihvola and three anonymous Reviewers for reviewing the paper.

REFERENCES

1. LeVine, D. M., A. Schneider, R. H. Lang, and H. G. Carter, "Scattering from thin dielectric disks," *IEEE Trans. Antennas Propagat.,* Vol. AP–33, No. 12, 1410–1413, 1985.
2. Borel, C. C., and R. E. McIntosh, "A backscattering model for various foliated deciduous tree types at millimeter wavelengths," *Proc. of IEEE Geosci. Remote Sens. Symp.,* Zurich, 8–11 Sept. 1986.
3. Senior, T. B. A., K. Sarabandi, and F. T. Ulaby, "Measuring and modeling the backscattering cross section of a leaf," *Radio Science,* Vol. 22, 1109–1116, 1987.
4. Ulaby, F. T., and M. El-Rayes, "Microwave dielectric spectrum of vegetation, Part II – Dual dispersion method," *Proc. of IEEE Geosci. Remote Sensing,* Vol. GE–25, 550–557, 1987.
5. Liepa, V. V., E. F. Knott, and T. B. A. Senior, "Scattering from two-dimensional bodies with absorber sheets," *Radiation Laboratory Report No. 011769–2–T,* The University of Michigan, May 1974.

Kamal Sarabandi was born in Tehran, Iran on November 4, 1956. He received the B.S. degree in Electrical Engineering from Sharif University of Technology, Tehran, Iran, in 1980. From 1980 to 1984 he worked as a microwave engineer in Iran's Telecommunication Research Center. In Fall 1984 he joined the graduate program in electrical engineering at the University of Michigan and received the M.Sc. degree in 1986. Currently he is working toward the Ph.D. degree in the area of microwave remote sensing.

Thomas B. A. Senior received the M.Sc. degree from the University of Manchester in 1950 and the Ph.D. degree from Cambridge University in 1954. From 1952 to 1957 he was at the Royal Radar Establishment in Malvern, England, and joined the University of Michigan in 1957. Having served as the Director of the Radiation Laboratory for 11 years, he is now Professor of Electrical Engineering and Computer Science, and Associate Chairman of the Department. He is Chairman of Commission B of the International Union of Radio Science, Fellow of the IEEE, and member of numerous technical and honorary societies.

Fawwaz T. Ulaby received his degree in Electrical Engineering from the University of Texas, Austin, in 1968. From 1968 to 1984, he was with the Electrical Engineering Department at the University of Kansas, where he was the J. L. Constant Distinguished Professor and Director of the Remote Sensing Laboratory. He is currently Professor of Electrical Engineering and Computer Science, the University of Michigan, Ann Arbor. His current research interests involve microwave propagation and active and passive microwave remote sensing.

Microwave Attenuation Properties of Vegetation Canopies

FAWWAZ T. ULABY, FELLOW, IEEE, AND EDWARD A. WILSON, MEMBER, IEEE

Abstract—A major impediment to the understanding and modeling of propagation through and backscattering and emission from vegetation canopies has been the lack of canopy attenuation data as a function of frequency, incidence angle, and polarization configuration. This paper presents the results of attenuation experiments conducted for canopies of winter wheat and soybeans in the late spring and early summer of 1984. Attenuation data were acquired at 1.55, 4.75, and 10.2 GHz for horizontal and vertical polarizations at incidence angles near 20° and 50°. In addition, wheat decapitation and soybean defoliation experiments were conducted to evaluate the relative importance of different canopy constituents (such as heads, leaves, and stalks) to the total canopy attenuation. The measured data were compared to calculations based on a model that treats the stalks as parallel elements of a uniaxial crystal and the leaves and branches as randomly oriented disks and needles, respectively. Very good agreement was obtained between theory and experimental observations for the soybean canopy for both polarizations and for the wheat canopy for vertical polarization; however, the model consistently underestimated wheat attenuation (relative to the data) for horizontal polarization. This deficiency of the model is attributed to the fact that it considers all the stalks to be vertically oriented, whereas in reality the stalks exhibit an orientation distribution, although it is centered around the vertical direction.

I. Introduction

AT MICROWAVE frequencies, a vegetation canopy is a highly inhomogeneous medium; moreover, because the scattering elements have a nonuniform orientation distribution, the canopy is likely to exhibit nonisotropic attenuation properties. In many types of canopies, the stalks may comprise the overwhelming majority of the biomass in the canopy, which suggests that an incident radar wave would be differentially attenuated by the canopy, depending on the direction of the incident electric field relative to the orientation of the stalks. The propagation properties of a vegetation canopy play a central role in modeling both the scattering and emission behavior of the canopy. Despite the critical need for such information, very few investigations have been conducted to date to determine the extinction properties of vegetation canopies on the basis of either their constituent parts (leaves, stalks, fruit) or as a whole. In 1970, Story *et al.* [1] reported that horizontal propagation (at 16 GHz) through a wheat canopy experienced higher attenuation for vertical polarization (E-field parallel to stalks) than for horizontal polarization (E-field perpendicular to stalks) and that the attenuation was higher by about 6 dB for propagation through the top layer (containing the wheat heads) than for the layer containing stalks only.

More recently, Ulaby and Jedlicka [2] reported the results of canopy attenuation measurements at 10.2 GHz, vertical polarization, and an angle of incidence of 56° relative to nadir. They observed that a soybean canopy, for example, may vary from appearing quasi-transparent to quasi-opaque, depending on its wet biomass. The variation of the canopy loss factor with polarization angle was examined by Le Toan *et al.* [3] in a laboratory setting. They observed that when a layer of standing wheat plants is illuminated along the horizontal direction (broadside), the loss factor of the layer varies from about 23 dB for vertical polarization down to about 1 dB for horizontal polarization. The results of this experiment, which was conducted at *X*-band ($\simeq$ 10 GHz), point out the important role that polarization can play in both the propagation through and backscattering from a vegetation canopy. Similar conclusions were reached by Allen and Ulaby [4] on the basis of attenuation measurements of wheat canopies and a uniaxial crystal model which was used to account for the polarization dependence of the canopy extinction coefficient.

This study extends the results of the preceding investigations by examining the canopy loss factor at three microwave frequencies (1.55, 4.75, and 10.2 GHz), for both horizontal and vertical polarizations, at two widely separated incidence angles, and at more than one stage of growth. In addition, both a wheat-decapitation experiment and a soybean-defoliation experiment were conducted in an attempt to evaluate the relative contributions of the various canopy constituents to the total loss factor of the canopy.

II. Experimental Procedure

The source of the electromagnetic energy used in these measurements was a set of *L*-, *C*- and *X*-band FM-CW radars mounted on a boom truck; their center frequencies were 1.55, 4.75, and 10.2 GHz, respectively. The radars were mounted on a positioner to allow flexibility in the selection of incidence angles. The receiver, which was placed on the ground surface beneath the canopy, consisted of antennas for *L*-, *C*-, and *X*-band, amplifiers for *C*-band and *X*-band, a detector, a wide-dynamic-range power meter, and a chart recorder. The antennas, amplifiers, and detector were mounted on a "sled," which was

Manuscript received February 1, 1985; revised June 1, 1985.

F. T. Ulaby is with the Department of Electrical Engineering and Computer Science, University of Michigan, Ann Arbor, MI 48109.

E. A. Wilson is with the North Central Association of Colleges and Schools.

0196-2892/85/0900-0746$01.00 © 1985 IEEE

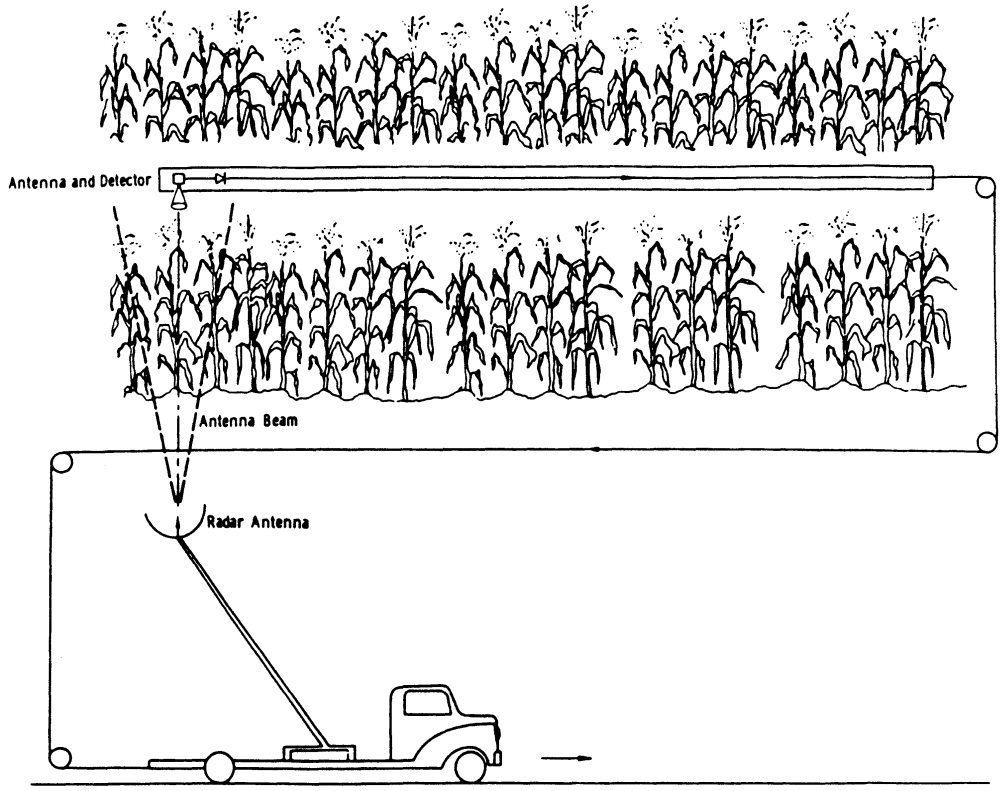

Fig. 1. Configuration used to measure canopy attenuation.

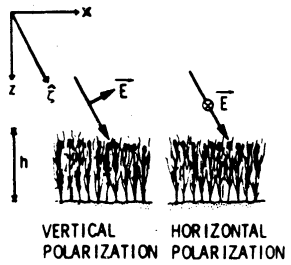

Fig. 2. Geometry of the problem.

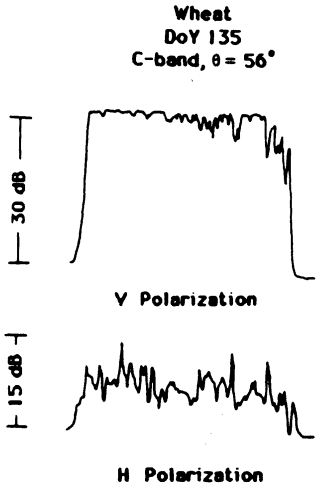

Fig. 3. Records of the canopy loss factor L of a wheat canopy for horizontal and vertical polarization at 4.75 GHz and $\theta = 56°$.

pulled along fiberglass rails in synchronism with the boom truck. Fig. 1 illustrates the setup, and Fig. 2 delineates the geometry of the problem. The L-band antenna was a microstrip patch antenna, and the C- and X-band antenna was a 4–18 GHz quad-ridged horn. The transmitting antennas had narrow beamwidths (3° at 10.2 GHz, 5° at 4.75 GHz, and 9° at 1.55 GHz) and the receiving antennas had wide beamwidths (greater than 40°). The C-band and X-band measurements required separate battery-powered amplifiers with approximately 25 dB of gain to ensure that signals remained above the noise floor under maximum attenuation conditions. The dynamic range of the detector and power-meter combination was 50 dB. The power meter had an analog output, which was used to drive the chart recorder.

Vegetation was cleared at each end of the fiberglass rails to provide a free-space reference for the measurements. A standard measurement included approximately 6 m of vegetation. The recorded data were digitized into intervals corresponding to approximately 14 cm and then averaged. In all cases, the 99-percent confidence limits (in decibels) were less than ± 0.15 of the mean value (in decibels) estimated from the digitized record. Fig. 3 shows sample records for vertical (V) and horizontal (H) polarizations for a wheat canopy measured on day-of-year (DoY) 135. The mean values of canopy loss are 27.4 dB for V polarization and 9.4 dB for H polarization. Similar records are shown in Fig. 4 to illustrate the role of frequency: the mean values of canopy loss increased from 7.4 dB at 1.55 GHz to 36.0 dB at 10.2 GHz.

III. Wheat Data

The wheat measurements were conducted at two widely separated sites within a single wheat field. Site W_1 was used for the frequency, angle, and polarization studies,

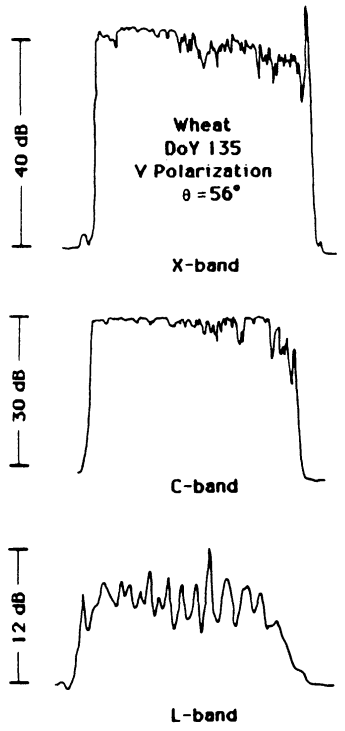

Fig. 4. Records of the canopy loss factor L for wheat at 1.55, 4.75, and 10.2 GHz.

whereas site W_2 was used for a wheat decapitation experiment. Attenuation measurements were performed at site W_1 on days 135 and 158 and at site W_2 on DoY 150. A summary of the canopy parameters measured in support of the microwave measurements is given in Table I.

In all cases, the quantity measured is the canopy loss factor $L_i(\theta)$

$$L_i(\theta) = 10 \log \left[\exp \left(\int_0^{h \sec \theta} \kappa_i(\zeta)\, d\zeta \right) \right] \text{ dB}$$

$$= 4.34 \int_0^{h \sec \theta} \kappa_i(\zeta), \qquad i = \text{V or H polarization}$$

where $\kappa_i(\text{Np m}^{-1})$ is the ith-polarized extinction coefficient for propagation along the ζ direction (see Fig. 2), and h is the height of the canopy. Since $\zeta = z \sec \theta$

$$L_i(\theta) = 4.34 \sec \theta \int_0^h \kappa_i(\theta, z)\, dz.$$

To factor out the dependence of $L_i(\theta)$ on the excess path length resulting from the oblique incidence, we define the modified loss factor as

$$L_i' = \frac{L_i}{\sec \theta} = 4.34 \int_0^h \kappa_i(\theta, z)\, dz.$$

For a uniform canopy with isotropic attenuation properties, κ_i is independent of both polarization and incidence angle, which means that L_i' would be similarly independent.

A. Frequency Behavior

The measured frequency variation of L_i' is shown in Fig. 5. We note the following observations:

1) If the wheat canopy had been an isotropic layer, the the four frequency plots would have been coincident. Th fact that L_i' is as much as one order of magnitude larger $\theta = 56°$ than at $\theta = 24°$ in some cases (4.75 GHz, polarization) is a clear indication that the canopy is highl anisotropic.

2) At $\theta = 24°$, the differences between L_H' and L_V' ar small and are statistically insignificant at all three fre quencies and for both canopy conditions.

3) At $\theta = 56°$, L_V' is always larger than L_H', and fc reasons that are not immediately obvious, the differenc is largest at C-band.

The observed variation of L_i' with θ is consistent wit the assumption that the anisotropic behavior is related t the vertical structure of the stalks. For example, at θ = 0°, L_V' should be equal to L_H'. As θ increases, the electri field vector maintains its orientation relative to the stalks orientation for H polarization, but for V polarization th component of the electric field vector parallel to the ver tical stalks increases as sin θ.

B. Temporal Variations

Between DoY 135 and DoY 158, the canopy increase in height from 0.73 to 1.16 m and acquired new heads each approximately 8 cm in length. The green-leaf are index (LAI), however, decreased from 8.0 to 4.0, and th plant water content decreased from 82.9 to 73.3 percer (by wet weight). The attenuation properties of the whea canopy on the preceding two dates are compared in Fig 6. We observe that for all three frequencies and both pc larizations, L_i either remains constant or decreases i magnitude between days 135 and 158, even though canop height increased by a factor of 1.6 during this perioc Clearly, the increase in height is of minor consequence (i terms of its effect on canopy loss) relative to the effects c the decrease in LAI by a factor of two and the presenc of the heads on DoY 158 (and their absence on the earlie date).

C. Wheat Decapitation Experiment

Fig. 7 compares the canopy loss factor L_i as measure before and after the wheat canopy was decapitated. Be cause of the uneven height distribution of the wheat plants the decapitation process not only cut off the wheat heads it also cut off part of the stalks. As a result, the decap tated wheat canopy was only 70 cm in height (compare to 111 cm prior to decapitation). The change in loss as result of decapitation is insignificant at L-band and is mo significant at X-band for V polarization.

IV. Soybean Data

The soybean measurements were conducted at a singl site on days 181 and 188. Comparing the canopy data in dicates that all parameters varied by less than 20 percent including the attenuation measurements. Hence, only th canopy data acquired on DoY 188 are given in Table II and the corresponding microwave data are shown in Fig 8. The general behavior of L_i' is similar to that observe

TABLE I
SUMMARY OF WHEAT CANOPY PARAMETERS

Day of Year	135	150	158
Mean Canopy Height (m)	0.73	1.11 (0.70 Decapitated)	1.16
Head Length (m)	--	0.08	0.08
Row Spacing (m)	0.15	0.15	0.15
Density (stems/m^2)	1694	1027	1694
Top 1/3 Leaf H_2O	80.0% (1.46 kg/m^2)	68.9% (0.18 kg/m^2)	72.6% (0.46 kg/m^2)
Mid 1/3 Leaf H_2O	80.2% (0.71 kg/m^2)	52.1% (0.15 kg/m^2)	53.7% (0.15 kg/m^2)
Low 1/3 Leaf H_2O	81.1% (0.11 kg/m^2)	8.3% (0.00 kg/m^2)	47.8% (0.07 kg/m^2)
Top 1/3 Stalk H_2O	86.1% (1.19 kg/m^2)	65.8% (0.41 kg/m^2)	75.7% (0.87 kg/m^2)
Mid 1/3 Stalk H_2O	84.1% (1.56 kg/m^2)	69.0% (0.75 kg/m^2)	78.2% (1.49 kg/m^2)
Low 1/3 Stalk H_2O	83.8% (1.46 kg/m^2)	63.4% (0.43 kg/m^2)	72.9% (1.00 kg/m^2)
Head H_2O	--	82.2% (1.11 kg/m^2)	72.5% (1.13 kg/m^2)
L123 Leaf H_2O	80.1% (2.28 kg/m^2)	55.2% (0.33 kg/m^2)	64.0% (0.69 kg/m^2)
L123 Stalk H_2O	84.6% (4.21 kg/m^2)	66.6% (1.59 kg/m^2)	75.9% (3.36 kg/m^2)
Whole Plant H_2O	82.9% (6.49 kg/m^2)	69.9% (3.03 kg/m^2)	73.3% (5.18 kg/m^2)
Leaf Area Index	8.0	3.6	4.0
Growth Stage*	23 (Flag Leaf Visible)	34 (Kernels Formed)	42 (Soft Dough)
Leaf Thickness (mm)	0.15	0.15	0.15
Stem Diameter (mm)	2.00	2.00	2.00
Look Direction	Perpendicular to Rows	Perpendicular to Rows	Perpendicular to Rows
Receiver Height (m)	0.10	0.22	0.10

*LACIE Crop Inventory System

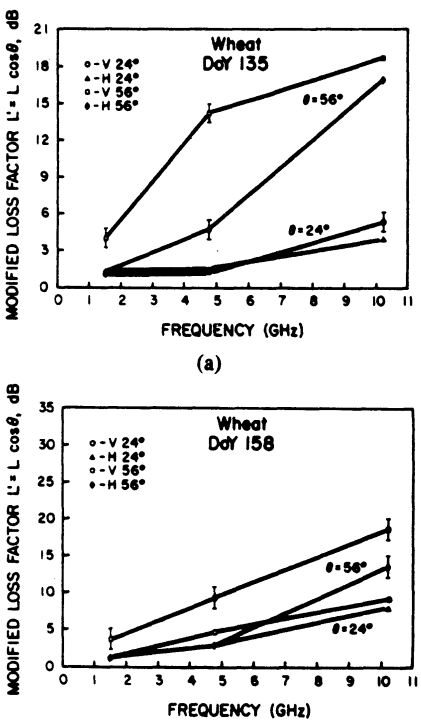

Fig. 5. Plots of the modified loss factor $L' = L \cos \theta$ for wheat on (a) DoY 135 and (b) DoY 158.

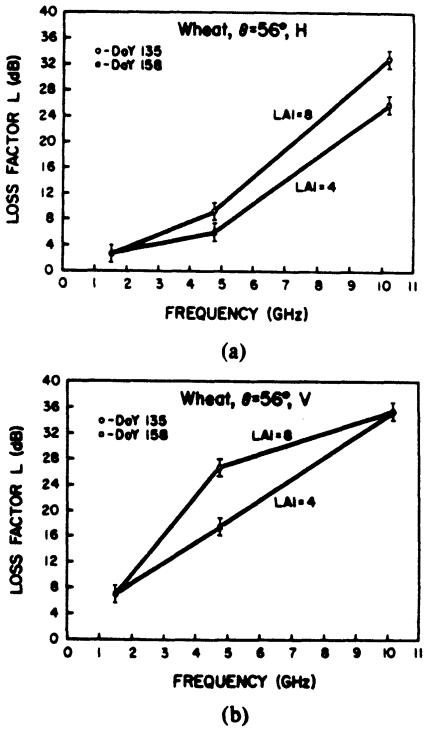

Fig. 6. Comparison of the wheat loss factor data for DoY 135 and DoY 158 for (a) horizontal polarization and (b) vertical polarization.

earlier for the wheat canopy (Fig. 5), although the role of polarization is not as outstanding as it was for wheat.

Shortly after the attenuation measurements were made on DoY 188, the soybean canopy was defoliated (by cutting and removing the leaves) and another set of measurements was made. The change in canopy loss due to defoliation was negligible at *L*-band (Fig. 9), somewhat significant for H polarization at *C*-band, and very significant for H polarization at *X*-band. Based on these data, we arrived at the following conclusions:

1) For V polarization, the leaves are secondary in importance to the stalks and branches of the soybean canopy. Assuming the total attenuation to be the algebraic sum of

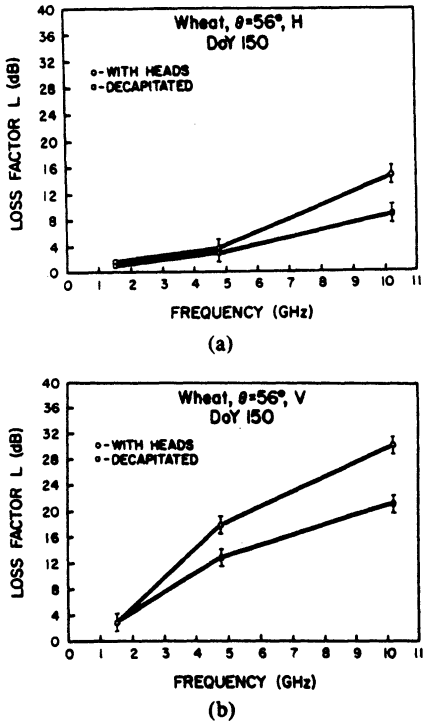

Fig. 7. Comparison of the wheat loss factor data before and after decapitation for (a) horizontal polarization and (b) vertical polarization.

TABLE II
SUMMARY OF SOYBEAN CANOPY PARAMETERS

Day of Year	188
Mean Canopy Height (m) - Low Angle (16°)	0.65
Mean Canopy Height (m) - High Angle (52°)	0.61 (0.54 Defoliated)
Row Spacing (m)	0.77
Row Width (m)	0.64
Density (plants/m^2)	42.0 (51.6)*
Leaf H_2O	72.1%* (0.62 kg/m^2)*
Main Stem H_2O	78.5%* (0.58 kg/m^2)*
Secondary Stem H_2O	81.7%* (0.60 kg/m^2)*
Whole Plant H_2O	77.2%* (1.80 kg/m^2)*
Leaf Area Index (m^2/m^2)	4.6 (5.5)*
Mean Main Stem Length (m)	0.44
Mean Secondary Stem Length (m)	0.22
Mean Secondary Stems per plant	11.1
Growth Stage**	32 (Full Bloom)
Leaf Thickness (mm)	0.2
Main Stem Diameter (mm)	5.6
Secondary Stem Diameter (mm)	1.9
Look Direction	Perpendicular to Rows
Receiver Height (m)	0.13

* Vegetated portion of field only (percent cover =83%)
** LACIE Crop Inventory System

an attenuation component due to the leaves and another due to the support structure (i.e., ignoring the attenuation loss resulting from the interaction between the leaves and the branches), the defoliation exercise resulted in a reduction of attenuation by about 10 percent at *L*-band and *C*-band and 30 percent at *X*-band.

2) For H polarization, the loss contribution attributed

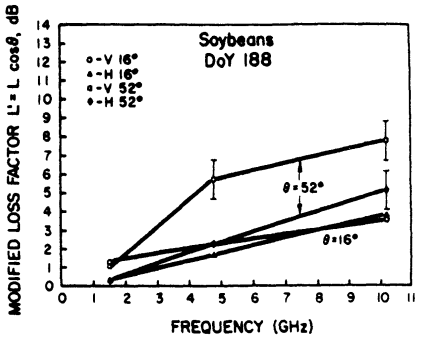

Fig. 8. Plots of the modified loss factor $L' = L \cos \theta$ for soybeans on Do' 188.

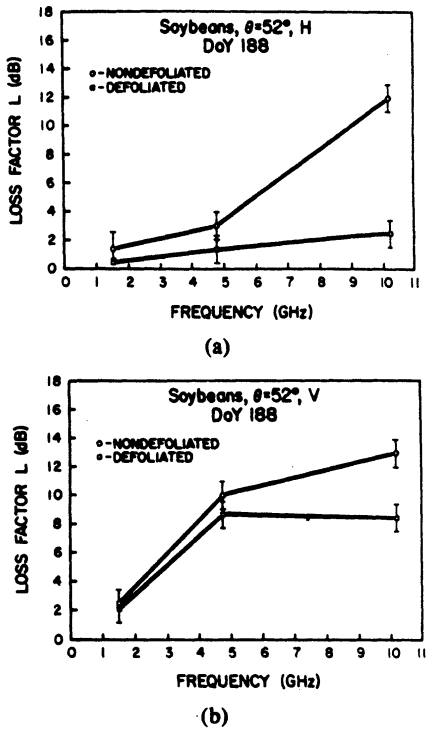

Fig. 9. Comparison of the soybean loss factor data before and after defo liation for (a) horizontal polarization and (b) vertical polarization.

to leaves was about 50 percent of the total loss at *L*-band and *C*-band and 70 percent of the total loss at *X*-band.

V. ATTENUATION MODELS

A vegetation canopy is a dielectric mixture consisting of discrete dielectric inclusions (such as leaves, stalks, and fruit) distributed in a host material (air). Because the dielectric inclusions are nonspherical, the canopy is an inhomogeneous anisotropic medium. Propagation through such a medium is subject to both absorption and scattering losses.

Because of the highly complex shapes and distribution of the canopy inclusions, it is very difficult to develop a deterministic model for wave propagation through a vegetation canopy. A probabilistic approach may be used when sufficient knowledge is available about the sizes, shapes and orientation distributions of the inclusions. In most situations, such information is not available, however. Hence we shall simplify the solution by making the following assumptions:

TABLE III
SUMMARY OF ESTIMATED WHEAT LEAF AND STALK DIELECTRIC CONSTANTS ON DAY OF YEAR 158

Plant Part	L-Band	C-Band	X-Band
Stalk	27-j3	30-j10	24-j11
Leaf	27-j10	17-j5	14-j7

1) The vegetation canopy may be treated in terms of an equivalent medium with homogeneous dielectric properties. The usual approach to estimating the equivalent dielectric constant of the canopy involves the use of dielectric mixing models. Such models usually are based on the assumption that the inclusions are much smaller than a wavelength in size. Since this condition is often violated at microwave frequencies, the validity of the results is open to question.

2) Scattering losses are ignored. This is a consequence of the preceding assumption. Being mostly water, vegetation material is highly absorptive, and absorption is likely to be the dominant loss factor at decimeter wavelengths; however, at *X*-band, no information is available either to support or refute such an assumption.

3) If the canopy consists of more than one type of inclusion, it will be assumed that there is no interaction between the different types of inclusions; thus, the absorption loss for each may be calculated separately and then summed to obtain the total canopy attenuation.

Starting with these assumptions, the following models were developed for the wheat and soybean canopies.

A. Wheat Attenuation Model

Wheat will be modeled as vertical stalks having randomly oriented leaves. Based on the results of the wheat decapitation experiment, the wheat head will be considered part of the stalk. Table III provides a summary of the dielectric constants of the wheat stalks and leaves. These values were established using the dielectric measurements reported in Ulaby and Jedlicka [2] and the moisture content values listed in Table I.

The loss factor of the wheat canopy is taken as the sum (in decibels) of the stalk and leaf loss factors

$$L_i(\theta) = L_i^{st}(\theta) + L^l(\theta) \quad \text{dB}$$

where the superscripts *st* and *l* denote stalk and leaf, respectively, and *i* is either V or H polarization.

1) Vertical Stalk Absorption Loss Factor: The wheat stalks will be modeled as a uniaxial crystal [4]. The model applies to a canopy of thin vertical stalks whose diameter is much smaller than the wavelength λ, where $\lambda = \lambda_0/\sqrt{\epsilon'_{st}}$ is the wavelength in the stalk material, and ϵ'_{st} is its relative permittivity. The applicability of this model therefore depends upon the stalk's diameter, its water content, and the signal wavelength λ_0. Although the model will not be strictly applicable at *X*-band, it will be used to provide an estimate of the stalk absorption loss. Upon adapting the expressions given by Allen and Ulaby [4] to the problem, we have

$$L_i^{st}(\theta) = 8.68\, \alpha_i h \sec\theta \quad \text{dB}$$

$$\alpha_i = \frac{2\pi}{\lambda_0} \begin{cases} |\text{Im}\,\{\sqrt{\epsilon_x}\}|, & \text{for } i = \text{H polarization} \\ [|\text{Im}\,\{\sqrt{\epsilon_x}|\}\cos^2\theta & \\ \quad + |\text{Im}\,\{\sqrt{\epsilon_z}\}|\sin^2\theta], & \text{for } i = V \end{cases}$$

$$\epsilon_z = 1 + V_{st}(\epsilon_{st} - 1)$$

$$\epsilon_x = 1 + 2V_{st}\left(\frac{\epsilon_{st} - 1}{\epsilon_{st} + 1}\right)$$

where ϵ_{st} is the stalk's complex dielectric constant, and V_{st} is the volume fraction of the stalks in the canopy (which can be calculated from the canopy information given in Table I).

2) Random Leaf Absorption Loss Factor: Assuming the leaves to be randomly distributed in both location and orientation, we arrive at the following approximate expression [5]:

$$L^l(\theta) = 8.68\left(\frac{2\pi}{3\lambda_0} V_l \epsilon_l'' h \sec\theta\right)$$

where V_l is the volume fraction of the leaves in the canopy, and ϵ_l'' is the dielectric loss factor of the leaf material.

3) Comparison With Measurements: The preceding expressions were used in conjunction with the data given in Tables I and III to compute the loss factor $L_i(\theta)$ for i = V and H polarization at $\theta = 24°$ and 56°. Table IV compares the calculated and measured values for DoY 158. The uncertainty ($\pm$) associated with each model-calculated loss value was determined by assuming that, in the worst case, stalk diameter and leaf thickness could be determined within only $\pm$ 20 percent and that the vegetation density and dielectric constant could be determined within $\pm$ 10 percent. The uncertainty associated with the measured values includes a $\pm$ 10 percent estimated accuracy error plus the precision estimates calculated from the digitized records.

An examination of the data reveals overlapping among the bands of the measured and calculated values for all of the V-polarization cases but none of the H-polarization cases. In all cases, the model underestimates the stalk term for H polarization. This is attributed to the assumption that all of the stalks and heads are vertically oriented, whereas a more reasonable assumption would have been that the stalks have a narrow orientation distribution centered around the vertical direction.

Similar observations were noted from analysis of the data for days 135 and 150.

B. Soybean Attenuation Model

The soybean canopy will be modeled as vertical stalks (primary stems), randomly oriented stalks (secondary

TABLE IV
PREDICTED VERSUS OBSERVED ATTENUATION DATA FOR WHEAT ON DAY OF YEAR 158

FREQUENCY (GHz)	POLARIZATION	ANGLE (°)	MODEL L^{st}(dB)	MODEL L^{ℓ}(dB)	MODEL L(dB)	MEASURED L(dB)
1.55	V	24	0.5 ± 0.3	0.6 ± 0.2	1.1 ± 0.5	1.3 ± 0.2
1.55	H	24	0.0 ± 0.0	0.6 ± 0.2	0.6 ± 0.2	1.3 ± 0.3*
4.75	V	24	4.2 ± 2.8	0.9 ± 0.5	5.1 ± 3.3	5.4 ± 1.3
4.75	H	24	0.1 ± 0.1	0.9 ± 0.5	1.0 ± 0.6	3.7 ± 0.8*
10.20	V	24	10.1 ± 6.6	2.9 ± 1.2	13.0 ± 7.8	10.9 ± 2.9
10.20	H	24	0.3 ± 0.2	2.9 ± 1.2	3.2 ± 1.4	9.4 ± 2.1*
1.55	V	56	2.9 ± 1.9	1.5 ± 0.3	4.4 ± 2.2	7.1 ± 1.1
1.55	H	56	0.0 ± 0.0	1.5 ± 0.3	1.5 ± 0.3	2.6 ± 0.9*
4.75	V	56	27.9 ± 18.4	1.6 ± 0.7	29.5 ± 19.1	17.8 ± 1.6
4.75	H	56	0.2 ± 0.2	1.6 ± 0.7	1.8 ± 0.9	6.0 ± 1.3*
10.20	V	56	67.2 ± 43.7	5.0 ± 2.0	72.5 ± 44.7	36.1 ± 3.7
10.20	H	56	0.6 ± 0.4	5.0 ± 2.0	5.6 ± 2.4	26.7 ± 3.6*

*Model and measured bands non-overlapping.

TABLE V
SUMMARY OF ESTIMATED DIELECTRIC CONSTANTS FOR SOYBEANS ON DAY OF YEAR 188

Plant Part	L-Band	C-Band	X-Band
Primary Stem	31-j3	38-j14	30-j15
Secondary Stem	35-j4	40-j15	35-j18
Leaf	27-j10	18-j6	16-j7

TABLE VI
PREDICTED VERSUS OBSERVED ATTENUATION DATA FOR SOYBEANS ON DAY OF YEAR 188

FREQUENCY (GHz)	POLARIZATION	ANGLE (°)	MODEL L^{st}(dB)	MODEL L^{rs}(dB)	MODEL L^{ℓ}(dB)	MODEL L(dB)	MEASURED L(dB)
1.55	V	16	0.0 ± 0.0	0.1 ± 0.1	1.1 ± 0.5	1.2 ± 0.6	2.6 ± 0.5*
1.55	H	16	0.0 ± 0.0	0.1 ± 0.1	1.1 ± 0.5	1.2 ± 0.6	0.8 ± 0.3
4.75	V	16	0.3 ± 0.2	0.7 ± 0.6	2.0 ± 0.9	3.0 ± 1.7	3.8 ± 0.8
4.75	H	16	0.0 ± 0.0	0.7 ± 0.6	2.0 ± 0.9	2.7 ± 1.5	3.6 ± 0.6
10.20	V	16	0.8 ± 0.6	1.7 ± 1.5	5.0 ± 2.2	7.5 ± 4.3	7.8 ± 1.5
10.20	H	16	0.1 ± 0.1	1.7 ± 1.5	5.0 ± 2.2	6.8 ± 2.8	10.9 ± 1.8
1.55	V	52	0.2 ± 0.1	0.1 ± 0.1	1.7 ± 0.8	2.0 ± 1.0	2.6 ± 0.5
1.55	H	52	0.0 ± 0.0	0.1 ± 0.1	1.7 ± 0.8	1.8 ± 0.9	0.7 ± 0.4
4.75	V	52	3.7 ± 2.5	1.0 ± 0.8	3.2 ± 1.4	7.9 ± 4.9	9.9 ± 1.6
4.75	H	52	0.0 ± 0.0	1.0 ± 0.8	3.2 ± 1.4	4.1 ± 2.2	3.1 ± 0.5
10.20	V	52	8.4 ± 6.1	2.5 ± 2.1	7.8 ± 3.5	18.7 ± 11.7	12.5 ± 2.6
10.20	H	52	0.1 ± 0.0	2.5 ± 2.1	7.8 ± 3.5	10.4 ± 5.6	12.1 ± 1.9

*Model and measured bands non-overlapping.

stems), and random leaves. The canopy loss factor is given by

$$L_i(\theta) = L_i^{st}(\theta) + L^{rs}(\theta) + L^{l}(\theta) \quad \text{dB}$$

where $L^{rs}(\theta)$ accounts for the absorption by the secondary stalks and is given by

$$L^{rs}(\theta) = \frac{8.68\pi}{\lambda_0} \epsilon'' h \sec\theta$$

where ϵ'' is the equivalent dielectric loss factor of the canopy attributed to the random stalks. Assuming that the random stalks are thin needles, the Polder-Van Santen

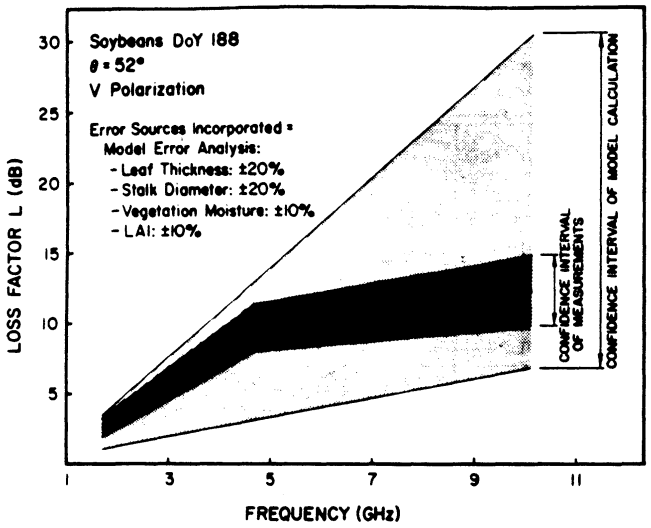

Fig. 10. Comparison of the measured and computed values of the loss factor for soybeans. The vertical bands represent confidence intervals of ±1 standard deviation.

mixing formula [6] gives

$$\epsilon = \epsilon' - j\epsilon'' = 1 + \frac{V_{rs}(\epsilon_{rs} - 1)(5 + \epsilon_{rs})}{3(1 + \epsilon_{rs})}$$

where V_{rs} is the volume fraction of the random stalks in the canopy, and ϵ_{rs} is its dielectric constant. The dielectric constants given in Table V were calculated on the basis of the data in Table II and the dielectric relations reported in Ulaby and Jedlicka [2]. The calculated values of the individual terms of the total loss factor are given in Table VI, where they are compared to the measured values. According to Fig. 10, which displays the same information for V polarization in graphical form, excellent agreement is obtained between the calculated and measured values of the canopy loss factor. We also observe that the models are very sensitive to the model parameters as exemplified by the large extent of the vertical bands associated with the calculated values of the loss factor; the band represents an uncertainty of ±20 percent of the ground-truth parameters around the measured values.

IV. Concluding Remarks

This study has established that vegetation canopies are both highly nonuniform and anisotropic at microwave frequencies. Although such a statement has often appeared in the literature, modelers have frequently ignored the role of the stalks in a canopy and have modeled emission and backscattering as being due to leaves only. The large differences between the vertical- and horizontal-polarization measurements of canopy attenuation clearly indicate that the relative importance of ground emission and backscattering is polarization dependent.

References

[1] A. G. Story, W. H. Johnson, and R. E. Stewart, "Remote measurement of concentration and height of standing grain with microwave energy," *Trans. ASAE*, vol.13, pp. 28-32, 1970.

[2] F. T. Ulaby and R. P. Jedlicka, "Microwave dielectric properties of plant materials," *IEEE Trans. Geosci. Remote Sensing*, vol. GE-22, pp. 406-414, 1984.

[3] T. Le Toan, A. Lopes, and M. Huet, "On the relationships between radar backscattering coefficients and vegetation canopy characteristics," in *1984 IEEE Int. Geosci. Remote Sensing Symp. (IGARSS'84) Dig.* (Strasbourg, France, Aug. 27-30, 1984).

[4] C. T. Allen and F. T. Ulaby, "Modeling the polarization dependence of the attenuation in vegetation canopies," in *1984 IEEE Int. Geosci. Remote Sensing Symp. (IGARSS'84) Dig.* (Strasbourg, France, Aug. 27-30, 1984).

[5] F. T. Ulaby, M. Razani, and M. C. Dobson, "Effects of vegetation cover on the microwave radiometric sensitivity to soil moisture," *IEEE Trans. Geosci. Remote Sensing*, vol. GE-21, pp. 51-61, 1983.

[6] D. Polder and J. H. Van Santen, "The effective permeability of mixtures of solids," *Physics*, vol. 12, pp. 257-271, 1946.

*

Fawwaz T. Ulaby (M'68-SM'74-F'80) was born in Damascus, Syria, on February 4, 1943. He received the B.S. degree in physics from the American University of Beirut, Lebanon, in 1964, and the M.S.E.E. and Ph.D. degrees in electrical engineering from the University of Texas, Austin, in 1966 and 1968, respectively.

Currently, he is a Professor in the Department of Electrical Engineering and Computer Science at the University of Michigan, Ann Arbor. Formerly, he was with the Electrical and Computer Engineering Department at the University of Kansas, where he was J. L. Constant Distinguished Professor. His research interests involve millimeter wave radar, microwave propagation, and active and passive microwave remote sensing. Along with R. K. Moore and A. K. Fung, he is co-author of the three-volume series *Microwave Remote Sensing: Active and Passive* (Addison Wesley/Benjamin Cummings). In addition, he served as a contributor to and co-editor of the second edition of the *Manual of Remote Sensing* (American Society of Photogrammetry).

Dr. Ulaby is a member of Eta Kappa Nu, Tau Beta Pi, and Sigma Xi. In recognition of his contributions to the application of radar to remote sensing in agriculture and hydrology, he was named an IEEE Fellow in 1980. He received the IEEE Geoscience and Remote Sensing Society's Outstanding Service Award in 1982, its Distinguished Service Award in 1983, and was honored as one of the recipients of the IEEE Centennial Medal in 1984. He was a President of the IEEE Geoscience and Remote Sensing Society, currently he is the Executive Editor of the Geoscience and Remote Sensing Society's TRANSACTIONS, 1985-1988, and is the Society's Distinguished Lecturer for 1985. He is also among the recipients of the American Society of Photogrammetry's 1984 Presidential Citations for Meritorious Service. He has received several awards for teaching excellence and service to higher education including the University of Kansas Gould Award in 1973, the Eta Kappa Nu MacDonald Award as an "Outstanding Electrical Engineering Professor in the United States in 1975," and the University of Kansas Chancellor's Award for Excellence in Teaching in 1980.

*

Edward A. Wilson (S'78-M'80) received the B.E.E. and E.E. degrees from Ohio State University, the M.S.E.E. degree from the University of Missouri, and the Ph.D. degree from the University of Kansas.

He has served as a member of the technical staffs of Rockwell International Corporation and RCA Corporation. He was a faculty member at the Ohio Institute of Technology, Dean of Faculty at the Missouri Institute of Technology, and a Vice President at DeVry, Inc. He served as a Project Engineer at the University of Kansas Center for Research, Remote Sensing Laboratory, while pursuing the Ph.D. degree, he was an IEEE Representative to and chairman of Region V of the Technology Accreditation Commission of the Accreditation Board for Engineering and Technology and is currently a consultant/evaluator for the North Central Association of Colleges and Schools. His current research interests include microwave sensor design and modeling the backscattering response of vegetation.

Relating Polarization Phase Difference of SAR Signals to Scene Properties

FAWWAZ T. ULABY, FELLOW, IEEE, DANIEL HELD, MEMBER, IEEE, MYRON C. DOBSON, MEMBER, IEEE, KYLE C. McDONALD, MEMBER, IEEE, AND THOMAS B. A. SENIOR, FELLOW, IEEE

Abstract—**This paper examines the statistical behavior of the phase difference $\Delta\phi$ between the HH-polarized and VV-polarized backscattered signals recorded by an *L*-band SAR over an agricultural test site in Illinois. Polarization-phase difference ($\Delta\phi$) distributions were generated for about 200 agricultural fields for which ground information had been acquired in conjunction with the SAR mission. For the overwhelming majority of cases, the $\Delta\phi$ distribution is symmetrical and has a single major lobe centered at the mean value of the disstribution $\overline{\Delta\phi}$. Whereas the mean $\overline{\Delta\phi}$ was found to be close to zero degrees for bare soil, cut vegetation, alfalfa, soybeans, and clover, a different pattern was observed for the corn fields; the mean $\overline{\Delta\phi}$ increased with increasing incidence angle θ from about zero at $\theta = 15°$ (near-range of the image) to about 140° at $\theta = 35°$. The explanation proposed for this variation is that the corn canopy, most of whose mass is contained in its vertical stalks, acts like a uniaxial crystal characterized by different velocities of propogation for waves with horizontal and vertical polarization. Thus, it is hypothesized that the observed backscatter is contributed by a combination of propagation delay, forward scatter by the soil surface, and specular bistatic reflection by the stalks. Model calculations based on this assumption were found to be in general agreement with the phase observations.**

I. INTRODUCTION

SHORTLY before its destruction with the NASA CV-990 aircraft on July 17, 1985, the JPL *L*-band SAR was configured to record both the amplitude and phase of the backscattered signal for each of the four linear polarization configurations (HH, HV, VV, and VH). The signals actually were recorded in complex notation from which their amplitudes and phases could be computed. The availability of phase information allowed the generation of polarization-phase-difference (PPD) images defined as follows. For a given image pixel, the received HH and VV signal voltages are given by

$$v_H = A_H e^{j\phi_H} \tag{1a}$$

$$v_V = A_V e^{j\phi_V} \tag{1b}$$

where A_H and A_V are the amplitudes of V_H and V_V, respectively, and ϕ_H and ϕ_V are their phases. The phases are measured with respect to a reference internal to the radar system. The quantity of interest is the polarization phase difference $\Delta\phi$, which is obtained from the product

$$v_H v_V^* = A_H A_V e^{j\Delta\phi} \tag{2}$$

where

$$\Delta\phi = \phi_H - \phi_V. \tag{3}$$

An example of a polarization phase-difference image (PPD) that was generated from a pair of four-look HH and VV complex images is shown in Fig. 1. The intensity (or brightness) of a given pixel is proportional to the magnitude A_H of the backscattered signal corresponding to that pixel. The color of the image pixel corresponds to $\Delta\phi$ in accordance with the scale indicated in the lower part of the image; the color purple corresponds to $\Delta\phi \cong 0°$, yellow corresponds to $\Delta\phi \cong -180°$, and cyan corresponds to $\Delta\phi \cong 110°$. Actually, the color assignment was made by setting the average value of $\Delta\phi$ of all pixels in the first five azimuth rows of the image equal to zero. In the image in Fig. 1, the first azimuth row corresponds to an angle of about 15° from normal incidence. Unless a target is azimuthaly unsymmetric, its backscattering properties should be identical for HH and VV polarizations at normal incidence. Hence, $\Delta\phi$ is expected to be $\cong 0°$ at and near normal incidence for most distributed targets. Consequently, in the near-range part of the image wherein $\theta \cong 15°$, it is expected that the majority of the pixels exhibit values $\Delta\phi$ in the neighborhood of 0°. In the color image, this expectation corresponds to having the near-range azimuthal strip take on a uniform color across the image. This is indeed the case for the image shown in Fig. 1 as demonstrated by the purple strip extending between $\theta = 15°$ and $\theta = 20°$. This behavior has been observed also for all other $\Delta\phi$ images generated by the JPL *L*-band SAR.

The rationale for using the average $\Delta\phi$ of the first five near-range azimuth rows as reference is because the *L*-band SAR system had not been calibrated to measure $\Delta\phi$ on an absolute scale. Thus, in a sense, the above procedure represents an approach for converting relative values of $\Delta\phi$ to absolute values.

Another point worth making relates to the use of $A_V A_H$ to modulate the intensity of the image. Although the focus of this study relates to an examination of $\Delta\phi$, which in-

Manuscript received April 10, 1986; revised October 20, 1986.

F. T. Ulaby, M. C. Dobson, K. McDonald, and T. B. A. Senior are with the Radiation Laboratory, University of Michigan, Ann Arbor, MI 48109.

D. Held is with the Jet Propulsion Laboratory, California Institute of Technology, Pasadena, CA 91109.

IEEE Log Number 8612328.

0196-2892/87/0100-0083$01.00 © 1987 IEEE

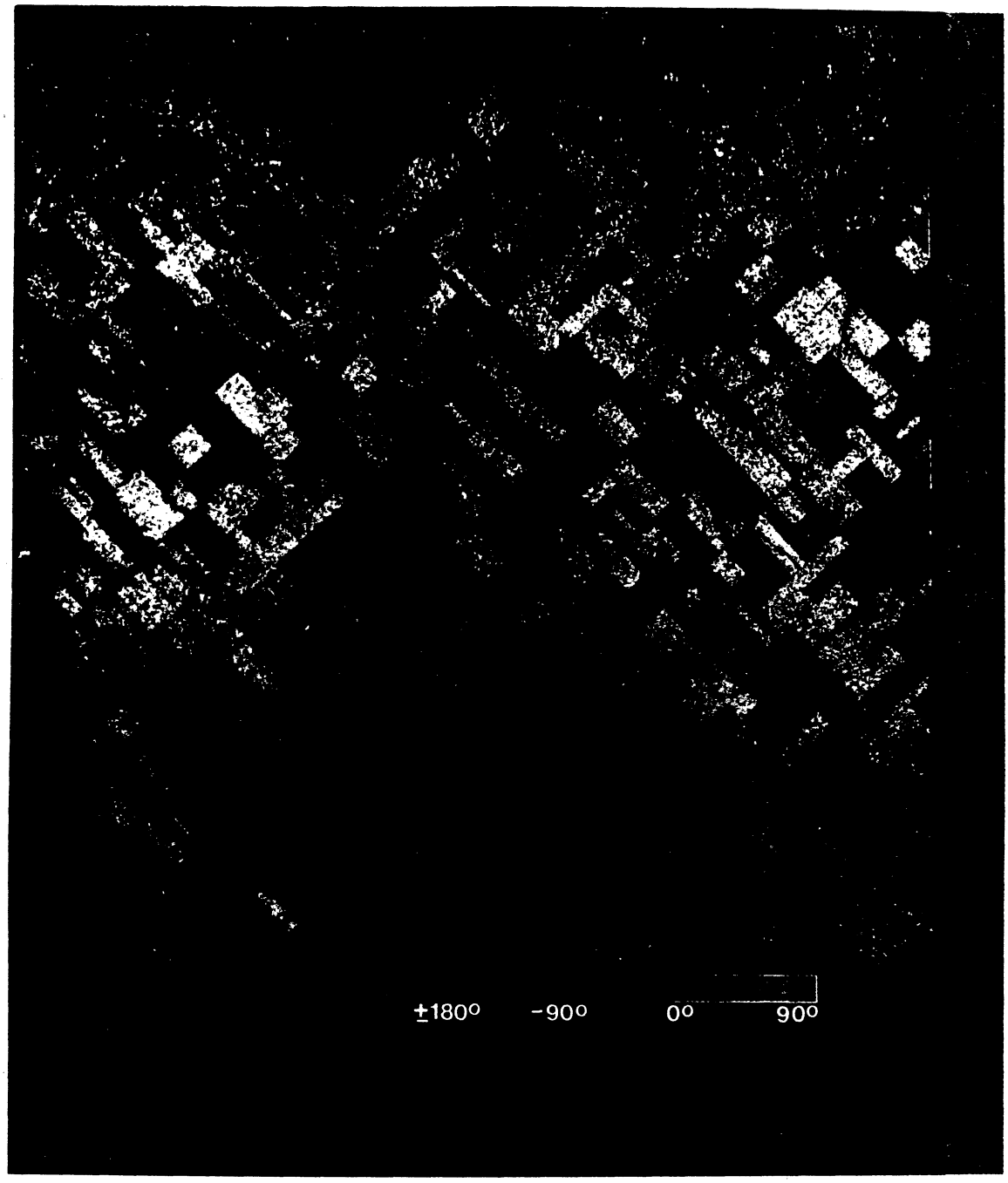

Fig. 1. Polarization-phase-difference image of an agricultural test site near McComb, Illinois. The image was generated by an *L*-band SAR that was flown by JPL on the NASA CV 990 aircraft. The color of a given pixel is related to the phase difference $\Delta\phi$, and its intensity is related to the HH-polarized backscattered power.

deed is the primary parameter displayed in the color image, the use of intensity modulation was incorporated in the generation of the PPD images because the intensity represents information about the strength of the backscattered signal. In our forthcoming discussion, however, attention will be limited to the phase information (color) only. Specifically, the goal of this paper is to examine the relationships, if any exist, between the phase difference $\Delta\phi$ of the signals corresponding to a given pixel, or to a collection of pixels, and the physical properties of the scattering target giving rise to the measured signals. To that end, we shall first describe the scene corresponding to the image in Fig. 1, and then follow it up with a proposed hypothesis to explain the relationship observed between the color of a field (i.e., its $\Delta\phi$) and its ground cover.

II. Image and Site Description

The image presented in Fig. 1 was generated from multipolarized data that were acquired by the NASA/JPL *L*-band SAR (operating at 1.225 GHz) over a largely agricultural test site near Macomb, Illinois. The data acquisition was made in conjunction with the Shuttle Imaging Radar (SIR-B) experiment in October 1984. An extensive

set of ground measurements were obtained throughout the test site and include biophysical and soil measurements of approximately 400 agricultural fields. The SAR data was digitally processed and recorded to produce four-look images with a pixel size of approximately 11 m in azimuth and 7.5 m in slant range (which corresponds to a ground range resolution of 29 m in the near range (at $\theta = 15°$) decreasing to 9 m in the far range (at $\theta = 55°$).

A. Test Site Description

The test site comprised an irregular area of roughly 250 km^2 within which approximately 400 agricultural fields were surveyed for ancillary data pertaining to physical and biophysical scene conditions. Extensive survey data included crop type, height, density, row direction, row spacing, and surface roughness.

Approximately half of the fields were sampled several times over a one-week period for canopy wet and dry biomass on a plant component basis (i.e., leaves, stalk, cob, and surface organic litter). Dry biomass was obtained after oven drying to equilibrium at 70°C. Additionally, roughly 200 fields were monitored daily for near-surface soil moisture conditions using a coring technique. On October 10, 1984, the average 0–5-cm soil moisture ranged from 0.18 to 0.40 g/cm^3 on a per field basis with a site mean of 0.28 ± 0.05 g/cm^3. An informal network of 56 raingauges operated by local farmers indicated widespread, but nonuniform, daily rainfalls of 0.2 to 0.5 cm and associated pre-dawn fog for the period from October 6 through 11.

Roughly 50 percent of the agricultural acreage contained corn with a 76-cm row spacing. In early October, the corn was harvest-ready with an average maximum height of 280 cm. In addition, the area had experienced widespread and occasionally severe infestations of European corn borer (*Ostrinia Nubilalis*). One effect of corn borer damage is to weaken the stalk and cause it to break (at a 170-cm height) and either topple to the ground or remain hinged at the breakpoint. Approximately 15 percent of the corn had been harvested prior to the October 10 aircraft data analyzed herein.

Unharvested corn fields were typically characterized by a relatively smooth soil surface with rms height variations σ on the order of 1.0 cm. The average quantity of water contained in plant material is determined by the difference between the wet and dry biomass of a particular canopy component. For corn, $\frac{1}{2}$ to $\frac{2}{3}$ of the water was located in the stalks, and the remainder is evenly split between the cobs and senescent leaf material.

Soybeans had been planted on 43 percent of the test site acreage. In early October, the soybeans were senescent and harvest-ready with a 100-cm average maximum height and a 76-cm row spacing. The remaining crop acreage was comprised of alfalfa, clover, and pasture of variable heights and biomass densities. The soil surface was always smooth (i.e., $\sigma << 1$ cm). Canopy heights ranged from 5 to 30 cm and plant water densities varies from 0.4 to 2.2 kg of water per square meter with an average of 1.22 kg/m^2.

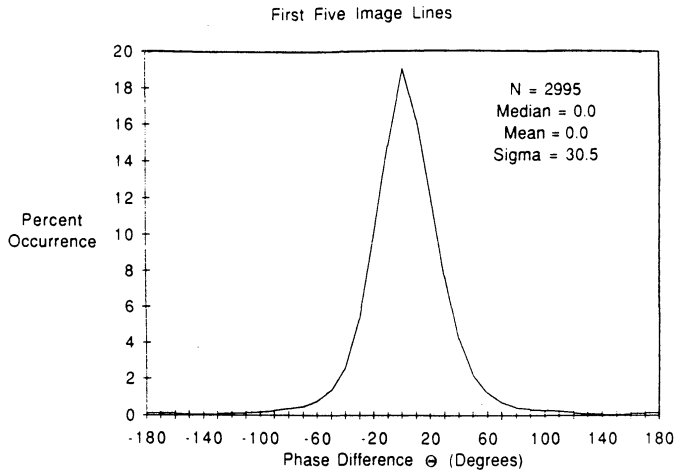

Fig. 2. PPD distribution for the first five lines of the image (corresponding to $\theta \cong 15°$).

B. PPD Distributions

1) Reference Distribution: Several bare soil and vegetation-covered fields were selected to examine the PPD statistics. Most fields were comprised of about 400 pixels. Fig. 2 shows the PPD distribution $p(\Delta\phi)$ for the first five near-range azimuth rows of the image. The mean value $\overline{\Delta\phi}$ is, of course, equal to zero because it was used as the zero reference for the whole image. The standard deviation σ_ϕ represents the variability in ϕ attributable to the stability of the measurement system and to factors related to the antenna patterns and polarization purity of the V and H ports; at $\theta \cong 15°$, it is very unlikely that the observed PPD for a given pixel is target related.

2) Bare-Soil Distribution: Fig. 3(a) and (b) shows PPD distributions for two bare-soil fields; one of them had been disked and the other one had been plowed prior to the flight. Both distributions have means $\overline{\Delta\phi}$ close to zero, but their standard deviations are very different. This difference is presumably related to the size and slope distributions of the soil clods; however, it is premature to speculate on how to relate these PPD distributions to the roughness parameters of the soil surface.

3) Vegetation-Cover Distribution: To examine the role of vegetation cover with regard to $\Delta\phi$, we start by showing a distribution for a soybean stubble field in Fig. 4(a) and for a field of standing soybean plants in Fig. 4(b). Although the two distributions have very different standard deviations, the mean values of both distributions are close to zero degrees. In fact, the mean value $\overline{\Delta\phi}$ was found to be within $\pm 25°$ of zero for all targets in the scene with the exception of fields of standing corn plants.

In contrast to the preceding examples all of which exhibited distributions with zero means regardless of the incidence angle, the PPD distributions for standing corn had non-zero means and exhibited a specific dependence on θ. Two examples are shown in Fig. 5. The first one corresponds to $\theta = 20°$ and its mean value $\overline{\Delta\phi}$ is 9°, whereas

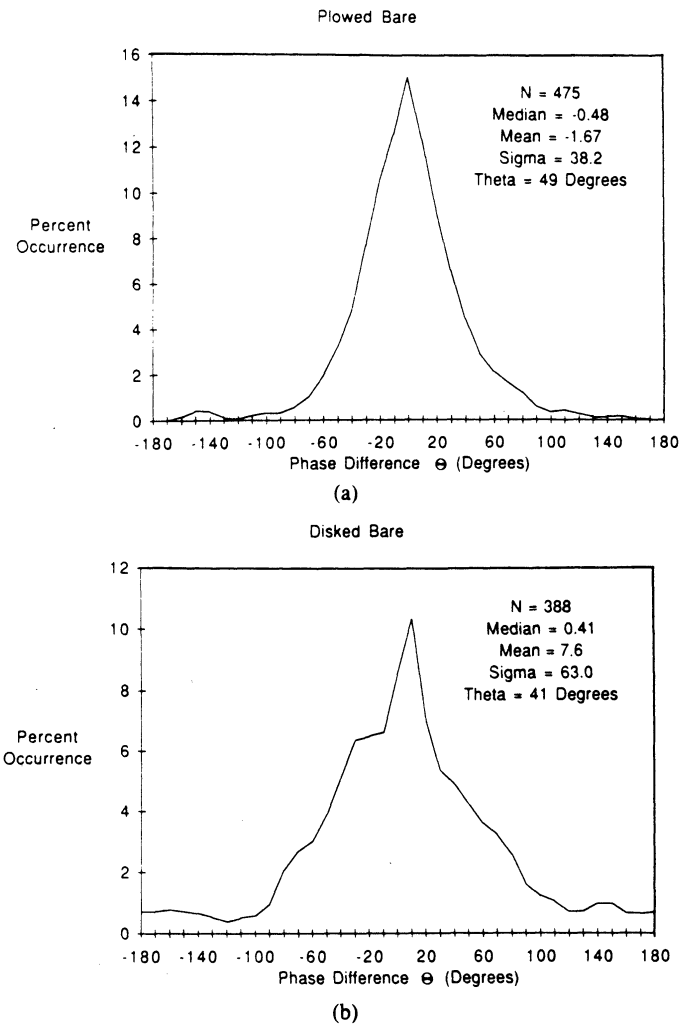

Fig. 3. PPD distribution for (a) plowed and (b) disked bare soil fields. Both distributions have means close to zero, but the distribution of the disked field has a much wider standard deviation.

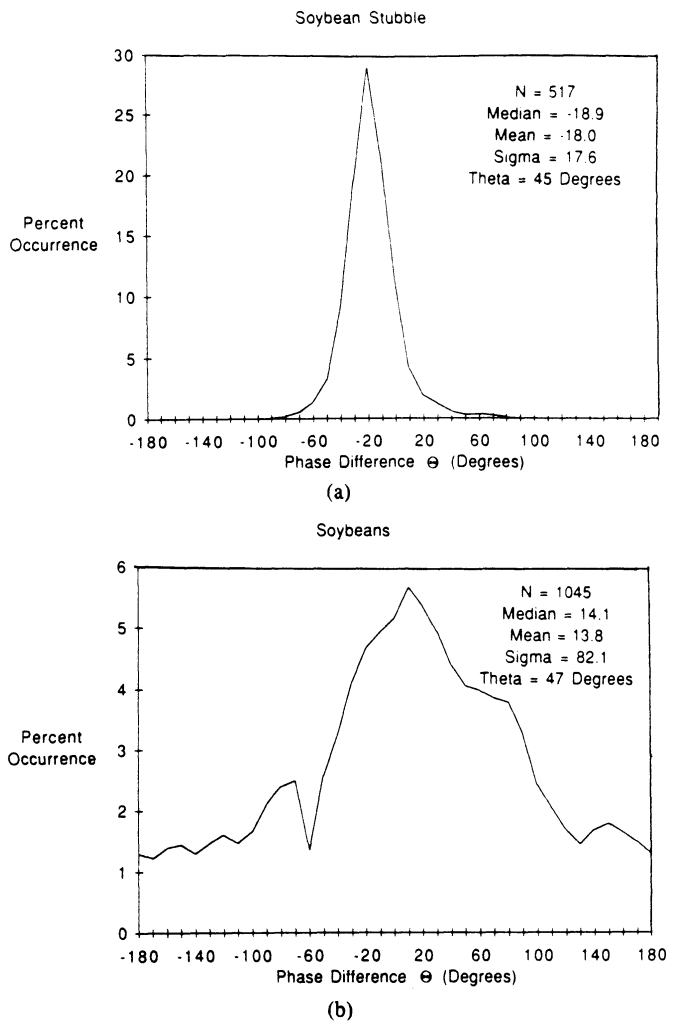

Fig. 4. PPD distributions for (a) soybean stubble and (b) standing soybeans. Note the large standard deviation of the soybeans distribution.

the second one corresponds to $\theta = 50°$ and its mean value is about 110°. When the distributions were generated and their means computed for several other fields of corn, we obtained the results shown in Fig. 6, which depicts the variation of the mean PPD, $\overline{\Delta\phi}$, versus the incidence angle θ. We observe that $\overline{\Delta\phi}$ starts at a value close to zero for $\theta = 18°$, increases rapidly with increasing θ to about 140° at $\theta = 35°$, and then decreases slowly as θ increases beyond 40°.

III. Propagation Through an Anisotropic Medium

The purpose of this section is to propose a mechanism that may possibly explain the observations discussed in the preceding section. Let us first summarize these observations:

1) Relative to the selected reference, namely the near-range strip of the image corresponding to $\theta \cong 15°$, all bare fields, stubble fields of corn and soybeans, fields of standing soybeans, and green alfalfa fields exhibit PPD distributions with means $\overline{\Delta\phi}$ within $\pm 25°$ of 0°.

2) Among all the targets in the image, the corn fields are the only ones having distributions with $\overline{\Delta\phi} > 25°$.

3) $\overline{\Delta\phi}$ of corn increases rapidly with increasing θ between $\theta = 20°$ and $\theta = 35°$.

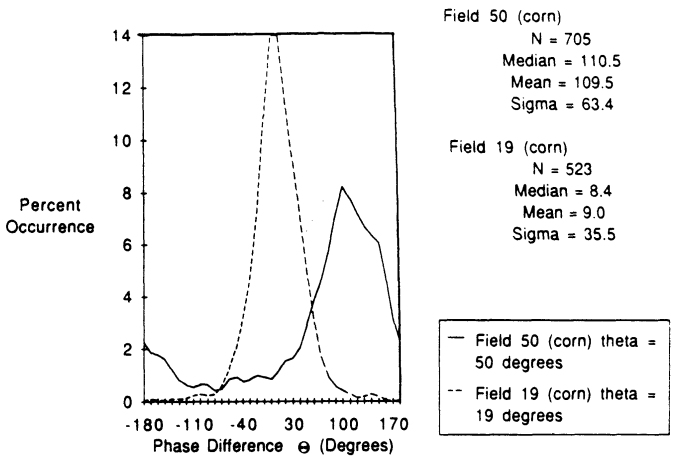

Fig. 5. PPD distributions for two corn fields, one observed at $\theta = 19°$ (relative to nadir) and the other at $\theta = 50°$. The mean values of the distributions are 9° for the near-range field and 110° for the far-range field.

Recalling the definition of $\Delta\phi = \phi_H - \phi_V$, we note that in order for the phase difference to be different from zero, at least one of the following conditions should be satisfied: 1) the phase difference is caused by the scatterers in the target, 2) $\Delta\phi$ is due to time delay resulting from the condition that the scatterers dominating the VV-polarized backscatter are at a range (from the radar antenna)

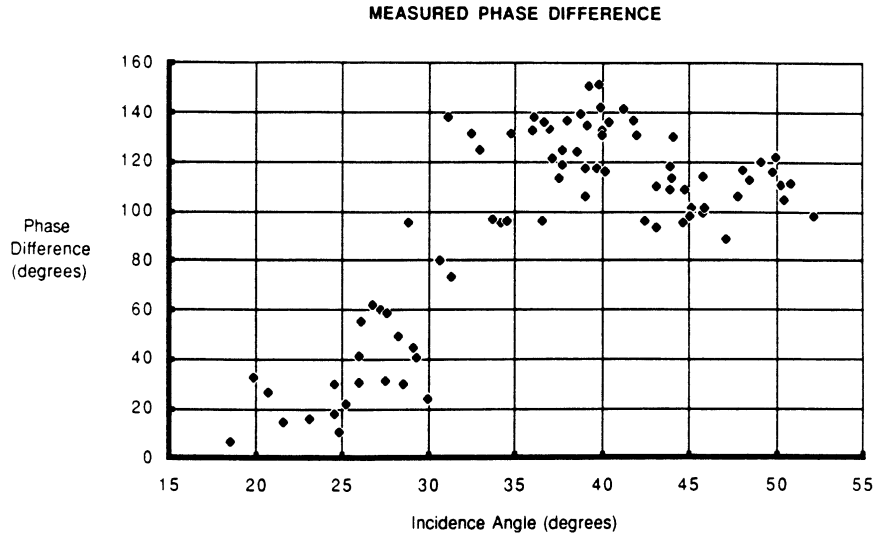

Fig. 6. Variation of the mean value $\overline{\Delta\phi}$ with incidence angle θ for fields of standing corn. The data points are based on distributions extracted from the digital-equivalent of the image in Fig. 1.

different from that for those dominating the HH-polarized backscatter, or 3) $\Delta\phi$ is due to time delay resulting from the condition that the phase velocity in the vegetation canopy for V polarization is different from that for H polarization.

Before we examine these possibilities in more detail, we should consider another piece of important information. According to the study reported by Dobson and Ulaby [1], SIR-B observations of the Illinois site (which covered the same fields shown in Fig. 1 and were made on the same day as the aircraft observations from which Fig. 1 was produced) indicate that the backscattering coefficient σ° of corn fields was highly correlated to their soil moisture content and exhibited a soil-moisture sensitivity comparable in magnitude to that observed for bare-soil fields. This response supports the contention that the backscattered energy was directly related to scattering by the soil surface and that the canopy is a low-loss medium. In their study, Dobson and Ulaby [1] examined three scattering mechanisms: 1) direct backscattering from the corn plants (see Fig. 7), 2) direct backscattering from the soil surface (including two-way attenuation by the canopy), and 3) indirect scattering resulting from foward scattering by the soil surface followed by bistatic scattering by the plants, or the reverse process. These contributions are referred to as σ°_{vol}, σ°_{surf}, and σ°_{int}, respectively. Dobson and Ulaby [1] concluded that the total return was governed by σ°_{int} and that the other two contributions were negligible in comparison. A consequence of this conclusion is that the total phase difference $\Delta\phi$ (between the HH and VV signals) consists of three primary sources

$$\Delta\phi = \Delta\phi_p + \Delta\phi_s + \Delta\phi_{st} \tag{4}$$

where $\Delta\phi_p$ is the phase difference due to two-way propagation through the canopy, $\Delta\phi_s$ is the phase difference due to Fresnel reflection by the soil surface, and $\Delta\phi_{st}$ is due to bistatic scattering by the stalks. Among these quantities, $\Delta\phi_s$ is the easiest to compute. If $\rho_H(\theta, \epsilon_s)$ and $\rho_V(\theta,$

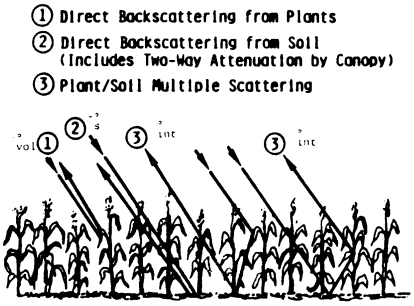

Fig. 7. Sketch of the three source terms contributing to the total backscattering by the canopy/soil scene.

ϵ_s) are the Fresnel reflection coefficients for a plane soil surface with relative dielectric constant ϵ_s, then

$$\Delta\phi_s = \tan^{-1}\left[\frac{\text{Im}\{\rho_H/\rho_V\}}{\text{Re}\{\rho_H/\rho_V\}}\right] - 180^\circ. \tag{5}$$

The 180° phase shift has been added to compensate for the difference in sign between ρ_H and ρ_V at normal incidence ($\theta = 0^\circ$). Expressions for the other two quantities, $\Delta\phi_p$ and $\Delta\phi_{st}$, are given by (A26) and (B6) in Appendices A and B, respectively.

In deriving these expressions, the corn canopy was modeled as a two-dimensional array of randomly located vertical cylinders. The plant leaves were ignored because, at the time of the radar observations, the leaves accounted for only 12 percent of the total mass of a corn plant and their average moisture content was about 0.1 (compared to 0.3 for the stalks).

IV. Comparison of the Model with Observations

At the time of image acquisition, ground observations were made for 89 fields of corn. The following average values were determined: canopy height (excluding tassle) = 2.5 m, stalk volume fraction = 4.8×10^{-3}, leaf volume fraction = 6.8×10^{-4}, stalk volumetric moisture content = 0.3, leaf volumetric moisture content = 0.1,

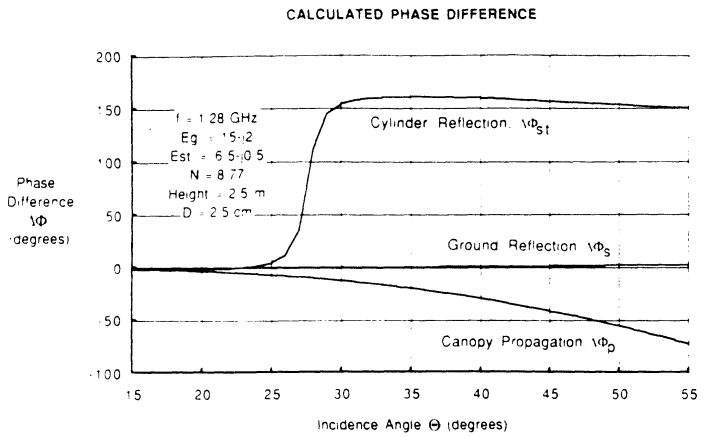

Fig. 8. Plots of the three phase-difference components, computed according to equations (5), (A26), and (B6).

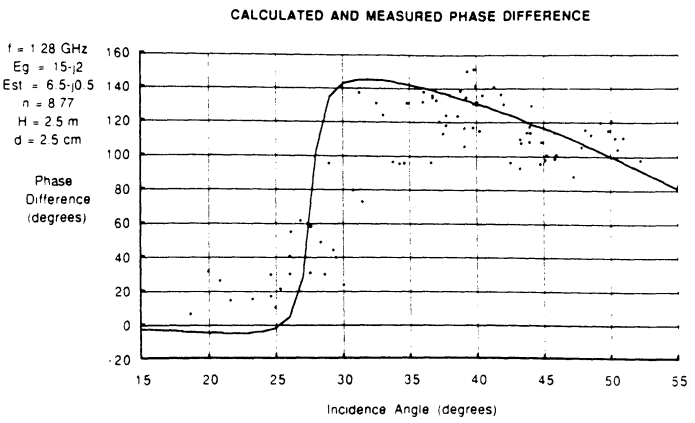

Fig. 9. Comparison of model-calculated polarization phase difference (sum of the three components shown in Fig. 8) with data extracted from the image in Fig. 1.

and soil volumetric moisture content = 0.28. Using the soil dielectric model defined in [2], the soil dielectric constant was set at $\epsilon_s = 15 - j2$. Based on laboratory measurements made for corn stalks as a function of moisture content, it was estimated that the stalk dielectric constant should be somewhere between $\epsilon_{st} = 6.5 - j0.3$ and $\epsilon_{st} = 9 - j1$. Fitting the model discussed in the preceding section to the data resulted in $\epsilon_{st} = 6.5 - j0.5$. The remaining model parameters are the stalk diameter D and the number density of stalks N. Both of these were specified on the basis of direct field measurements.

Fig. 8 shows each of the three components of (4) plotted as a function of the incidence angle θ from 15° to 55° Being less than 5°, the ground component $\Delta\phi_s$ is inconsequential. The propagation component $\Delta\phi_p$ is negative and its magnitude increases monotonically with increasing θ, which is in agreement with the results of direct transmission measurements made for a canopy of corn plants using transmitters mounted on a truck-mounted boom and receivers mounted on a rail system at ground level [4]. The stalk bistatic scattering component, $\Delta\phi_{st}$, exhibits a very rapid change between $\theta = 24°$ and $\theta = 30°$. The Brewster angle for Fresnel reflection off a surface material with $\epsilon = 6.5 - j0.5$ is about 68°, whose complement is $\theta = 22°$.

The combination of $\Delta\phi_p$ and $\Delta\phi_{st}$ is reponsible for the negative slope of $\Delta\phi$ versus θ for $\theta \geq 35°$ (see Fig. 9). Overall, the model is in good agreement with the data; it is important to note that the model calculations are based on "average" field conditions and, as such, do not incorporate the natural field-to-field variability inherent in the scene. Furthermore, based on an analysis of the polarization coupling properties of the antenna, it is estimated that the error associated with the measurement of $\Delta\phi$ is on the order of 6°–12°.

V. Concluding Remarks

The polarization phase difference observed for the corn canopies is attributed to a combination of two primary sources: 1) bistatic reflection by the vertical stalks and 2) propagation delay between the H-polarized and V-polarized waves as they travel through the canopy down to the soil surface and back (subsequent to specular reflections by the soil surface and the stalk, in either order). An important condition that needs to be satisfied in order for the polarization phase difference to be significantly different from zero is for the primary source of the backscattered signal to be the result of forward scattering by the soil surface and the vertical stalks. This condition, in turn, requires that the canopy medium be a relatively low-loss medium, which was satisfied in this case by the fact that the observations were made late in the growing season (the leaves were essentially dry).

Appendix A
Equivalent Medium Model

This appendix provides the formulation for the propagation constant γ of the corn canopy. The canopy is modeled as a slab-like region consisting of identical vertically oriented cylinders (the stalks). The cylinders point in the z direction; they are randomly positioned in the x–y plane; and for the purposes of this treatment, the slab extends from $x = -d/2$ to $x = d/2$. First, we shall consider the case where the slab is illuminated by a normally incident plane wave propagating in the x direction, as shown in Fig. 10, and then we shall generalize the expression for γ to the case where incidence is at any angle θ relative to the $-z$ direction.

A. Horizontal Propagation ($\theta = 90°$)

We consider the layer in Fig. 10 to contain N cylinders per unit area. The cylinders are sufficiently far apart to allow us to ignore multiple scattering, but not so far apart laterally to force us to consider other than forward scattering, and the cylinders are sufficiently long compared to the wavelength λ to be considered infinite in extent. With plane wave illumination incident as shown in the figure, we seek an expression for the transmitted field $U(P)$ at a point $P(x_0, 0)$ located well beyond the layer (i.e., P is in the far-field of the scattering cylinders). The field $U(P)$ stands for the electric field $E(P)$ if the incident wave is vertically polarized (TM) and for the magnetic field $H(P)$ if the wave is horizontally polarized (TE).

The total field at P consists of an unscattered compo-

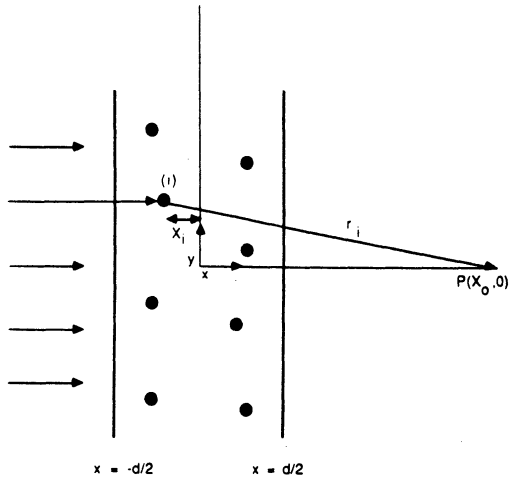

Fig. 10. Top view of the canopy. The solid circles represent the vertical stalks.

nent due to the incident wave U_0, and a component due to forward scattering by the cylinders U_{sc}. Relative to the field at the origin

$$U_0 = e^{jkx_0} \tag{A1}$$

where $k = 2\pi/\lambda$ is the wave number in air. For the ith scatterer (cylinder) located at (x_i, y_i), the incident field is

$$U_i^{\text{inc}} = e^{jkx_i} \tag{A2}$$

and the forward scattered field observed at P is [3]

$$U_i^{sc} = U_i^{\text{inc}}\left[\frac{2}{\pi kr_i}\right]^{1/2} \exp\left[j\left(kr_i - \frac{\pi}{4}\right)\right] T(\phi')$$

$$= \left[\frac{2}{\pi kr_i}\right]^{1/2} \exp\left[j\left(kr_i + kx_i - \frac{\pi}{4}\right)\right] T(\phi') \tag{A3}$$

where r_i is the distance between the ith scatterer and point P, $T(\phi')$ is the normalized far-field amplitude of the scattered field, and ϕ' is the azimuth angle defined with respect to the $-x$ direction (backscattered direction). In this treatment, we shall consider only the contributions of cylinders present in a narrow region in the y direction, extending from $y = -b/2$ to $y = b/2$ such that $x_0 >> b/2$, in which case $\phi' \cong \pi$. Moreover, the distance r_i may be approximated as follows:

$$r_i = \left[(x_0 - x_i)^2 + y_i^2\right]^{1/2}$$

$$\cong (x_0 - x_i) + \frac{y_i^2}{2x_0} \tag{A4}$$

where we have assumed that $x_0 >> x_i, y_i$, If n cylinders contribute to the scattered field at P

$$U^{sc}(x_0, 0) = \sum_{i=1}^{n} U_i^{sc}(x_0, 0)$$

$$= \left[\frac{2}{\pi kx_0}\right]^{1/2} \exp\left[j\left(kx_0 - \frac{\pi}{4}\right)\right] T(\pi) \sum_{i=1}^{n} \exp\left(\frac{jky_i^2}{2x_0}\right), \tag{A5}$$

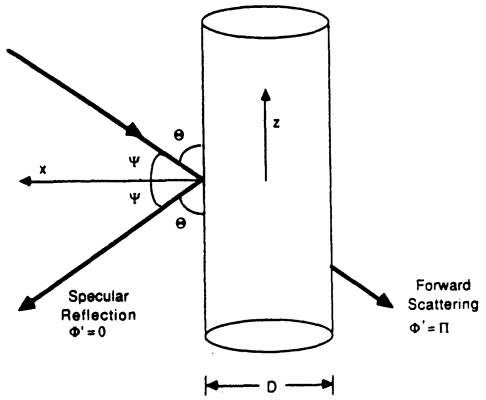

Fig. 11. Scattering geometry showing the angles pertaining to specular reflection ($\phi' = 0$) and forward scattering ($\phi' = \pi$).

where use was made of (A3) and (A4), ϕ' was set equal to π, and r_i in the amplitude part of U_i^{sc} was set equal to x_0. If there are N cylinders per unit area, and these are randomly distributed over the region $-d/2 \le x \le d/2$ and $-b/2 \le y \le b/2$, then

$$U^{sc}(x_0, 0) = \left[\frac{2}{\pi kx_0}\right]^{1/2} \exp\left[j\left(kx_0 - \frac{\pi}{4}\right)\right] T(\pi) N$$

$$\int_{-d/2}^{d/2} \int_{-b/2}^{b/2} \exp\left(\frac{jky^2}{2x_0}\right) dy\, dx. \tag{A6}$$

The x integration gives d, and the y integration is

$$\int_{-b/2}^{b/2} \exp\left(\frac{jky^2}{2x_0}\right) dy = 2\int_0^{b/2} \exp\left(\frac{jky^2}{2x_0}\right) dy$$

$$= 2\left(\frac{2x_0}{k}\right)^{1/2} \left[\int_0^{\infty} - \int_{b/2(k/2x_0)^{1/2}}^{\infty}\right] e^{jy_1^2}\, dy_1. \tag{A7}$$

But

$$\int_0^{\infty} e^{jy_1^2}\, dy_1 = \tfrac{1}{2}\sqrt{\pi}\, e^{j\pi/4} \tag{A8}$$

and the remaining integral is negligible if 1) $kb^2/8x_0 >> 1$, or 2) if we assume that k has a positive imaginary component $k'' = 2\pi n''/\lambda$ (where n'' is the imaginary part of the average index of refraction of the layer) and that $\exp(-k''b^2/8x_0) << 1$. The former condition, when combined with the previously stated condition $x_0 >> b/2$, leads to

$$b << 2x_0 << \pi b^2/2\lambda \tag{A9}$$

which is always satisfied if we choose $b = 200\,\lambda/\pi$ and $x_0 = 1000\,\lambda/\pi$.

The net scattered field at P is therefore

$$U^{sc}(x_0, 0) = \frac{2Nd}{k} e^{jkx_0} T(\pi)$$

$$= \frac{2Nd}{k} T(\pi) U_0 \tag{A10}$$

and the total field is

$$U = U_0 + U^{sc}$$
$$= U_0\left[1 + \frac{2Nd}{k} T(\pi)\right]. \quad \text{(A11)}$$

Now suppose we were to replace the given layer with an equivalent homogeneous layer of complex index of refraction n and the same thickness d. With reference to the coordinate system shown in Fig. 10, the transmitted field at P is

$$U = e^{-jkd/2} \cdot e^{jk(x_0 - d/2)}$$
$$= U_0 \exp\left[j(k_e - k)d\right]$$
$$= U_0 \exp\left[jk(n-1)d\right] \quad \text{(A12)}$$

where $k_e = kn$ is the wavenumber of the equivalent medium. Because air usually constitutes more than 0.99 of the total volume of the vegetation canopy, the magnitude of n usually is only slightly larger than unity and $(n-1) \ll 1$. Hence, if d is such that $kd(n-1) \ll 1$, then

$$U \cong U_0[1 + jkd(n-1)]. \quad \text{(A13)}$$

Upon equating the field U derived for the actual layer containing the dielectric cylinders, (A11), to the field given by (A13) for the equivalent medium, we have

$$n \cong 1 - j\frac{2N}{k^2} T(\pi) \quad \text{(A14)}$$

implying

$$n' \cong 1 + \frac{2N}{k^2} \operatorname{Im}\left\{T(\pi)\right\} \quad \text{(A15)}$$

and

$$n'' \cong -\frac{2N}{k^2} \operatorname{Re}\left\{T(\pi)\right\}. \quad \text{(A16)}$$

It should be noted that $\operatorname{Im}\{T(\pi)\} \geq 0$ and $\operatorname{Re}\{T(\pi)\} \leq 0$.

B. Oblique Incidence

For incidence at an angle θ relative to $-z$, a repeat of the preceding steps leads to

$$n_p' \cong 1 + \frac{2N}{k^2} \sin\theta \operatorname{Im}\left\{T_p(\theta, \pi)\right\}, \quad p = \text{V or H} \quad \text{(A17)}$$

and

$$n_p'' \cong -\frac{2N}{k^2} \sin\theta \operatorname{Re}\left\{T_p(\theta, \pi)\right\}, \quad p = \text{V or H} \quad \text{(A18)}$$

which is a result of changing the number density in the propagation plane from N to $N \sin\theta$.

In the preceding expressions, n and T were assigned a subscript p to denote polarization, where p = V (vertical TM) or H (horizontal, TE). The normalized amplitudes T_V and T_H are given by

$$T_V(\theta, \pi) = \frac{1}{\sin\theta} \sum_{n=-\infty}^{\infty} C_n^{TM}(\theta) \quad \text{(A19)}$$

$$T_H(\theta, \pi) = \frac{1}{\sin\theta} \sum_{n=-\infty}^{\infty} C_n^{TE}(\theta) \quad \text{(A20)}$$

and the constants $C_n^{TM}(\theta)$ and $C_n^{TE}(\theta)$ are given in Ruck *et al.* [3, pp. 273–274] in terms of the angle $\psi = \pi/2 - \theta$, the cylinder radius a_0, and the relative complex dielectric constant of the cylinder material ϵ.

The propagation constant γ is related to n_p by

$$\gamma_p = kn_p = k(n_p' + jn_p'') \quad \text{(A21)}$$

and since $j\gamma_p = -\alpha_p + j\beta_p$, the attenuation constant α and phase constant β are given by

$$\alpha_p = kn_p'', \quad p = \text{V or H} \quad \text{(A22)}$$

$$\beta_p = kn_p', \quad p = \text{V or H.} \quad \text{(A23)}$$

The extinction width of an infinitely long cylinder is given by

$$\sigma_p^E(\theta) = -2\lambda/\pi \operatorname{Re}\left\{T_p(\theta, \pi)\right\} \quad \text{(A24)}$$

which, when combined with (A18) and (A20), leads to

$$\alpha_p(\theta) = \frac{\sin\theta}{2} N\sigma_p^E(\theta), \quad p = \text{V or H} \quad \text{(A25)}$$

and is attributable to both scattering and any intrinsic absorption by the cylinders.

C. Phase Difference

For propagation at an incidence angle θ through a canopy of height h, the polarization phase difference for two-way propagation is

$$\Delta\phi_p = 2h \sec\theta(\beta_H - \beta_V)$$
$$= \frac{4Nh}{k} \tan\theta\left[\operatorname{Im}\left\{T_H(\theta, \pi)\right\} - \operatorname{Im}\left\{T_V(\theta, \pi)\right\}\right]. \quad \text{(A26)}$$

Appendix B
Bistatic Scattering by Dielectric Cylinder

To compute the phase difference between the H-polarized and V-polarized waves bistatically reflected by the corn stalks, we shall treat the stalks as infinitely long cylinders (the length of the stalks does not affect the phase difference) and consider specular scattering only. For a TM wave of amplitude E_0^{TM} incident at angle θ relative to the axis of the cylinder, the field of the specularly reflected wave is given by [3, p. 269]

$$E_z^{sc} = E_0^{TM} F(k, \psi, z, r)\, T_H(\theta, 0°) \quad \text{(B1)}$$

and for a TE wave of H_0^{TE}

$$H_z^{sc} = H_0^{TM} F(k, \psi, z, r)\, T_V(\theta, 0°) \quad \text{(B2)}$$

where $F(h, \psi, z, r)$ is a complex function, and $T_H(\theta, 0°)$

and $T_V(\theta, 0°)$, which are normalized amplitudes evaluated at the scattering azimuth angle $\phi' = 0$, are given by

$$T_H(\theta, 0°) = \sum_{n=-\infty}^{\infty} (-1)^n C_n^{TM}(\theta) \quad \text{(B3)}$$

$$T_V(\theta, 0°) = \sum_{n=-\infty}^{\infty} (-1)^n C_n^{TE}(\theta). \quad \text{(B4)}$$

The constants $C_n^{TM}(\theta)$ and $C_n^{TE}(\theta)$ are the same as those given in (A19) and (A20).

The polarization phase difference due to bistatic scattering by N identical cylinders is the same as that due to scattering by a single cylinder and is equal to the phase of the product

$$E_z^{TM}(H_z^{TE})^* = E_0^{TM} H_0^{TE} |F|^2 T_H T_V^*$$
$$= E_0^{TM} H_0^{TE} |F|^2 |T_H| |T_V| e^{j\Delta\phi_{st}} \quad \text{(B5)}$$

where

$$\Delta\phi_{st} = \tan^{-1}\left\{\frac{\text{Im}\,[T_H/T_V]}{\text{Re}\,[T_H/T_V]}\right\}. \quad \text{(B6)}$$

References

[1] M. C. Dobson and F. T. Ulaby, "Preliminary evaluation of the SIR-B response to soil moisture, surface roughness, and crop canopy cover," *IEEE Trans. Geosci. Remote Sensing*, vol. GE-24, pp. 517–526, 1986.

[2] M. T. Hallikainen, F. T. Ulaby, M. C. Dobson, M. A. El-Rayes, and L. K. Wu, "Microwave dielectric behavior of wet soil—Part I: Empirical models and experimental observations," *IEEE Trans. Geosci. Remote Sensing*, vol. GE-23, pp. 25–34, 1985.

[3] G. T. Ruck, D. E. Barrick, W. D. Stuart, and C. K. Krichbaum, *Radar Cross-Section Handbook*. New York: Plenum, 1970.

[4] F. T. Ulaby, A. Tavakoli, and T. B. A. Senior, "Amplitude and phase characteristics of microwave propagation in vegetation canopies," Univ. of Michigan Tech. Rep. RL-022132-2, 1986.

*

Fawwaz T. Ulaby (M'68–SM'74–F'80) was born in Damascus, Syria, on February 4, 1943. He received the B.S. degree in physics from the American University of Beirut, Lebanon, in 1964 and the M.S.E.E. and Ph.D. degrees in electrical engineering from the University of Texas, Austin, in 1966 and 1968, respectively.

From 1968 to 1984, he was with the Electrical Engineering Department at the University of Kansas, Lawrence, where he was the J. L. Constant Distinguished Professor, and the University of Kansas Center for Research, where he was Director of the Remote Sensing Laboratory. He is currently with the Radiation Laboratory and the Department of Electrical and Computer Engineering, University of Michigan, Ann Arbor. His current research interests involve microwave propagation and active and passive microwave remote sensing. Along with R. K. Moore and A. K. Fung, he is a coauthor of the three-volume series *Microwave Remote Sensing: Active and Passive* (Reading, MA: Addison-Wesley). In addition, he is coeditor of the *Manual of Remote Sensing*, 2nd ed., vol. I, American Society of Photogrammetry.

Dr. Ulaby is a member of Eta Kappa Nu, Tau Beta Pi, and Sigma Xi. He has been named the Executive Editor for IEEE TRANSACTIONS ON GEOSCIENCE AND REMOTE SENSING, 1984–1985, and was the Geoscience and Remote Sensing Society's Distinguished Lecturer for 1987. He was named an IEEE Fellow in 1980 "for contributions to the application of radar to remote sensing for agriculture and hydrology," received the GRS Society's Outstanding Service Award in 1982, and its Distinguished Service Award in 1983. In 1984, he also received a Presidential Citation for Meritorious service from the American Service of Photogrammetry. He received the University of Kansas Chancellor's Award for Excellence in Teaching in 1980, the University of Kansas Gould Award for "distinguished service to higher education" in 1973, and the Eta Kappa Nu MacDonald Award as an "outstanding electrical engineering professor in the United States of America" in 1975.

*

Daniel N. Held (S'67–M'68) received the B.S., M.S., and Sc.D. degrees from Columbia University in 1968, 1971, and 1977, respectively.

He is currently a Supervisor in the Radar Science and Engineering Section of the Jet Propulsion Laboratory, California Institute of Technology. He has been the Principal Investigator for a number of NASA research projects involved with the quantitative analysis and use of synthetic aperture radar data. He has recently been responsible for the Seasat SAR Engineering Performance Evaluation which demonstrated the ultimate capability of that sensor to provide accurate cartographic and amplitude information. He has served in a radar system engineering capacity on the SIR-A, SIR-B, VOIR, and VRM programs. Prior to his employment at JPL, he worked at the NASA Goddard Institute for Space Studies, where he was the System Engineer/Manager for the design, construction and testing of a millimeter-wave radio astronomy facility. It was at Goddard where he wrote his thesis and several papers on millimeter-wave mixer design. Prior to Goddard, he worked for the Columbia University Astrophysics Laboratory on the HEAO-A, X-Ray Astronomy Satellite. His work there centered on the development of position-sensitive proportional counters, and the measurement systems that surrounded them. Prior to the work at Columbia, he worked for the Bendix Corporation, Navigation and Control Division, on high-resolution solid-state star trackers.

Dr. Held is a member of the A.A.A.S. and Sigma Chi. He has served as a member of the administrative Committee of the Geoscience and Remote Sensing Society of the IEEE. Two of his papers were awarded the 1978 "Microwave Prize" by the IEEE Microwave Theory and Technique Society for the best published paper of the year.

*

Myron C. Dobson (M'83) was born in Rochester, NY, on October 25, 1951. He received the B.A. degree in both geology and anthropology from the University of Pennsylvania, Philadelphia, in 1973 and the M.S. degree in geography from the University of Kansas, Lawrence, in 1981.

In 1975, he joined the Remote Sensing Laboratory at the University of Kansas Center for Research where he was the Project Manager of the soil-moisture-sensing program. His research interests are in the areas of microwave remote sensing, target-sensor interaction physics, image processing and simulation, and renewable-resource management. His ongoing projects include satellite image simulations and the measurement of soil dielectric properties. He is now with the Computer Science Department, University of Michigan, Ann Arbor.

*

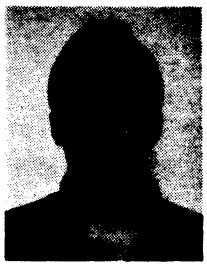

Kyle C. McDonald (S'84–M'85) was born in Columbus, OH, on October 23, 1960. He received the Bachelor of Electrical Engineering degree from the Georgia Institute of Technology in 1983. He received the M.S. degree in numerical science from The Johns Hopkins University. He is currently working toward the Ph.D. degree at the University of Michigan, Ann Arbor.

In 1983, he joined The Johns Hopkins University Applied Physics Laboratory where he was involved in the development of oceanographic sensor systems. His current research interests lie in modeling radar backscatter from vegetation canopies.

Thomas B. A. Senior (SM'66-F'72) received the M.Sc. degree in applied mathematics from the University of Manchester, England, in 1950 and the Ph.D. degree in research from Cambridge University in 1954.

In 1952 he was appointed as an Established Scientific Officer and accepted a position with the Ministry of Supply at the Radar Research and Development Establishment (now the Royal Radar Establishment) at Malvern, England. In 1955 he was promoted to Senior Scientific Officer. He joined the Radiation Laboratory, University of Michigan, Ann Arbor, in June 1957. He was appointed Professor of Electrical Engineering in 1969 and Director of Radiation Laboratory in 1975. His primary interests are in the study of diffraction and propagation of electromagnetic waves, with applications to physical problems.

Dr. Senior has been an Associate Editor for *Radio Science* and served as Editor from 1973 through 1978, and is now an Associate Editor for *Electromagnetics*. He is the Vice Chairman of Commission B of the International Union of Radio Science, the past Chairman of the U.S. National Committee for URSI and served as Chairman of U.S. Commission B. He is a member of Sigma Xi, Tau Beta Pi and Eta Kappa Nu, and is listed in American Men and Women of Science.

Microwave Propagation Constant for a Vegetation Canopy With Vertical Stalks

FAWWAZ T. ULABY, FELLOW, IEEE, AHAD TAVAKOLI, AND THOMAS B. A. SENIOR, FELLOW, IEEE

Abstract—**An equivalent-medium model is developed to relate the propagation constant γ, associated with propagation of the mean field through a vegetation canopy, to the geometrical and dielectric parameters of the canopy constituents. The model is intended for media containing vertical cylinders, representing the stalks, and randomly oriented discs, representing the leaves. The formulation accounts for both absorption and scattering by the cylinders, but uses a quasi-static approximation with respect to the leaves. The model was found to be in good agreement with experimental results at 1.62 and 4.75 GHz, but underestimates the extinction loss at 10.2 GHz. The experimental component of the study included measurements of the attenuation loss for horizontally polarized and vertically polarized waves transmitted through a fully grown corn canopy, and of the phase difference between the two transmitted waves. The measurements were made at incidence angles of 20°, 40°, 60°, and 90° relative to normal incidence. The major conclusion of this study is that the proposed model is suitable for corn-like canopies, provided the leaves are smaller than λ in size.**

I. INTRODUCTION

IN THE MICROWAVE region, most vegetation canopies are considered inhomogeneous media, and in some cases, anisotropic also. Efforts to model the radar backscattering and radiometric emission from vegetation follow one of two basic approaches. In the first approach, the canopy is treated as a *continuous* random medium with an average dielectric constant ϵ_a and a fluctuating component $\epsilon_f(x, y, z)$, which, in the general case, may be formulated as a tensor [1], [2]. When modeled using the second approach, the canopy is treated as the sum of discrete elements each characterized by a scattering phase function that relates the directional distribution of energy scattered by the element to the energy incident upon it [3], [4]. Although numerous papers have been published to document the merits of the two approaches and many more have reported the results of experimental observations, there remain many unresolved questions about the nature of the wave-target interaction process, both in the canopy volume and between the canopy elements and the underlying soil surface. For the most part, the applicability of a given model to a given target type (such as vegetation) is evaluated by comparing the model-calculated scattering coefficient or brightness temperature to measured values of the same quantity. The model is based on certain assumptions and is a function of a set of electromagneti and physical parameters of the target, many of which ai difficult to measure and are, therefore, selected such th the fit between the model and the observations are optin ized. Because of the broad latitude afforded the "fitting process, it is often possible to fit the same data to mode with distinctly different assumptions and implications.

Does this mean that the available theoretical scatterin models are inappropriate and/or unimportant to the prob lem at hand, namely, the development of techniques fc the utilization of microwave observations to derive infor mation about the biophysical properties of the canopy Definitely not; theoretical models are extremely importar and should play a vital role in the research process. A though most theoretical models may prove to be too dif ficult to invert, they are indispensable for conducting ser sitivity analyses and for pointing the direction of futur research.

What is the solution? A search through the literatur reveals three approaches that microwave remote-sensin researchers have taken in this regard. They include: 1 direct measurements of some of the canopy parameters such as the leaf-angle-distribution and the dielectric con stant of the vegetation elements [5], 2) high-resolutio measurements of the backscattering cross section per un volume as a function of range (or depth) using probin scatterometers [6], [7], and 3) measurement of the trans mission properties of vegetation canopies [5], [8], [9] The information provided by these investigations has im proved the understanding of the interaction process an has tightened the constraints that have to be met by th theoretical models. For example, all volume scatterin models include formulations for computing the extinctio coefficient of the medium. Requiring that the model-cal culated total transmission loss through the canopy b comparable in magnitude and exhibit similar spectral an polarization variations to the measured loss represents a excellent test for evaluating the applicability of the mode to the medium.

The present study extends previous studies of the trans mission properties of vegetation canopies along the fol lowing lines: 1) it includes greater simultaneous coverag of the three wave parameters: wavelength, incidence an gle, and polarization, 2) it presents measurements of th phase difference between horizontally polarized and ver tically polarized simultaneously transmitted waves, an 3) it provides a model for wave propagation in a vegeta

Manuscript received January 21, 1987; revised July 30, 1987. This work was supported by NASA Grant NAG 5-480, NASA/GSFC, Beltsville, MD.

The authors are with the Radiation Laboratory, Department of EE-CS, the University of Michigan, Ann Arbor, MI 48109-2122.

IEEE Log Number 8717092.

tion medium comprised of vertically oriented stalks and randomly oriented leaves.

II. The Experiment

Several types of experiments were conducted to measure the transmission loss for a mature corn canopy at incidence angles of 20°, 40°, 60°, and 90°. The configurations used are illustrated in Fig. 1. The transmitters for the 20°, 40°, and 60° measurements were placed on a truck-mounted platform at a height of 11.5 m above the ground surface, and the receivers were placed underneath the canopy. For the 90° measurements, the transmitter platform was placed on the truck bed and the receivers were placed on a wooden platform whose height above the ground was the same as that of transmitters. Fig. 2 shows photographs of the transmitters in the configurations corresponding to Fig. 1(a) and (b). The transmitters used three dual-polarized antennas with center frequencies of 1.62, 4.75, and 10.2 GHz.

Because a vegetation canopy is an inhomogeneous medium at microwave frequencies, its coherent attenuation coefficient should be treated as a random variable. Consequently, to measure (estimate) the mean attenuation with a reasonable degree of precision, it is necessary that the estimate be an average over a large number of statistically independent samples. In addition, it is of interest to record the spatial variations of the canopy attenuation. To meet these requirements, the measurements were performed using the arrangement shown in Fig. 3; the receiving platform was placed on a rail system on which it slid in synchronism with the motion of the truck as it was pulled by a rope connected to the truck through a pulley system. Fig. 4 shows photographs of the ground rail used in conjunction with the 20°–60° measurements and of the elevated rail used with the 90° measurements.

A. The Hardware System

Table I presents a summary of the overall system specifications, including antenna sizes, beamwidths, and relevant dimensions, and Fig. 5 is a block diagram of the receiver configurations used for the power (amplitude) and phase measurements. The amplitude receiver consisted of a small antenna (microstrip patches were used at *L*-band and small dual-polarized corrugated horns were used at both *C*-band and *X*-band) connected to a microwave detector, which was, in turn, connected to a power meter through a 50-m coaxial cable. The output of the power meter was recorded on a strip-chart recorder for immediate display in the field as well as on a digital cassette recorder (using an HP 85 computer) for later analysis. The canopy loss L is defined in dB as

$$L = 10 \log (P_0/P_r) \quad (1)$$

where P_r is the power received when the canopy is present and P_0 is the free-space level received under identical conditions (antenna pointing, range between transmitter and receiver, etc.) but without an intervening canopy between the transmitter and the receiver.

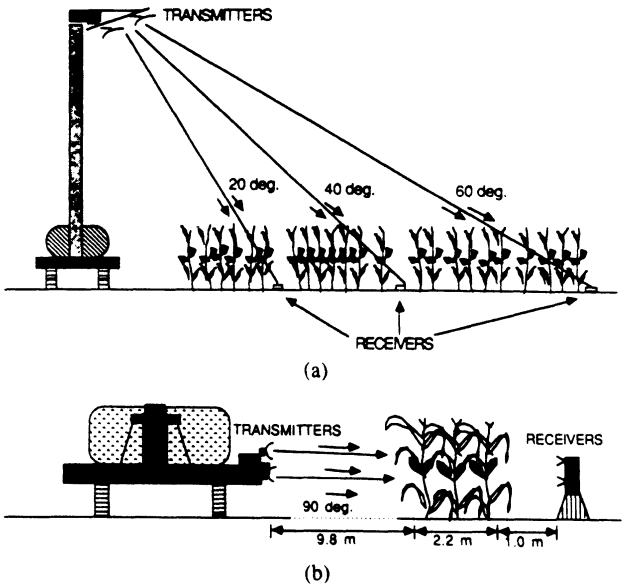

Fig. 1. Configurations used for the transmission measurements at (a) 20°, 40°, 60° and (b) 90°.

The phase measurement refers to the phase difference $\Delta\phi$ between the vertically polarized (V) and horizontally polarized (H) waves transmitted through the canopy. On the transmitting side, H- and V-polarized waves were transmitted simultaneously by the dual-polarized antennas. At the receiver, the outputs of the antenna H- and V-polarization ports were down-converted in frequency to 20 MHz and then relayed to a network analyzer through a pair of 50-m coaxial cables. The phase difference measured by the network analyzer was recorded on a strip-chart recorder and on a digital recorder.

B. Calibration and Interference Tests

By cutting and removing the corn plants from an approximately 3-m wide strip on both ends of the canopy area (Fig. 3), it was possible to establish a free-space reference signal for both the amplitude and the phase measurements. Furthermore the stability of the signal across each of the 3-m wide strips provided an indication of the presence (or absence) of multiple ground reflections. As an additional test, the entire corn canopy was cut and removed at the conclusion of the experiment and direct free-space transmission measurements were made across the entire 10-m wide test area. The variability in the reference signal was found to be within ±0.3 dB for amplitude and ±4° for phase.

C. Types of Measurements

Amplitude measurements were conducted at 1.62 GHz (*L*-band), 4.75 GHz (*C*-band), and 10.2 GHz (*X*-band) for V and H polarizations at 20°, 40°, 60°, and 90°. The measurements were made for three canopy conditions designated as follows:

1) *Full*, which refers to the canopy in its natural condition.

2) *Defoliated*, which refers to the canopy condition after the leaves had been stripped off and removed.

(a)

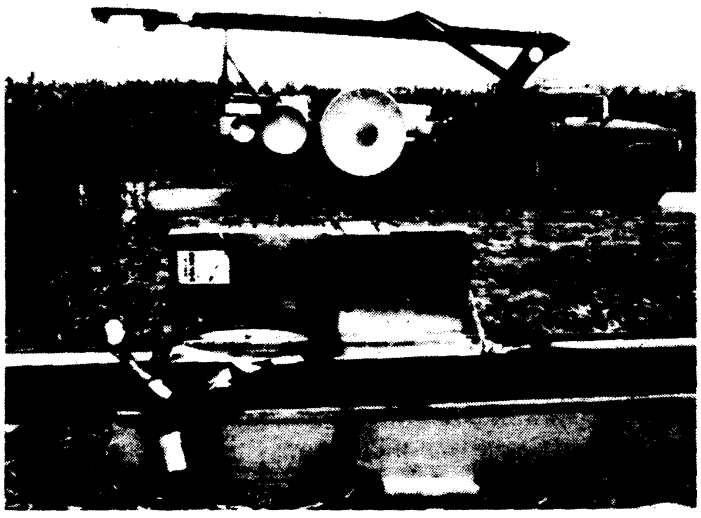

(b)

Fig. 2. Photograph of the transmitting section (a) atop the truck-mounted boom (for the 20° and 40°, and 60° measurements) and (b) on the truck bed for the 90° measurements. The rail system in the foreground shows the back side of the sliding mount on which the receiving antennas were mounted.

3) *Stalks*, which refers to the condition after removing the leaves and the cobs, thereby leaving behind standing stalks only.

Analysis of the data reveals that the difference in attenuation between the Defoliated and Stalks conditions is inconsistent and statistically insignificant. Consequently, only the data for Full and Stalks conditions will be presented in this paper.

The polarization phase-difference measurements were made at *L*-band and *C*-band only, and the incidence angles were limited to 20°, 40°, and 90°.

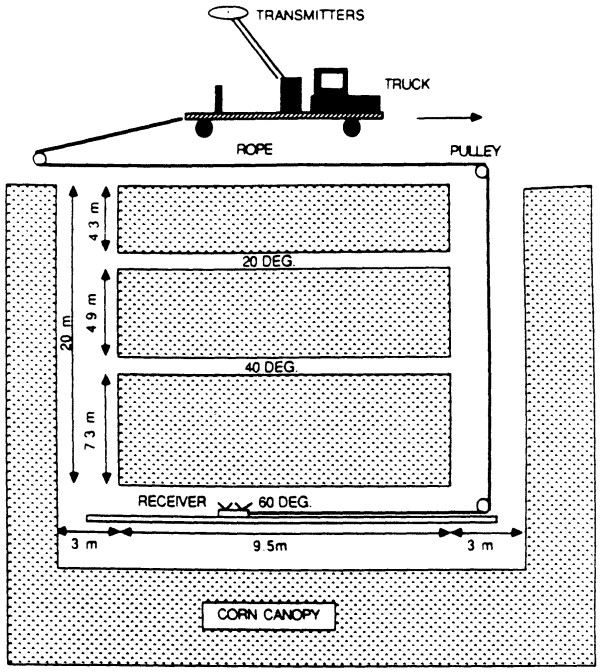

Fig. 3. The pulley system was used so that as the truck moved forward, the transmit and receive antennas moved in space at exactly the same speed, thereby maintaining line of sight.

(a)

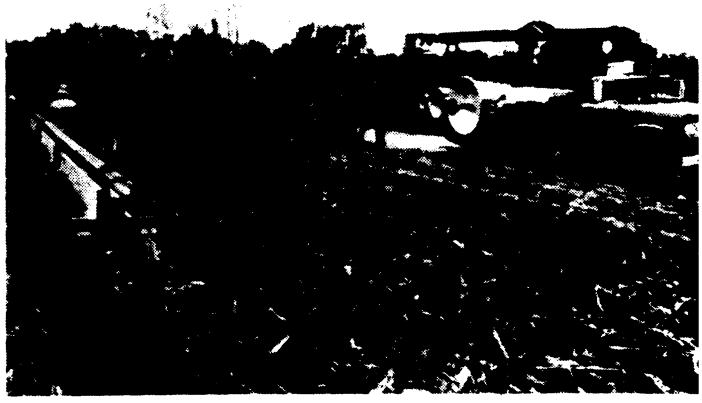

(b)

Fig. 4. Photographs of (a) the ground rail system with the receiving antenna mount and (b) the elevated rail (Photograph taken after defoliating the plants.)

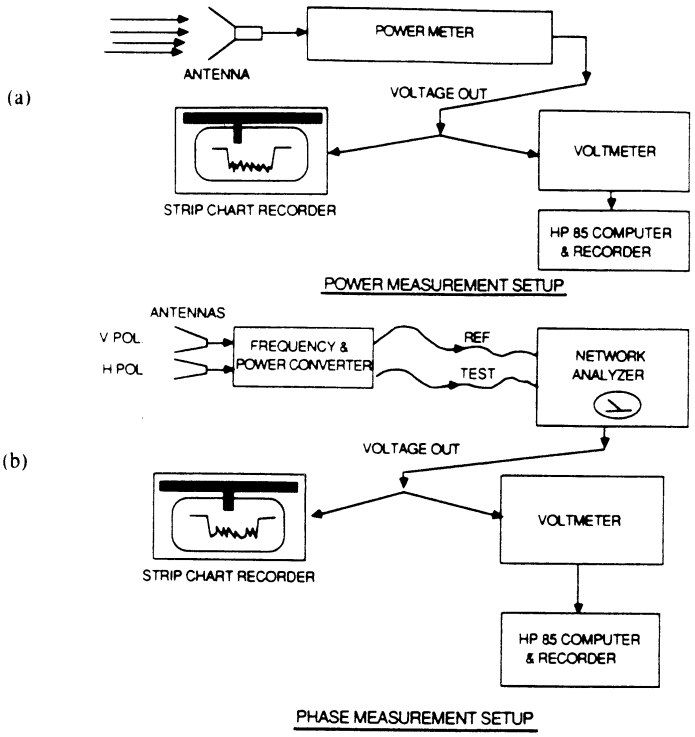

Fig. 5. Block diagrams of the receivers used to measure (a) the amplitude of the received signal and (b) the phase difference between the V-polarized and H-polarized signals.

TABLE I
CHARACTERISTICS OF THE MEASUREMENT SYSTEM

Antenna Beamwidths

	L-Band (1.6 GHz)	C-Band (4.75 GHz)	X-Band (10.2 GHz)
Transmitter	7.8°	4.6°	4.7°
Receiver	90.2°	53.1°	24.7°

Incidence Angle Information

	20°	40°	60°	90°
Distance between Transmitter and Receiver	11.7 m	14.3 m	22.0 m	13.0 m
Transmitter Height	11.5 m	11.5 m	11.5 m	1.2 m
Receiver Height	0.3 m	0.3 m	0.3 m	1.2 m
Slant path in canopy	2.6 m	3.1 m	4.8 m	2.2 m

Canopy Parameters

Row spacing: 76 cm	Stalk volume fraction = 3.5×10^{-3}
Average plant spacing: 19.8 cm	Leaf volume fraction: 5.8×10^{-4}
Average plant height: 2.7 m	Stalk volumetric moisture: 0.47
Stalk diameter: 2.8 cm at base	Leaf volumetric moisture: 0.65
1.8 cm at 1.2 m	Average number of leaves per plant: 13.7
0.6 cm at top	Leaf area index: 2.8

Field measurements were performed to determine the density of plants, the row spacing, and the volume fractions of leaves, stalks, and cobs. In addition, samples were processed in the laboratory to determine their volumetric moisture contents (Table I). Fig. 6 shows spectral plots of the relative dielectric constant of corn leaves and stalks at the moisture contents given in Table I. These curves

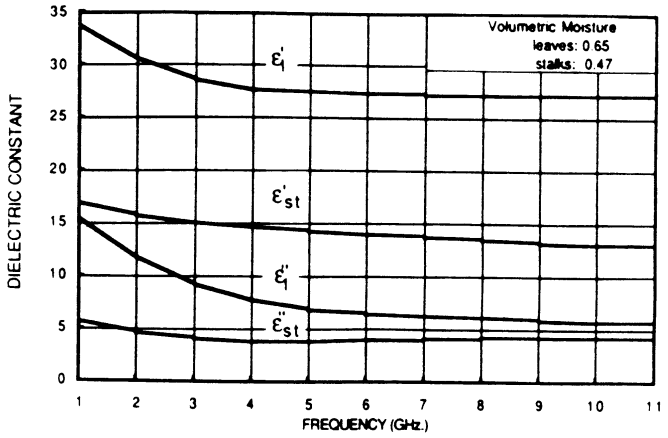

Fig. 6. Dielectric constant of corn leaves and stalks as a function of frequency.

are based on dielectric measurements that were made for corn stalks over a wide range of moistures [10].

III. Sample Results

Because of the large volume of data acquired in this study, we will present only a few samples of the measured records of the transmission loss L and then provide a summary of the overall behavior. Comparison of data with model calculations is given in Section IV.

Figs. 7–9 display the power level recorded by the digital tape recorded at L-band, C-band, and X-band. Each figure contains records for both H and V polarizations. The relatively flat levels at the ends of each record represent the free-space reference level of the received signal. The canopy transmission loss $L(x)$ is measured in decibels relative to this reference level. Close inspection of the records shown in Figs. 7–9, which pertain to a Full canopy condition at $\theta = 60°$, reveals the following observations:

1) At L-band (Fig. 7), the mean value of the V-polarized loss $\bar{L}_V$ is 8.57 dB, compared to only 2.82 dB for the mean of the H-polarized loss $\bar{L}_H$. The standard deviation σ_L is a measure of the fluctuating component of $L(x)$ relative to the mean $\bar{L}$. We observe that $\sigma_V \cong \sigma_H$ at L-band and both $L_V(x)$ and $L_H(x)$ vary slowly as a function of position x. These observations lead to the conclusion that at L-band ($\lambda = 20$ cm) the corn canopy appears quasi-continuous with relatively few discontinuities.

2) At C-band (Fig. 8) the situation is the reverse of what was observed at L-band. The mean values $\bar{L}_V$ and $\bar{L}_H$ are approximately equal, whereas the standard deviations are quite different. The much larger standard deviation of $L_V(x)$ is due to the deep fades shown in Fig. 8(b), which are attributed to attenuation by the stalks. The high spatial-frequency variations of $L_V(x)$ and, to a lesser extent, $L_H(x)$, indicate that the corn canopy is discontinuous at C-band, and, therefore, the discrete approach to modeling scattering in the canopy should be preferred over the continuous-medium approach.

3) At X-band (Fig. 9), $L_V(x)$ and $L_H(x)$ are quite similar to one another. Their means are about the same, and

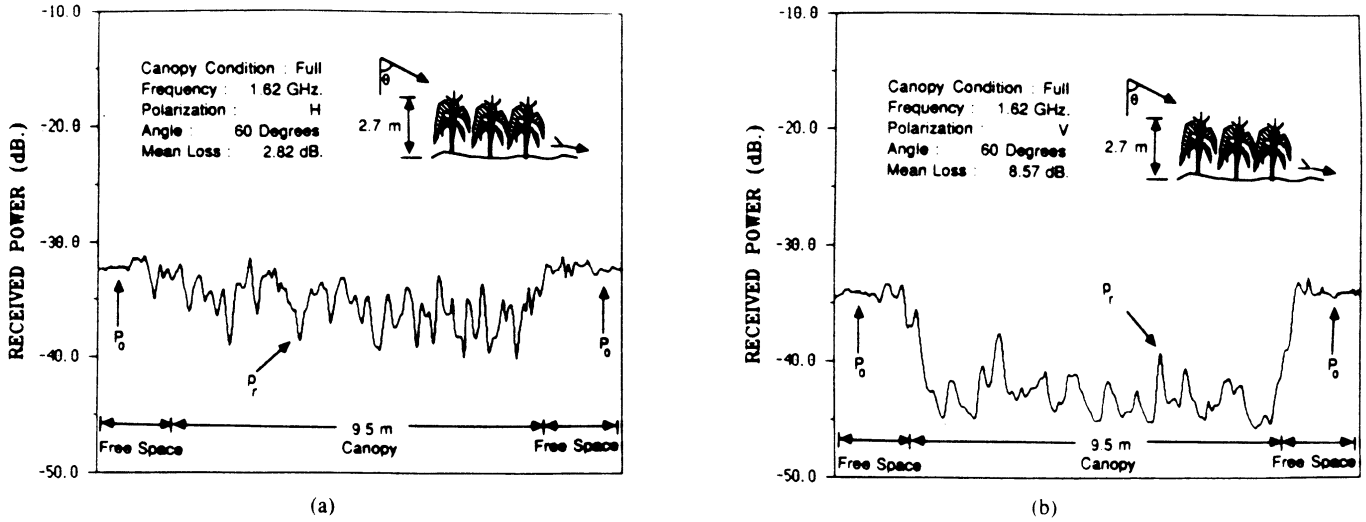

Fig. 7. Received power at L-band as a function of spatial position for (a) H polarization and (b) V polarization.

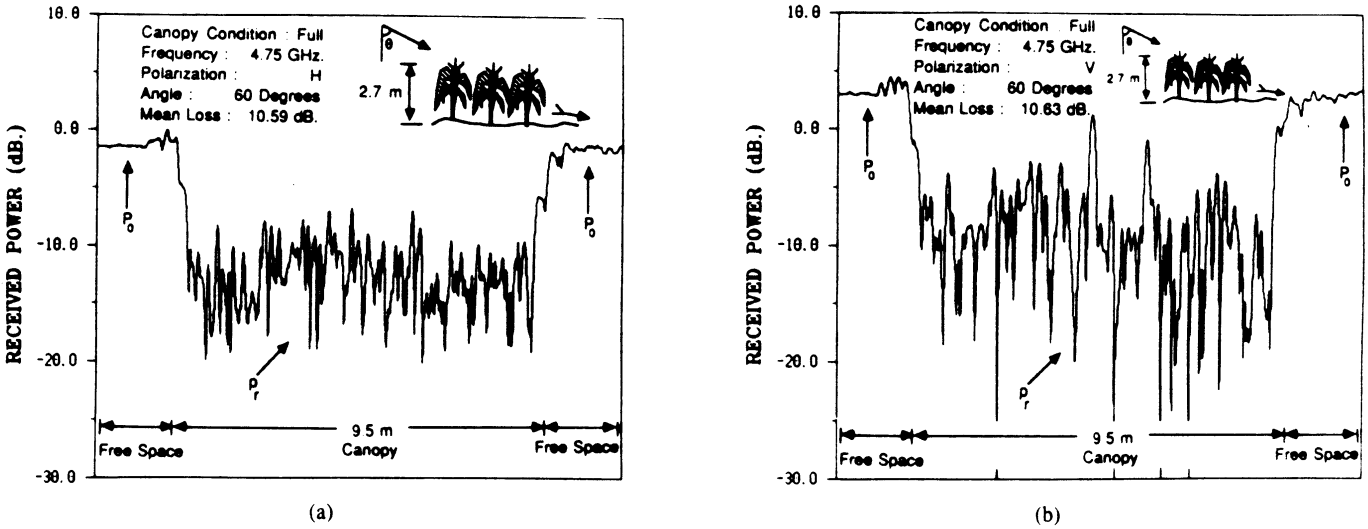

Fig. 8. Received power at C-band as a function of spatial position for (a) H polarization and (b) V polarization.

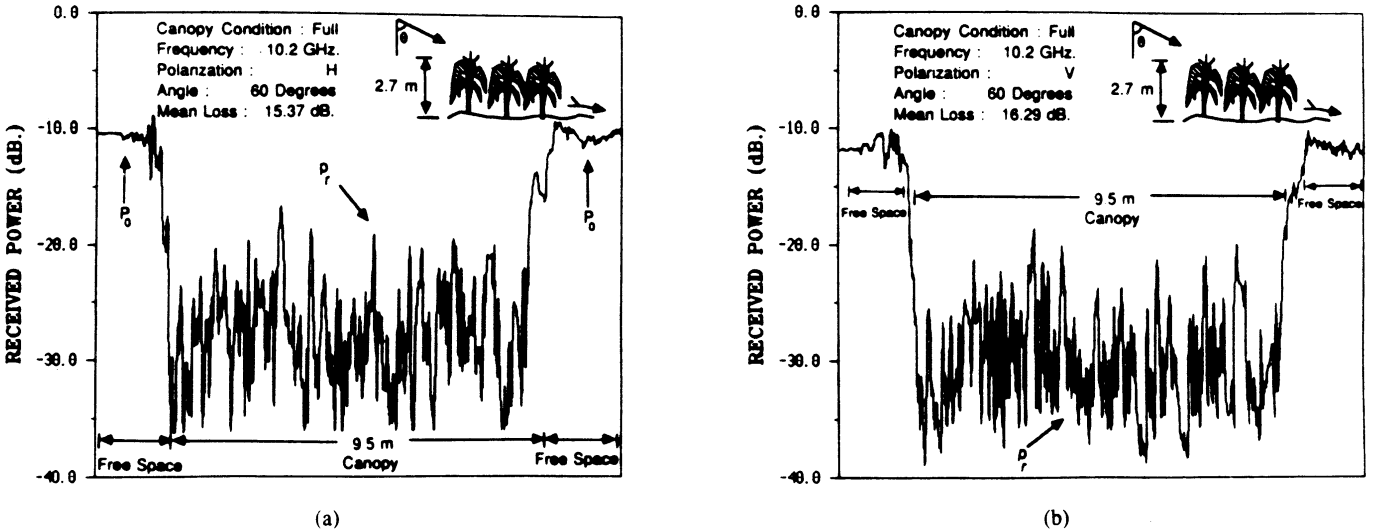

Fig. 9. Received power at X-band as a function of spatial position for (a) H polarization and (b) V polarization.

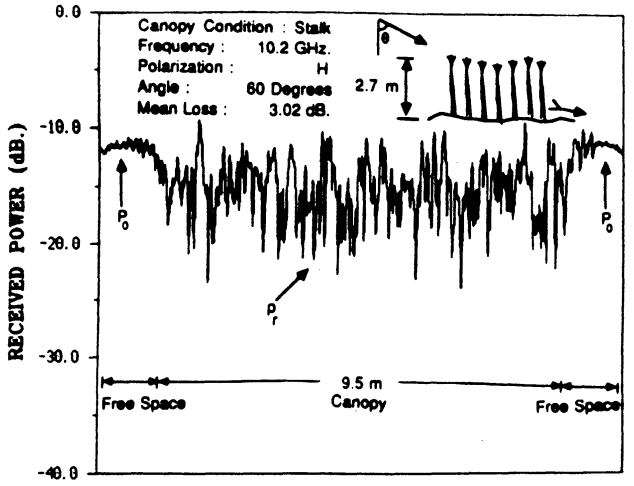

Fig. 10. Received power at *X*-band as a function of spatial position, measured for a defoliated corn canopy with (a) H polarization and (b) V polarization.

so are their standard deviations. As will become apparent later, this similarity is attributed to the fact that the loss at *X*-band is dominated by the leaves, and the stalks exercise a small influence in comparison.

To examine the role played by the stalks relative to that played by the leaves, we present in Fig. 10 records of $L_V(x)$ and $L_H(x)$ for the Stalk condition at *X*-band. We note that $\bar{L}_H$ is 3.02 dB compared to 15.37 dB for the Full canopy, and $\bar{L}_V = 4.12$ dB for Stalks compared to 16.29 dB for Full. Thus, the Stalks are indeed a minor contributor to the total attenuation; even for V polarization $\bar{L}_V$ (Stalk) $- \bar{L}_V$ (Full) $= -12.17$ dB, which is a ratio of 0.06 when converted to natural units.

Another observation worth noting is that in the absence of leaves, the record of $L_V(x)$ contains more high-frequency fluctuations than the record of $L_H(x)$ does, which indicates that even at a wavelength as short at 2.94 cm, the coupling between the propagating wave and a canopy constituent (such as a stalk) is strongly dependent on the constitutent's orientation relative to the direction of the wave's electric field. When leaves are present, diffuse scattering increases, thereby reducing the sensitivity of $L(x)$ to the polarization of the propagating wave.

IV. Propagation Models

The following treatment pertains to a vegetation canopy comprised of vertically oriented stalks (or trunks) and randomly oriented leaves. The canopy is modeled as a slab-like region, its stalks as infinitely long, identical cylinders pointing in the z direction, and its leaves as thin circular discs. We seek an expression for the propagation constant γ of an equivalent dielectric medium such that it is applicable at any incidence angle θ relative to the $-z$ direction and for both H- and V-polarization configurations. This will be realized in two steps. First, we shall consider the case of the defoliated canopy (Stalks condition) and propose a model that incorporates the effect of both absorption and scattering by the dielectric cylinders. This will result in expressions for the equivalent dielectric medium with the complex refractive index n. In the second step, a new set of expressions are derived for the Full canopy case by treating the leaves as small circular discs randomly oriented and randomly distributed in a background medium of refractive index n. By assuming the disc diameter to be small relative to λ, we avoid the problems associated with computing the scattering from a leaf and the need to define a leaf orientation distribution. The results shown later suggest that for a corn canopy this assumption is quite acceptable at *L*-band, barely acceptable at *C*-band, and unacceptable at *X*-band.

A. Defoliated Corn Canopy

1) Single Stalk: Before we treat the problem of wave propagation through a canopy comprised of many corn stalks, we shall briefly examine the electromagnetic properties of a single stalk. Fig. 11 depicts a plane wave incident upon an infinitely long circular cylinder in the $-x$ direction ($\theta = 90°$ and $\phi = 0$) and a scattered wave of the same polarization propagating in the x-y plane at an angle ϕ' relative to $\hat{x}$. The cylinder has a radius a_0 and a relative complex dielectric constant ϵ_{st}. If $\mathbf{U}_V^i$ stands for the electric field of the incident wave $\mathbf{E}^i$ when the wave is vertically polarized (TM) and $\mathbf{U}_H^i$ stands for the magnetic field of the incident wave $\mathbf{H}^i$ when the wave is horizontally polarized (TE), the far-zone scattered field is given by [11, pp. 207]

$$\mathbf{U}_p^{SC}(r, \phi') = \mathbf{U}_p^i \left[\frac{2}{\pi kr}\right]^{1/2} \exp\left[j(kr - \pi/4)\right] T_p(\phi'), \quad p = \text{V or H} \tag{2}$$

where $k = 2\pi/\lambda_0$, λ_0 is the free-space wavelength, $T_p(\phi')$ is the p-polarized normalized far-field amplitude of the scattered field, and p is a polarization index. The amplitudes $T_V(\phi')$ and $T_H(\phi')$ are given by

$$T_V(\phi') = \sum_{n=-\infty}^{\infty} (-1)^n C_n^{TM} e^{jn\phi'} \tag{3a}$$

and

$$T_H(\phi') = \sum_{n=-\infty}^{\infty} (-1)^n C_n^{TE} e^{jn\phi'} \tag{3b}$$

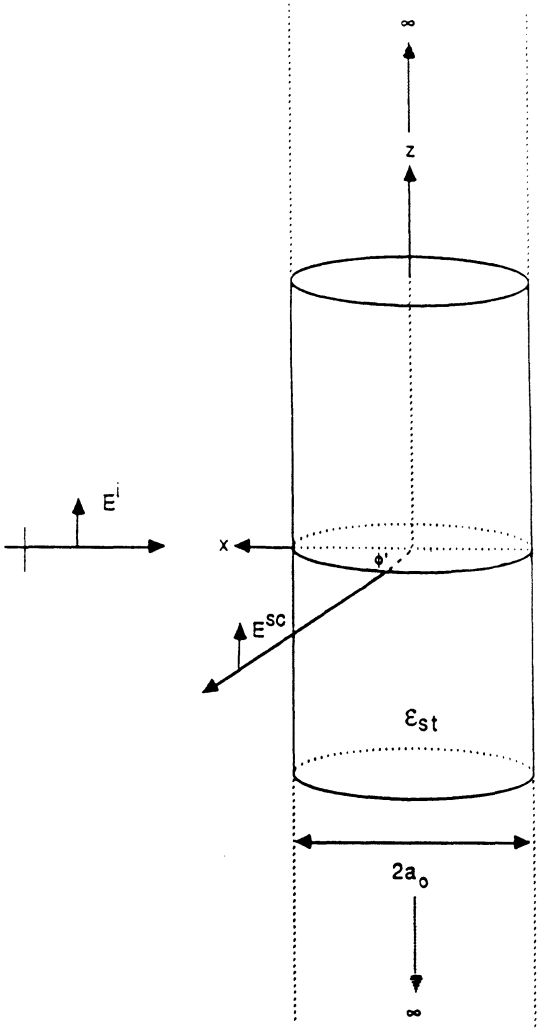

Fig. 11. Scattering geometry for an infinite cylinder.

and the functions C_n^{TM} and C_n^{TE} are given in Ruck *et al.* [11, pp. 273–274] for incidence at any angle Ψ relative to the surface normal of the cylinder ($\Psi = \pi/2 - \theta$). In the present case $\theta = \pi/2$ and $\Psi = 0$.

For a three-dimensional body, its scattering behavior is described by its bistatic scattering cross section, which relates the power of the wave scattered (into a given direction) to that of the incident wave

$$\sigma^{bs} = 4\pi \lim_{r\to\infty} r^2 \frac{(\mathbf{E}^{SC} \cdot \mathbf{E}^{SC*})}{(\mathbf{E}^{i} \cdot \mathbf{E}^{i*})}$$

$$= 4\pi \lim_{r\to\infty} r^2 \frac{(\mathbf{H}^{SC} \cdot \mathbf{H}^{SC*})}{(\mathbf{H}^{i} \cdot \mathbf{H}^{i*})}, \quad \text{m}^2. \tag{4}$$

The analogous quantity for a two-dimensional body, such as an infinite cylinder, is the bistatic scattering width

$$\sigma^{bs} = 2\pi \lim_{r\to\infty} r \frac{(\mathbf{E}^{SC} \cdot \mathbf{E}^{SC*})}{(\mathbf{E}^{i} \cdot \mathbf{E}^{i*})}$$

$$= 2\pi \lim_{r\to\infty} r \frac{(\mathbf{H}^{SC} \cdot \mathbf{H}^{SC*})}{(\mathbf{H}^{i} \cdot \mathbf{H}^{i*})}, \quad \text{m}. \tag{5}$$

Inserting (2) into (5) leads to the following expression for the bistatic scattering width:

$$\sigma_p^{bs}(\phi') = \frac{2\lambda_0}{\pi} \left| T_p(\phi') \right|^2, \quad p = \text{V or H}.$$

The total scattering width is given by

$$\sigma_p^S = -\frac{1}{2\pi} \int_0^{2\pi} \sigma_p^{bs}(\phi')\, d\phi', \quad p = \text{V or H}$$

and using the forward-scattering theorem, the extinc width may be obtained from

$$\sigma_p^E = -\frac{2\lambda_0}{\pi} \text{Re}\left\{T_p(\pi)\right\}, \quad p = \text{V or H}.$$

Finally, the absorption width σ_p^A of the cylinder is de mined from

$$\sigma_p^A = \sigma_p^E - \sigma_p^S.$$

Fig. 12 shows spectral plots of σ^A, σ^E, and σ^S c puted for a 1.7-cm diameter cylinder using the above mulation. The relative dielectric constant was assigned value $\epsilon_{st} = 16.9 + j5.6$. This is appropriate for a c stalk at 1 GHz when its volumetric moisture conter 0.47 (see Fig. 6), which is the value measured for stalks examined in this study. We observe that the s tering and absorption components of σ^E are compar in magnitude for H polarization, but σ^S is significa larger than σ^A for V polarization. All three quantiti σ^S, σ^A, and σ^E—exhibit strong variations with freque below 3 GHz, which corresponds to a wavelength of at 2.5 cm in the stalk medium and approximately equa the stalk diameter. Particularly relevant to the experim tal results discussed in the next section is the fact σ_V^E is about an order of magnitude larger than σ_H^E at 1 GHz and only slightly larger at 4.75 and 10.2 GHz.

2) Many Stalks: Ulaby *et al.* [12] have shown propagation in a layer comprised of identical vertical c inders randomly positioned in the x-y plane may be m eled in terms of an equivalent dielectric medium cha terized by a complex index of refraction given by

$$n_p' \cong 1 + \frac{2N}{k^2} \sin\theta \,\text{Im}\left\{T_p(\theta, \pi)\right\}, \quad p = \text{V or H}$$

(1

and

$$n_p'' \cong -\frac{2N}{k^2} \sin\theta \,\text{Re}\left\{T_p(\theta, \pi)\right\}, \quad p = \text{V or H}$$

(1

where N is the number density of cylinders (per unit are θ is the angle of incidence relative to $\hat{\mathbf{z}}$, and $T_p(\theta, \pi$ the p-polarized normalized scattering amplitude evalua for $\phi' = \pi$ (forward scattering), and is given by

$$T_V(\theta, \pi) = \frac{1}{\sin\theta} \sum_{n=-\infty}^{\infty} C_n^{TM}(\theta) \tag{1}$$

$$T_H(\theta, \pi) = \frac{1}{\sin\theta} \sum_{n=-\infty}^{\infty} C_n^{TE}(\theta) \tag{1}$$

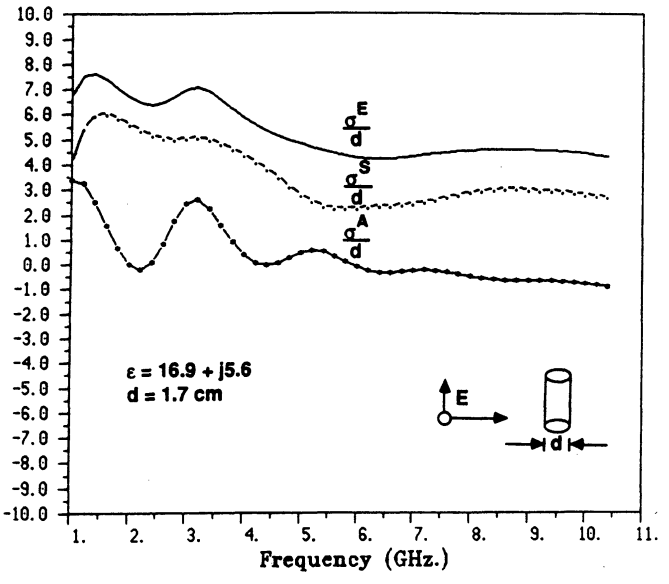

(a)

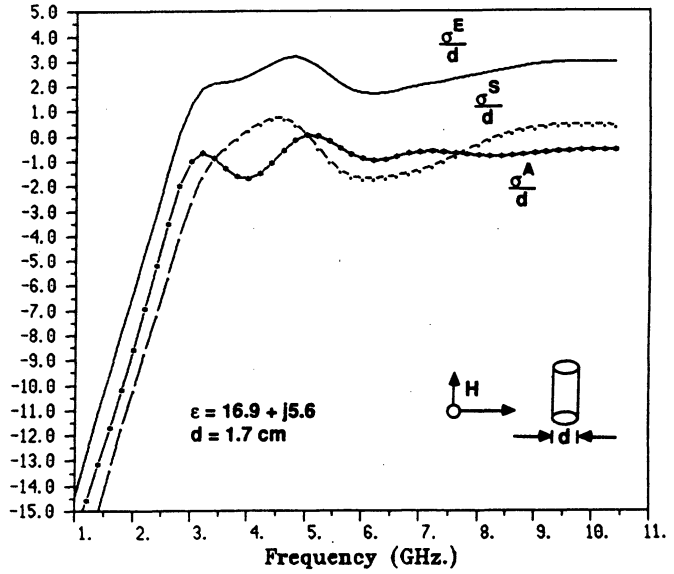

(b)

g. 12. Calculated spectral variation of the normalized absorption, scattering, and extinction widths for an infinite cylinder illuminated with (a) a V-polarized wave and (b) an H-polarized wave. d is the cylinder diameter.

he functions $C_n^{TM}(\theta)$ and $C_n^{TE}(\theta)$ are the same as those troduced earlier in connection with (3).

The propagation constant of the equivalent medium γ_p related to n_p by

$$\gamma_p = kn_p = k(n_p' + jn_p'') \tag{12}$$

nd since $j\gamma_p = -\alpha_p + j\beta_p$, the attenuation constant α_p nd phase constant β_p are given by

$$\alpha_p = kn_p'', \quad p = \text{V or H} \tag{13a}$$

$$\beta_p = kn_p', \quad p = \text{V or H}. \tag{13b}$$

he extinction width of an infinite cylinder is given by

$$\sigma_p^E(\theta) = -\frac{2\lambda_0}{\pi} \operatorname{Re}\left\{T_p(\theta, \pi)\right\} \tag{14}$$

which, when combined with (13a) and (14), leads to

$$\kappa_p(\theta) = 2\alpha_p = N\sigma_p^E(\theta) \sin\theta, \quad p = \text{V or H}. \tag{15}$$

The (power) extinction coefficient $\kappa_p(\theta)$ is associated with propagation of the "mean" field through the layer and incorporates losses due to both scattering and absorption by the cylinders. For propagation over a distance d, the mean loss $L_p(\theta)$ is given by

$$\begin{aligned} L(\theta) &= 10 \log\left[e^{\kappa_p(\theta) d}\right] \\ &= 4.34\, \kappa_p(\theta)\, d. \end{aligned} \tag{16}$$

The polarization phase difference for one-way propagation is given by

$$\begin{aligned} \Delta\Phi &= (\beta_H - \beta_V)\, d \\ &= \frac{2N\,d}{k} \sin\theta \left[\operatorname{Im}\left\{T_H(\theta, \pi)\right\}\right. \\ &\quad \left. - \operatorname{Im}\left\{T_V(\theta, \pi)\right\}\right]. \end{aligned} \tag{17}$$

3) Comparison with Experimental Observations: Fig. 13 provides spectral plots of $L_p(\theta)$ for the 1–11 GHz range, all computed in accordance with the formulation given in the preceding section and using the dielectric function given in Fig. 6. Also included are the data measured at 1.62, 4.75, and 10.2 GHz, presented in the form of the mean value of the measured loss and the associated ±25-percent confidence interval. Overall, good agreement is observed between the measured data and the theoretical curves. The same data were used in Fig. 14 to display the angular variation of the extinction coefficient $\kappa_p(\theta)$.

As was mentioned previously in Section II-C, the polarization phase-difference measurements were made at 1.62 and 4.75 GHz. The variation of $\Delta\Phi$ with frequency was calculated using (17) and is compared with the measured data in Fig. 15. Considering the broad extent of the confidence intervals associated with the measured data, it is reasonable to conclude that there is good qualitative agreement between the theory and the experimental observations.

B. Full Corn Canopy

When in the Full condition, the corn canopy includes both stalks and leaves. Although conceptually the extinction attributable to leaves may be treated in a manner similar to that presented in the preceding section for stalks, the problem is somewhat more difficult for leaves because: 1) the leaves have an irregular shape whereas the stalks may be approximated as cylinders and 2) the leaves are nonuniform in orientation whereas the stalks are essentially vertical. Consequently, we shall make certain simplifying assumptions in order to reduce the complexity of the problem to a manageable state, seek a solution for the extinction coefficient of a Full canopy, and then compare the results to the experimental data.

If we consider the leaves to be thin circular discs, small

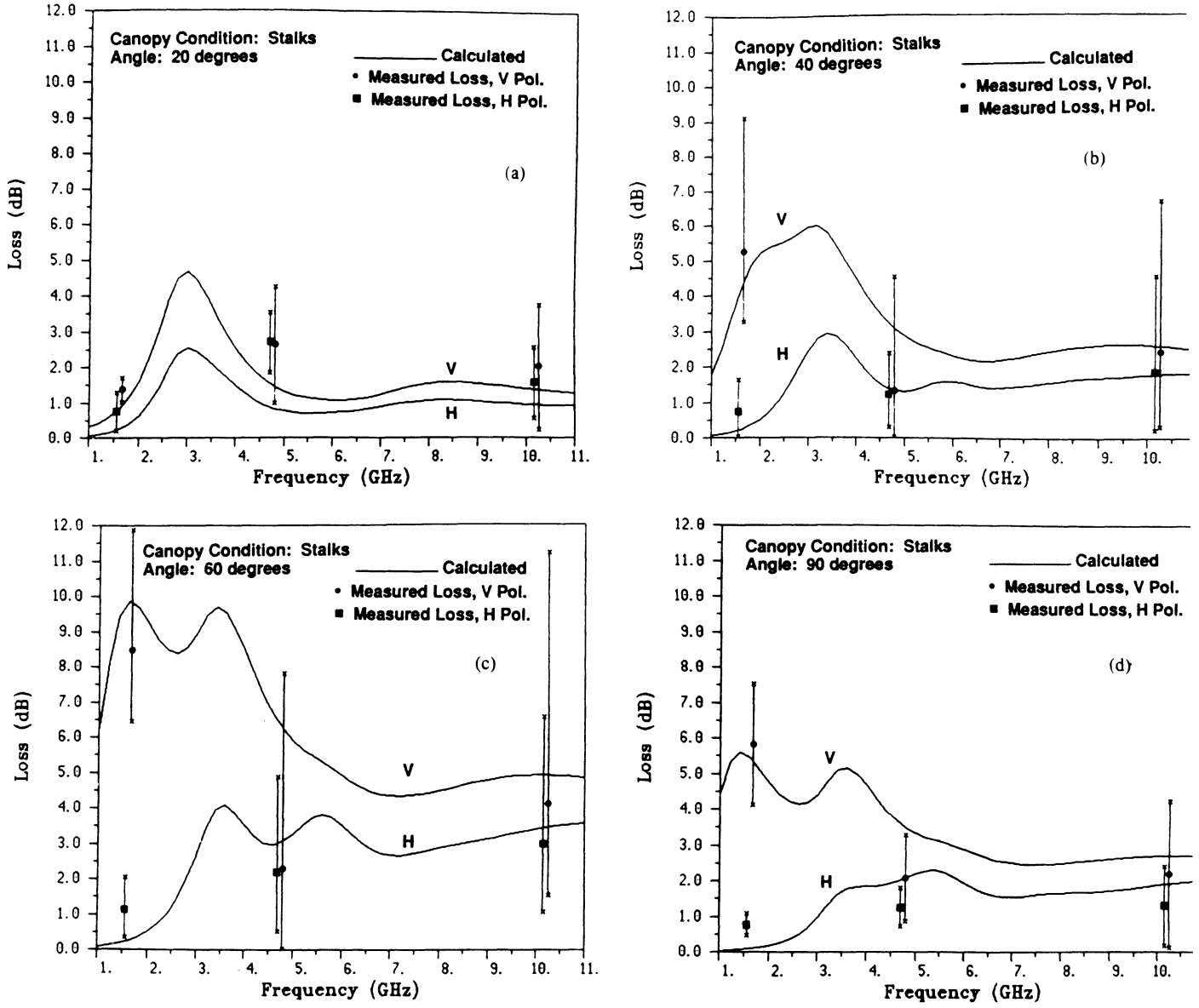

Fig. 13. Comparison of the calculated loss spectrum for stalks with measured data at incidence angles of (a) 20°, (b) 40°, (c) 60°, and (d) 90°.

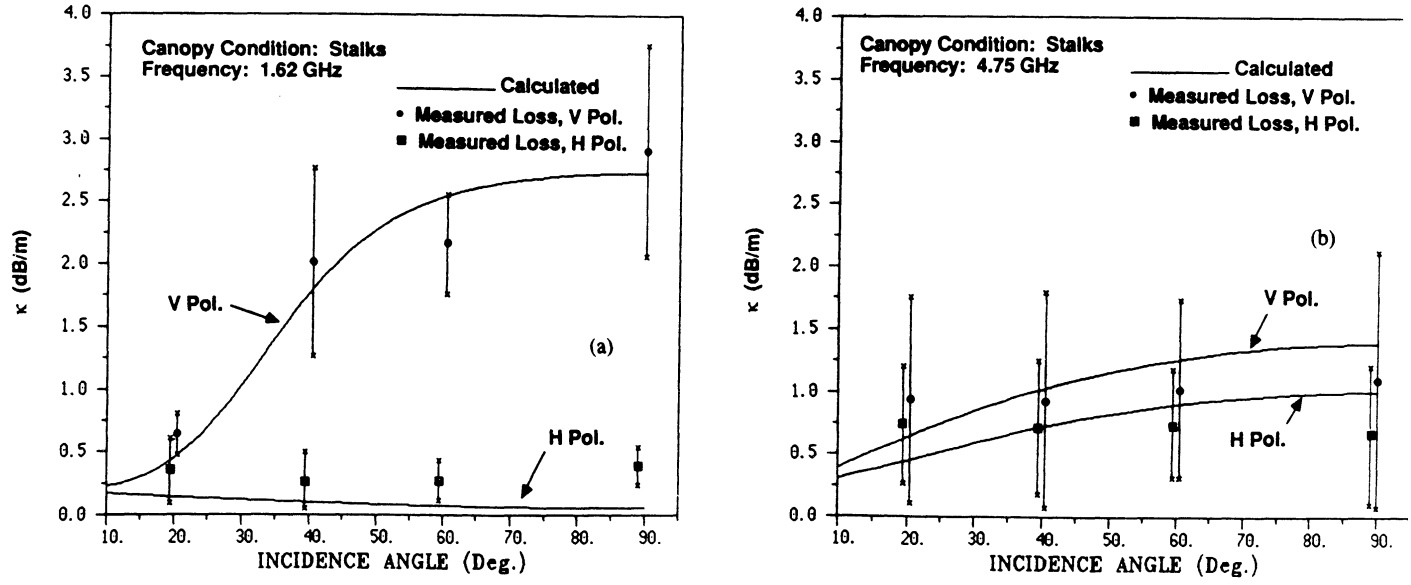

Fig. 14. Comparison of calculated extinction coefficient for stalks with measured values at (a) *L*-band and (b) *X*-band.

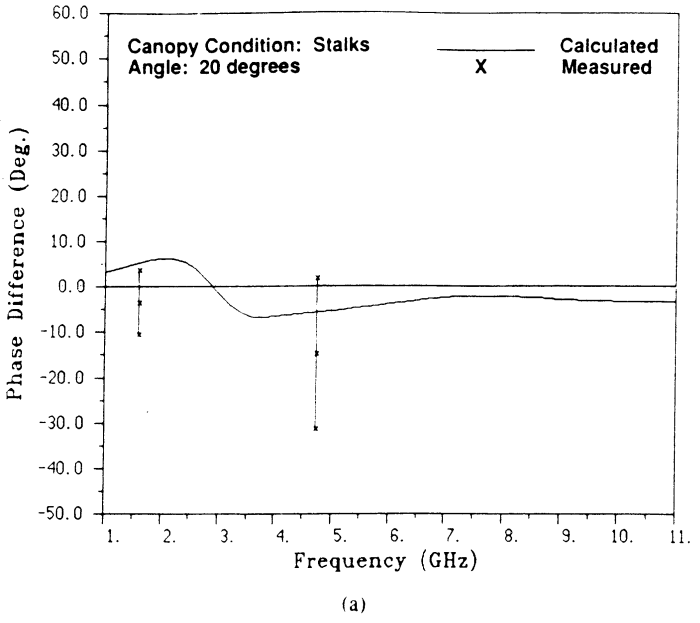

(a)

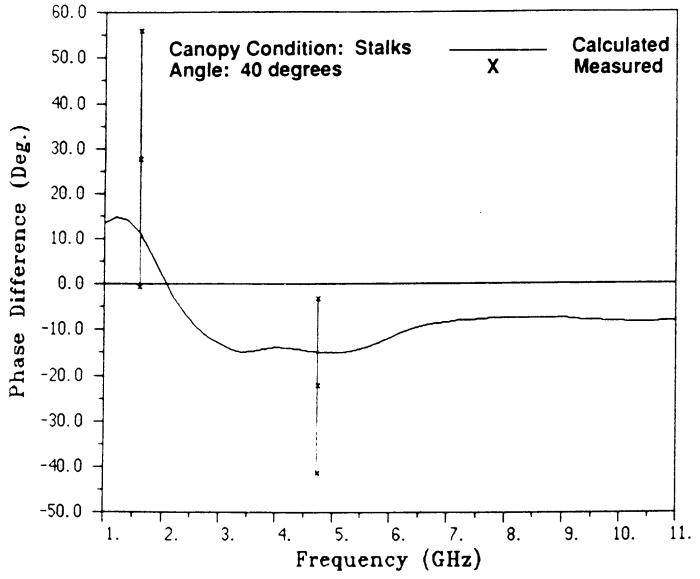

(b)

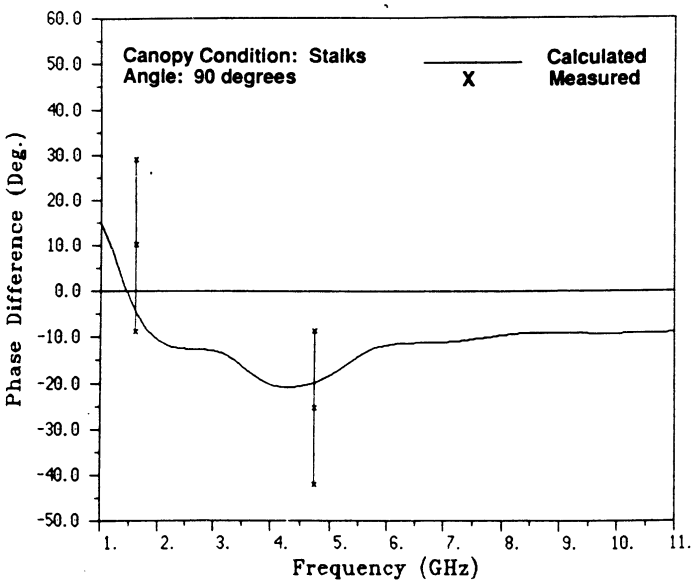

(c)

Fig. 15. Comparison of calculated polarization phase difference $\Delta\Phi$ with measured data at incidence angles of (a) 20°, (b) 40°, and (c) 90°.

in size relative to λ, and randomly oriented, we can use the de Loor mixing formula [13; 14, p. 2040] to relate the relative dielectric constant of the leaf material ϵ_l to that of a medium with equivalent propagation properties for the mean field. The equivalent medium, which is comprised of a background dielectric material of dielectric constant ϵ, representing the stalks in air, and inclusions (the leaves) of dielectric constant ϵ_l and volume fraction v_l, has a relative dielectric constant ϵ_c given by

$$\epsilon_c = \epsilon + \frac{v_l}{3}(\epsilon_l - \epsilon)\left(2 + \frac{\epsilon}{\epsilon_l}\right) \tag{18}$$

Because the background dielectric $\epsilon = \epsilon_p(\theta)$ is a function of both the incidence angle θ and the polarization configuration p, so is the canopy dielectric constant ϵ_c. The background dielectric constant is related to the index of refraction defined by (10) through

$$\epsilon = \epsilon_p = (n_p' + jn_p'')^2 \tag{19}$$

and the extinction coefficient of the Full canopy medium is given by

$$\begin{aligned} \kappa_c &= 2\alpha_c \\ &= 2kn_c \end{aligned} \tag{20}$$

with $n_c = \sqrt{\epsilon_c}$. Although not denoted explicitly, both κ_c and n_c are functions of θ and the polarization index p.

Using the preceding formulation, κ_c was computed for V and H polarizations at 1.62, 4.75, and 10.2 GHz and the results are presented in Fig. 16. Comparison of the theoretical results with the measured data indicates very good agreement at 1.62 GHz, fair agreement at 4.75 GHz, and poor correspondence at 10.2 GHz. At 10.2 GHz, the measured data are consistently higher in level than the computed curves. This is attributed to the assumption that extinction by the corn leaves is dominated by intrinsic absorption and that scattering losses are negligibly small, which is an inherent assumption of the model leading to (18). The results suggest that this assumption is reasonably acceptable at 1.62 GHz ($\lambda \cong 20$ cm), but is strongly violated at 10.2 GHz.

V. Conclusions

The propagation model developed in this paper accounts for both scattering and intrinsic absorption by the canopy cylinders (stalks), but treats the leaves as small randomly oriented discs. Good agreement between theory and experiment is obtained for the defoliated canopy at 1.62, 4.75, and 10.2 GHz and for the canopy with leaves also, but only at 1.62 GHz. In order to extend the frequency coverge of the present model, it should be modified to incorporate the scattering phase function and slope distribution of the leaves.

References

[1] J. K. Lee and J. A. Kong, "Active microwave remote sensing of an anisotropic random-medium layer," *IEEE Trans. Geosci. Remote Sensing*, vol. Ge-23, no. 6, pp. 910–923, Nov. 1985.

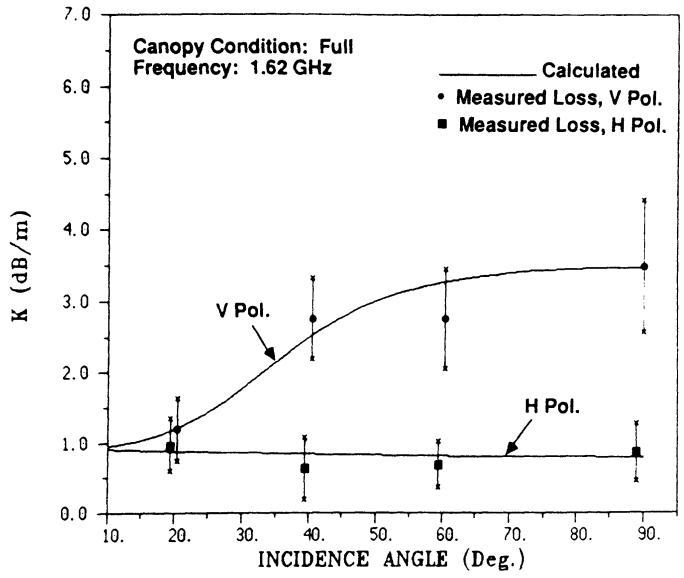

(a)

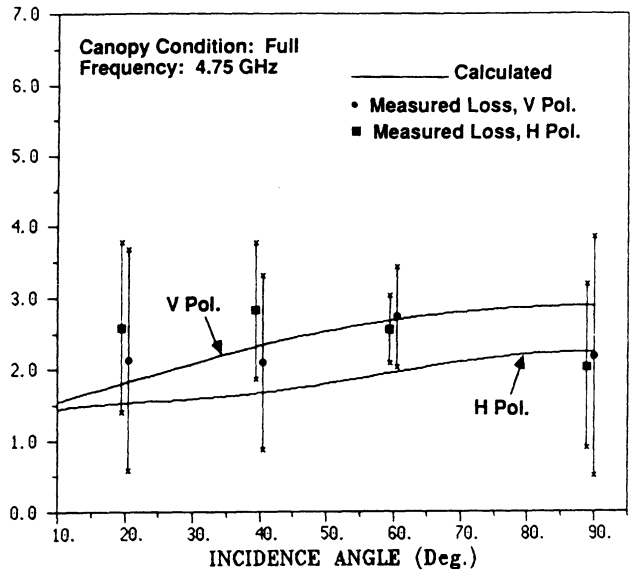

(b)

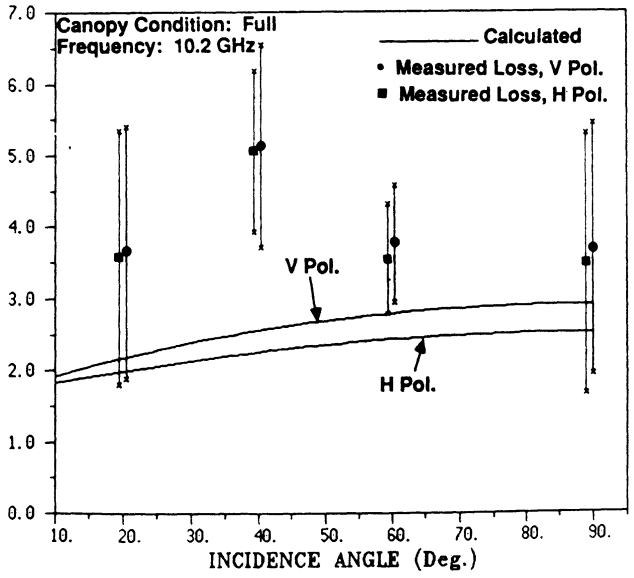

(c)

Fig. 16. Comparison of calculated extinction coefficient with measured values for a full corn canopy at (a) *L*-band, (b) *C*-band, and (c) *X*-band.

[2] ——, "Passive microwave remote sensing of an anisotropic randoi medium layer," *IEEE Trans. Geosci. Remote Sensing*, vol. GE-2 no. 6, pp. 924-932, Nov. 1985.

[3] R. H. Lang, S. S. Seker, and D. M. Levine, "Vector solution for t mean electromagnetic fields in a layer of random particles," *Raa Sci.*, vol. 21, pp. 771-786, 1986.

[4] J. J. Eom and A. K. Fung, "A scatter model for vegetation up to K band," *Remote Sensing Environ.*, vol. 15, pp. 185-200, 1984.

[5] F. T. Ulaby and R. P. Jedlicka, "Microwave dielectric properties plant materials," *IEEE Trans. Geosci. Remote Sensing*, vol. GE-2 pp. 406-414, 1984.

[6] L. K. Wu, R. K. Moore, R. Zoughi, A. Afifi, and F. T. Ulaby, "Pr liminary results on the determination of the sources of scattering fro vegetation canopies at 10 GHz," *Int. J. Remote Sensing*, vol. 6, n 2, pp. 299-313, 1985.

[7] J. F. Paris, "Probing thick vegetation canopies with a field micr wave scatterometer," *IEEE Trans. Geosci. Remote Sensing*, vol. GI 24, no. 6, pp. 886-893, Nov. 1986.

[8] C. T. Allen and F. T. Ulaby, "Modeling the polarization dependen of the attenuation in vegetation canopies," in *IEEE Int. Geosci. R mote Sensing Symp. (IGARSS) Dig.* (Strasbourg, France), Aug. 2 30, 1984.

[9] F. T. Ulaby and E. A. Wilson, "Microwave attenuation propertie of vegetation canopies," *IEEE Trans. Geosci. Remote Sensing*, vo GE-23, pp. 746-753, no. 5, Sept. 1985.

[10] F. T. Ulaby and M. El-Rayes, "Microwave dielectric spectrum vegetation material," in *Proc. IGARSS Symp.* (Zurich), Sept. 8-1 1986.

[11] G. T. Ruck, D. E. Barrick, W. D. Stuart, and C. K. Krichbaun *Radar Cross Section Handbook.* New York: Plenum 1970.

[12] F. T. Ulaby, D. Held, M. C. Dobson, K. McDonald, and T. B. A Senior, "Relating polarization phase difference of SAR signals scene properties," *IEEE Trans. Geosci. Remote Sensing*, vol. GI 25, no. 1, pp. 83-92, Jan. 1987.

[13] G. P. de Loor, "Dielectric properties of heterogeneous mixtures co taining water," *J. Microwave Power*, vol. 3, pp. 67-73, 1968.

[14] F. T. Ulaby, R. K. Moore, and A. K. Fung, *Microwave Remote Sen ing: Active and Passive*, vol. 3. New York: Artech House, 1986.

*

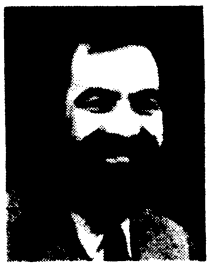

Fawwaz T. Ulaby (M'68-SM'74-F'80) was bo in Damascus, Syria, on February 4, 1943. He r ceived the B.S. degree in physics from the Ame ican University of Beirut, Lebanon, in 1964 a the M.S.E.E. and Ph.D. degrees in electrial e gineering from the University of Texas, Austi in 1966 and 1968, respectively.

From 1968 to 1984, he was with the Electric Engineering Department at the University of Ka sas, where he was the J. L. Constant Disti guished Professor, and the University of Kans Center for Research, where he was Director of the Remote Sensing Lab ratory. He is currently Professor of Electrical Engineering and Comput Science, the University of Michigan, Ann Arbor. His current research i terests involve microwave propagation and active and passive microwa remote sensing. Along with R. K. More and A. K. Fung, he is a coauth of the three-volume series *Microwave Remote Sensing: Active and Passi* (Reading, MA: Addison-Wesley). In addition, he is coeditor of the *Manu of Remote Sensing*, 2nd ed., vol. I (American Society of Photogrammetry

Dr. Ulaby is a member of Eta Kappa Nu, Tau Beta Pi, and Sigma X He is the Executive Editor for the IEEE TRANSACTIONS AND GEOSCIEN AND REMOTE SENSING, 1984-1988, and was the Geoscience and Remo Sensing Society's Distinguished Lecturer for 1986-1987. He received t GRS Society's Outstanding Service Award in 1982, and its Distinguish Service Award in 1983. In 1984, he also received a Presidential Citatic for Meritorious Service from the American Society of Photogrammetry ar the IEEE Centennial Medal. He received the University of Kansas Cha cellor's Award for Excellence in Teaching in 1980, the University of Ka sas Gould Award for "distinguished service to higher education" in 197 and the Eta Kappa Nu MacDonald award as an "outstanding electrical e gineering professor in the United States of America" in 1975, the Unive sity College of Engineering Reserch Excellence Award in 1986, and t Kuwait Prize in applied science for 1986.

had Tavakoli was born in Teheran, Iran, on March 8, 1959. He received ıe B.S. and M.S. degrees in electrical engineering from the University of ansas, Lawrence, in 1982 and 1984, respectively. He is working toward ıe Ph.D. degree in electrical engineering and computer science at The Iniversity of Michigan, Ann Arbor.

His areas of interest are microwave remote sensing and dielectric propıties of materials.

*

Thomas B. A. Senior (SM'66-F'72) received the M.Sc. degree in applied mathematics from the University of Manchester, England, in 1950 and the Ph.D. degree in research from Cambridge University in 1954.

In 1952 he was appointed as an Established Scientific Officer and accepted a position with the Ministry of Supply at the Radar Research and Development Establishment (now the Royal Radar Establishment) at Malvern, England. In 1955 he was promoted to Senior Scientific Officer. He joined the Radiation Laboratory, University of Michigan, Ann Arbor, in June 1957. He was appointed Professor of Electrical Engineering in 1969 and Director of Radiation Laboratory in 1975. His primary interests are in the study of diffraction and propagation of electromagnetic waves, with applications to physical problems.

Dr. Senior has been an Associate Editor for *Radio Science* and served as Editor from 1973 through 1978, and is now an Associate Editor for *Electromagnetics*. He is the Vice Chairman of Commission B of the International Union of Radio Science, the past Chairman of the U.S. National Committee for URSI and served as Chairman of the U.S. Commission B. He is a member of Signa Xi, Tau Beta Pi, and Eta Kappa Nu, and is listed in American Men and Women of Science.

Microwave Emission from Row Crops

DAVID R. BRUNFELDT AND FAWWAZ T. ULABY, FELLOW, IEEE

Abstract—**In order to examine the emission properties of vegetation without taking into consideration the effects of variations in the soil background, strips of metal screening were used to cover the soil surface between adjacent rows of plants. Temporal measurements were made at 2.7 and 5.1 GHz for soybean, wheat, and corn canopies. Several special experiments were conducted to evaluate the sensitivity of brightness temperature to look direction (relative to row direction), polarization configuration, and incidence angle, and to evaluate the emission contributions of defoliated stalks. In general, the results show that the canopy is highly anisotropic, the emission exhibits a strong dependence on polarization and look direction, and the scattering albedo is, typically less than 0.1. Canopy transmissivity was estimated from the radiometric observations and then related empirically to the canopy's integrated water content. Using this relation in a zero-order radiative transfer model led to good agreement between the experimental observations and the model predictions.**

I. Introduction

AT CENTIMETER wavelengths, a vegetation canopy may be modeled as an inhomogeneous medium comprised of discrete scatterers (such as leaves and stalks) distributed in an air background. The sizes, shapes, and dielectric properties of the scatterers determine the angular, spectral, and polarization behavior of canopy scattering and emission. The backscattering coefficient of a vegetation layer over a soil background represents the sum of backscattering contributions related to the canopy alone, the soil alone (except for two-way attenuation), and interactions between the canopy volume and the soil surface. A similar statement applies in the emission case.

Because of the complexity of the scattering and emission problems, it is difficult to study the microwave scattering and emission behavior of the canopy independently of the soil background. This has often led to multiple interpretations of experimental observations. In order to circumvent this difficulty, Brunfeldt and Ulaby [1] used metal screens to isolate the soil surface from the vegetation canopy and then proceeded to make radiometric observations of the canopy as a function of several parameters. The screens were wire meshes with an interwire spacing of 1.6 mm and wire thickness of 0.3 mm. Such an arrangement was sufficiently large to allow normal water drainage and vegetation growth, yet sufficiently small for the screen to act (electromagnetically) as a reflecting (nonemitting) surface at the wavelengths under consideration (5 and 11 cm). This technique was used in the study reported here to investigate the following questions:

a) Is the brightness temperature T_B of a vegetation canopy polarization-independent? If not, what is the role of the polarization configuration of the radiometer antenna with regard to emission by the canopy?

b) Is it a reasonable assumption to regard the canopy as being symmetrical in azimuth?

c) For canopies planted in parallel rows, does the brightness temperature depend on row direction (relative to the observation direction)?

d) Is it possible to relate the brightness temperature of a canopy to its biophysical properties?

This paper describes a set of experiments conducted at 2.7 and 5.1 GHz to examine the preceding questions for soybean and corn canopies.

Manuscript received September 6, 1985; revised December 4, 1985.

D. R. Brunfeldt is with the Applied Microwave Corporation, Lawrence, KS 66046.

F. T. Ulaby is with the Radiation Laboratory, University of Michigan, Ann Arbor, MI 48109.

IEEE Log Number 8607734.

II. Canopy Emission

To examine the emission from a vegetation canopy, the following zero-order solution of the radiative transfer equation will be used:

$$T_B = (1 + \Upsilon\,\Gamma_g)(1 - \Upsilon)(1 - \omega)T_v + \Upsilon(1 - \Gamma_g)T_g + \Upsilon^2 T_{SKY}\Gamma_g \quad (1)$$

where T_B is the brightness temperature, Υ is the one-way transmissivity of the canopy, Γ_g is the reflectivity of the underlying ground surface, ω is the scattering albedo of the vegetation layer, T_V and T_g are the physical temperatures of the vegetation and ground media, and T_{SKY} is the downwelling sky brightness temperature. The model ignores diffuse scattering in the medium and reflection at the air-vegetation boundary. At the frequencies under consideration (2.7 and 5.1 GHz), T_{SKY} is of the order of 5 K, which means that the last term in the above equation may be neglected (since $\Upsilon^2\Gamma_g < 1$). Also, we may set $T_v = T_g = T_0$, in which case (1) reduces to

$$T_B = [(1 - \omega + \omega\Upsilon) + \Gamma_g(\omega\Upsilon^2 - \Upsilon^2 - \omega\Upsilon)]T_0. \quad (2)$$

For the purpose of the discussion that follows, we shall simplify the above expression further. However, we shall not use the resulting expression for comparison with data. The albedo ω is of the order of 0.1, and Υ usually is smaller than 0.5 (except for very dry and/or short canopies). Hence, terms involving the products $\omega\Upsilon$ and $\omega\Upsilon^2$ are much smaller than the other terms in (2) and may be neglected.

$$T_B \simeq [(1 - \omega) - \Gamma_g\Upsilon^2]T_0. \quad (3)$$

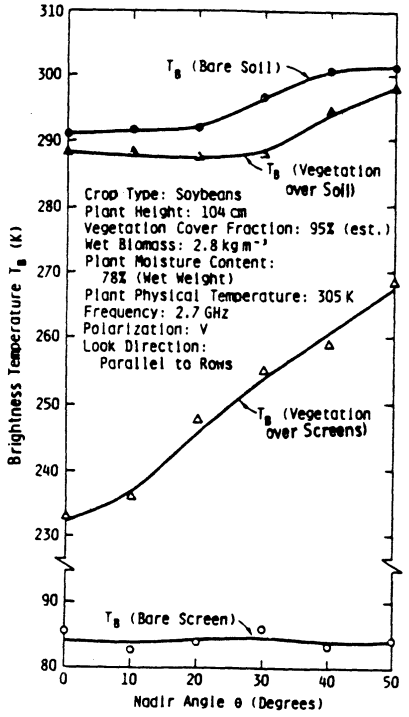

Fig. 1. Measured brightness temperature of vegetation over soil, vegetation over screen, bare soil, and bare screen. The frequency is 2.7 GHz.

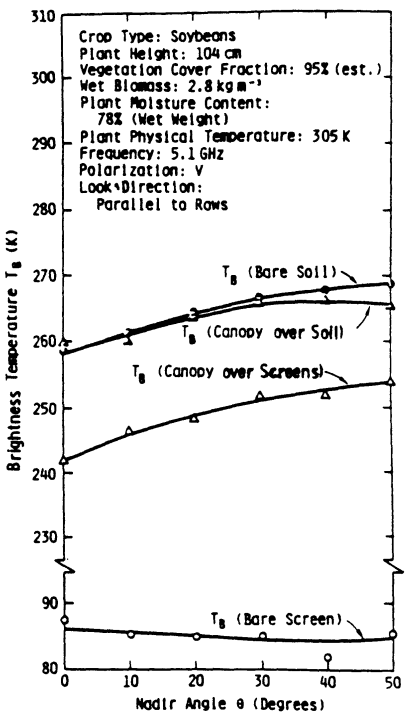

Fig. 2. Measured brightness temperature of vegetation over soil, vegetation over screen, bare soil, and bare screen. The frequency is 5.1 GHz.

For a dry soil background, $\Gamma_g \simeq 0.1$ at nadir. In contrast, a metal plate has $\Gamma_g = 1.0$. This large difference in reflectivity suggests that the use of metal screens to cover the soil surface enhances the sensitivity of T_B to canopy variations. The scattering albedo is a parameter of the scattering medium (vegetation layer) and is therefore independent of variations in the vertical thickness of the vegetation layer as long as the canopy maintains an approximately constant structure. We know that the canopy structure changes over the growth cycle, but its influence on ω is likely to be much smaller than its effect on Υ. The transmissivity Υ is related to the total propagation loss through the canopy along the direction of observation. Hence, height variations have a direct effect on Υ. Variations in canopy moisture also exercise a direct effect on Υ through the extinction coefficient κ_e. In contrast, the albedo is equal to the ratio of the scattering coefficient κ_s to the extinction coefficient κ_e, both of which increase with increasing moisture content. Although the rates of increase with moisture may not be the same for the scattering and absorption coefficients, the ratio $\omega = \kappa_s/(\kappa_s + \kappa_a)$ is much less sensitive to moisture than κ_e.

Based on the preceding arguments, we expect the time variation of T_B to be governed primarily by the second term in (3)

$$\frac{\partial T_B}{\partial t} \simeq -2\Gamma_g T_0 \Upsilon \frac{\partial \Upsilon}{\partial t}. \tag{4}$$

A similar statement applies to the variation of T_B with incidence angle.

Figs. 1 and 2 illustrate the effect of the canopy background on the emitted radiation from a soybean canopy. The data were acquired in 1983 by a dual-frequency (2.7 and 5.1 GHz), dual-polarization radiometer mounted atop a truck-mounted boom. The photograph in Fig. 3 shows strips of metal screening in place over the soil surface, between rows of corn plants. The plants in the foreground have been defoliated, whereas those in the background have not. Because the screens do not cover the entire soil surface, some radiation escapes through the narrow strips

Fig. 3. Photograph of a section of corn field showing strips of metal screening covering the soil surface between the rows of plants. The plants in the foreground were defoliated before the photo was taken.

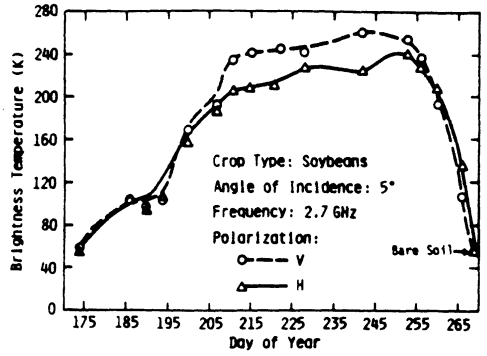

Fig. 4. Temporal variation of the brightness temperature of a soybean canopy over a screen-covered soil surface.

of exposed soil between the screens. The observed brightness temperature of about 85 K for the bare screen (measured following removal of the soybean plants) consists of about 50 K due to the exposed soil strips, about 15 K due to leakage through the holes in the screen mesh, about 5 K due to downwelling sky emission reflected by the screen, and about 15 K due to emission from the surrounding fields received through the sidelobes. The effective reflectivity of the screen background may be calculated from

$$\Gamma_{sc} = \frac{T_s - T_B}{T_s - T_{SKY}} \tag{5}$$

where T_s is the physical temperature of the screen and T_B is the brightness temperature measured for bare screen. For $T_B \simeq 85$ K (Fig. 1), $\Gamma_{sc} \simeq 0.73$. It is worth noting that it is possible to reduce the level of T_B of screens by more careful placement of the screens; in a similar experiment conducted in 1982, T_B was about 55 K (see Fig. 4).

At nadir, the presence of the screen causes T_B of vegetation to be lower than it is with a soil background by about 60 K at 2.7 GHz and 20 K at 5.1 GHz (Figs. 1 and 2). This difference is attributed to the fact that T is smaller at 5.1 GHz than at 2.7 GHz.

III. Temporal Observations of Brightness Temperature

Fig. 4 displays temporal measurements of the brightness temperature of a soybean canopy recorded over a period of three months in 1982. The first measurement, recorded on Day of Year (DoY) 173, was made shortly after planting, at which time the plants were only a few centimeters high. The brightness temperature was found to be about 55 K for both polarizations. The last measurement (DoY 269), which was made after harvesting and removing the soybean plants, was at approximately the same level as that recorded at the beginning of the growing season.

The overall temporal variation of T_B was as expected, but the observed difference in level between the horizontal-polarization and vertical-polarization curves was quite unexpected because the observations were made at a nadir angle of 5°. In midseason, the difference in level was as much as 40 K. Such a polarization dependence at angles near nadir had been observed for periodic soil surfaces [2], [3] but had not been reported for vegetation canopies. The data presented in Fig. 4 are part of a data set acquired as a function of θ for $\phi = 90°$ (Fig. 5). In such a configuration, which will be referred to as the "perpendicular look direction," H-polarization corresponds to an electric field vector parallel to row direction (i.e., $\vec{E} = \times E$), and V-polarization corresponds to $\vec{E}$ being in the yz plane. Measurements made by varying θ while maintaining ϕ equal to 0° will be referred to as "parallel look-direction" data. The dependence of T_B (θ, ϕ, p) on incidence angle θ, azimuth angle ϕ, and polarization configuration p is discussed in the next section.

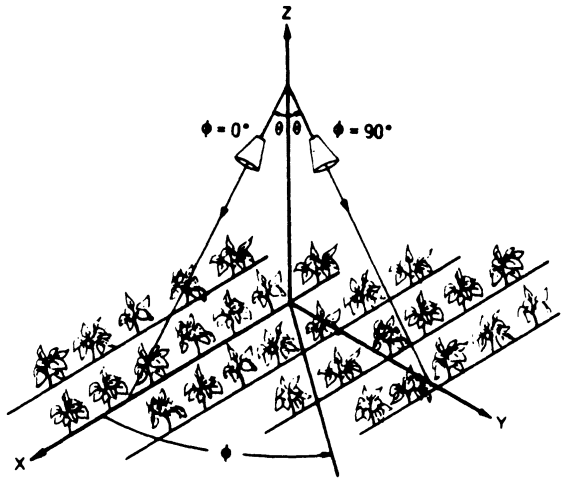

Fig. 5. Definition of look direction and polarization. Measurements as a function of θ at $\phi = 0°$ (xz plane) refer to parallel look-direction observations; $\vec{E}$ in y-direction is H-polarization and $\vec{E}$ in xz plane is V-polarization. For $\phi = 90°$, measurements as a function of θ in yz plane are perpendicular look-direction observations; $\vec{E}$ in x-direction is H-polarization and $\vec{E}$ in yz plane is V-polarization.

A similar, though lesser polarization dependence was observed for a corn canopy. An explanation related to leaf slope distribution is proposed in the next section.

IV. Row-Direction Experiments

A. Soybean Canopy

A row-direction experiment was conducted on July 26, 1983 (DoY 207) to evaluate the response of T_B to row direction and polarization. The soybean plants were approximately 80 cm in height and the canopy's wet-biomass was 2.3 kg · m^{-2}. The brightness temperature was measured as a function of θ for $\phi = 0°$ (parallel look direction) and $\phi = 90°$ (perpendicular look direction) at 2.7 and 5.1 GHz. The 2.7-GHz results are shown in Fig. 6.

The curves show that for perpendicular look direction $T_B(\theta, 90°, V)$ is higher than $T_B(\theta, 90°, H)$ by 20–30 K. At nadir, $T_B(0°, 90°, V) = T_B(0°, 0°, H)$, which is expected, since both configurations represent an orthogonal orientation of the electric field relative to the row direction. Similarly, $T_B(0°, 90°, H) = T_B(0°, 0°, V)$. However, the nadir brightness temperature of the canopy is 23 K higher in level when $\vec{E}$ is orthogonal to row direction

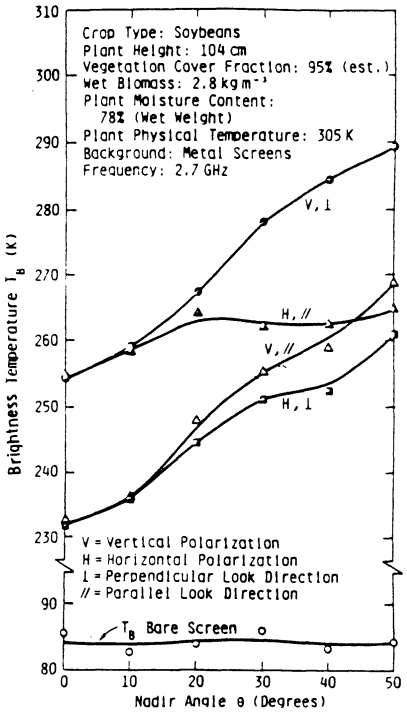

Fig. 6. Angular measurements of T_B at 2.7 GHz for various combinations of look direction and polarization.

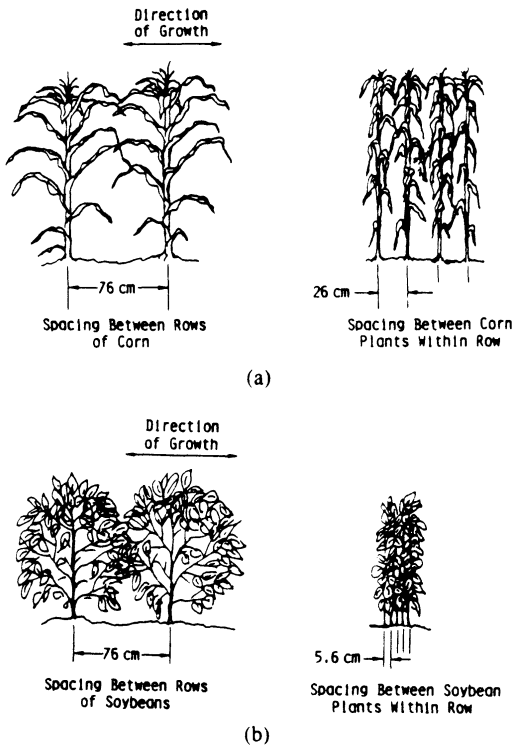

Fig. 7. Along-row and across-row views of (a) a corn field and (b) a soybean field.

than when it is parallel to row direction. This behavior is somewhat puzzling. For periodic soil surfaces, the polarization/row-direction dependence of T_B is attributed to the Fresnel reflectivity at the soil-air interface [2], [3]. An analogous explanation for a vegetation canopy would require that the canopy be regarded as having an undulating periodic air-vegetation boundary and that the average permittivity of the vegetation layer be of the order of 4 or higher. However, the effective permittivity of a vegetation canopy rarely exceeds 1.3.

Ruling out the large-scale periodicity of the canopy as being the factor directly responsible for the polarization dependence, we offer an alternative explanation based on the azimuthal variation of the slope distribution of the canopy scatterers (leaves and branches). The standard planting practice for corn and soybeans is to sow the crops in rows 76 cm apart. Measurements for the fields observed in this investigation yielded a within-row plant spacing of 26 cm for corn and 5.6 cm for soybeans. As the plants grow, the stalks grow vertically, but the leaves (corn) and branches (soybeans) tend to spread into the space (76 cm wide) between the rows. Fig. 7(a) and (b) illustrates the structure for corn and soybeans, respectively. The net result of this process is that the leaves and branches have a distinctly different slope distribution in the plane parallel to the rows than in the plane orthogonal to row direction. If the emission by an individual leaf or branch is polarization-dependent and has a nonuniform angular distribution, then the emission by the canopy as a whole will, in general, have an azimuthal dependence also.

B. Corn Canopy

The corn observations included an additional variable that was not examined for soybeans. This variable was

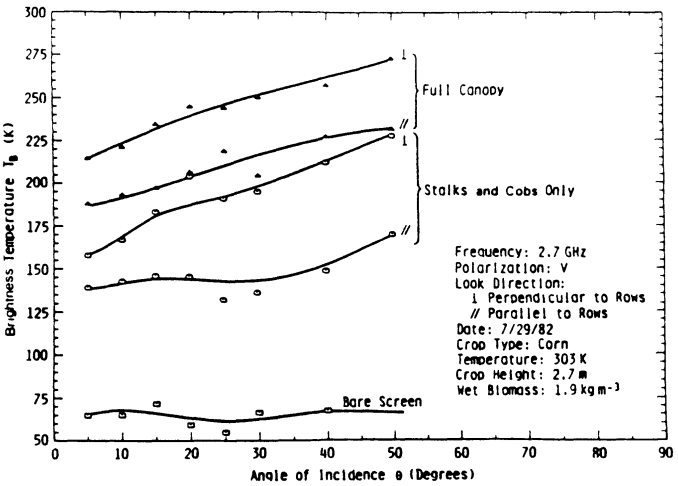

Fig. 8. Results of the corn defoliation experiment for the screen-covered soil field.

the presence or absence of leaves on the canopy. After measuring the foliated canopy, the leaves were stripped off and another set of measurements was made. Finally, the plants were cut and removed, and T_B of the background was recorded. This process was conducted for canopy plots with soil as background and with screen-covered soil as background. Fig. 8 displays the angular behavior of T_B based upon observations made in the planes parallel and perpendicular to the rows for both the full canopy and for stalks and cobs only. The measurements were made with screens as background. Bare-screen measurements were made for parallel and perpendicular look directions for both H- and V-polarizations. The variations in the four measurements were typically less than 5 K. Hence, only one curve is displayed in Fig. 8. The curves

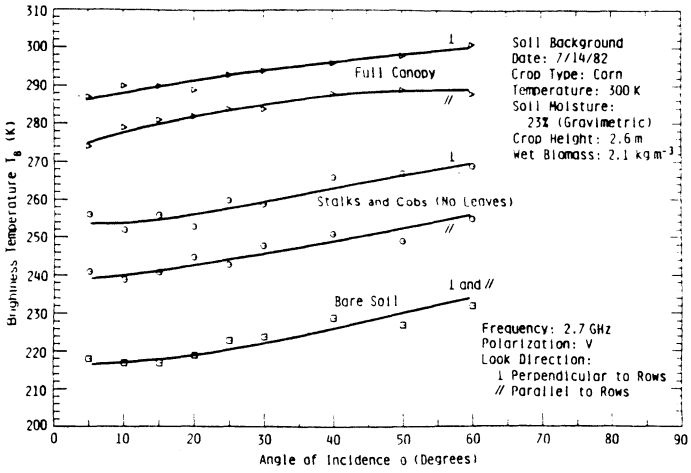

Fig. 9. Results of the corn defoliation experiment (with no screen used).

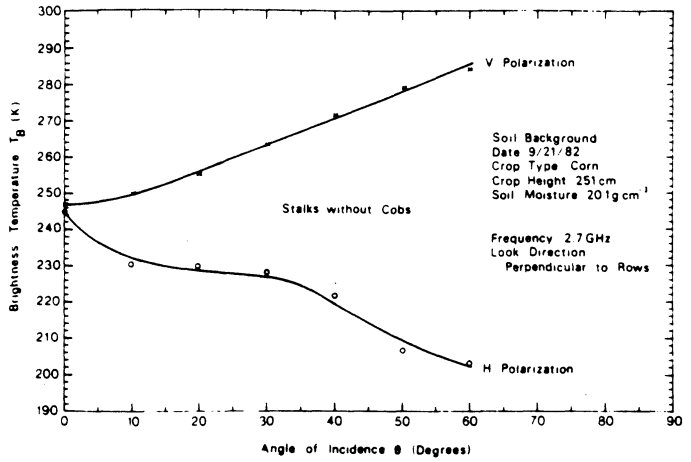

Fig. 10. Angular variation of T_B for bare stalks over soil background.

for the defoliated canopy (stalks and cobs only) clearly show that the emission from the stalks and cobs is substantial and should not be ignored (some models have assumed that the leaves are the source of most of the emission and that the stalks and cobs are inconsequential). The overall T_B pattern displayed in Fig. 8 also is visible in Fig. 9, which pertains to measurements made without screens (soil background), although the differences in level between the curves for perpendicular and parallel look directions are smaller (note that the scale of T_B is different in Figs. 8 and 9). We again observe that the brightness temperatures for parallel and perpendicular look directions do not converge to the same value as θ approaches 0° (nadir). For the full canopy case, we attribute the lack of convergence to the azimuthal variation of the leaf slope distribution, and for the stalks and cobs cases we attribute it to the nonuniform azimuthal density of the cob's locations on the stalks. This last contention is based on measurements that were made two months later for stalks alone (Fig. 10) and for stalks and cobs together; when cobs were not present, T_B was the same for both V- and H-polarizations at nadir.

V. Canopy Model

The results reported in the previous section provide information about the general behavior of canopy emission

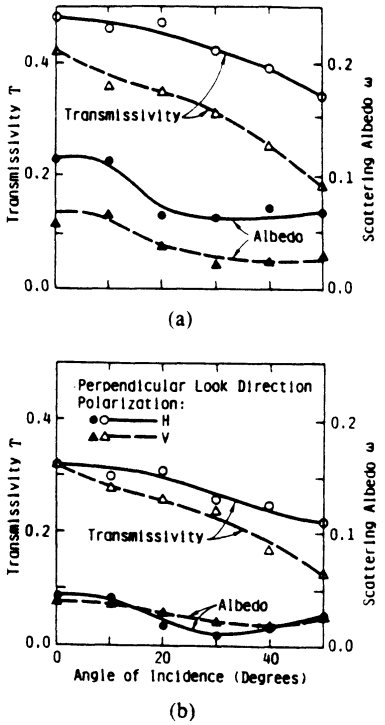

Fig. 11. Angular variation of effective canopy transmissivity Γ and albedo ω for perpendicula look direction at (a) 2.7 GHz and (b) 5.1 GHz.

and about the roles of the incidence angle θ, the look direction defined by the azimuth angle ϕ, the polarization configuration p (V or H), and the frequency f (limited to 2.7 and 5.1 GHz in this study). To model the emission from a vegetation canopy, we will a) adopt the model given by (1); b) regard the two canopy parameters, ω and Γ, as effective model parameters that are functions of θ, ϕ, p, and f; c) use radiometric observations to determine ω and Γ; and d) relate ω and Γ to the physical parameters of the canopy. As a test, we will evaluate the performance of the model against the measured data.

To determine ω and Γ, the brightness temperature was measured for a) bare screens (which provided Γ_{sc}), b) canopy over screens, c) bare absorbing material with an emissivity close to unity, and d) canopy over the absorbing material. From these four observations, it is then possible to calculate ω and Γ, using the form of (1) appropriate to each of the four conditions. Figs. 11 and 12 display the results in the form of angular plots for ω and Γ at 2.7 and 5.1 GHz for $\phi = 0°$ and 90°. We observe that

a) Γ is smaller at 5.1 than at 2.7 GHz.

b) Γ exhibits a strong dependence on θ for $\phi = 90°$ compared to the absence of a discernible variation for $\phi = 0°$.

c) The albedo ω is generally smaller at 5.1 GHz than at 2.7 GHz. This result is contrary to expectations based on Rayleigh scattering.

d) ω generally decreases with increasing θ, particularly in the near-nadir angular region.

e) Near nadir, ω is much larger when the electric field vector is parallel to the row direction (p = H and $\phi = 90°$, or p = V and $\phi = 0°$) than when it is perpendicular

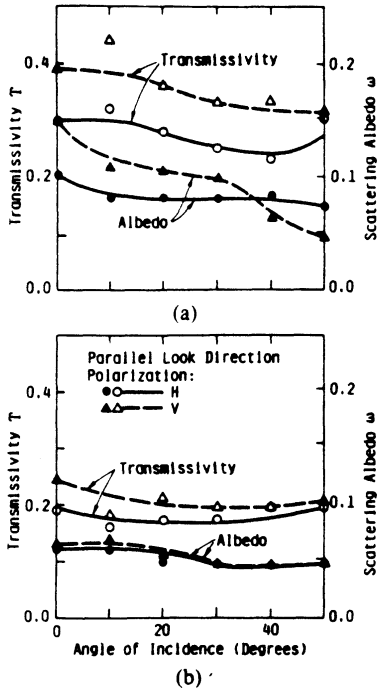

Fig. 12. Angular variation of effective canopy transmissivity Υ and albedo ω for parallel look direction at (a) 2.7 GHz and (b) 5.1 GHz.

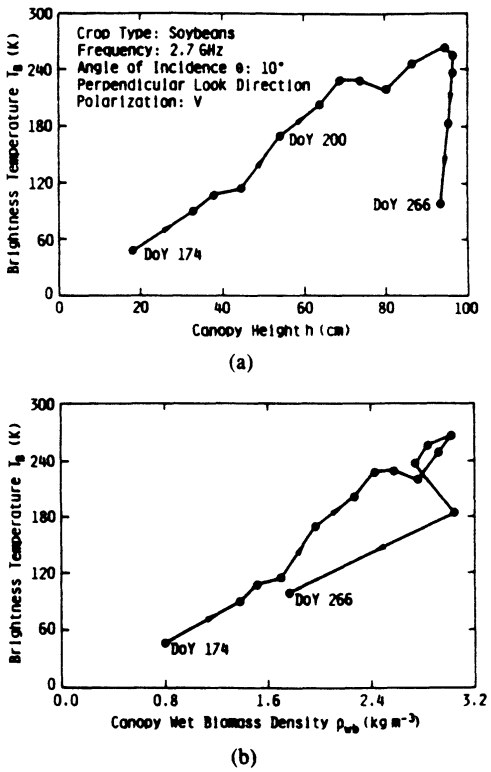

Fig. 13. Variation of brightness temperature at 2.7 GHz with (a) canopy height and (b) wet biomass density ρ_{wb}.

to the row direction (p = V and $\phi = 90°$, or p = H and $\phi = 0°$).

Next, we shall summarize the results of attempts made to relate T_B and Υ to the physical parameters of the canopy. The data, which were acquired as a function of time over the growing season, included T_B measurements for perpendicular look direction and measurements of several canopy and soil biophysical parameters. Statistical regression analyses were performed for T_B and Υ as a function of canopy height h, wet biomass density ρ_{wb} (kg · m^{-3}), canopy water density ρ_w (kg · m^{-3}), dry biomass density ρ_{ab}, integrated water content $W = \rho_w h$ (kg · m^{-2}), and other products of biomass density and height. It was found that T_B and Υ correlate highly with h, ρ_{wb}, and ρ_w for the first half of the growing cycle but not for the entire cycle. Examples are shown in Fig. 13.

The experiment leading to the results shown in Figs. 11 and 12, which included radiometric measurements of the canopy with both screen-covered soil and absorber-covered soil, was conducted only once during the growing season. The availability of data for the low-emissivity screen-covered soil and high-emissivity absorber-covered soil allowed us to estimate effective values for the albedo ω and the transmissivity Υ. As discussed earlier, we expect ω to exhibit a much weaker dependence on the biophysical properties of the canopy than Υ would. To obtain approximate estimates of the variation of Υ with time, we shall assume that the values of ω given in Figs. 11 and 12 remain constant with time. This assumption allows us to use the record of T_B (measured over the growing season) for the canopy over the screen-covered soil to compute Υ and then to relate it to the canopy's biophysical parameters. The result of this procedure is illustrated in Figs. 14 and 15 for soybeans at 2.7 GHz. In Fig. 15, the trans-

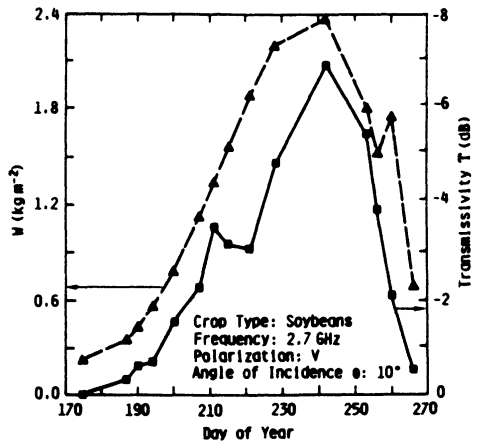

Fig. 14. Temporal variations of canopy integrated water W and transmissivity Υ.

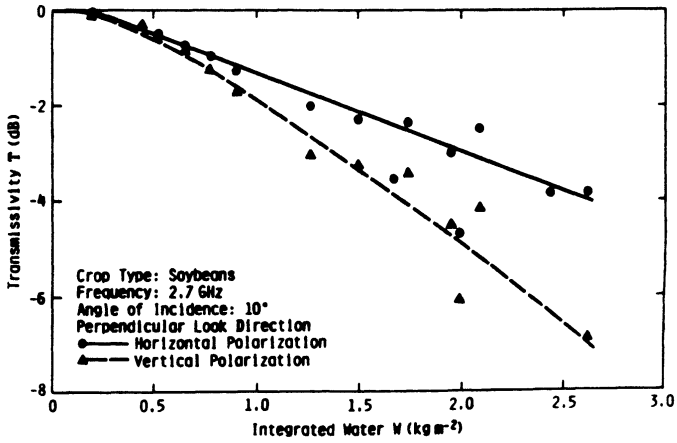

Fig. 15. Variation of the transmissivity Υ with integrated water W at 2.7 GHz.

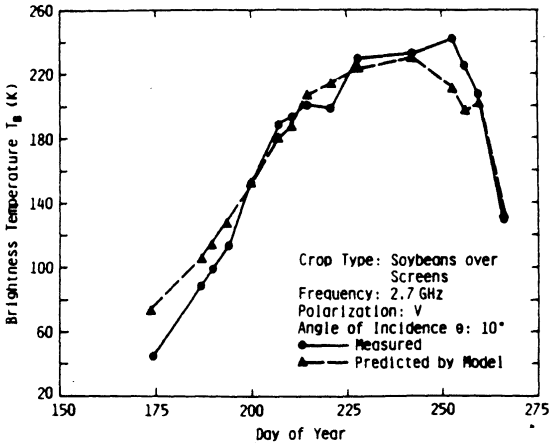

Fig. 16. Comparison of model prediction versus measured temporal record of T_B for a soybean canopy over a metal screen background.

missivity Υ may be related to the integrated water W through a simple formula based on linear regression. Using this formula in (1), T_B was calculated for each of the dates on which data were available and then compared to the measured values, as shown in Fig. 16. The albedo was treated as a time-independent constant, and the reflectivity of the screen-covered soil Γ_{sc} also was assumed constant; its value was obtained from the bare-screen observations discussed earlier.

To evaluate the model for the case in which the soil surface is not covered by a screen, the model was applied, with one modification, to the data acquired for the "natural" soybeans field: the ground reflectivity was taken as a function of the volumetric soil moisture content m_v

$$\Gamma_g = 0.0112\, m_v - 0.05$$

$$\theta = 10°$$

$$p = \mathrm{H}$$

$$f = 2.7\ \mathrm{GHz}.$$

The above expression was based on radiometric observations made for a bare-soil surface that had been prepared for soybean planting, but which was left bare instead. Fig. 17 compares the model predicted values of T_B with the experimental observations. Considering the relative simplicity of the model and the narrow dynamic range of T_B, the overall agreement between the model and the data is fairly good.

VI. Concluding Remarks

This study has shown that the microwave emission from vegetation canopies planted in parallel rows exhibits a) nonisotropic behavior in azimuth and b) a polarization dependence related to the slope distribution of the canopy scatterers (such as leaves, stalks, and branches). For a given look direction, polarization configuration, and microwave frequency, it is possible to use a simple zero-order radiative transfer model to predict the emission from the canopy. The next step, which is the subject of future research, will be to relate canopy albedo and transmissivity to a) large-scale canopy structure (row orientation and spacing), and b) dielectric constants, sizes, and slope distributions of the scatterers.

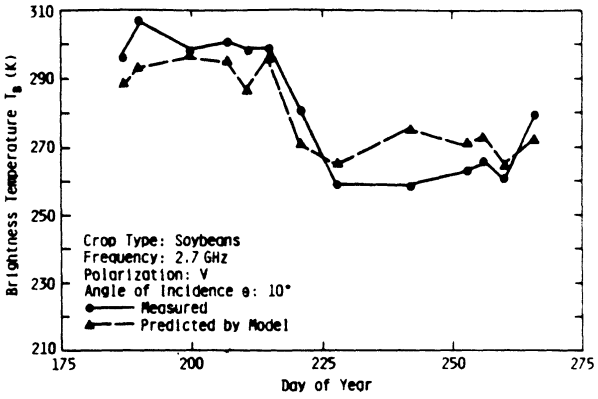

Fig. 17. Comparison of model prediction versus measured temporal record of T_B for a soybean canopy over a soil background.

References

[1] D. R. Brunfeldt and F. T. Ulaby, "Measured microwave emission and scatter in vegetation canopies," *IEEE Trans. Geosci. Remote Sensing*, vol. GE-22, pp. 520-524, 1984.

[2] F. Kouyate, F. T. Ulaby, and A. K. Fung, "Microwave emission from a periodic soil surface," University of Kansas Center for Research, Inc., Lawrence, Kansas, RSL Tech. Rep. TR460-7, 1981.

[3] J. R. Wang, R. W. Newton, and J. W. Rouse, "Passive microwave remote sensing of soil moisture: The effect of tilled row structure," *IEEE Trans. Geosci. Remote Sensing*, vol. GE-18, pp. 288-295, 1980.

*

David R. Brunfeldt was born in Bartlesville, OK, on June 2, 1952. He received the B.S., M.S., and Ph.D. degrees from the University of Kansas in 1974, 1979, and 1985, respectively.

He is currently in charge of engineering for microwave remote sensing systems at the Applied Microwave Corporation, Lawrence, KS. He was formerly with the Remote Sensing Laboratory at the University of Kansas Center for Research.

*

Fawwaz T. Ulaby (M'68-SM'74-F'80) was born in Damascus, Syria, on February 4, 1943. He received the B.S. degree in physics from the American University of Beirut, Lebanon, in 1964 and the M.S.E.E. and Ph.D. degrees in electrical engineering from the University of Texas, Austin, in 1966 and 1968, respectively.

From 1968 to 1984, he was with the Electrical Engineering Department at the University of Kansas, where he was the J. L. Constant Distinguished Professor, and the University of Kansas Center for Research, where he was Director of the Remote Sensing Laboratory. He is currently with the Radiation Laboratory and the Department of Electrical and Computer Engineering, University of Michigan, Ann Arbor. His current research interests involve microwave propagation and active and passive microwave remote sensing. Along with R. K. Moore and A. K. Fung, he is a coauthor of the three-volume series *Microwave Remote Sensing: Active and Passive*, Reading MA: Addison-Wesley. In addition, he is coeditor of the *Manual of Remote Sensing*, 2nd ed., vol. I, American Society of Photogrammetry.

Dr. Ulaby is a member of Eta Kappa Nu, Tau Beta Pi, and Sigma Xi. He is the Executive Editor for IEEE Transactions on Geoscience and Remote Sensing, 1984-1987, and the Geoscience and Remote Sensing Society's Distinguished Lecturer for 1986. He was named an IEEE Fellow in 1980 "for contributions to the application of radar to remote sensing for agriculture and hydrology," received the GRS Society's Outstanding Service Award in 1982, and its Distinguished Service Award in 1983. In 1984, he also received a Presidential Citation for Meritorious service from the American Service of Photogrammetry. He received the University of Kansas Chancellor's Award for Excellence in Teaching in 1980, the University of Kansas Gould Award for "distinguished service to higher education" in 1973, and Eta Kappa Nu MacDonald Award as an "outstanding electrical engineering professor in the United States of America" in 1975.

RADAR POLARIMETRIC OBSERVATIONS OF A TREE CANOPY

F T Ulaby, M W Whitt & M C Dobson

The Radiation Laboratory
Department of Electrical Engineering and Computer Science
The University of Michigan
Ann Arbor, MI 48109-2122, U.S.A

ABSTRACT

This paper introduces an effective technique for characterizing the propagation properties of a forest canopy. The technique requires the use of a polarimetric scatterometer, which is a calibrated radar capable of measuring the complete backscattering matrix (amplitude and phase) of the scene it illuminates. A truck-mounted 1.6 GHz polarimetric scatterometer was used from a 19 m high platform to measure the backscattering from a dense canopy of pine trees at an incidence angle of 40°. Two sets of measurements were made at each of many spatial locations, one set with and the other without a trihedral corner reflector present on the ground surface underneath the canopy. From the two sets of polarimetric measurements, it was possible to determine the mean values and the statistical distributions of the canopy attenuation factors for horizontal and vertical polarizations. The mean values of the one-way attenuation factors were found to be 9.31 dB for horizontal polarization and 9.16 dB for vertical polarization.

1. INTRODUCTION

The propagation properties of a forest canopy play a fundamental role in the development of microwave remote sensing models that relate the radar backscatter to the biophysical properties of the canopy. To date, however, only a few experimental investigations have been conducted (Refs. 1-4) to measure the attenuation of forest canopies at microwave frequencies. This is attributed in part to the difficulties associated with measuring the propagation properties of a forest canopy. The difficulties are related to the inhomogeneous, random, and possibly anisotropic nature of the medium.

The approaches traditionally used to measure the propagation characteristics of an inhomogeneous random medium are of two types. The first type involves the use of a transmitter on one side of the layer whose propagation properties are to be measured and a receiver on the other side. Because the medium is inhomogeneous, it is necessary to measure the loss and phase delay through many paths in the layer to establish the mean values and associated statistics of the attenuation coefficient a_p and phase constant b_p. The subscript p denotes the polarization configuration under consideration. Usually, the quantities of interest are a_h, a_v, and $Db = b_v - b_h$, where the subscripts h and v denote horizontal and vertical polarizations, respectively, and $\hat{h}$ is defined to be parallel to the earth's surface.

For a forest canopy, the transmitter-receiver technique is somewhat cumbersome to use, particularly at oblique incidence, because of problems associated with proper pointing and positioning of the antennas.

In the second approach, which is a modified version of the first one, the transmitter and receiver are co-located (radar mode) on one side of the layer (Fig. 1), and the quantity measured by the

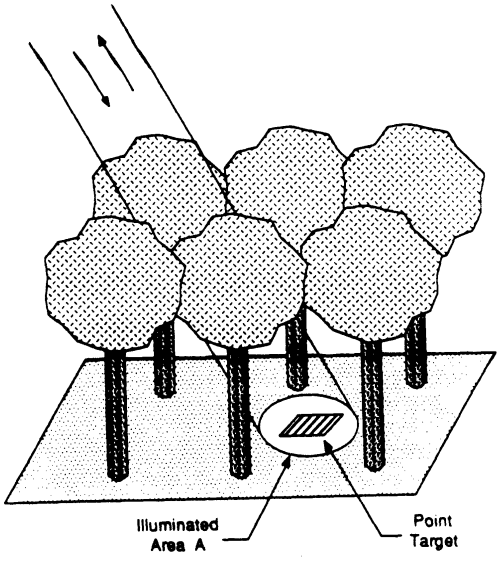

Figure 1. Sketch showing a radar beam illuminating a tree canopy with a point target underneath.

receiver is the signal backscattered from a strong target of known radar cross section placed on the other side of the layer. Because the received signal contains backscattering contributions from both the reference target located behind (or below) the layer and from the layer itself, the precision associated with the measured two-way attenuation of the layer, is governed by the amplitude ratio $|E_r| / |E_b|$. The quantities E_r and E_b are the fields backscattered from the reference target and the "background" layer, respectively.

A traditional radar measures $|E|^2$, where $E = E_r + E_b$, and through calibration, $|E|^2$ is converted to units of radar cross section s. If the background contribution is negligible, the radar will measure the radar-cross- section of the reference target (s_r) attenuated by the intervening canopy,

$$\sigma = \sigma_r e^{-2\tau} \qquad (1)$$

Proceedings of IGARSS '88 Symposium, Edinburgh, Scotland, 13–16 Sept. 1988. Ref. ESA SP-284 (IEEE 88CH2497-6).
Published by ESA Publications Division, August 1988.

where t is the one-way slant path optical thickness of the canopy.

In order to measure t with good accuracy, it is necessary to select the reference target such that its cross section s_T is sufficiently large to insure that

$$\sigma_r e^{-2\tau} / \sigma_b >> 1 \ . \qquad (2)$$

If the objective is to measure t with a precision of ±1 dB, the ratio on the left-hand side of Eq. 5 should be equal to or greater than 100 (Ref. 5, pp. 768-770).

Let us now consider a specific example. Assume that a narrow-beam 1.6 GHz radar antenna is used to illuminate a flat metal plate oriented normal to the illumination and placed underneath a tree canopy. If the antenna footprint area A on the ground is about 5 m^2, and the backscattering coefficient of the trees alone (with no metal plate present) is σ_b^0=0.1 $m^2 m^{-2}$, then $\sigma_b=\sigma_b^0 A$=0.5 m^2. Assuming a 10 dB one-way loss due to the layer, the two-way loss term exp(-2t) = 0.01. A flat metal plate is chosen for this example because among passive reflectors it provides the highest radar cross section for a given physical cross section A_T. If we set $s_T \exp(-2\,t) / s_b = 100$ and use the values given above, we find that s_T should be 5000 m^2. From the relationship $\sigma_r=4\pi A_r^2/\lambda^2$, we find that A_r should be 3.7 m^2 at 1.6 GHz. The half-power beamwidth of a square or circular metal plate with such an area is about 2.5°, which makes it difficult to point the reflector properly with respect to the radar antenna. In essence, the pointing accuracy has to be better than about 0.7° in order for the error associated with the estimated value of t to be less than 1 dB. A wider- beam trihedral corner reflector may be used instead, but in that case the length L of its aperture edges will have to be 3.6 m each in order for s_T to be 5000 m^2; for a trihedral corner reflector, $s_T = p\,L^4/3l^2$ (Ref. 5, p.776). Clearly, this is a large trihedral to use in a forest canopy. Moreover, if a measurement precision of better than ±1 dB is desired, the trihedral will have to be even larger and heavier.

Instead of this "brute force" approach, we propose to use a polarimetric technique that involves measuring the scattering matrix of the tree canopy with and without a trihedral reflector underneath. The propagation parameters of the canopy may be derived from these measurements using a much smaller trihedral reflector, and the associated accuracy is far superior to that associated with the traditional amplitude-only technique.

2. POLARIMETRIC RADAR MODEL

When a point target is present underneath a vegetation canopy (Fig. 1), the backscattered signal is composed of a contribution due to the canopy, a contribution due to the point target and attenuated by the intervening medium (the canopy), and a third contribution due to interaction (multiple scattering) between the canopy and the point target. We assume that the interaction contribution is negligible small in comparison to the other two contributions, and therefore ignore it. This assumption is supported by measurements that were conducted for a canopy of pine trees with and without a trihedral corner reflector present in the illuminated area. The measurements for trees alone indicated that the canopy produces significant depolarization. When the trihedral was placed under the canopy, the co-polarized returns (hh and vv) exhibited a measurable change, as expected, but the cross- polarized returns (hv and vh) did not. This implies that an insignificant amount of the co-polarized energy backscattered from the trihedral reflector is converted by the canopy to cross-polarized energy. Thus, as a first order model, it is reasonable to ignore the interaction contribution and to model the scattering matrix of the canopy with the point target present as:

$$[S] = [T] + [L]\,[P]\,[L]\ , \qquad (3)$$

where the phase reference is taken to be the top of the canopy, and

- [S] = scattering matrix of trees with point target,
- [L] = one-way propagation (loss) matrix of canopy,
- [P] = scattering matrix of point target,
- [T] = scattering matrix of trees alone.

The matrices [S] and [L] are given by

$$[S] = e^{j\phi_{hhs}} \begin{bmatrix} S_{hh} & S_{hv} e^{j\phi'_{hvS}} \\ S_{vh} e^{j\phi'_{vhS}} & S_{vv} e^{j\phi'_{vvS}} \end{bmatrix} \qquad (4)$$

$$[L] = \begin{bmatrix} L_h e^{j\phi_{hL}} & 0 \\ 0 & L_v e^{j\phi_{vL}} \end{bmatrix}\ , \qquad (5)$$

$$L_\mu = \exp\left(-\int_0^R \alpha_\mu \, dR\right),\ \phi_{\mu L} = \int_0^R \beta_\mu \, dR,\ \mu \in \{h,v\}, \qquad (6)$$

where R is the total path length through the canopy to the point target, a_m and b_m are the canopy attenuation coefficient and phase constant for polarization m, and

$$\phi'_{rtS} = \phi'_{rtS} - \phi'_{hhS} \ . \qquad (7)$$

Matrices [P] and [T] are identical with [S] except for replacing the symbol S with P and T everywhere, respectively. Using a polarimetric scatterometer, we can measure [S], [P], and [T], and then use Eq. 3 to determine the loss matrix [L].

3. PROPAGATION EXPERIMENT

3.1 Polarimetric Scatterometer

The measurement system consists of an L-band polarimeter operating from the end of an extendable boom mounted on a truck (Fig. 2). A variable-angle mount is used to connect the polarimeter to the boom allowing the incidence angle of the radar illumination to be varied. The polarimeter consists of a HP8753 vector network analyzer, a pulse generator and switching network, and a transmit-receive RF unit section. A detailed description of a similar system that operates at millimeter wavelengths is given in (Refs. 7, 8). The HP8753 network analyzer and the switching network are housed on the bed of the truck while the transmit- receive RF unit is mounted at the top of the boom.

Figure 2 depicts the layout used to measure the propagation properties of the pine canopy. The average canopy height was approximately 13.7 m, the radar antenna was at a height of 19 m above the ground, and the observations were made at an incidence angle of 40° relative to normal incidence. The truck boom was rotated in a conical scan arrangement, thereby maintaining the range to the ground constant for all measurements. Measurements were made at 30 locations approximately 1 m apart. The first four locations were outside

Figure 2. Photograph showing truck-mounted radar next to the pine-tree forest canopy.

the canopy, and the remaining locations were inside the canopy. At each of the 30 locations, two scattering matrix measurements were made, one with the trihedral reflector placed in the illuminated area and another without the trihedral reflector (grass or trees alone). The proper location for placing the trihedral reflector was determined using a simple telescopic and ranging arrangement referenced to the base of the boom and its azimuth orientation. The dimensions of the antenna footprint on the ground were 2.3 m in the azimuth direction and 2.5 m in the range direction, and the triangular front surface of the trihedral corner reflector had 85-cm edges.

3.2 Canopy Description

The experimental data described in this study was obtained from a small plot of mature red pines *(pinus resinosa)* located within the University of Michigan's Nichols Arboretum on a river terrace south of the Huron River. This particular plot of red pines was selected because (1) it is densely planted, which results in the gross stand morphology characteristic of a "closed canopy," (2) its dense planting and high biomass per unit area yields a somewhat extreme case in terms of the foliage penetration problem, and (3) it is adjacent to a level grassy area that provides an unobstructed (by the canopy) view of point targets used for system calibration.

The red pine plot consists of a pure stand of trees (averaging 13.7 m height) with a crown layer of foliage approximately 4 m thick. The tree boles (trunks) are gently tapered cylinders with diameters at breast height (dbh) ranging from 15 cm to 25 cm (average dbh = 19 cm). The stand is densely spaced with 0.23 boles/m^2 (2,291 boles/ hectare). Hence, approximately 12% of the stand area is covered with trunks.

The relative dielectric constant of the boles was measured at L-band (1.2 GHz) in situ using a field portable dielectric probe. The technique is based upon reflection from an open-ended coaxial probe. The average relative dielectric constants measured are e = 3-j0.1 for the bark layer and e = 18-j6 for the sapwood.

3.3 Reference Target

The theoretical scattering matrix for a trihedral corner reflector is given by

$$P = -P_0 \begin{bmatrix} 1 & 0 \\ 0 & 1 \end{bmatrix}, \qquad (8a)$$

with

$$P_0 = \sqrt{\frac{\pi}{3}} \frac{L^2}{\lambda}.$$

For L = 85 cm and l = 18.75 cm, P_0 = 3.93 m corresponding to a maximum radar cross section of sp = 11.9 dBm^2. The scattering matrix measured by the polarimetric scatterometer (with the phase of the hh term as reference) was

$$P = 4.29 \begin{bmatrix} 1 & 0.028 \\ 0.029 & 1.04\, e^{j5^\circ} \end{bmatrix}. \qquad (8b)$$

Comparison of Eq. 8a with Eq. 8b shows that (1) the measured value of P_0 is within 10 percent of the calculated value, (2) the measured P_{vv} deviates from the measured P_{hh} by only 4 percent, and (3) the measured cross-polarized terms are very small. The ratio P_{hv}/P_{vv} = 0.028 is equivalent to -31 dB, which is approximately equal to the polarization isolation of the antenna.

3.4 Results

Using the polarimetric scatterometer, the matrices [S], [P], and [T] were measured and then used in Eq. 3 to compute [L]. This technique was applied to each of the 26 sets of measurements made, and the results are shown in Fig. 3. Parts (a) and (b) of Fig. 3 show the distributions for L_h^2 and L_v^2, the one-way power loss factors, in dB. The mean values are -9.31 dB for h polarization and -9.16 dB for v polarization. Part (c) of Fig. 3 shows the distribution for the phase difference $2(f_{vL} - f_{hL})$; its mean value is 4.23°. These results, namely that the mean values of L_v and L_h are approximately equal and the mean value of the propagation phase difference is approximately zero, suggest that the pine canopy is approximately an isotropic medium.

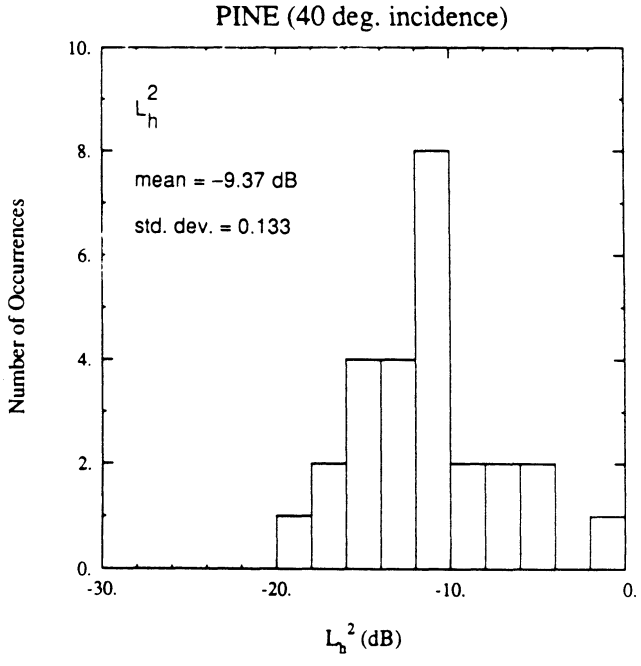

(a) Loss for h polarization

Figure 3. Distribution functions for the one-way power losses L_h^2 and L_v^2 and the two-way phase difference $2(\phi_{vL} - \phi_{hL})$ for pine trees.

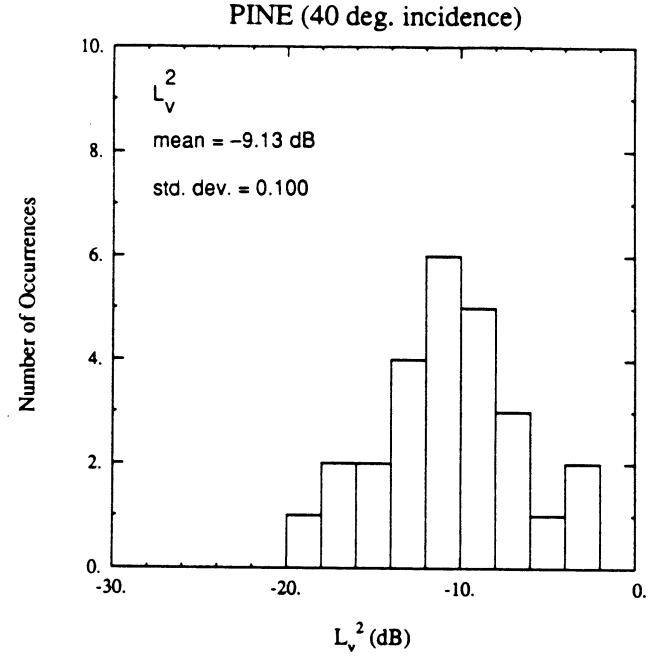

(b) Loss for v polarization

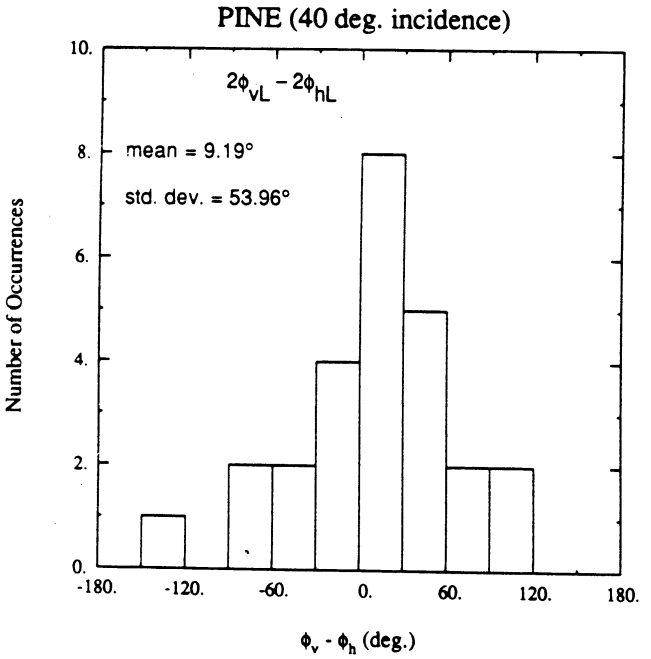

(c) Phase difference

4. CONCLUDING REMARKS

The precision associated with the values of the canopy loss factor measured using the polarimetric technique is estimated to be on the order of ± 0.3 dB. The primary source of error is due to orientation-related variations in P_0, (the scattering amplitude of the trihedral reflector) arising from deployment errors. The trihedral reflector used in the experiment described in the preceding section had an aperture $A_t = \sqrt{3}\ L^2/4 = 0.3\ m^2$.

In comparison, with the amplitude-only measurement technique. A_t would have had to be about 17.7 m^2 in order to achieve the above accuracy of ±0.3 dB, even if we ignore the deployment-related errors altogether.

5. REFERENCES

1. Brown, G. S. and W. J. Curry, "A theory and model for wave propagation through foliage," *Radio Science*, Vol. 17, 1982, pp. 1027-1036.

2. Currie, N. C., F. B. Dyer, and E. E. Martin, "Millimeter foliage penetration measurements," *1976 Int. IEEE Antennas and Prop. Soc. Symposium Digest*, Amherst, Massachusetts.

3. Violette, E. J., R. H. Espeland, and F. K. Schwering, "Millimeter wave propagation at street level in an urban environment," *IEEE Transactions on Geoscience and Remote Sensing,"* Vol. 26, No. 3, 1988, pp. 368-380.

4. Ulaby, F. T., T. E. van Deventer, J. East, T. F. Haddock, and M. Coluzzi, "Millimeter-wave bistatic scattering from ground and vegetation targets," *IEEE Transactions on Geoscience and Remote Sensing*, Vol. 26, No. 3, 1988, pp. 229-243.

5. Ulaby, F. T., R. K. Moore, and A. K. Fung, *Microwave Remote Sensing: Active and Passive, Vol. II -- Radar Remote Sensing and Surface Scattering and Emission Theory*, Addison-Wesley, Advanced Book Program, Reading, MA, 1982, 609 pages.

6. Ruck, G. T., D. E. Barrick, W. D. Stuart, and C. K. Krichbaum, *Radar Cross Section Handbook*, Vol. I, Plenum Press, New York, pp. 17-21, 1970.

7. Whitt, M. W. and F. T. Ulaby, "Millimeter-wave polarimetric measurements of artificial and natural targets," in *International Geoscience and Remote Sensing Symposium (IGARSS '87) Digest*, Ann Arbor, Michigan, pp. 537-543, 1987.

8. Ulaby, F. T., T. F. Haddock, J. East, and M. W. Whitt, "A millimeter-wave network analyzer based scatterometer," *IEEE Transactions on Geoscience and Remote Sensing*, Vol. 26, No. 1, pp. 75-81, January, 1988.